Modeling Results for the ITER Cryogenic Fore Pump

By

Dongsheng Zhang

A dissertation submitted in partial fulfillment of

the requirements for the degree of

Doctor of Philosophy

(Mechanical Engineering)

at the

UNIVERSITY OF WISCONSIN-MADISON

2014

Date of final oral examination: 05/16/2014

The dissertation is approved by the following members of the Final Oral Committee:

John M. Pfotenhauer, Professor, Mechanical Engineering & Engineering Physics
Franklin K. Miller, Professor, Assistant Professor, Mechanical Engineering
Gregory F. Nellis, Professor, Mechanical Engineering
Christopher J. Rutland, Professor, Mechanical Engineering
James Blanchard, Professor, Engineering Physics

Dedication

给妈妈黄云。

Acknowledgements

Thanks to my principle advisor Prof. John M. Pfotenhauer,

Thanks to my co-advisor Prof. Franklin K. Miller,

Thanks to my committee members: Prof. Gregory F. Nellis, Prof. Christopher J. Rutland, and Prof. James Blanchard,

Thanks to the University of Wisconsin-Madison, the US Department of Energy, and the Oak Ridge National Lab.

Table of Contents

List of Tables

List of Figures

Abstract

The work presented here is the analysis and modeling of the ITER-Cryogenic Fore Pump (CFP), also called Cryogenic Viscous Compressor (CVC). Unlike common cryopumps that are usually used to create and maintain vacuum, the cryogenic fore pump is designed for ITER to collect and compress hydrogen isotopes during the regeneration process of the torus cryopumps. Different from common cryopumps, the ITER-CFP works in the viscous flow regime. As a result, both adsorption boundary conditions and transport phenomena contribute unique features to the pump performance. In this report, the physical mechanisms of cryopumping are studied, especially the diffusion-adsorption process and these are coupled with the standard equations of species, momentum and energy balance, as well as the equation of state. Numerical models are developed, which include highly coupled non-linear conservation equations of species, momentum, and energy and equation of state. Thermal and kinetic properties are treated as functions of temperature, pressure, and composition of the gas fluid mixture. To solve such a set of equations, a novel numerical technique, identified as the Group-Member numerical technique is proposed.

This document presents three numerical models: a transient model, a steady state model, and a hemisphere (or molecular flow) model. The first two models are developed based on analysis of the raw experimental data while the third model is developed as a preliminary study. The modeling results are compared with available experiment data for verification.

The models can be used for cryopump design, and can also benefit problems, such as loss of vacuum in a cryomodule or cryogenic desublimation. The scientific and engineering investigation being done here builds connections between Mechanical Engineering and other disciplines, such as Chemical Engineering, Physics, and Chemistry.

Chapter 1 Introduction: ITER and the cryogenic fore pump

This section introduces the ITER tokamak fusion device and focuses on the use of cryo-pump technology to separate the by-products or 'exhaust' components from the fusion reaction. It presents a review of cryogenic adsorption, cryo-pumps, commonly applied numerical methods used to model the physical processes inside the cryo-pump, and the unique characteristics of the ITER-Cryogenic Fore Pump.

The cryogenic fore pump (CFP), also called the cryogenic viscous compressor (CVC), is being developed for use in ITER (C. Day D. B., 2005) (Foster, 2005) (C. Day D. M., 2009) (M. Dremel, 2009) (Baylor, et al., 2011) (Robert C. Duckworth, 2011) (D. S. Zhang, 2014). The CFP is the first part of the roughing pump system, which pumps the fusion exhaust gas during the regeneration process of the torus cryopumps.

1.1. ITER

ITER (ITER, 2013) is a joint international project and is one of the largest scientific projects in the world. It aims to demonstrate the commercial use of fusion energy. The science will benefit all of mankind. Countries representing half of the world's population participate in the project. **FIGURE 1-1** shows the seven domestic agencies, representing 35 countries, that are involved in the development of ITER.

FIGURE 1-1. ITER domestic agencies (http://www.iter.org/).

The ITER machine is designed to produce 10 times the amount of energy that it consumes. That is, 500 MW of fusion power will be produced from 50 MW of input power.

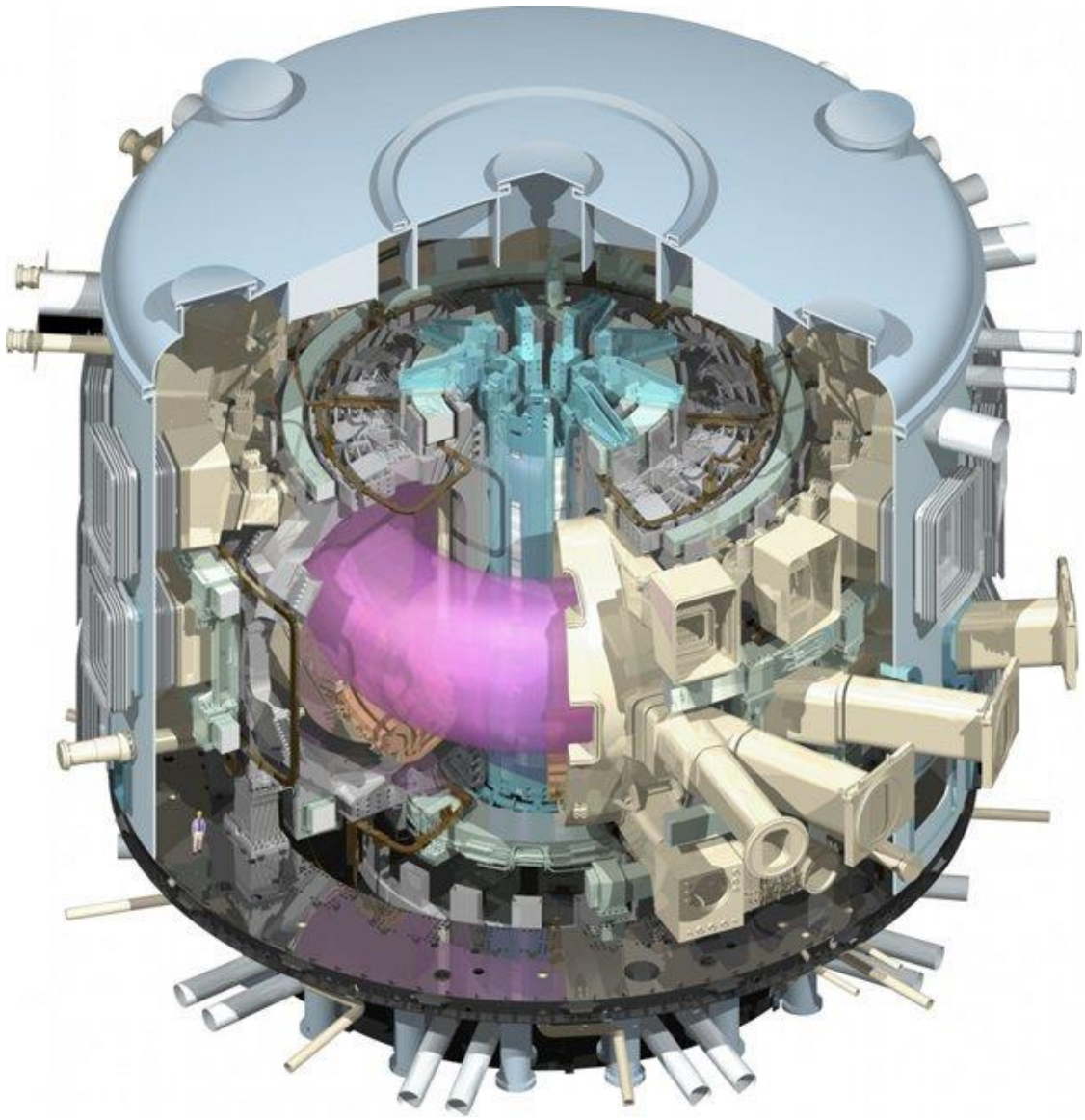

FIGURE 1-2. The ITER Tokamak (http://www.iter.org/).

FIGURE 1-2 shows the ITER tokamak. It is the largest tokamak in the world. Note significantly, that the small figure at the lower left corner is a normal-size human being. The tokamak includes a doughnut-shaped vacuum vessel in which hydrogen isotopes (deuterium and tritium) form a plasma at temperatures in excess of 150 million ˚C. The

plasma is constrained by a high magnetic field. At such extreme temperatures, a fusion reaction occurs. The results of the fusion reaction are the large amount of energy being released and the helium nucleus and neutron being formed. Most of the produced energy is carried by the neutron and is transferred to the surrounding walls of the tokmak. The other particles with charge are constrained in the vessel.

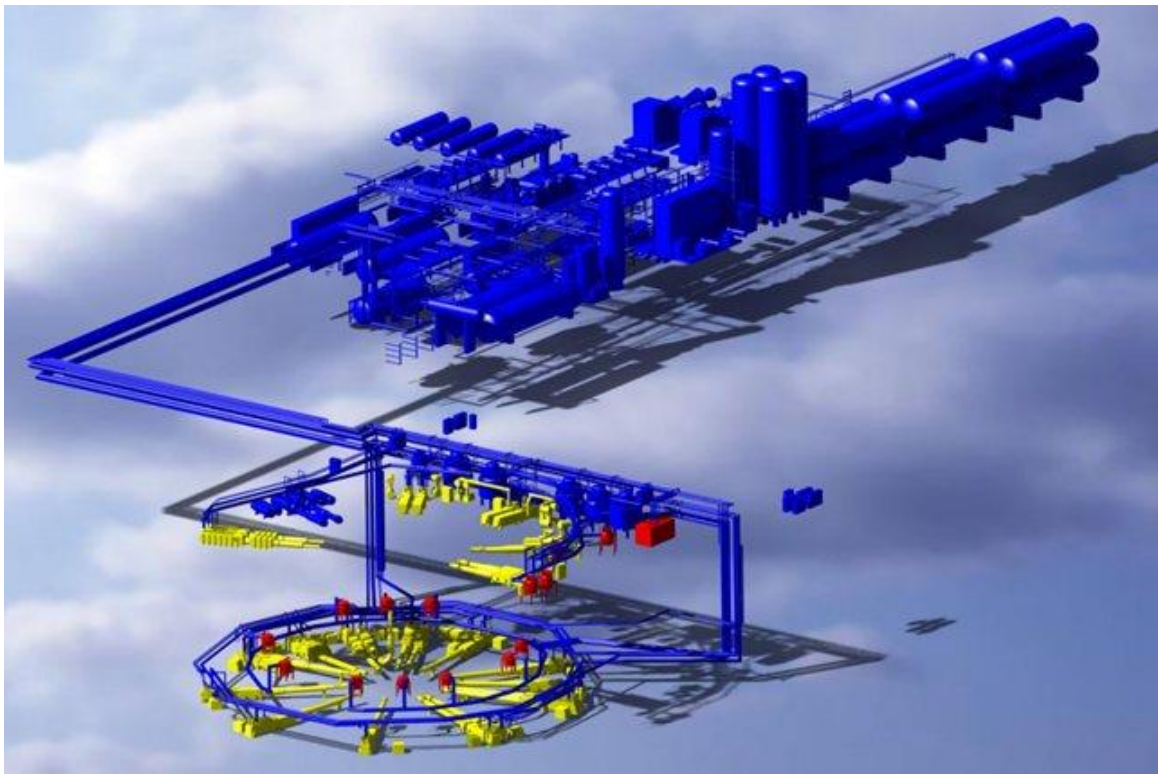

FIGURE 1-3. The ITER cryogenic system (http://www.iter.org/).

To create and maintain the vacuum condition for the tokmak together with other purposes, cryogenic technology is extensively used at ITER. **FIGURE 1-3** shows the ITER cryogenic system. It will be the largest concentrated cryogenic system in the world. The

system includes 50 cold boxes, 3-kilometers of cryo-lines, and 4500 components. The installed cooling power will be 65 KW at 4.5 K that is provided by helium and 1300 KW at 80 K that is provided by nitrogen.

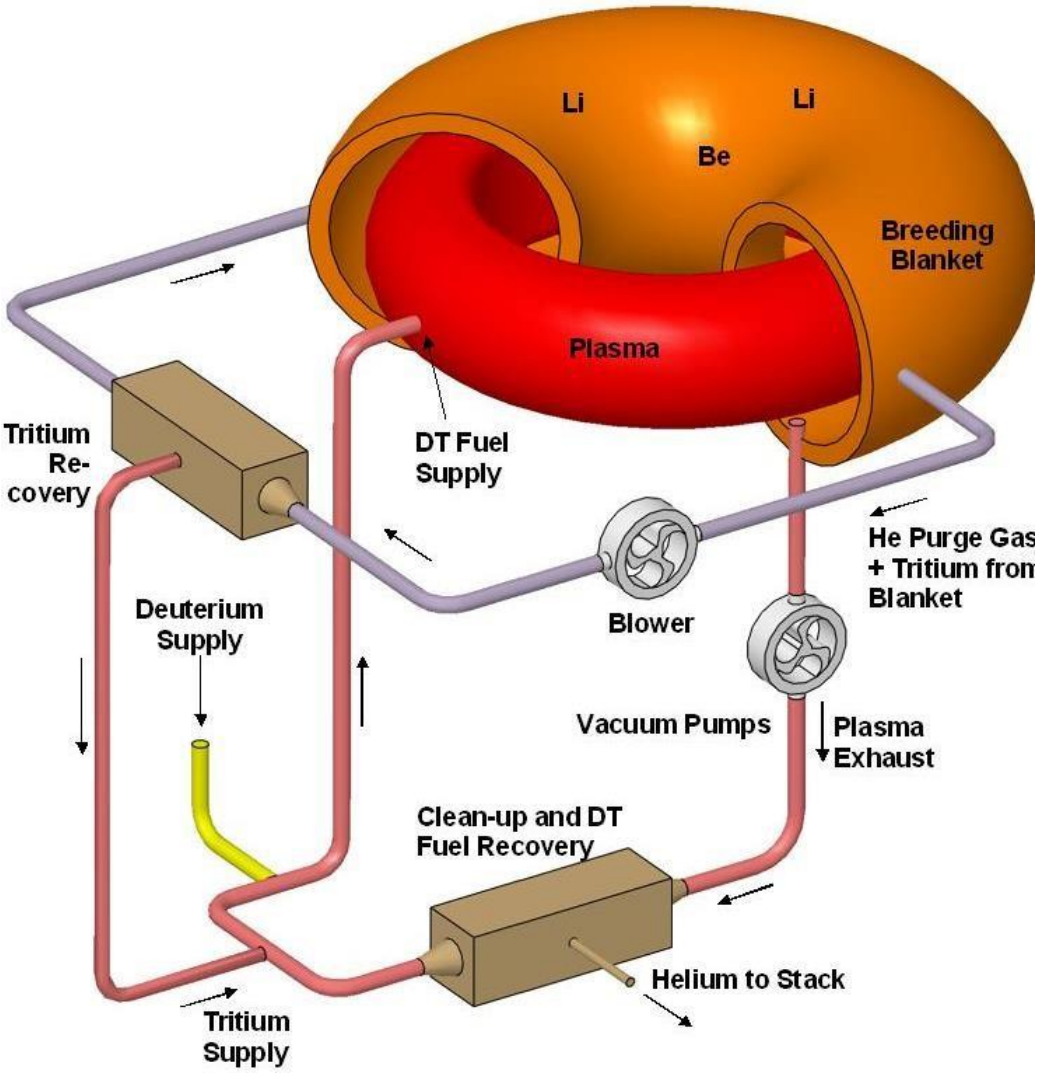

FIGURE 1-4. ITER fuel cycle (http://www.iter.org/).

The fuel supply (deuterium and tritium) at ITER is in a closed system as shown in **FIGURE 1-4**. Pellets of solid deuterium and tritium are injected as fuel into the tokmak (J.W. Leachman, 2008).

The ITER vacuum system is also among the largest ever built. The cryogenic fore pump is part of the ITER vacuum system.

1.2. Cryogenic fore pump

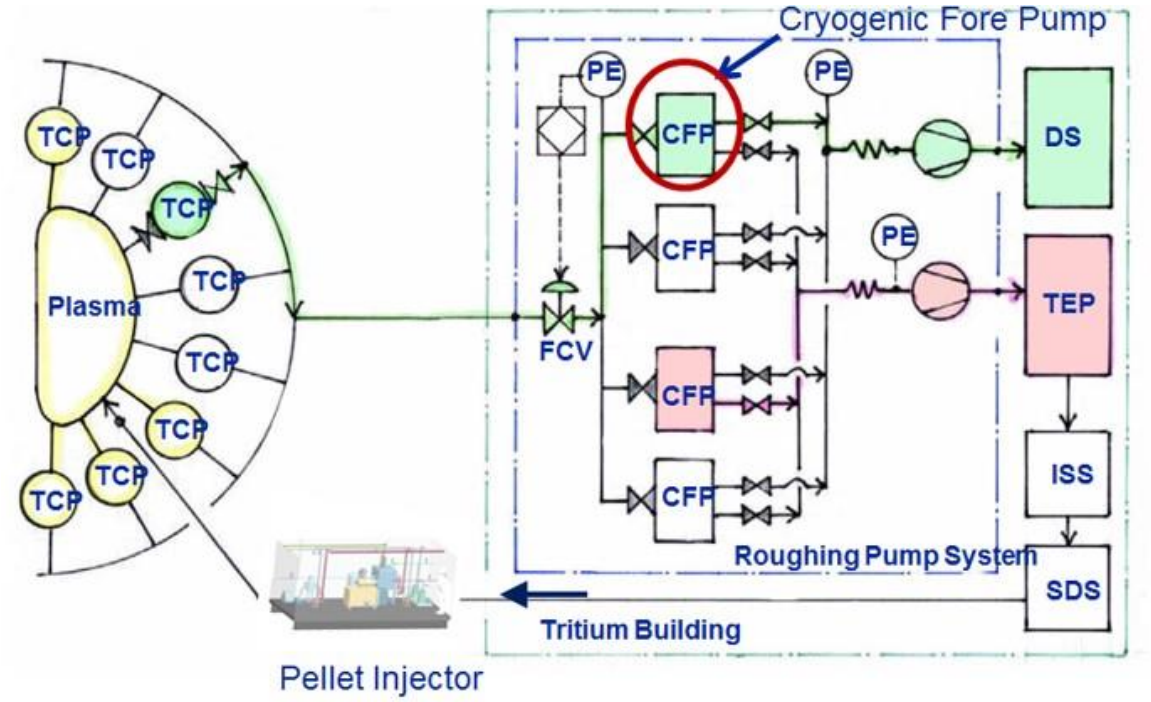

FIGURE 1-5. Simplified ITER fuel cycle flow diagram (courtesy of Oak Ridge National Lab).

FIGURE 1-5 shows the simplified ITER fuel cycle flow diagram. Eight Torus Cryogenic Pumps (TCP) are connected to the tokmak. The TCPs pump trash molecules out

of the plasma by adsorption onto activated charcoal at 4.5 K. Only 4 of them operate at the same time, while the other 4 are under regeneration. During the regeneration of the TCPs, the roughing pump system takes away the exhaust gas from the TCPs. The exhaust gas is comprised of hydrogen isotopes with trace amounts of helium.

The Cryogenic Fore Pumps (CFP) are the first part of the roughing pump system. They are designed to collect the hydrogen isotopes and send them to a tritium reprocessing facility while allowing the trace helium to pass through. Experimental and theoretical investigations have been carried out in order to develop the CFP. At the Oak Ridge National Lab, a prototype CFP has been built and tested (Foster, 2005) (Baylor, et al., 2011) (Robert C. Duckworth, 2011), while efforts at the University of Wisconsin-Madison (Zhang, 2014) have focused on the physical analysis and modeling. The experimental data provide a reference for the theoretical models, and the theoretical work can provide guidance for the future experiments.

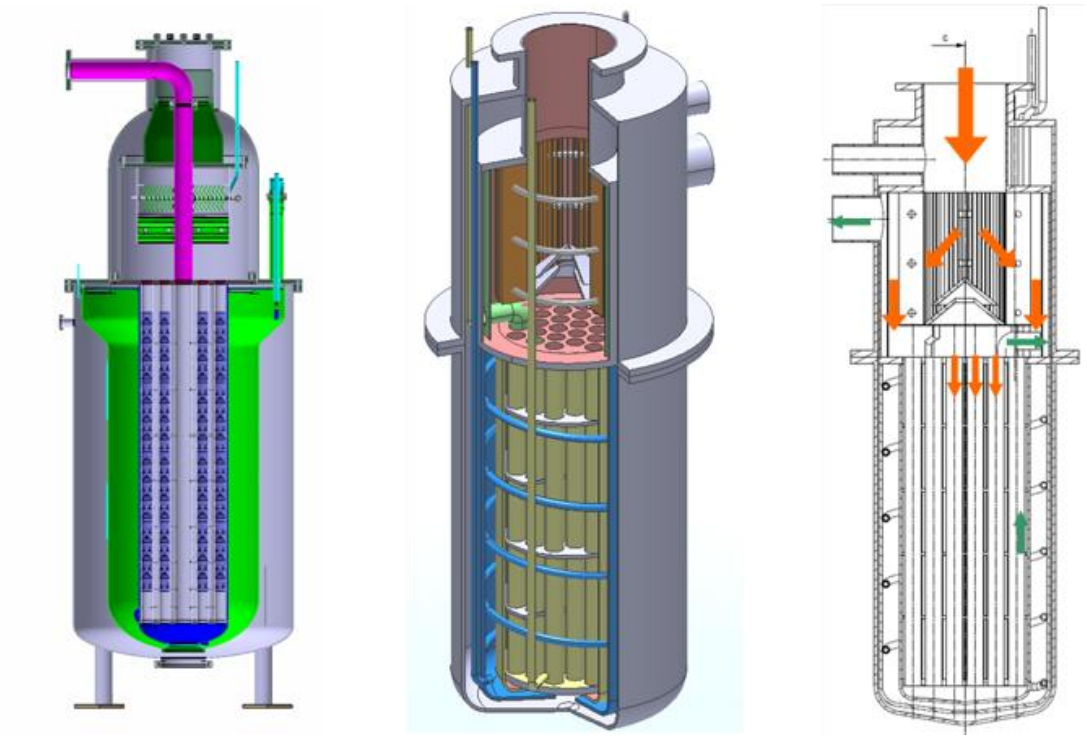

FIGURE 1-6. Initial conceptual design of the cryogenic fore pump (courtesy of Oak Ridge National Lab).

FIGURE 1-6 shows the initial design of the cryogenic fore pump. The prototype being tested at the Oak Ridge National Lab provides a simplified form of the same design.

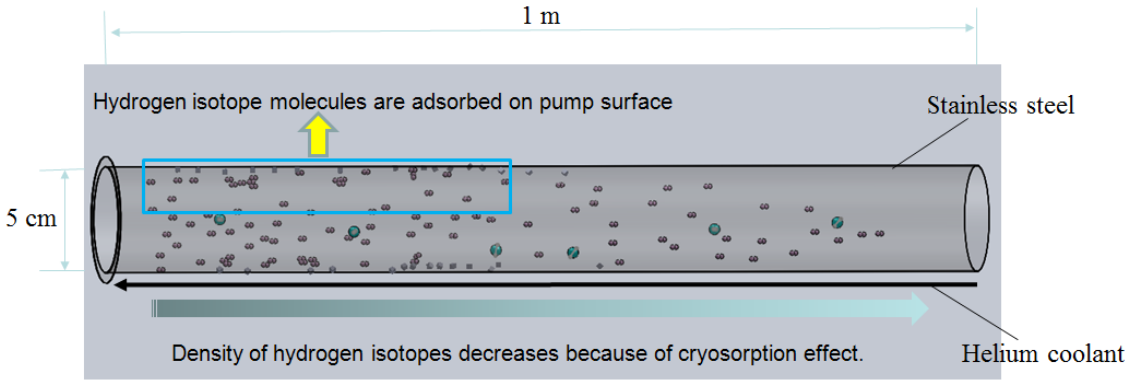

FIGURE 1-7. Cartoon representation of the cryogenic fore pump.

FIGURE 1-7 shows the key operating features of the cryogenic fore pump. The cartoon provides a helpful starting point for the modeling. The cryogenic fore pump is modeled as a tube-in-tube counter-flow heat exchanger that includes adsorption of hydrogen molecules on the inside of the inner tube (pump) surface. The CFP has a length of about 1 m, an inner diameter of 5 cm, and an overall outer diameter of 15.24 cm. Hydrogen gas with trace amounts of helium (about 1 %) flows through the inner tube. A helium coolant (supercritical helium or cold helium gas) flows through the outer annular tube.

Common cryopumps are used to create or maintain a relatively high vacuum, and typically operate in the rarefied gas regime. The pumping process results from a chemical or physical adsorption mechanism that depends on factors such as surface condition and molecule species. As a result, a Monte Carlo method is usually applied to model the physical processes. The ITER cryogenic fore pump differs from common cryopumps in

that it operates in the viscous flow regime and therefore requires a different modeling approach.

1.2.1. Cryogenic adsorption mechanism

Molecules can be trapped on solid surfaces at cryogenic temperatures. For a rarefied gas, the gas-surface interaction is determined mainly by the relationship between individual molecules and the surface. For viscous flow, the dominant interaction is between the bulk flow and its surface boundary. The mechanisms are quite different.

Rarefied gas-surface interactions, generally referred to as gas surface interactions, have been widely studied (Kennard, 1938) (Ruthven, 1984). Once a gas molecule collides with a solid surface, the molecule can have several possible destinies: elastic scattering, accommodation, physical adsorption, molecular chemical adsorption and dissociated chemical adsorption. Elastic scattering means that molecules conserve the translational and internal energy, maintain their momentum parallel to the surface, and retain the same amount of perpendicular momentum but with the opposite direction. Accommodation, also called inelastic scattering, is scattering of molecules with loss of partial energy to the surface; and thermodynamically molecules are scattered away with some temperature between the original molecule temperature and the surface temperature. Physical adsorption is the situation that molecules are trapped in the potential energy well of the gas-surface system, and lose all of their original information, such as thermal velocity. Molecular chemical adsorption and dissociated chemical adsorption both involve forming chemical bonds between the incident molecules and the surface, and as a result, the adsorption energy is orders of magnitude higher than that in physical adsorption. In

molecular chemical adsorption, molecules maintain their chemical form while in dissociated chemical adsorption molecules break internal chemical bonds and the resulting atoms form new chemical bonds with the surface.

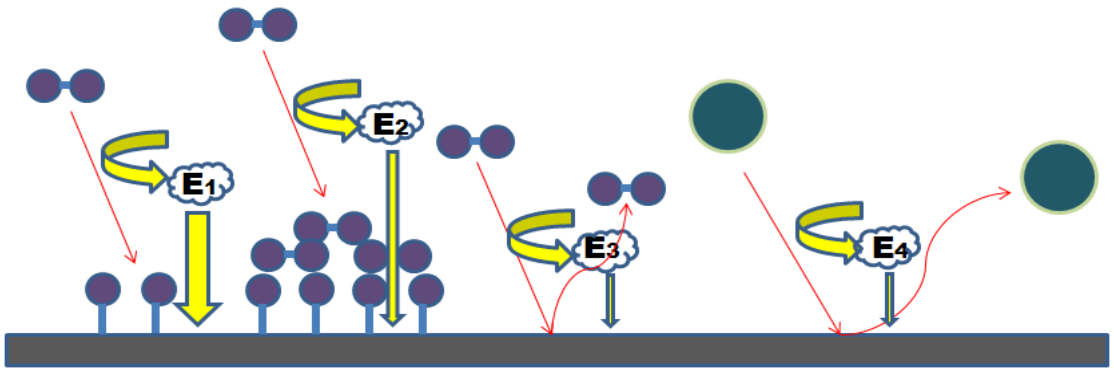

FIGURE 1-8. Illustration of gas-surface interaction and the associated energy deposited.

FIGURE 1-8 shows the energy deposited to the surface in the gas-surface interaction. Modified equations (Govers, 1980) are provided to describe the energies in the figure.

$$E_1 = S(E_{kinetic} + E_{internal} + \Delta E_{adsorption} - k_b T_{surface}) \quad 1)$$

$$E_2 = E_{sublimation} \quad 2)$$

$$E_3, E_4 = \alpha(E_{kinetic} + E_{internal} + \Delta E_{adsorption} - 2k_b T_{surface}) \quad 3)$$

Where S is the sticking coefficient, k_b is Boltzmann's constant, and α is the accommodation coefficient.

Physical adsorption and chemical adsorption are strong gas-surface interactions that can catch molecules on the surface. Both of the adsorptions are kinematic processes, which means that desorption happens at the same time as adsorption. Mean surface lifetime is an averaged time period during which an adsorbed molecule can stay on the surface, and it is a strong function of surface temperature. With a decrease of the surface temperature, the mean surface lifetime increases significantly. If the surface temperature is low enough, any kind of molecules can be trapped on the surface. As a result, cryogenic adsorption can be used to provide a vacuum (Lafferty, 1998) (O'Hanlon, 2004). The adsorption process is also affected by many factors, such as impingement rates, sticking coefficients, and adsorption energy.

Among all the molecules, hydrogen receives the most research attention in many disciplines, such as physics and chemistry, and the adsorption of hydrogen molecules is extensively studied for both metal surfaces and composite-material surfaces. Handy experimental data regarding the adsorption of hydrogen are available (Nordlander, 1984), and adsorption energy for hydrogen molecules on many materials can be accurately computed. At cryogenic temperatures, hydrogen molecules are adsorbed on a metal surface by chemical adsorption. Chemical adsorption is limited by the availability of adsorption sites.

Unlike hydrogen molecules, helium molecules are very hard to be adsorbed. If the surface temperature is not low enough which is true in the cryogenic fore pump case, helium molecules are not adsorbed on the surface. Instead helium molecules interact with a surface through accommodation, and the energy deposited to the surface is orders of magnitude smaller than the adsorption energy.

In the viscous flow regime, large amounts of molecules quickly occupy all available adsorption sites and thus chemical adsorption and physical adsorption effects are not important in the whole picture. Instead, the bulk flow's interaction with the surface is important and determines the physical properties near the surface, such as the temperature and velocity. The adsorption of molecules is accompanied with a phase change from vapor to liquid or solid, depending on the conditions. The adsorption rate is not determined by the molecular (thermal) velocity but by the gradient in density, temperature, and pressure. The adsorption energy is the sum of the enthalpy difference between the molecules at the mean flow temperature and those at the phase equilibrium temperature, and the phase change energy, which depends on the phase equilibrium temperature.

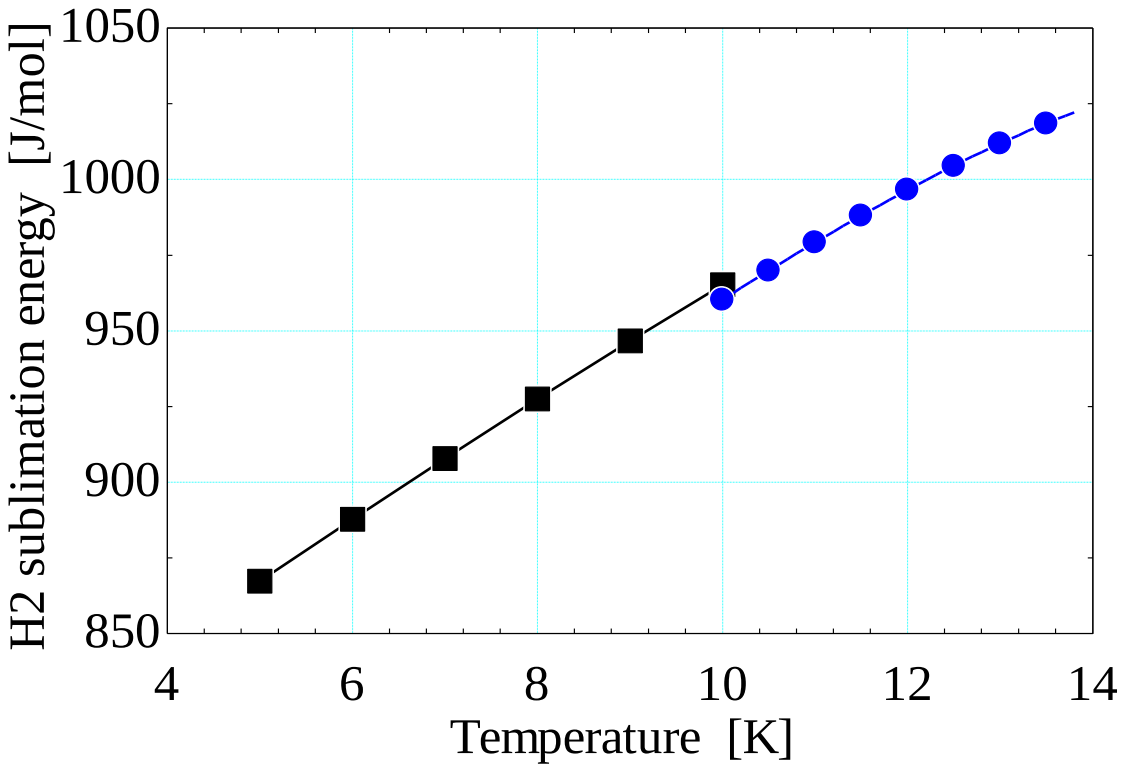

FIGURE 1-9. Hydrogen sublimation energy as a function of temperature

FIGURE 1-9 shows hydrogen sublimation energy as a function of temperature, which is plotted from the experimental data (Ahlers, 1963) (Mullins, Ziegler, & Kirk, 1961) (Roder, The thermodynamic properties of slush hydrogen and oxygen, 1977) (Roder, Childs, McCarty, & Angerhofer, 1973) (McCarty, 1981).

1.2.2. Cryogenic pumps and models

Cryogenic pumps, also called cryogenic adsorption pumps or cryopumps, are the devices that are used to capture gas molecules on the pump surface (Hands, 1976) (Bentley, 1980). Usually cryogenic pumps are designed to work in the molecular regime, to create and maintain a vacuum, and the mechanism of cryopumping is adsorption of molecules on

the pump surface (gas–surface interaction). However, in the situation where the gas flow is in the viscous flow regime, the cryogenic pumps will have different functions, such as to collect molecules, and have different mechanism of cryopumping.

Cryogenic pumping speed and energy load are two important characteristics of a cryogenic pump. For a cryogenic pump working in the molecular flow regime, the pumping speed depends on the impingement rate of molecules onto the pump surface and the sticking coefficient. The impingement rate sets the limit for cryogenic pumping. By substituting ideal gas law for pressure, the impingement rate can be expressed as the following. The equation indicates that the impingement rate is determined by the target molecule gas itself. Higher density and higher temperature of the gas produce a higher impingement rate.

$$I = \frac{\rho R\sqrt{T}}{\sqrt{2\pi m k_b}} \qquad 4)$$

Here R is the universal gas constant, and m is the mass of the molecule species.

In contrast, for cryogenic pumps working in the viscous flow regime, the pumping speed is determined by both the properties of the bulk flow and the conditions at the pump surface.

The energy load for these two kinds of cryogenic pumps is quite different as well. For cryopumps working in the rarefied gas regime, the energy load is dominantly

determined by bonding energy. For cryopumps working in the viscous flow regime, the energy load is mainly determined by the phase change energy.

As a result, modeling of a cryogenic pump can generally be placed into two categories: the molecular flow regime or the viscous flow regime.

A Monte Carlo technique is usually adopted for modeling molecular-flow-regime cryogenic pumps. In ITER, the torus cryogenic pumps, which are used to provide and maintain vacuum and thus work in the rarefied gas regime, are modeled using a Monte Carlo technique (Luo, 2011) (S Varoutis, 2011) (Stylianos Varoutis, 2012).

Methods in classical mechanical engineering (Sanford Klein, 2011) (Gregory Nellis, 2008) and chemical engineering (RB Bird, 2007) (Deen, 1998) are suitable for modeling cryogenic pumps working in the viscous flow regime. Various modeling efforts have been carried out for similar problems (C. Tzemos, 1986) (P Dwivedi, 2004) (Nastaj, 2006) (K. Munakataa, 2007). These models are generally one dimensional, rely on the existing mass diffusivities that are developed by others (Reid, Prausnitz, & Poling, 1987) (Edwards, 1968) (Wakao N. T., 1978) (Schork, 1988) (J. M. COULSON, 1990) (Yang, 1997), at times do not include a momentum balance, and do not consider the thermal and kinetic properties' dependence on temperature and pressure.

Mass diffusivity varies significantly in different conditions and is modeled for different driving forces. For example, there is the Chapmann-Enskog correlation for isothermal and isobaric mass diffusivity (Reid, Prausnitz, & Poling, 1987). Thermal diffusion of mass is also presented (Furry, 1939). Besides density and thermally driven diffusion, chemical potential driven diffusion has also been discussed (Yang, 1997). The

above numerical models are limited by their ability to solve complex coupled non-linear equations.

In modeling of the cryogenic fore pump, numerical methods are widely used, and have many advantages over analytical methods, such as their ability to solve real-world problems. However, numerical methods present disadvantages as well, such as complexity of programming, cost of calculation, and numerical error. The downsides become significant once the problem to be solved becomes complicated.

Numerical methods are extensively used in solving problems in fluid mechanics and heat transfer (Ferziger, 1996) (Tannehill, Anderson, & Pletcher, 1997) (Gregory Nellis, 2008) (Myers, 1998). With the development of software, such as the Engineering Equation Solver (EES), the techniques of solving non-linear equations have been improved.

Chapter 2 Experiment

The prototype of the cryogenic fore pump has been built and tested at the Oak Ridge National Lab. The experimental setup and flow conditions set the frame for the numerical analysis and modeling.

The analysis of the raw experimental data boosts the development of the numerical models. Note significantly, that the experimental data set I (2.2.1. Experimental data set I) is explained by the transient model (Chapter 3).

2.1. Scale analysis

In this section, the geometry of the pump test and the important associated time scales are presented. These provide a reference frame for the space-and-time scales addressed in the analysis and modeling.

2.1.1. Experiment setup and geometry scaling

The prototype of the ITER cryogenic fore pump being tested at the Oak Ridge National Lab is a tube-in-tube double pipe heat exchanger. The hydrogen gas flows in the inner tube, while the helium coolant counter flows in the outer annular tube.

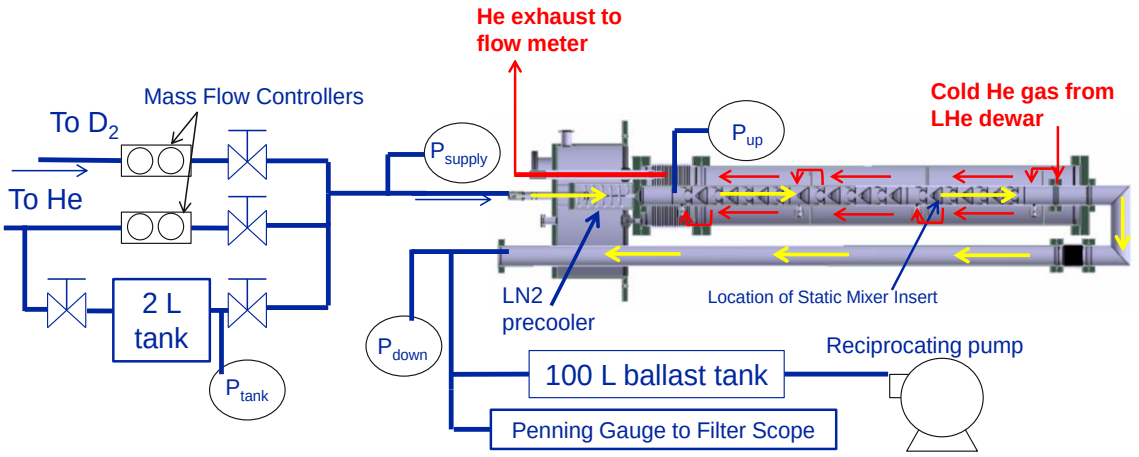

FIGURE 2-1. Experiment setting for testing the prototype CVC single tube cryogenic pump (courtesy of the colleague at Oak Ridge National Lab).

FIGURE 2-1 shows the experiment setup, including the prototype of the cryogenic fore pump, mass flow controllers, measurement systems, and roughing pump. Pure hydrogen gas, or a mixture of hydrogen isotopes and helium gas, flows through the inner tube while helium coolant flows through the outer annular tube.

The cryopump (tube) is 1.07 m long. Including the additional 0.085 m long adaptor plate, the entire cooling length is about 1.16 m. The tube-in-tube cryopump has an inner diameter of 5 cm and an overall outer diameter of 15.24 cm.

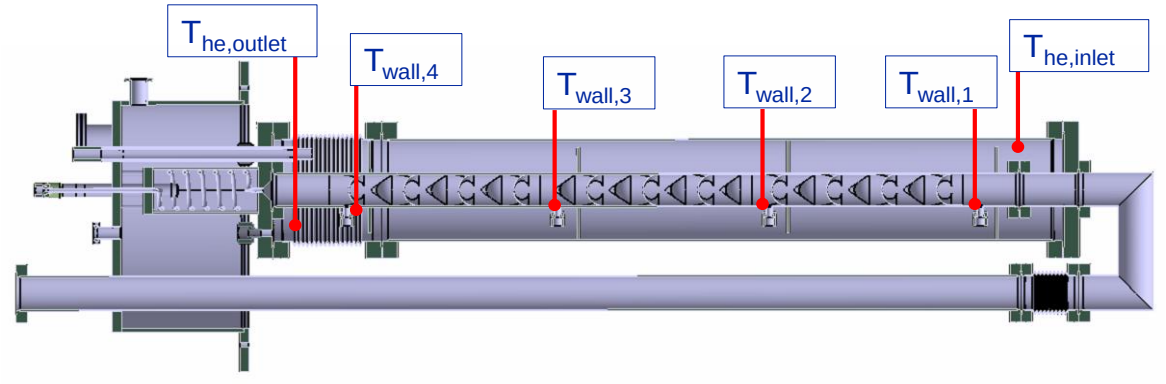

FIGURE 2-2. Location of thermometers on the testing single tube cryogenic pump (courtesy of the colleague at Oak Ridge National Lab).

As shown in **FIGURE 2-2**, 4 silicon diode type thermometers are mounted on the outer surface of the cryopump tube to measure the tube wall temperature. To avoid communication with the helium coolant flow stream, some insulation is added. As measured from the top of the tube (hydrogen flow entrance end), the first thermometer (measuring $T_{wall,4}$) is located 10.2 cm down the tube length. The three subsequent thermometers are mounted 30.5 cm apart along the tube length, and they measure $T_{wall,3}$, $T_{wall,2}$, and $T_{wall,1}$ respectively. Two silicon diode type thermometers are used to measure the inlet and outlet temperatures of the helium coolant. The thermometer measuring the helium coolant inlet temperature is mounted on a Teflon screw secured to a baffle and located about 7.5 cm axially beyond the $T_{wall,1}$ thermometer near the bottom of the tube (106.7 cm from the top of the tube) and radially about 5 cm from the wall. The thermometer measuring the helium coolant outlet temperature is mounted on a Teflon rod about 10.2 cm

from the top of the tube and secured with Teflon nuts approximately 2.5 cm radially inside the outer tube wall.

Two pressure gauges are used to measure upstream and downstream hydrogen flow pressures. The pressure gauges are the MKS 722B Baratron type Capacitance Manometers. The model numbers are 722B11TCD2FA and 722B13TCD2FA for the upstream and downstream (10 Torr) locations respectively, and these provide absolute pressure measurements. The upstream pressure gauge is mounted with a capillary tube located 7 cm from the top of the tube, while the downstream pressure gauge is mounted on the exit of the entire setup. An axial distance of approximately 2.16 m separates the two pressure transducers, where the pipe extending from the bottom of the tube to the downstream pressure gauge location has an inner diameter of approximately 5 cm. When the downstream pressure is unreported, the experimenters have assumed that pressure drop through the piping is minimal because of its large diameter. Additionally, pressure gauges are used to measure the pressure of the hydrogen gas supply and the ballast tank. The gauge for the hydrogen gas supply is mounted downstream of the flow controllers but before the precooler.

Model 1480A MKS Instruments flow controllers are used as mass controllers. For hydrogen flow, the controller is a 0-10000 sccm controller (model number 1480A00714CR1BM12). For helium flow, the controller is a 0-1000 sccm controller (model number of 1480A00713CR1BM12). Both of the controllers are calibrated for hydrogen flow, and the helium flow controller, when used, incorporates a correction factor

of 1.44. The controllers have a 0-5 V control signal and the control signal is adjusted to set the incoming flow rates.

The u-tube at the bottom of the test rig has an outer diameter of 5.08 cm with a wall thickness of 0.9 mm. Each leg is nominally 10 cm long and the connecting piece is approximately 15 cm long. The buffer volume of the ballast tank is approximately 30 inches long with a 40.6 cm diameter. The wall thickness is nominally 3 mm.

2.1.2. Relevant scales and order of magnitude

When the helium coolant flow rate is about 0.5 g/s, the resulting velocity is about 3 mm/s. If the tube length is divided to 50 nodes, the time for the helium coolant to travel from one node to its adjacent neighbor is about 8 seconds.

When the inlet hydrogen flow is about 0.001 g/s, the inlet velocity is about 4 m/s. The velocity decreases quickly as the gas is cooled.

For the inlet condition of hydrogen flow at 80 K and 100 Pa, the speed of sound is 733.1 m/s and it thus takes about 0.001 s for a (viscous) pressure signal to travel through a 1 m cryogenic fore pump. The diffusion coefficient is about 0.01335 m^2/s, and it thus takes about 0.01 s for molecules to diffuse from the centerline to the surface of a tube with a 5 cm diameter.

At 80 K, the thermal velocity of hydrogen molecules is about 916.6 m/s. If the cryogenic fore pump is maintained at 5 K, the vapor pressure of hydrogen is 0.00476 Pa. Hydrogen molecules traveling at their thermal velocity thus take about 0.0005 seconds to form 5 adsorption layers on the surface of the cryogenic pump.

At 80 K and 100 Pa, the mean free path of hydrogen and helium are about 0.0329 mm and 0.0523 mm respectively. Both are much smaller than the 50 mm pump diameter. When the flow pressure approaches 0.066 Pa, the mean free path becomes comparable to the pump diameter. Note that the saturation temperature of hydrogen at 0.00476 Pa is approximately 5 K.

The diffusion coefficient for hydrogen gas is about 0.0004 m^2/s to 0.03 m^2/s, and it depends significantly on temperature.

2.2. Analysis of experimental data

The prototype cryogenic fore pump has been tested at the Oak Ridge National Lab, and the raw experimental data was generously rendered to the author (private communication from Robert C. Duckworth). The access to the raw date has enabled a comparison and verification of the transient model results.

Experimental data is not available to compare with two additional numerical models, the steady-state model and the hemisphere model. Nevertheless, although they cannot be directly verified by experimental data, they are built on the investigation of the available experimental data.

2.2.1. Experimental data set I

The first set of the experimental data is used to compare with the transient model. In this case pure hydrogen gas is used to test the prototype cryogenic fore pump. Three separated time blocks make up the first set of data, and before each of them, the pump has been regenerated, that is warmed sufficiently to remove all condensed or de-sublimated gases.

The following three figures (**FIGURE 2-3**, **FIGURE 2-4**, and **FIGURE 2-5**) display the data for three important variables over the complete experimental time range. **FIGURE 2-3** shows the time dependence of the inlet helium coolant temperature. **FIGURE 2-4** shows the time dependence of the inlet hydrogen gas mass flow rate, that is well controlled by the mass flow controller. **FIGURE 2-5** shows the time dependence of the inlet helium coolant mass flow rate, and it is also well controlled. Although this parameter is very important for the cryopumping performance, it is not well controlled.

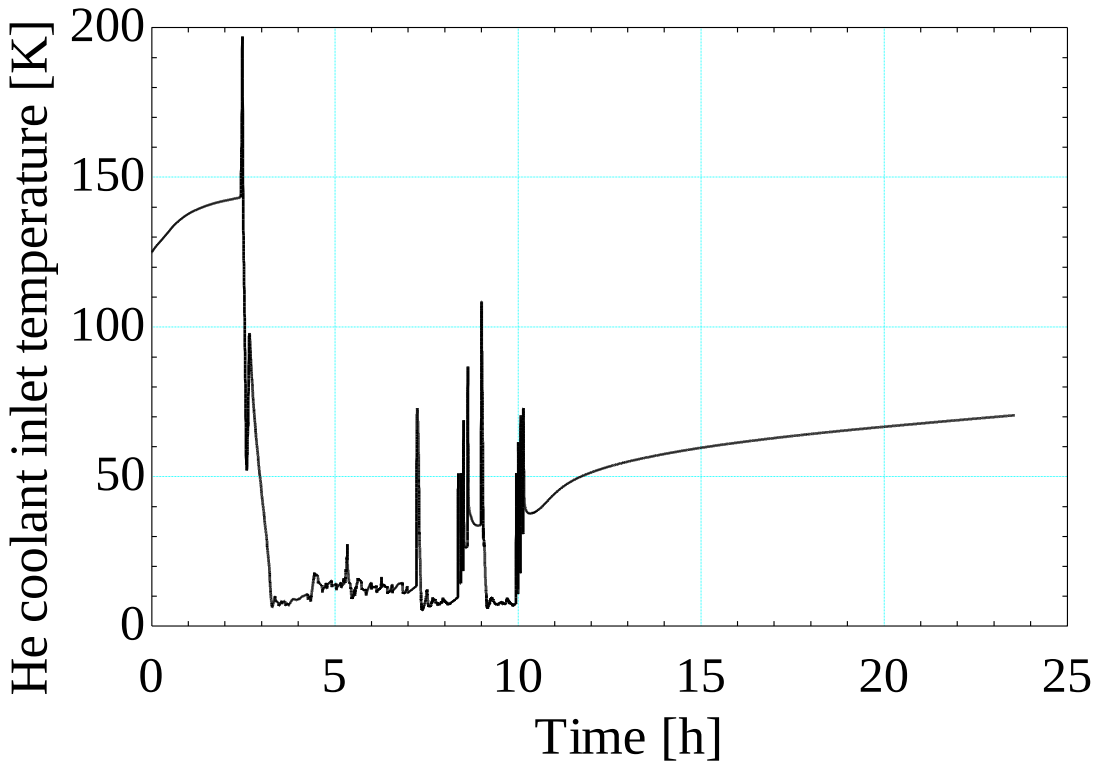

FIGURE 2-3. Inlet helium coolant temperature as a function of time.

FIGURE 2-3 shows the time dependence of the inlet helium coolant temperature. Three tests are the blocks that are between the 5.5 and 7 hour mark, between the 7.95 and 8.15 hour mark, and between the 9.68 and 9.88 hour mark respectively. The inlet helium coolant temperature is raised above 50 K before each test to regenerate the pump. The inlet helium coolant is supplied at different temperatures for different tests. Note that between the 5.5 and 7 hour mark, the helium temperature is generally above 12 K. Between the 7.5 and 8.5 hour marks, the temperature varies between 6 K and 9 K. Between the 9 and 10 hour mark, the helium temperature varies between 7 K and 10 K. Even for the same test, the variation in the temperature is noticeable. And as said before, that variation significantly affects the pumping performance.

Note significantly, that the vapor pressure of hydrogen near the wall is determined by the pump wall temperature, and that temperature is dominantly determined by the inlet helium temperature. The vapor pressure of the hydrogen near the wall must be smaller than the hydrogen gas pressure in the radial center of the tube in order to generate adsorption. At 12 K, the vapor pressure of hydrogen is about 2000 Pa. The pressure of the hydrogen gas at its inlet to the pump does not exceed 100 Pa. As a result, it is not necessary to investigate the data whenever the inlet helium coolant temperature that is greater than 12 K, since there is definitely no adsorption at that temperature.

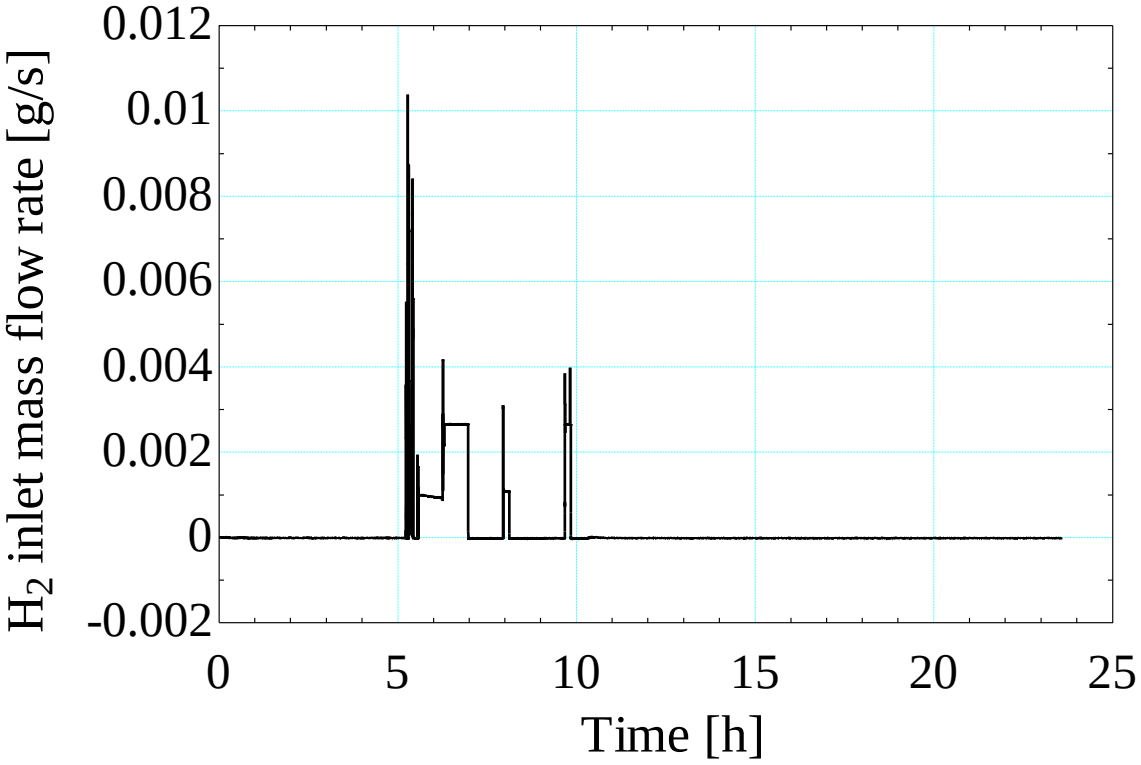

FIGURE 2-4. Inlet hydrogen gas mass rate as a function of time.

FIGURE 2-4 shows the time dependence of the inlet hydrogen gas mass flow rate. The region between 5 hour and 10 hours displays peaks at approximately 5, 8, and 9.5 hours that correspond to the beginning of the three separate time blocks. Values greater than 0.004 g/s are noise.

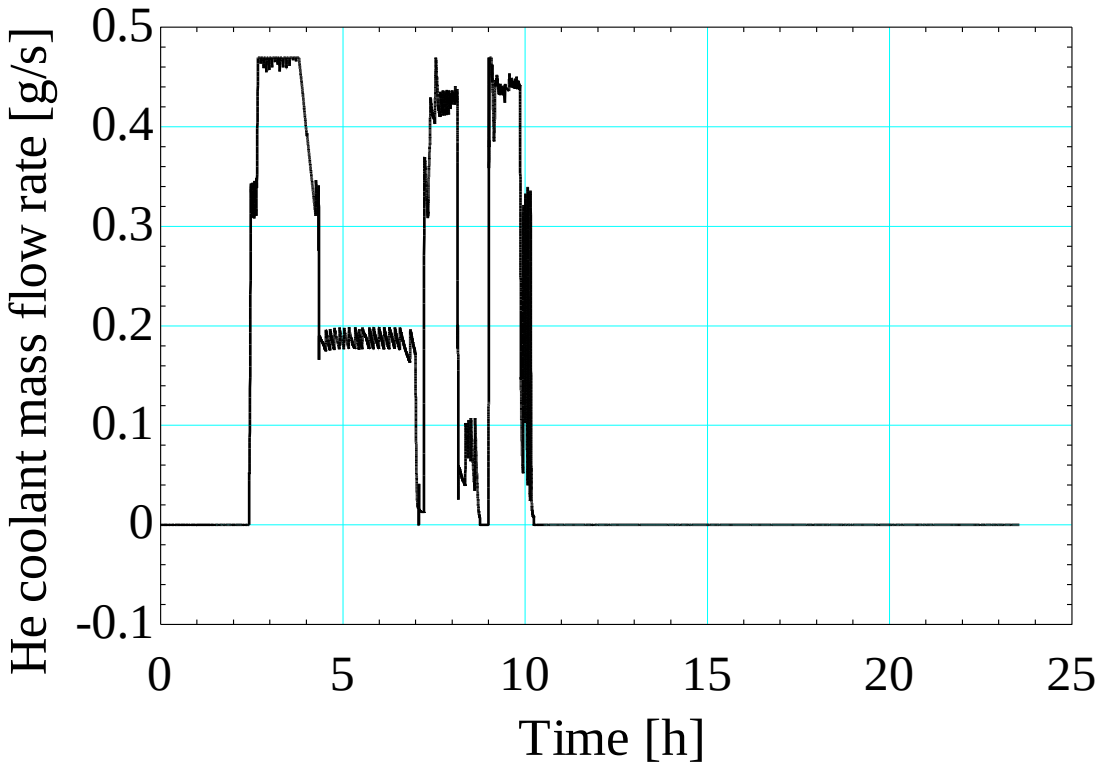

FIGURE 2-5. Inlet helium coolant mass flow rate as a function of time.

FIGURE 2-5 shows the time dependence of the inlet helium coolant mass flow rate. Compared with **FIGURE 2-4**, there are several observations. First, the helium coolant mass flow rate varies with time. However, it is almost constant for each of the 3 independent tests. Note that between the 5.5 and 7 hour mark, the helium mass flow rate is about 0.2 g/s. Between the 7.5 and 8.5 hour marks, the helium mass flow rate is about 0.45 g/s. Between the 9 and 10 hour mark, the helium mass flow rate is about 0.45 g/s. Secondly, the helium coolant is introduced into the pump before the hydrogen gas. And that is to precool the pump before the tests.

Based on these considerations, the following figures only display the experimental data in the meaningful region.

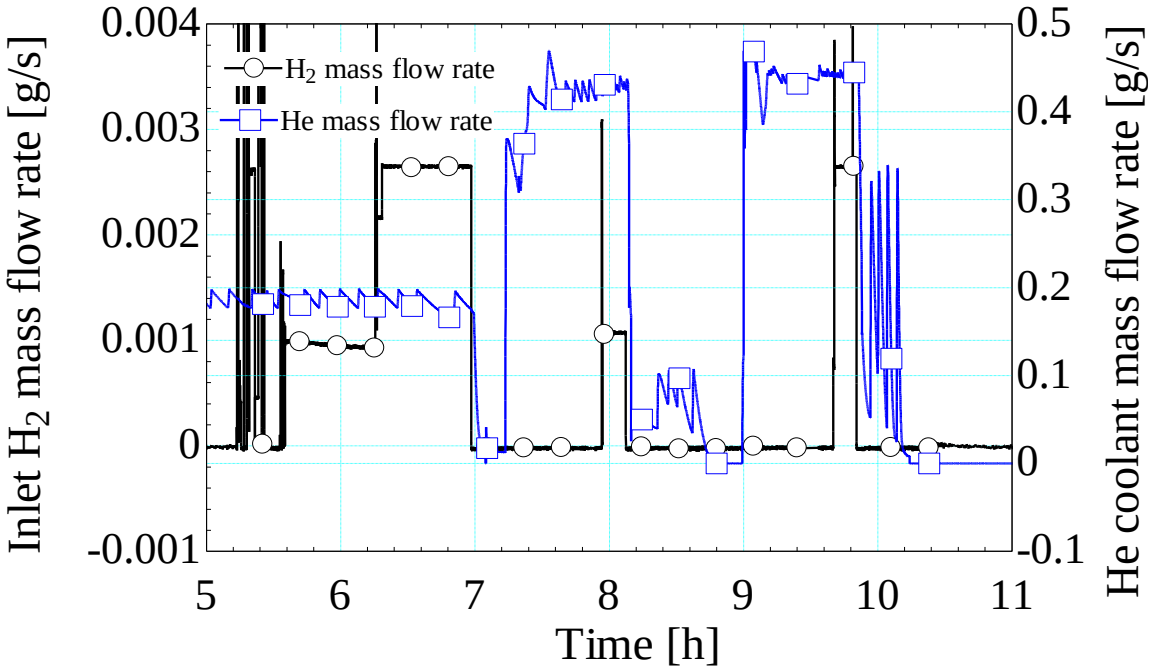

FIGURE 2-6. Inlet hydrogen mass flow rate and inlet helium coolant mass flow rate as a function of time.

FIGURE 2-6 shows the time dependence of the inlet hydrogen mass flow rate and the inlet helium coolant mass flow rate. The two mass flow rates are controlled nearly as constants. It is clear that precooling is provided by the helium coolant. The helium mass flow rate is different for the 3 tests, presumably to adjust the cooling power. However, compared to the mass flow rate, the inlet helium temperature is a more important factor that determines the cooling power.

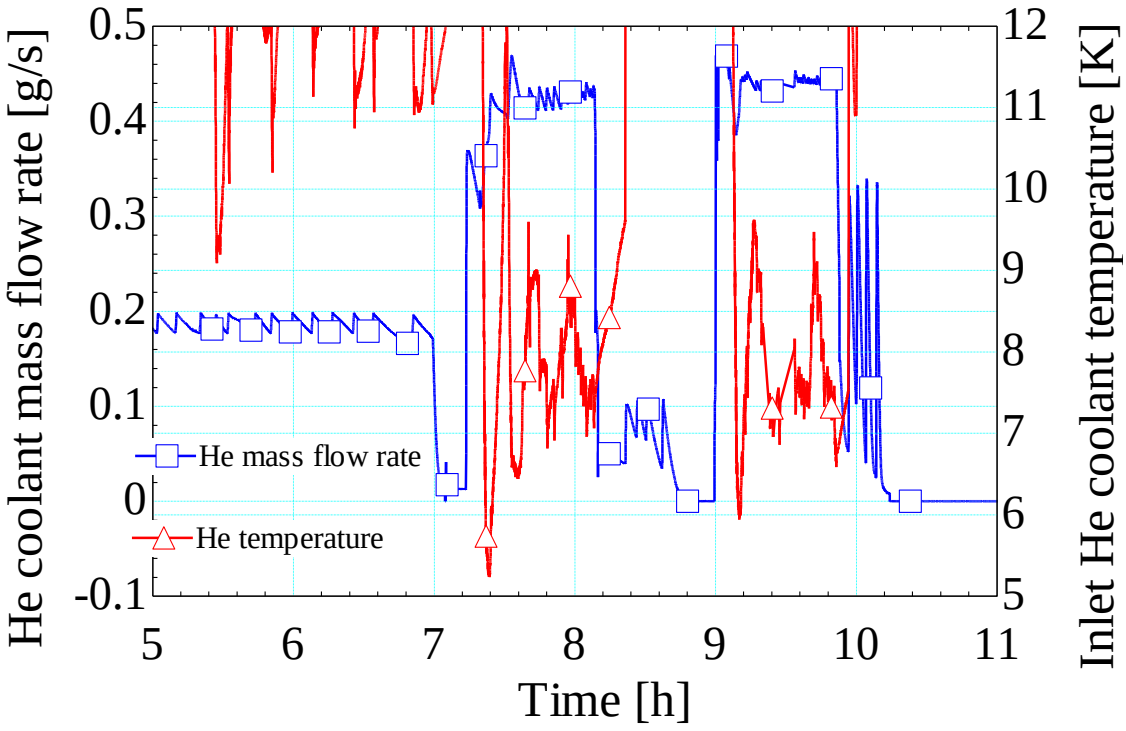

FIGURE 2-7. Inlet helium mass flow rate and inlet helium coolant temperature as a function of time.

FIGURE 2-7 shows the time dependence of the inlet helium coolant mass flow rate and the inlet helium coolant temperature. As mentioned above, the inlet helium coolant temperature has a significant influence on the cryopump performance because it determines the vapor pressure of the hydrogen at the wall. In addition, the dependence of the hydrogen vapor pressure on the temperature is very strong. For example, in the temperature range reflected in **FIGURE 2-7**, a 1-K change in the temperature leads to orders of magnitude change of the vapor pressure. The range of helium inlet temperatures spanned by **FIGURE 2-7** yields all the interesting behaviors of the hydrogen cryogenic pump.

The transient model has been developed in order to explain the observed pumping behavior. It uses the experimental measurement of the inlet helium coolant temperature as one input parameter.

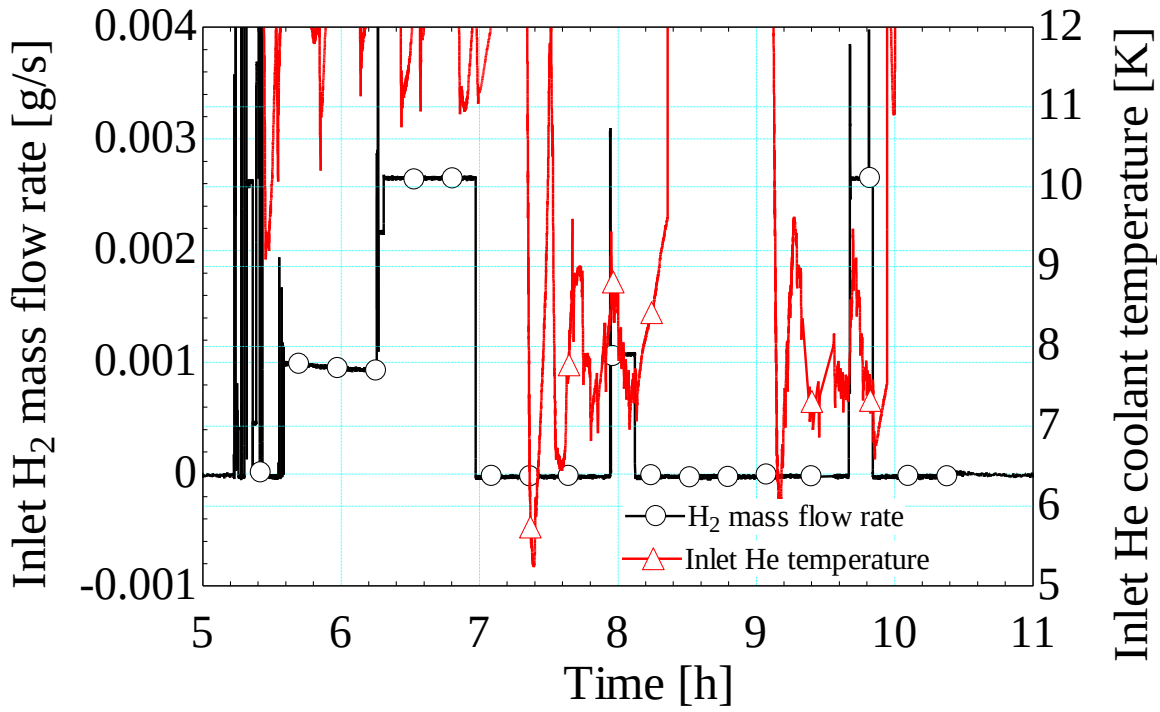

FIGURE 2-8. Inlet hydrogen mass flow rate and inlet helium coolant temperature as a function of time.

FIGURE 2-8 shows the time dependence of the inlet hydrogen mass flow rate and the inlet helium coolant temperature. The hydrogen vapor pressure is about 2000 Pa at 12 K. The inlet hydrogen gas pressure is not higher than 100 Pa in the experiments. As a result, the helium coolant in the first test (between the time of 5 hour to the time of 7 hour) provides no cryopumping power.

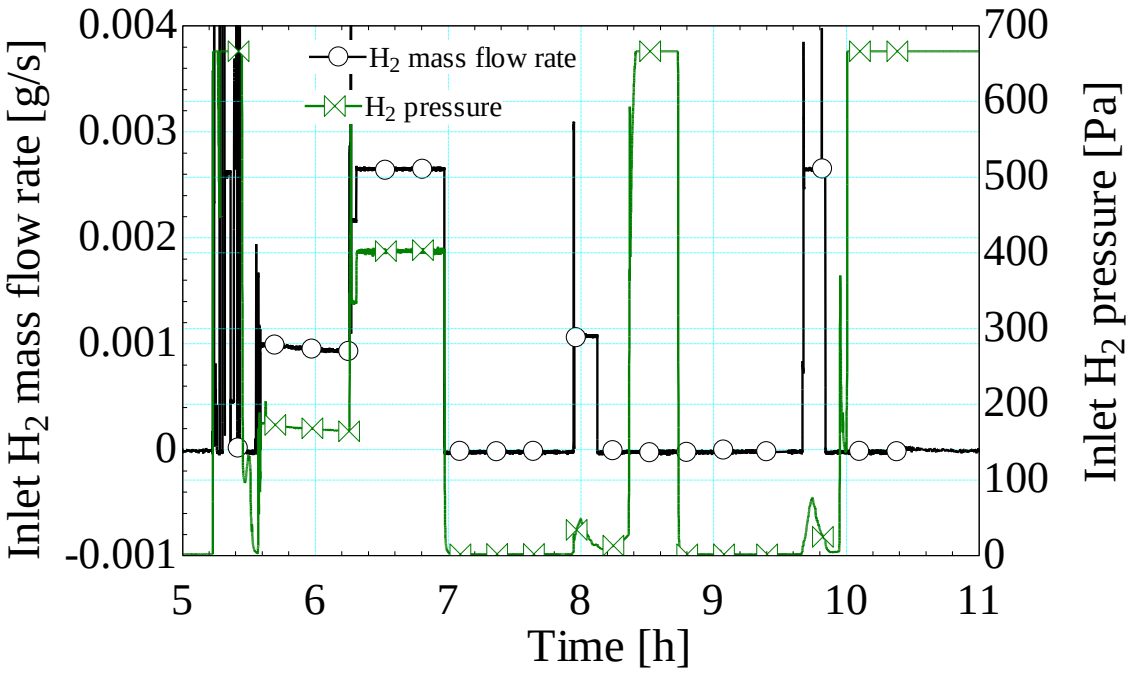

FIGURE 2-9. Inlet hydrogen mass flow rate and inlet hydrogen gas pressure as a function of time.

FIGURE 2-9 shows the time dependence of the inlet hydrogen mass flow rate and the inlet hydrogen gas pressure. The data is cut off by the pressure meter limit at 700 Pa.

In the first test (between the time of 5 hour to the time of 7 hour), there is no adsorption. Notice that the inlet hydrogen pressure stays constant, and there is no pressure peak in the regeneration process after the test (see the helium temperature spike near 7 hours in **FIGURE 2-3**).

In the second test (around the time of 8 hour) and the third test (near the time of 10 hour) hydrogen molecules are adsorbed by the pump. This feature is reflected by the fact that the inlet hydrogen pressure varies with time during the test, and that there exist pressure

peaks in the regeneration process after the tests (hydrogen pressures approaching 700 Pa). Note in particular how large the pressure rise is compared with the much smaller inlet hydrogen pressure in the second and third tests.

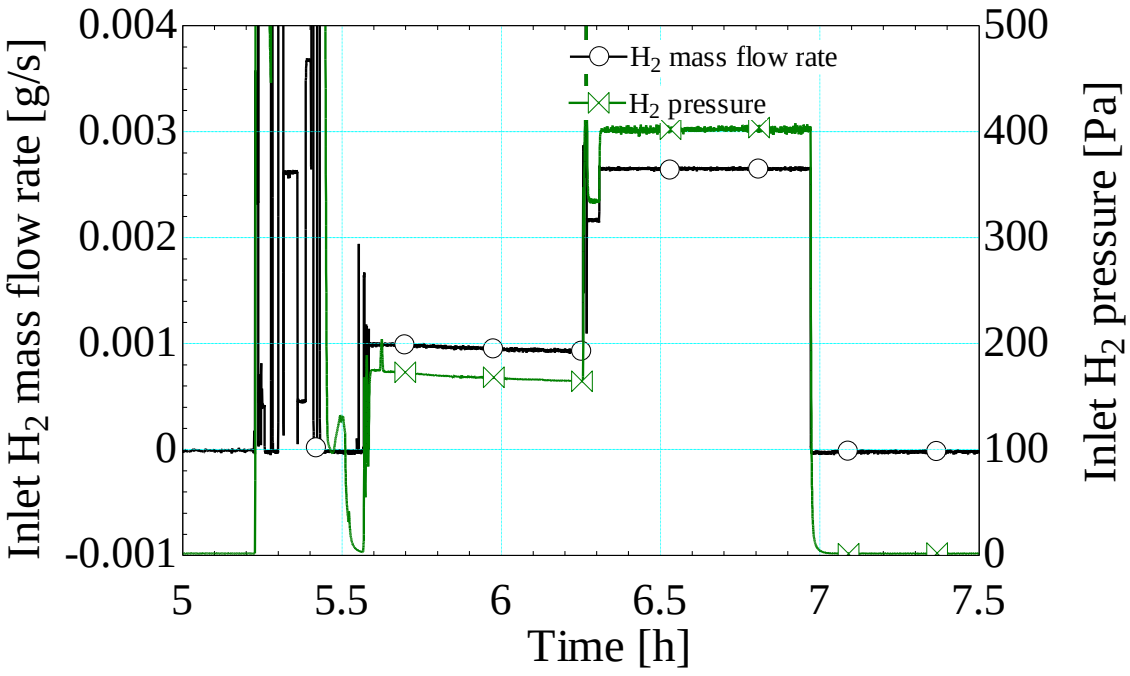

FIGURE 2-10. 1st test: Inlet hydrogen mass flow rate and inlet hydrogen gas pressure as a function of time.

FIGURE 2-10 shows the time dependence of the inlet hydrogen mass flow rate and the inlet hydrogen gas pressure for the test 1.

In the viscous flow regime, the information of the pressure travels at the speed of sound. If adsorption occurs, the inlet hydrogen pressure is affected immediately. Saturation conditions occur only if the inlet hydrogen pressure approaches the hydrogen vapor

pressure that is determined by the pump wall temperature. As a result, the inlet hydrogen pressure is also an important factor determining whether adsorption occurs or not.

The constant inlet hydrogen pressure reflects the fact that there is no adsorption in this test. Friction at the pump wall is the only mechanism reducing the hydrogen pressure, and this effect is very small for the hydrogen gas.

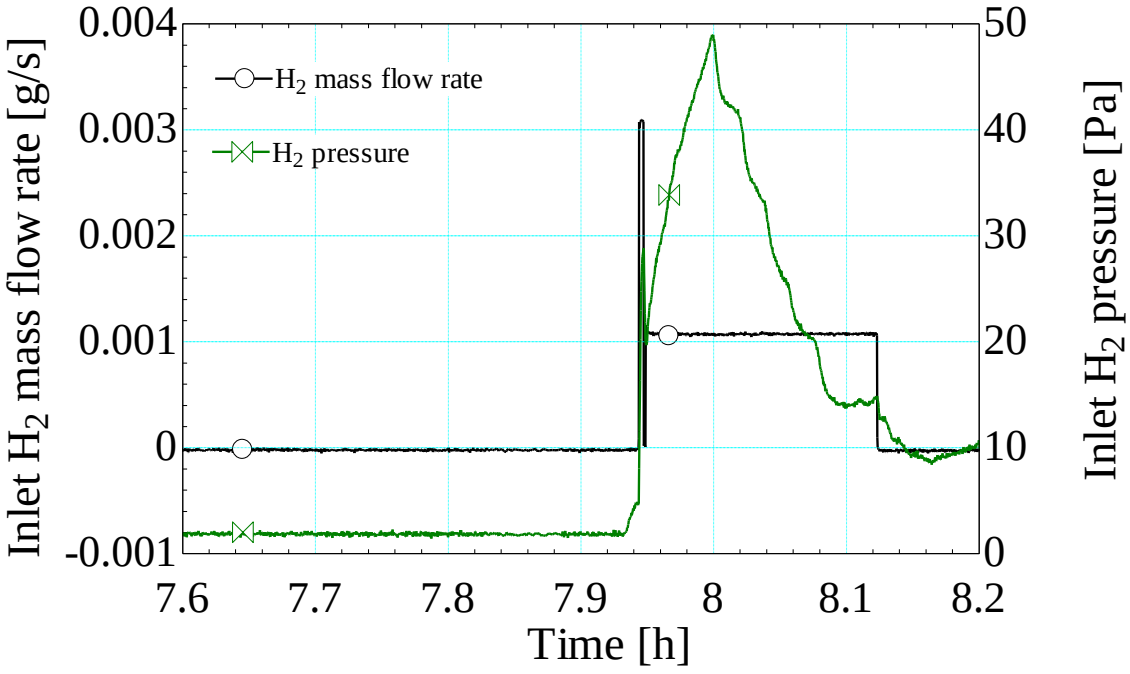

FIGURE 2-11. 2nd test: Inlet hydrogen mass flow rate and inlet hydrogen gas pressure as a function of time.

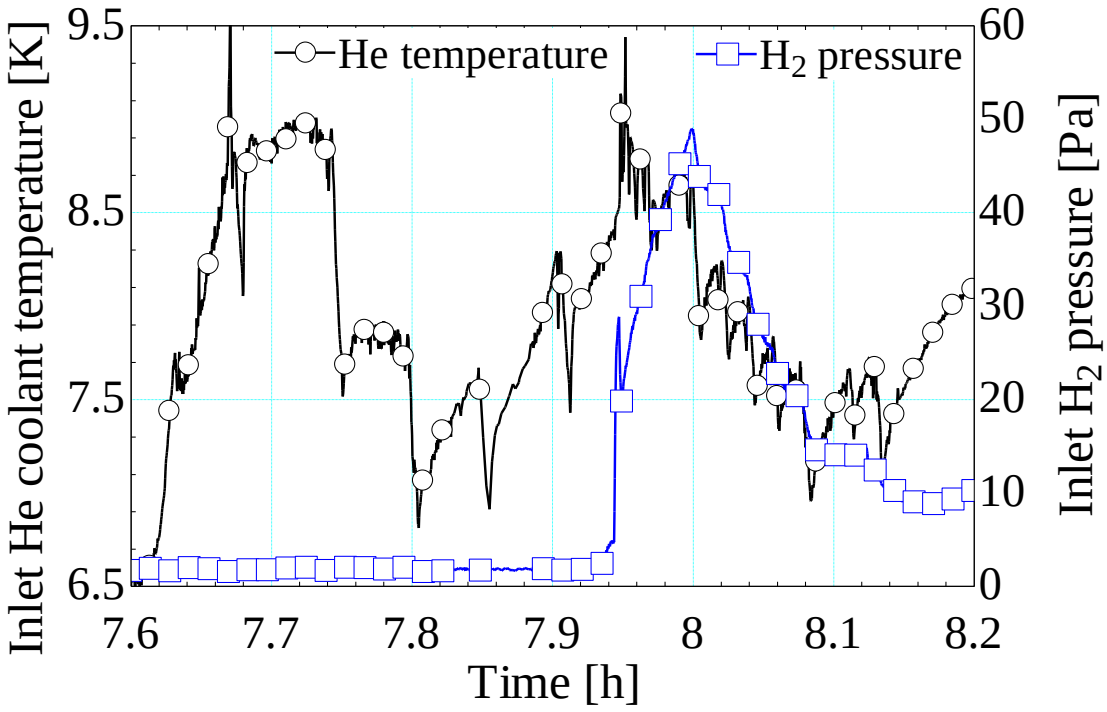

FIGURE 2-12. 2nd test: Inlet helium coolant temperature and inlet hydrogen gas pressure as a function of time.

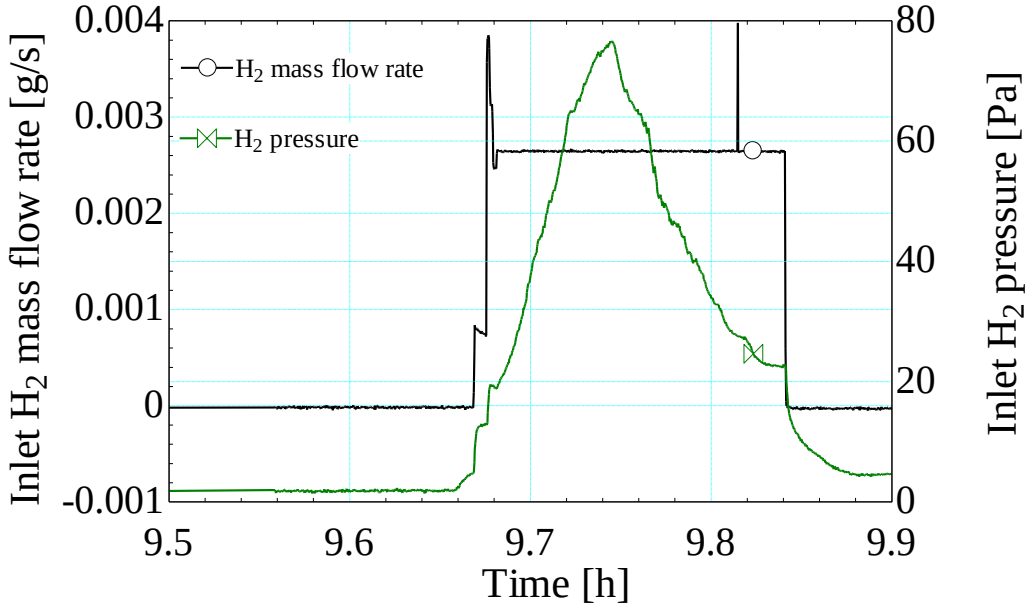

FIGURE 2-13. 3rd test: Inlet hydrogen mass flow rate and inlet hydrogen gas pressure as a function of time.

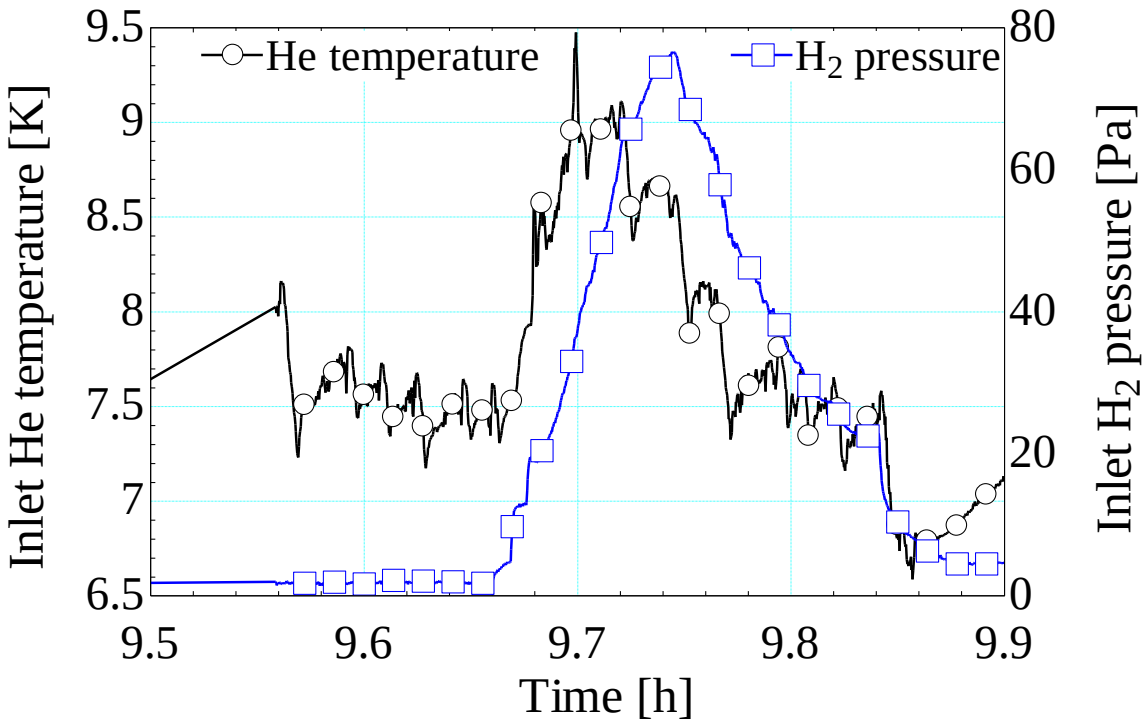

FIGURE 2-14. 3nd test: Inlet helium coolant temperature and inlet hydrogen gas pressure as a function of time.

FIGURE 2-11 and **FIGURE 2-13** show the time dependence of the inlet hydrogen mass flow rate and the inlet hydrogen gas pressure. Compared to **FIGURE 2-10** the pressures in the second and third tests are much smaller, and they vary with time. And that is a clear indicator that the adsorption of the hydrogen molecules occur in the latter two tests.

FIGURE 2-12 and **FIGURE 2-14** show the time dependence of the inlet helium coolant temperature and the inlet hydrogen pressure. The pressure follows the same trend as the temperature.

The following 3 figures (**FIGURE 2-15**, **FIGURE 2-16**, and **FIGURE 2-17**) show and compare the temperature measurements in the 3 tests. Three of the four thermometers mounted on the pump wall provided useful temperature measurements. The thermometers are mounted on the outer surface of the inner tube, and thus they actually measure an intermediate temperature between that of the pump wall and that of the helium coolant. $T_{wall,4}$ is the temperature measurement reported by the thermometer close to the pump entrance (the hydrogen gas inlet and the helium coolant outlet). Two additional thermometers are used to measure the inlet and outlet helium coolant temperatures.

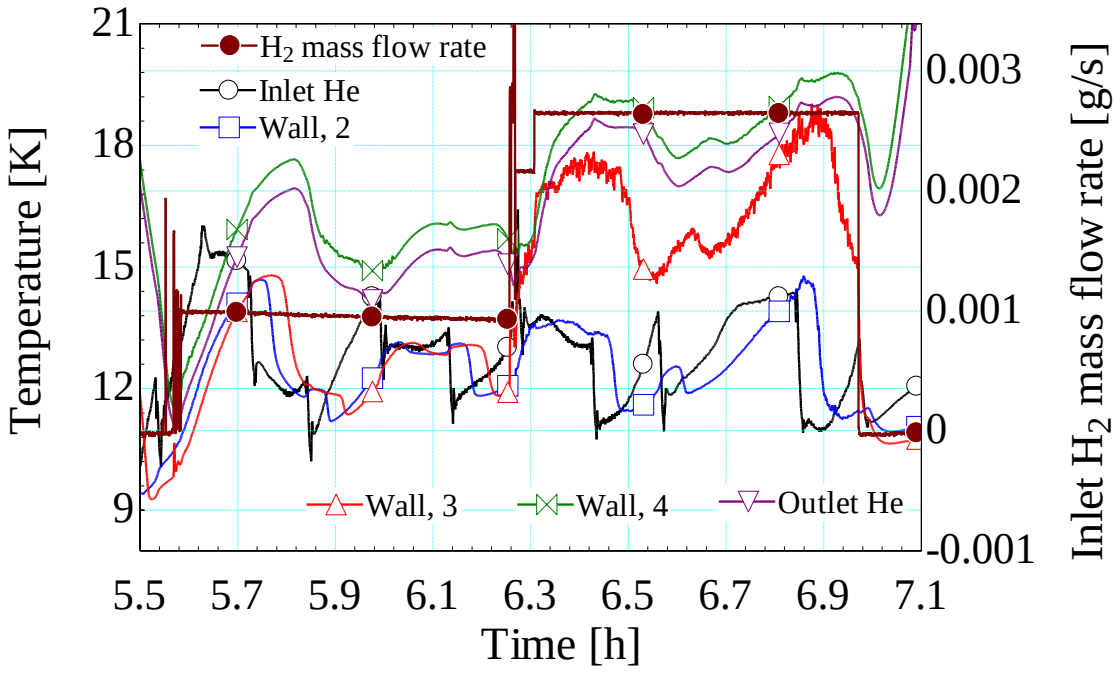

FIGURE 2-15. 1st test: Inlet hydrogen mass flow rate, inlet and outlet helium coolant temperatures, and pump wall temperatures as a function of time.

FIGURE 2-15 shows the time dependence of the inlet hydrogen mass flow rate, the inlet and outlet helium coolant temperatures, and the three pump wall temperatures for the first test. $T_{wall,4}$ and $T_{outlet,He}$ follow each other. $T_{wall,3}$ approaches $T_{wall,4}$ when the hydrogen mass flow rate is large, indicating that the wall temperature at the pump entrance is mainly affected by the inlet hydrogen gas. The effect of the hydrogen gas increases as its mass flow rate increases.

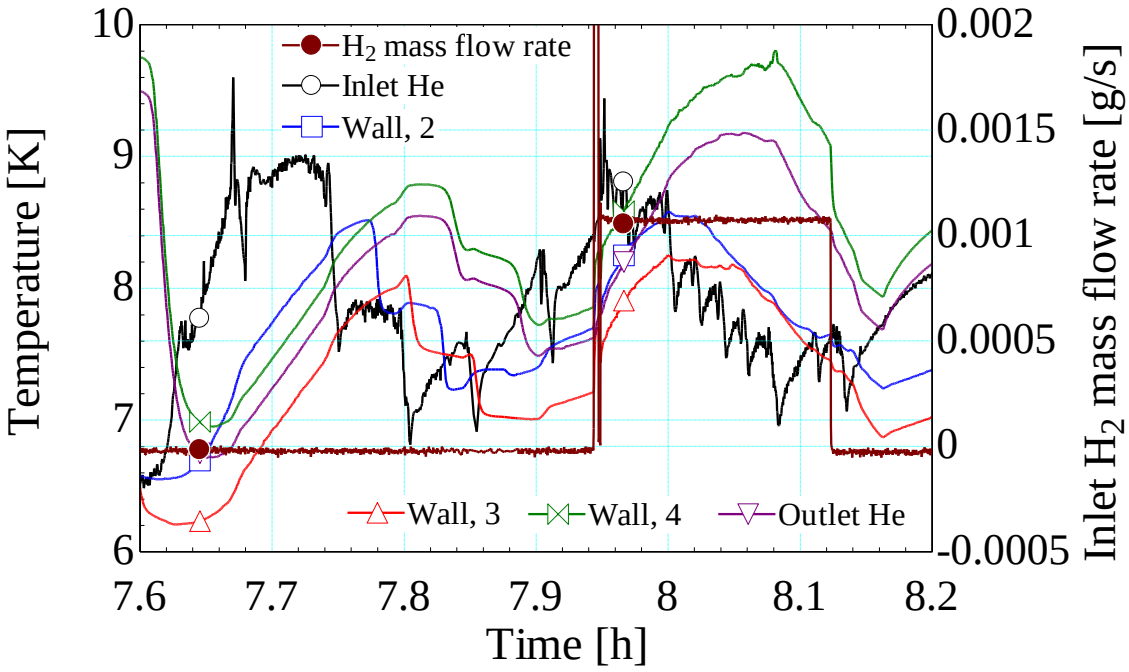

FIGURE 2-16. 2nd test: Inlet hydrogen mass flow rate, inlet and outlet helium coolant temperatures, and pump wall temperatures as a function of time.

FIGURE 2-16 displays the time dependence of the inlet hydrogen mass flow rate, the inlet and out let helium coolant temperatures, and the three pump wall temperatures for the second test. Note significantly that the wave of the inlet helium coolant temperature

yields the same but delayed waves in the pump wall temperatures. This phenomena is clearly shown when the inlet hydrogen mass flow rate is 0 kg/s. When the inlet hydrogen mass flow rate is not 0 kg/s, the pump wall temperature is affected by both the inlet helium coolant and the inlet hydrogen gas.

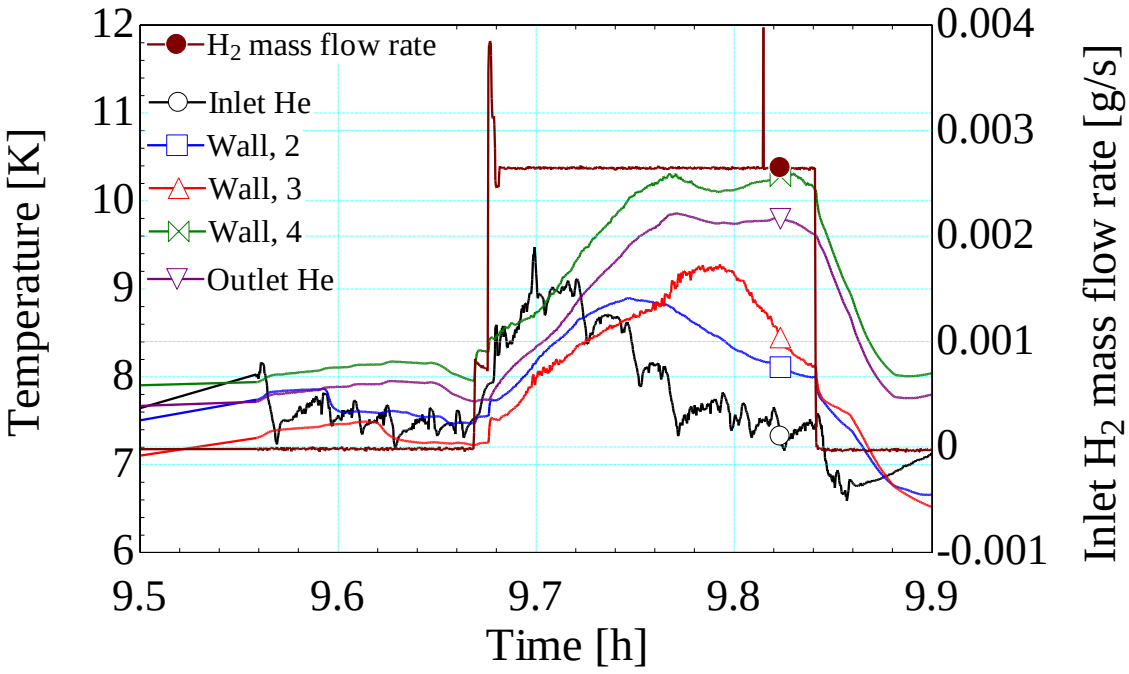

FIGURE 2-17. 3rd test: Inlet hydrogen mass flow rate, inlet and outlet helium coolant temperatures, and pump wall temperatures as a function of time.

FIGURE 2-17 shows the time dependence of the inlet hydrogen mass flow rate, the inlet and outlet helium coolant temperatures, and the three pump wall temperatures for the third test. It is observed that the shape of the inlet helium coolant temperature is reflected by the pump wall temperature ($T_{wall,2}$ and $T_{wall,3}$). $T_{wall,4}$ and $T_{outlet,He}$ are

close to the pump entrance where the hydrogen gas is introduced and are therefore more affected by the warm hydrogen gas at the pump inlet.

2.2.2. Experimental data set II

The second set of experimental data was gathered during another test of the prototype cryogenic fore pump. As with the first set, the gas being pumped was pure hydrogen gas. In addition to the same variables that were measured in experimental data set I, the upstream and downstream hydrogen pressures at the pump test rig, were measured and reported.

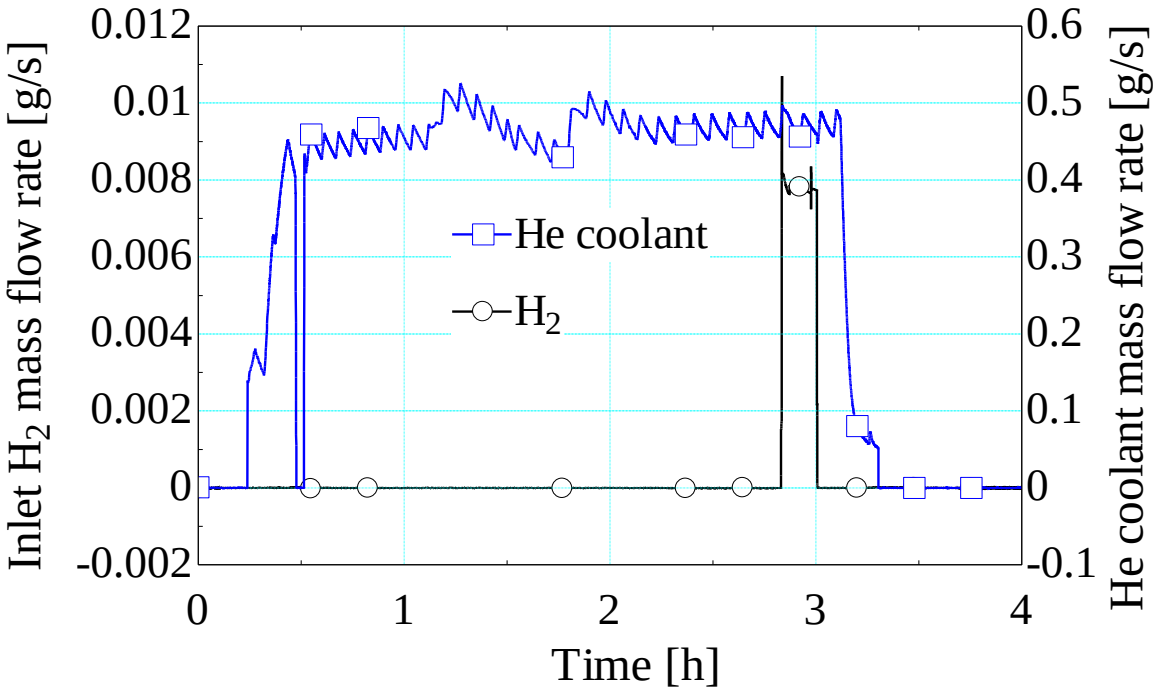

FIGURE 2-18. Inlet hydrogen mass flow rate and inlet helium coolant mass flow rate as a function of time.

FIGURE 2-18 shows the time dependence of the inlet hydrogen mass flow rate and the inlet helium coolant mass flow rate. In this case, the hydrogen mass flow rate is about 0.008 g/s, that is about 4 times higher than the flow rates used in experimental data set I. As before, the helium coolant is introduced before the hydrogen gas to precool the cryogenic pump.

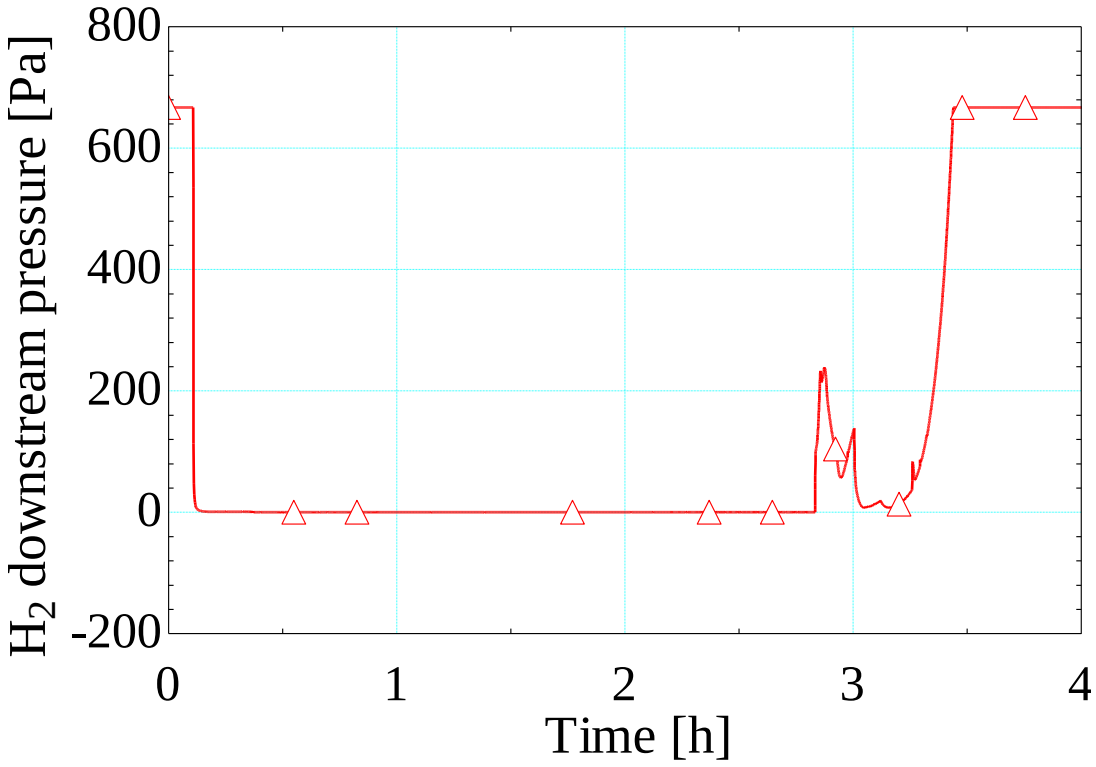

FIGURE 2-19. Downstream hydrogen gas pressure as a function of time.

FIGURE 2-19 shows the time dependence of the hydrogen gas pressure by the downstream pressure tap. The pressure is capped at about 700 Pa due to the pressure meter

limit. The two pressure caps at the two ends of the profile are shown because they reflect the regeneration process before and after the test.

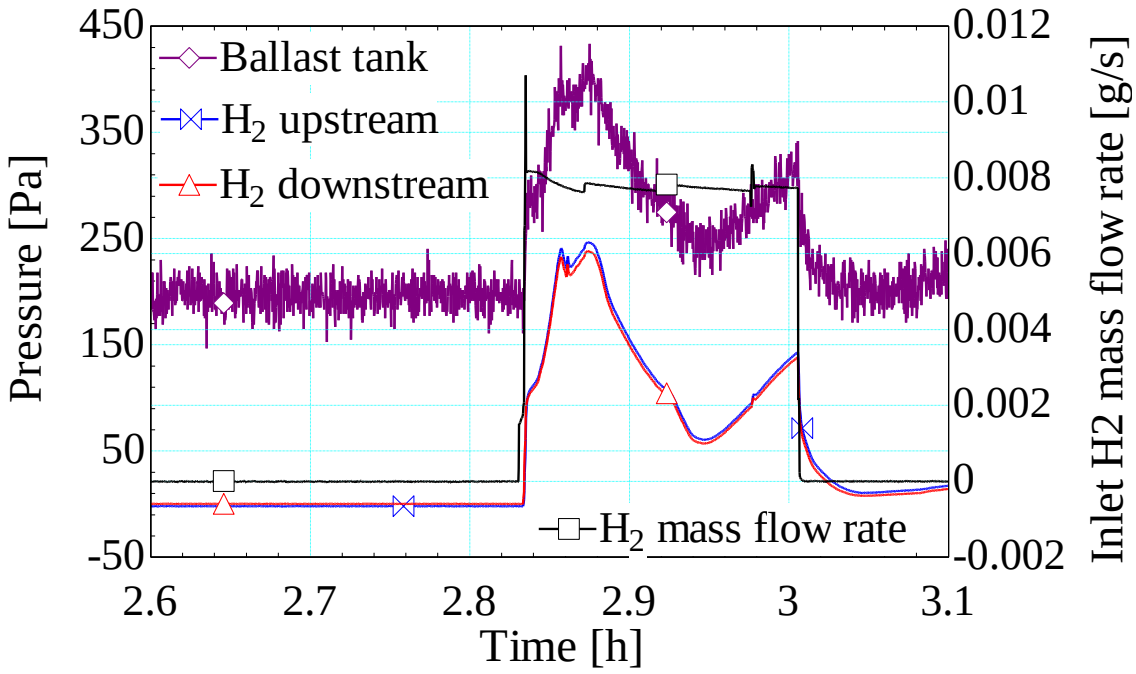

FIGURE 2-20. Upstream hydrogen gas pressure, downstream hydrogen gas pressure, hydrogen gas pressure in the ballast tank, and inlet hydrogen mass flow rate as a function of time.

FIGURE 2-20 shows the time dependence of the upstream hydrogen gas pressure, the downstream hydrogen gas pressure, the hydrogen gas pressure in the ballast tank, and the inlet hydrogen mass flow rate. This is an important figure. It shows that the pressure drop in the cryogenic pump is very small, because the upstream pressure and the downstream pressure are almost identical. The hydrogen gas is in the viscous flow regime, and the friction between the gas and the wall is small.

The time dependence of the hydrogen gas pressure in the ballast tank mimics the inlet hydrogen gas pressure as well. Since the tank is located downstream of the cryogenic pump, its pressure should be lower than those measured in the pump. An explanation for this experimental discrepancy is not available at this time, but it seems plausible that an artificial offset was present in the measurement.

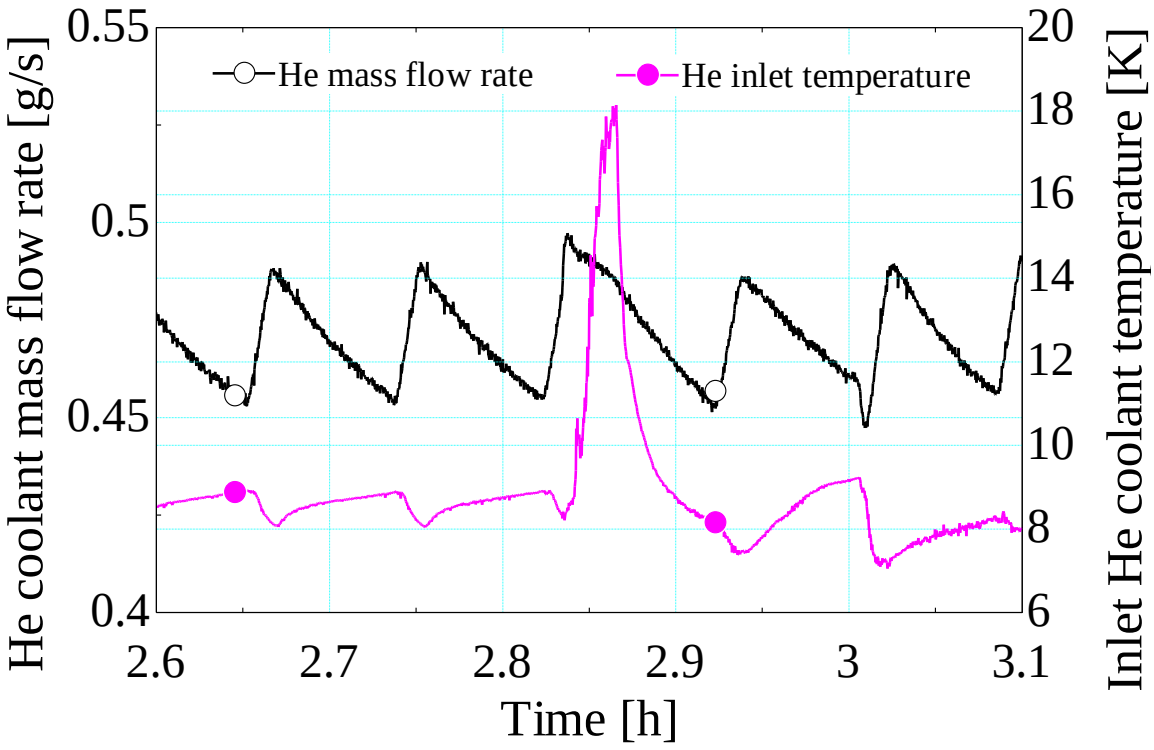

FIGURE 2-21. Inlet helium coolant mass flow rate and inlet helium coolant temperature as a function of time.

FIGURE 2-21 shows the time dependence of the inlet helium coolant mass flow rate and the inlet helium coolant temperature. The inlet helium mass flow rate is reasonably constant. However, the inlet helium coolant temperature is not maintained at a constant

value. One may suggest that the hydrogen load on the coolant is responsible for the sharp temperature rise, but the reason for the subsequent sharp drop in coolant temperature is unknown.

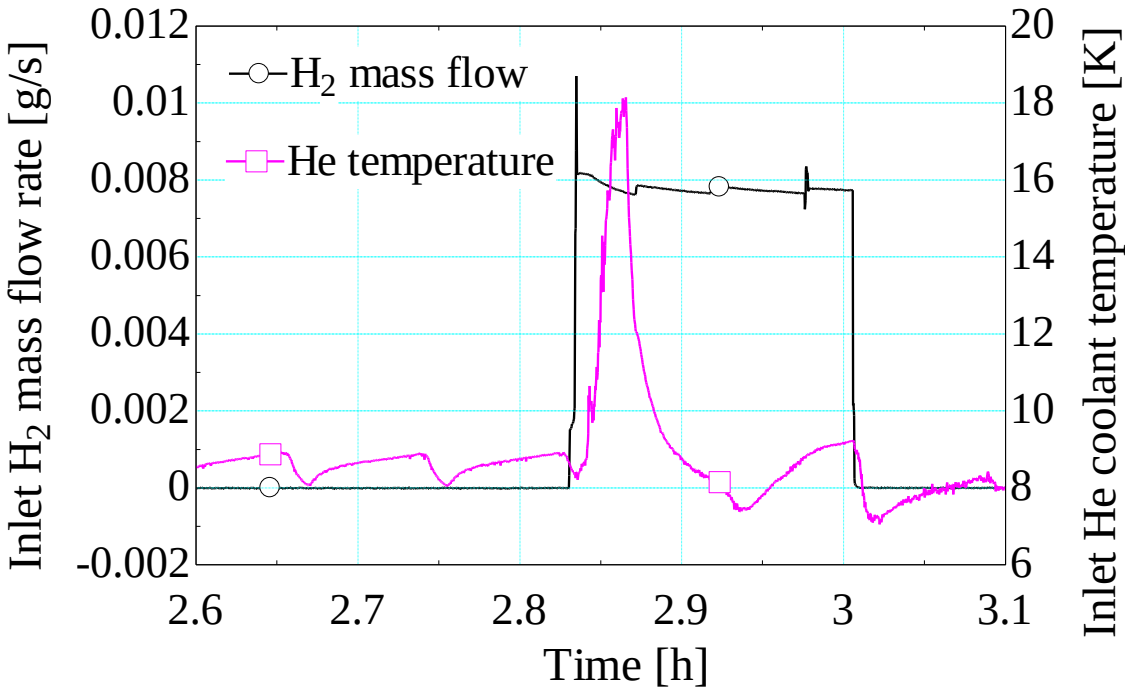

FIGURE 2-22. Inlet hydrogen mass flow rate and inlet helium coolant temperature as a function of time.

FIGURE 2-22 shows the time dependence of the inlet hydrogen mass flow rate and the inlet helium coolant temperature.

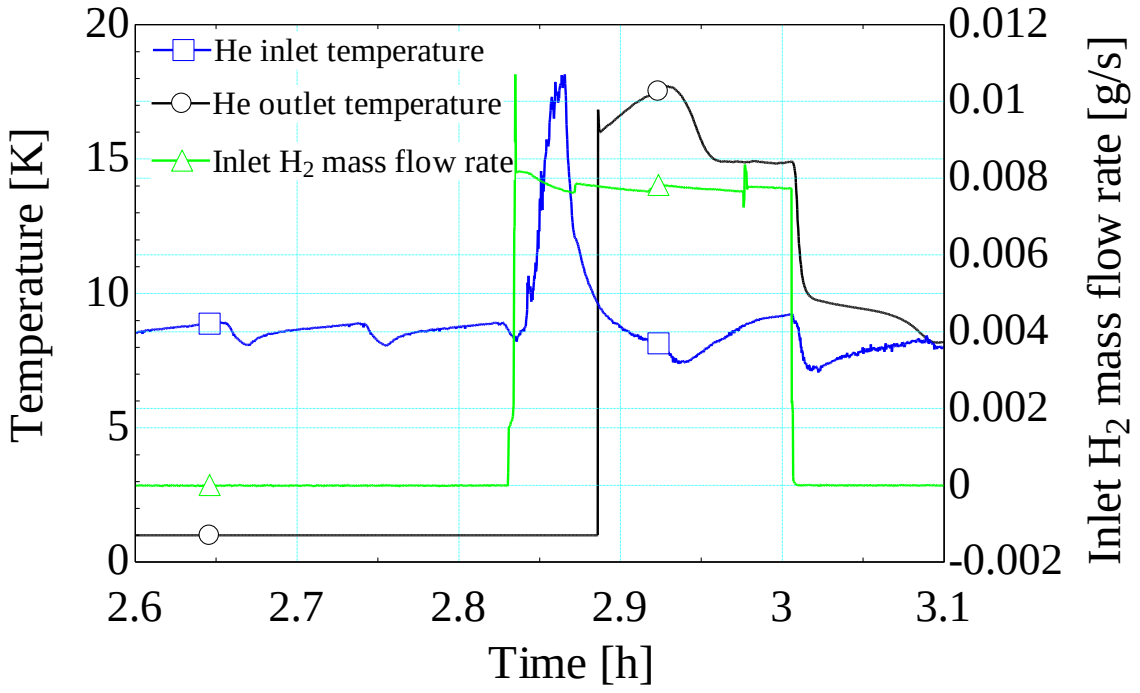

FIGURE 2-23. Inlet helium coolant temperature, outlet helium coolant temperature and inlet hydrogen mass flow rate as a function of time.

FIGURE 2-23 shows the time dependence of the inlet helium coolant temperature, the outlet helium coolant temperature, and the inlet hydrogen gas mass flow rate. It appears that the outlet thermometer was activated after the hydrogen gas was introduced.

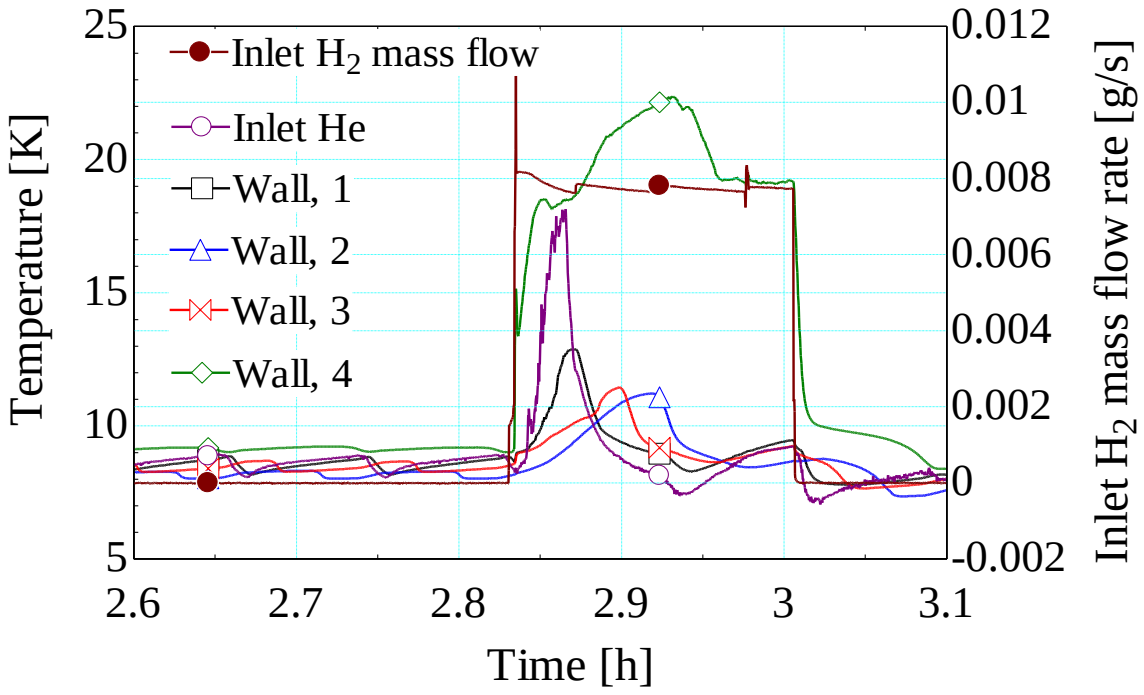

FIGURE 2-24. Inlet helium coolant temperature, 4 pump wall temperatures, and inlet hydrogen mass flow rate as a function of time.

FIGURE 2-24 shows the time dependence of the inlet helium coolant temperature, the four pump wall temperatures and the inlet hydrogen gas mass flow rate. $T_{wall,1}$, $T_{wall,2}$, and $T_{wall,3}$ respond to and mimic $T_{inlet,He}$ in sequence. The delayed responses are obvious. Note that $T_{wall,4}$ is different and is dominantly affected by the hydrogen gas. The temperature recorded by $T_{wall,4}$ is much higher than that by $T_{wall,3}$. The distance between the two thermometers measuring $T_{wall,4}$ and $T_{wall,3}$ is about 1/3 of the pump length. That means that the impact of the 'warm' hydrogen gas at the pump inlet on the pump wall temperature occurs within a small length at the pump entrance. Additionally, the hydrogen

gas temperature must have decreased significantly in the same region. This observation agrees with our numerical models.

Chapter 3 Transient model

The cryogenic fore pump is designed to separate hydrogen isotopes from helium during the regenerating process of the torus cryo-pumps. During their residence in the CFP, hydrogen isotopes are captured along the wall while helium flows through. Such problems are not widely encountered nor studied in Mechanical engineering or Chemical engineering; instead these type of flow problems are usually simplified by assuming a constant density or velocity profile and then calculating the associated bulk temperatures using various estimation methods. Even though from an engineering point of view, such simplifications or estimations could adequately characterize the flow, we are strongly interested in pursuing the full detailed physical mechanisms associated with the flow. We believe that in addition to the applicability for the cryogenic fore pump, as well as other systems with solid-precipitating gas-flow, our work will provide generic value to the fundamental disciplines of Thermodynamics, Fluid Mechanics, Heat Transfer, and Mass Transfer.

The transient numerical model is developed to explain the experimental data set I from the test results of the prototype ITER cryogenic fore pump (CFP) using pure hydrogen. Although the model has been developed for a hydrogen-helium mixture, it is simplified here in order to compare with the experimental data.

The transient model is valid in the viscous flow regime. In the experiment the hydrogen flow is also in the viscous flow regime because the inlet helium coolant temperature remains above 7 K.

3.1. Physical analysis

The pumping process within the ITER cryogenic fore pump involves a variety of physical phenomena. The analysis of the process has included considerations for molecular kinetic, surface chemistry, heat transfer, thermodynamics and fluid mechanics. Each consideration provides a unique perspective, and by integrating them together an overall view of the pumping process has been obtained.

3.1.1. Cryogenic adsorption and boundary condition

The purpose for developing the ITER cryogenic fore pump (CFP) is to cryogenically adsorb hydrogen. Several questions of interest are: What pump condition is required to adsorb hydrogen? (3.4.3. Hydrogen pressure and adsorption) How strong is the adsorption power? (4.2.1. Inlet hydrogen pressure and inlet helium coolant temperature) What is the capacity of the pump? (4.2.2. Best pumping performance) To answer those questions, it is necessary to identify the physical nature of adsorption for the cryogenic fore pump.

Common cryogenic pumps adsorb molecules through gas-surface interaction, mainly chemical adsorption and physical adsorption. Such pumps operate in the rarefied gas regime and they see small amounts of target molecules during the cryogenic adsorption process. As a result, the adsorbed molecules are not enough to form adsorption layers covering the pump surface. Incoming molecules always see and interact with the pump surface. For adsorption to occur, the pumps should be very clean with surfaces un-contaminated by impurity molecules. The forces between target molecules and the cryopump surface trap the molecules, and the bonding energy between the molecules and

the surface is the adsorption energy. Molecules in the rarefied gas regime have a long mean free path compared to the dimension (here, the diameter) of the cryogenic pump. The total projected area of the adsorbed molecules is small compared to the cryogenic pump surface, and the adsorbed molecules do not form a solid structure but remain as separate individual molecules. In other words, the molecules do not see each other much before and after adsorption. As a result, factors affecting the gas-surface interaction are key to determining the performance of a common cryogenic pump. For example, pump surface temperature and adsorption energy (bonding energy) determine the mean surface lifetime. The thermal velocity is the characteristic velocity of the molecules impinging on the cryopump surface. The capacity of a conventional cryopump is then determined by the available adsorption sites of the pump. Once all the available sites have been occupied, the cryogenic pump has to be regenerated.

In contrast with common cryogenic pumps, the nature of the ITER cryogenic fore pump is the cryogenic deposition of the hydrogen molecules from a viscous gas flow into the hydrogen solid on the pump surface. The crucial point is that the ITER cryogenic fore pump (CFP) works in viscous flow regime. As long as the inlet pressure is greater than 5 Pa, the 1% contribution of helium gas creates a viscous, rather than a molecular flow regime. The incoming hydrogen molecules collide with other molecules more frequently than with the pump surface, and they behave as a bulk gas flow. Additionally the ITER CFP processes many more molecules than those being processed by a common cryogenic pump.

As a result, neither chemical adsorption nor physical adsorption are the major mechanism for cryogenic pumping in the ITER cryogenic fore pump. It is possible though that the gas-surface interaction is important at the very beginning of the cryogenic pumping given the condition that the pump surface is initially clean and free of contamination. The available sites for chemical or physical adsorption are too few compared to the large amount of hydrogen molecules entering the pump. The process of the gas-surface interaction is very short and unimportant in the entire cryogenic pumping process. The available sites are soon occupied, and the surface of the ITER CFP is quickly covered by the solid hydrogen molecules.

After the first five or so monolayers are deposited, the hydrogen molecules in the gas flow see and interact with the solid hydrogen molecules on the pump surface instead of the pump surface directly (or indirectly). This interaction is the main mechanism for the ITER cryogenic fore pump. In other words, deposition, the phase change of the hydrogen molecules from vapor to solid, is the main adsorption mechanism for the ITER cryogenic fore pump.

Deposition is a kinematic process. Molecules enter the solid phase from the vapor phase and leave the solid phase to the vapor phase at the same time. Molecules leaving the solid phase, going directly into the vapor phase is sublimation. When the net effect of the molecular flow in both directions is balanced, that is when there is no change in the number of molecules in either phase, the pressure of the vapor phase is called the solid vapor pressure, or just the vapor pressure. In other words, the vapor pressure is the pressure at which the vapor phase and the solid phase reach equilibrium. Whenever the gas pressure

adjacent to a solid is larger than the vapor pressure associated with the solid temperature, there will be a net transfer of molecules going from the gas into the solid phase.

The vapor pressure of solid hydrogen is a strong function of temperature. The experimental data (Ahlers, 1963) (Mullins, Ziegler, & Kirk, 1961) (Roder, The thermodynamic properties of slush hydrogen and oxygen, 1977) (Roder, Childs, McCarty, & Angerhofer, 1973) (McCarty, 1981) are plotted in **FIGURE 3-1** and **FIGURE 3-2**.

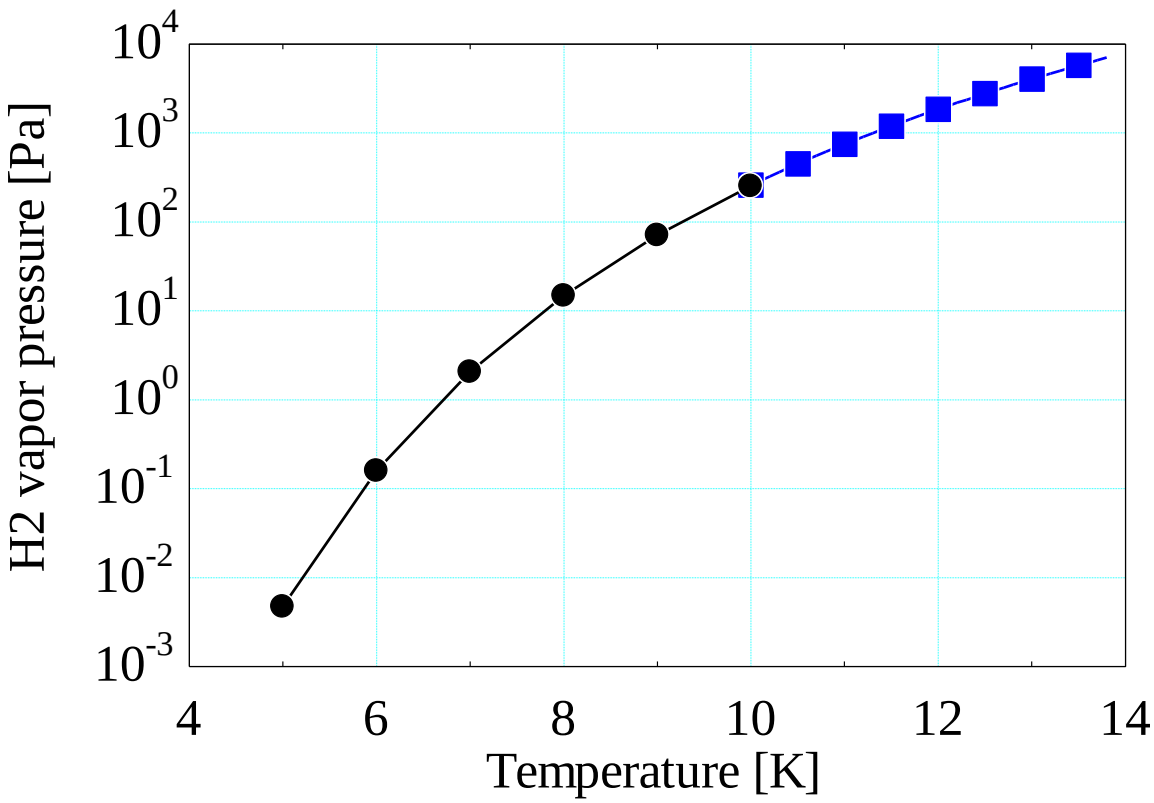

FIGURE 3-1. Hydrogen solid vapor pressure as a function of temperature [5 K, 14 K].

FIGURE 3-1 shows the hydrogen vapor pressure for the temperature range from 5 K to 14 K. The vapor pressure drops from about 7000 Pa to about 200 Pa when the solid temperature decreases from about 14 K to 10 K.

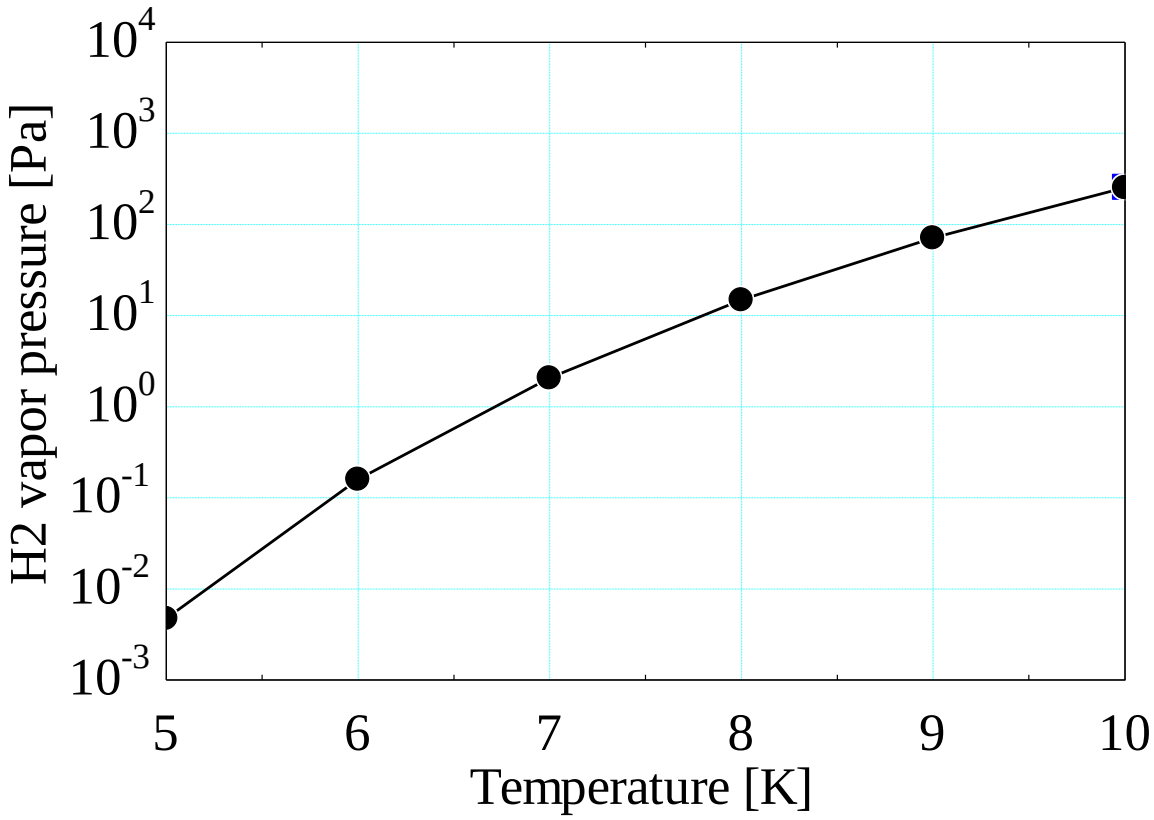

FIGURE 3-2. Hydrogen solid vapor pressure as a function of temperature [5 K, 10 K].

FIGURE 3-2 shows the hydrogen vapor pressure from 5 K to 10 K. And the data is summarized in the following table as well because of its importance.

TABLE 1. Hydrogen vapor pressure as a function of temperature

Temperature [K]	5	6	7	8	9	10
Vapor pressure [Pa]	0.00476	0.16	2.08	14.91	71.23	255.58

It is obvious that the pump surface temperature is a key factor for the pumping performance. The hydrogen pressure is very sensitive to the temperature change. A one-degree change in temperature produces an order-of-magnitude change in the hydrogen vapor pressure.

3.1.2. Transport phenomena

The ITER cryogenic fore pump presents unique features for transport phenomena. Because of the adsorption of hydrogen molecules on the pump surface and its sensitivity to the surface temperature, the transport of species, momentum, and energy in the control volume of the hydrogen gas flow are all significantly affected by the boundary condition defined by the surface. That boundary condition varies with time and position, and is strongly influenced by the inlet helium coolant.

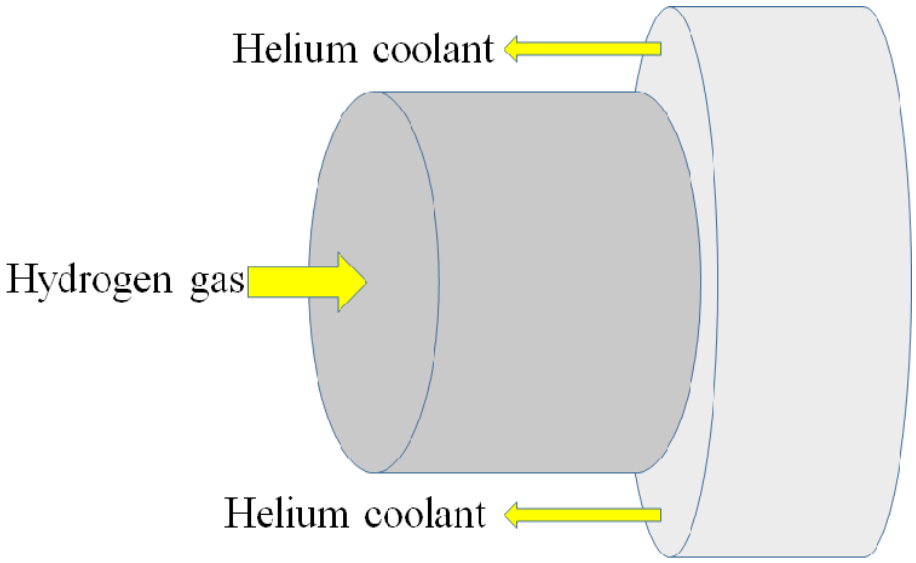

FIGURE 3-3. A drawing of the configuration of the cryogenic fore pump.

As shown in **FIGURE 3-3**, the ITER cryogenic fore pump (CFP) is modeled as a concentric tube-in-tube heat exchanger. The hydrogen gas (or a hydrogen-helium gas mixture) flows through the inner tube, while the helium coolant flows through the annulus. The tube wall separating the two flows develops a temperature profile that is determined by the heat transfer between the two fluids, which in turn is influenced by accumulation of solid hydrogen on the wall. As hydrogen gas flows through the tube, heat is transferred from the bulk gas flow to the cryopump surface and then is taken away by the helium coolant. As a result, the temperature of the hydrogen flow decreases as it flows through the tube. Because of its relatively low pressure, a sufficient decrease in the temperature of the hydrogen flow results in the deposition of solid, rather than liquid hydrogen on the pump wall. Deposition occurs wherever the wall temperature is sufficiently low, so that the corresponding vapor pressure of solid hydrogen is lower than the pressure of the adjacent

bulk hydrogen gas. Since the vapor pressure of solid hydrogen is a strong function of temperature, the ITER CFP performance is strongly affected by the inlet temperature and mass flow rate of the helium coolant. The mass of hydrogen deposited on the wall not only influences the conservation of species, momentum, and energy, it introduces an additional thermal resistance to the heat flow through the tube wall. The conductivity of solid hydrogen is about 0.2 to 0.6 W/m-K. And that is in the same order as the conductivity of the stainless steel (about 0.5 W/m-K). Therefore the adsorption of hydrogen molecules on the pump wall is like to increase the wall thickness. However, that thermal resistance is not included in the current model.

The cryopump inner surface specifies the physical and computational boundary for the hydrogen flow inside the inner tube. To be specific, the surface temperature sets the temperature boundary for the hydrogen flow, and the axial bulk velocity is zero at the pump surface. In the situation where the pump surface temperature is below the triple-point temperature of hydrogen, hydrogen molecules in the bulk flow start to deposit onto the pump surface, which is a phase change from vapor to solid.

Transport can be defined as the sum of convection and diffusion. Because of the similarity of transport for species, momentum, and energy, the transport of species (mass flux) is taken as the illustration example.

Mass flux M is the sum of convection flux ρu and diffusion flux J .

$$M = \rho u + J \qquad 5)$$

Convection flux is characterized by the bulk velocity u. That velocity is the mass-averaged velocity of the bulk flow. To a certain extent the bulk velocity is a mathematical term, since it is back-calculated from the mass flux and density. If the molar flux is used, the bulk velocity will accordingly be a molar-averaged velocity.

Diffusion is defined as the additional movement relative to a mass (or molar) averaged bulk velocity in a mixture. In an isothermal and isobaric environment, diffusion is driven by the concentration gradient of species. Species tend to move down their concentration gradient. The diffusion speed can be described by a diffusion coefficient.

Besides concentration driven diffusion, one may also have thermal diffusion that is driven by the temperature gradient. Thermal diffusion is mainly considered in the mixture of isotopes. In such a mixture, molecules of different molecular weight move towards different directions in a non-isothermal environment. The thermal diffusion coefficient is related to, and can be calculated from, the concentration diffusion coefficient, and is generally smaller than the concentration diffusion coefficient.

A rigorous expression of diffusion should adopt an apparent gradient $\nabla(\Pi)$. The apparent gradient includes all the potentials that are summed to be Π. Then the general diffusive mass flux is determined from

$$J = -D\nabla(\Pi) \qquad 6)$$

Here D represents the diffusion coefficient, and $\nabla(\Pi)$ represents the gradient of all the potentials that drive the diffusion.

3.1.3. Variables for performance and design

In this section a few short but important discussions are provided on the hydrogen gas pressure, inlet hydrogen gas velocity, and the cooling power of the helium coolant. The discussions either stress the importance of the terms or clarify the related information.

In experiment set I, the upstream hydrogen pressure is measured. In experiment set II, both the upstream hydrogen pressure and downstream hydrogen pressure are measured.

The upstream pressure is used as an indicator for adsorption. When the upstream pressure stays constant, no adsorption occurs. When the upstream pressure varies with time, adsorption of hydrogen happens. The adsorption slows down the initial rise of the upstream pressure. And as the inlet helium coolant temperature rises, the adsorbed hydrogen molecules can come back to the bulk flow again. In addition, the figures (**FIGURE 2-11** and **FIGURE 2-13**) show the initial pressure rise from 0 Pa when the hydrogen gas is just introduced. It is due to the initial strong cryopumping power.

In experiment set II, the downstream hydrogen pressure mimics the upstream hydrogen pressure, and the difference between them (the pressure drop) is negligibly small. The cause of the small pressure drop in the ITER cryogenic fore pump is the relatively small friction between the gas and the pump wall.

The information associated with pressure travels at the speed of sound in the viscous flow regime. Any change of hydrogen pressure inside the ITER cryogenic fore

pump (CFP) is immediately reflected in the upstream hydrogen pressure. With adsorption, the wall boundary condition (the wall temperature and the associated hydrogen vapor pressure) changes. And that change is affected by the time dependence of the hydrogen inlet pressure. In other words, the change of the upstream hydrogen pressure is in fact the result of the adsorption happening in the CFP. The vapor pressure of the solid hydrogen implies the adsorption power. Given the same inlet hydrogen gas conditions, the smaller hydrogen vapor pressure is, the stronger the adsorption power is. As a result, the upstream hydrogen pressure, or hydrogen flow pressure in the CFP, should follow the same trend as the hydrogen vapor pressure, and that in turn will be determined by the time dependence of the minimum wall temperature. This feature is confirmed by comparing the modeling results with the experimental data in **SECTION** 3.4.2. Time dependence of variable) below.

In the experiment the inlet mass flow rate of the hydrogen gas is controlled by a mass flow controller. The data show that that mass flow rate can be well maintained as a desired constant. In addition, the inlet hydrogen gas is precooled by a 77-K liquid nitrogen bath, so that the inlet hydrogen gas temperature can be reasonably assumed constant at 77 K.

As shown in the following equation, the mass flow rate $\dot{m}$ is the product of density ρ, bulk velocity u and cross-sectional area A. Also, the hydrogen density is a function of pressure P and temperature T. Thus, the inlet hydrogen flow velocity is fixed by knowing the upstream hydrogen pressure.

$$\dot{m} = \rho(P,T)uA \quad 7)$$

Without adsorption or sublimation, the upstream hydrogen pressure and inlet hydrogen velocity are constant. When adsorption or sublimation occurs, both of them change with time.

As the hydrogen gas flows through the ITER cryogenic fore pump, its bulk velocity decreases. There are three reasons for the decrease, one being friction, one being a cooling effect, and the last one being adsorption of hydrogen molecules. The decrease in velocity due to friction is constrained by the conservation of momentum. The decrease in velocity due to the cooling effect and adsorption is in fact the result of the conservation of species.

The cooling power is a term used to describe the cooling effect provided by the helium coolant. It is determined by the inlet helium coolant temperature, mass flow rate and geometry of the ITER cryogenic fore pump.

As mentioned above, a one-degree change in the surface temperature of the pump wall yields orders of magnitude change in the hydrogen vapor pressure. Thus, to the degree that the inlet helium coolant temperature and mass flow rate influence the wall temperature of the cryopump, they influence its cooling power. The pump geometry also influences the cooling power through its influence on the heat transfer coefficients associated with convection along the inner wall and in the annular region.

3.2. Model and governing equations

SECTION 3.2.1. Model for hydrogen-helium mixture) presents the model developed for the control volume of the hydrogen gas that is a mixture of hydrogen and helium. The **SECTION** 3.2.2. Model for comparing with experimental data set I) presents the model developed to explain the experimental data set I.

3.2.1. Model for hydrogen-helium mixture

This section describes the numerical model that solves for the temperature, pressure, velocity, density, and composition of a hydrogen-helium gas mixture as they flow through the cryogenic pump. Thermal and kinetic properties, such as conductivity and viscosity, in turn depend on the temperature, pressure and composition.

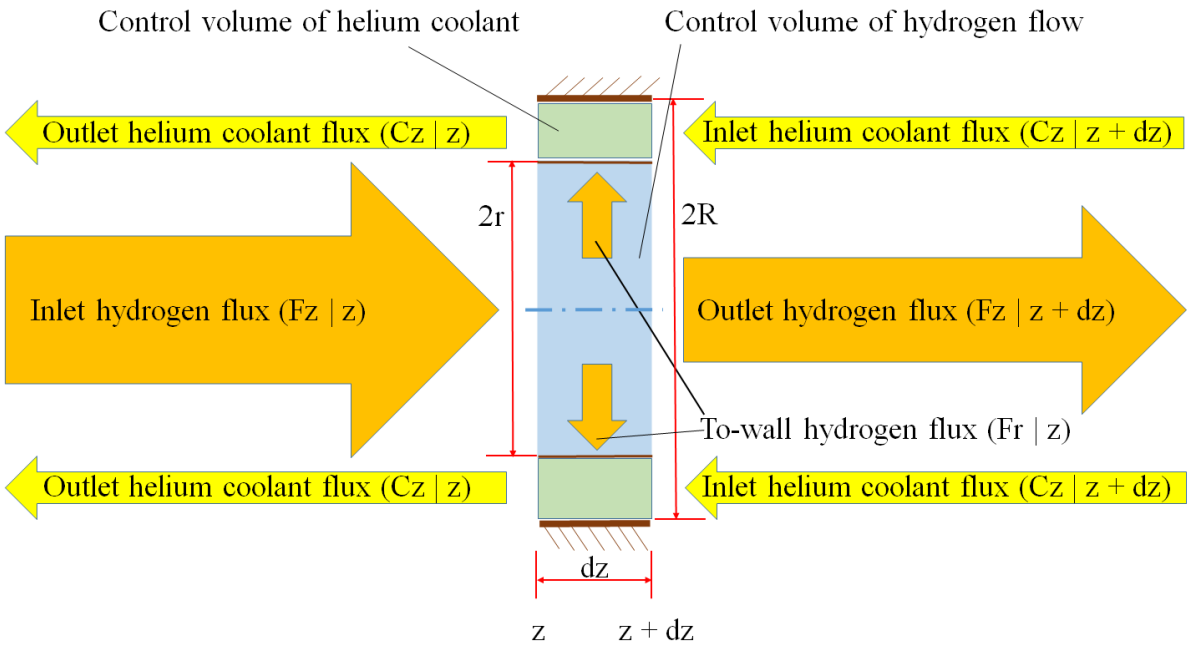

FIGURE 3-4. A control volume of the hydrogen gas flow and the helium coolant. The inner tube has a diameter of 2r, and the outer tube has a diameter of 2R. The differential length is dz.

The analysis on the control volume of the hydrogen-helium gas (represented as hydrogen flow) is shown in **FIGURE 3-4**. The control volume is a cylinder with a differential length of dz and a radius of r. Fz and Fr are general flux terms and can be flux of species, momentum, or energy. F_z represents the cross-sectional-area-averaged flux in the axial (z) direction. As the axial flux flows through the control volume, some portion is transferred out of the control volume to the cryopump surface, and the rest flows out. By applying either of the conservation laws, a general form is obtained for the steady-state flux balance as shown in the following equation.

$$r\frac{d\left[F_z\right]}{dz}+2F_r=0. \quad 8)$$

Substituting species, z-momentum, and energy flux into the general equation, the steady-state governing equations for the control volume of the hydrogen-helium gas are given as follows.

$$r\frac{d\left[M_{z,H_2}\right]}{dz}+2M_{r,H_2}=0. \quad 9)$$

$$\frac{d\left[M_{z,He}\right]}{dz}=0. \quad 10)$$

$$r\frac{d\left[\Phi_{zz}\right]}{dz}+2\Phi_{rz}=0. \quad 11)$$

$$r\frac{d\left[E_z\right]}{dz}+2E_r=0. \quad 12)$$

In the conservation equation of the hydrogen species, M_{z,H_2} is the axial hydrogen mass flux, and M_{r,H_2} is the radial hydrogen mass flux being adsorbed onto the cryopump surface. Expressions for M_{z,H_2} and M_{r,H_2} are given as follows.

$$M_{z,H_2} = \rho_{H_2} u_z \tag{13}$$

$$M_{r,H_2} = h_m(\rho_{H_2} - \rho_{H_2,w}) \tag{14}$$

Here, ρ_{H_2} is the hydrogen density in bulk flow, $\rho_{H_2,w}$ is hydrogen density at the cryopump surface temperature (T_w) and solid hydrogen vapor pressure, u_z is the axial bulk velocity, and h_m is the hydrogen mass transfer coefficient. The definition of h_m is similar to the heat transfer coefficient (h_t) and is obtained through the Reynolds analogy for a gas.

$$h_t = \frac{Nu \cdot k}{2r}, h_m = \frac{Sh \cdot D_{ab}}{2r} \tag{15}$$

Where Nu is the Nusselt number, k is the thermal conductivity, Sh is the Sherwood number, and D_{ab} is the mass diffusivity.

In the conservation equation of the helium species, $M_{z,He}$ is the axial helium mass flux, a product of helium density (ρ_{He}) and axial velocity (u_z).

$$M_{z,He} = \rho_{He} u_z \quad 16)$$

Helium molecules cannot be adsorbed onto the cryopump surface given the condition of the helium coolant, and thus there is no radial mass flux of helium.

In the conservation equation for the z-momentum, Φ_{zz} is the z-momentum flux transferred in axial (z) direction. With negligible viscous dissipation, it is sum of the momentum flux associated with mass flow and the pressure (P). Φ_{rz} is the z-momentum loss to the cryopump surface due to friction (friction momentum loss $\Delta P_{friction}$) and adsorption of hydrogen (adsorption momentum loss $M_{r,H_2} u_z$).

$$\Phi_{zz} = \rho_{H_2} u_z u_z + \rho_{He} u_z u_z + P \quad 17)$$

$$\Phi_{rz} = \Delta P_{friction} + M_{r,H_2} u_z \quad 18)$$

The pressure drop $\Delta P_{friction}$ represents the momentum loss due to the pump surface friction.

$$\Delta P_{friction} = (\rho_{H_2} + \rho_{He}) f \frac{u_z^{\,2}}{2} \frac{dz}{2r} \qquad 19)$$

Where f is the friction factor.

In the conservation equation of the energy, E_z is the axial energy flux, and E_r is the radial energy flux transported to the cryopump surface. E_z is the sum of the enthalpy and kinetic energy (negligibly small in this case) terms. E_r is the sum of enthalpy and convection heat terms. Here, h_{H_2} and h_{He} are the specific enthalpy of hydrogen and helium respectively. T is the bulk flow temperature.

$$E_z = \rho_{H_2} u_z h_{H_2} + \rho_{He} u_z h_{He} + (\rho_{H_2} + \rho_{He})\, u_z (\frac{1}{2} u_z^{\,2}) \qquad 20)$$

$$E_r = M_{r,H_2} (h_{H_2} + \frac{1}{2} u_z^{\,2}) + h_t (T - T_w) \qquad 21)$$

An additional equation is the equation of state. The ideal gas law is adopted because for all conditions involved the compressibility factor is close to 1.

$$P = \rho R_m T \qquad 22)$$

Note significantly, that in the momentum balance equation, the static pressure at each face of each control volume is determined by the corresponding particle flux (density x velocity) at that location, that being decreased by mass deposition at the pump surface.

Assuming steady state for the control volume of the helium coolant, the energy given up by the hydrogen-helium gas is equal to that adsorbed by the helium coolant. (The transient process is discussed in the following section.) This energy balance along with the inlet conditions of hydrogen gas and helium coolant determine the cryopump surface temperature. When hydrogen is adsorbed on the pump surface, the total energy flux $E_{r,w}$, taken away by the helium coolant is the sum of the adsorption energy and the heat transferred by convection. Here Δh_{H_2} is the enthalpy change of hydrogen from the gas phase to the solid phase.

$$E_{r,w} = M_{r,H_2}(\Delta h_{H_2} + \frac{1}{2}u_z{}^2) + h_t(T - T_w) \qquad 23)$$

Correlations (Hornbeck, 1965) (R. K. Shah, 1978) (Gregory Nellis, 2008) are available for heat transfer coefficients of both inner pipe flow and the outer annular flow. Nu is a function of the Reynolds number (Re) and Prandtl number (Pr), while similarly Sh is calculated from Re and the Schmidt number (Sc).

$$Nu = Nu(\mathrm{Re}, \mathrm{Pr}), Sh = Sh(\mathrm{Re}, Sc) \quad 24)$$

Additionally, the viscosity and conductivity of the combined hydrogen-helium flow are considered as properties of the gas mixture (Lindsay, 1950) (Wilke, 1950).

3.2.2. Model for comparing with experimental data set I

The transient numerical model is developed to explain the time-dependent changes of the variables in experimental data set I. That experimental data is the test results of cryopumping pure hydrogen gas.

The available experimental data that vary with time are five temperature measurements (two for the helium coolant and three for the pump wall surface) and one pressure measurement for the inlet hydrogen flow pressure (upstream hydrogen flow pressure).

The mass flow rates of the hydrogen gas and the helium coolant are quite stable with time. Therefore, the transient model treats the mass flow rates of the hydrogen gas and the helium coolant as constants, and treats the inlet hydrogen gas pressure and inlet helium coolant temperature as variables. More specifically, the transient model takes the experimental data of the inlet hydrogen gas pressure and the inlet helium coolant temperature as inputs. And based on those inputs, the transient model calculates the other variables at each spatial node for discrete time steps. The modeling results are compared with the rest of the experimental data.

The helium coolant velocity is about 0.3 cm/s, that is orders of magnitude smaller than the hydrogen gas velocity. The numerical time step size is set as about half of the time during which the helium coolant travels between two adjacent nodes. As a result, the hydrogen gas is treated as a steady-state control volume, while the helium-coolant-plus-pump-wall is treated as a transient-state control volume. The reasons are as follows:

For the control volume of the hydrogen gas, the number of hydrogen molecules traveling through a numerical node in one time step is much more than the change in the number of molecules contained in the node. Considering the energy balance for the node in the form: IN = OUT + STORED, the energy represented by the IN or OUT term is thus much larger than the energy represented by the change in the STORED term. In other words, the hydrogen gas gives energy away to the helium coolant by passing a large amount of flow through the node and decreasing the enthalpy of the flow, but not by decreasing the internal energy of the molecules stored in the node. As a result, the hydrogen gas is treated as a control volume at steady state.

For the control volume of the helium-coolant-plus-the-pump-wall, the amount of helium traveling through one numerical node in one time step is much smaller than that contained in the node. In the energy equation IN = OUT + STORED, the energy represented by the change in the STORED term is much larger than the energy represented by the IN or OUT terms. In other words, the helium coolant (plus the pump wall) primarily absorbs energy from the hydrogen gas by increasing the internal energy associated with the STORED term, but not by carrying it away with the enthalpy of the coolant passing through the node (the IN and OUT terms). As a result, the temperature at each node increases with

time. The control volume of the helium-coolant-plus-the-pump-wall is thus treated as a transient control volume.

The transient model is built in the following manner: First, the temperatures of the pump wall and the helium coolant are set at the initial time. Next, the inlet condition of the hydrogen gas and the helium coolant are read from the experimental measurements and used as input parameters to the transient model. Then, the properties for the hydrogen-gas control volume (temperature, pressure, density, and velocity) are calculated for each axial position based on the inlet hydrogen gas condition and the pump wall temperature at that time. The heat flux from the hydrogen gas to the pump wall is also calculated. Next, for the control volume of the helium-coolant-plus-the-pump-wall, the heat flux from the hydrogen gas is used together with the inlet helium coolant condition to calculate the coolant properties at all the nodes for the next time step. Finally, the new pump wall temperature together with the inlet hydrogen gas condition is used to calculate the steady-state profiles for the hydrogen gas at the next time step.

The analysis of the transient model is based on **FIGURE 3-5**. The two control volumes are the steady-state hydrogen gas and the transient-state helium-coolant-plus-the-pump-wall.

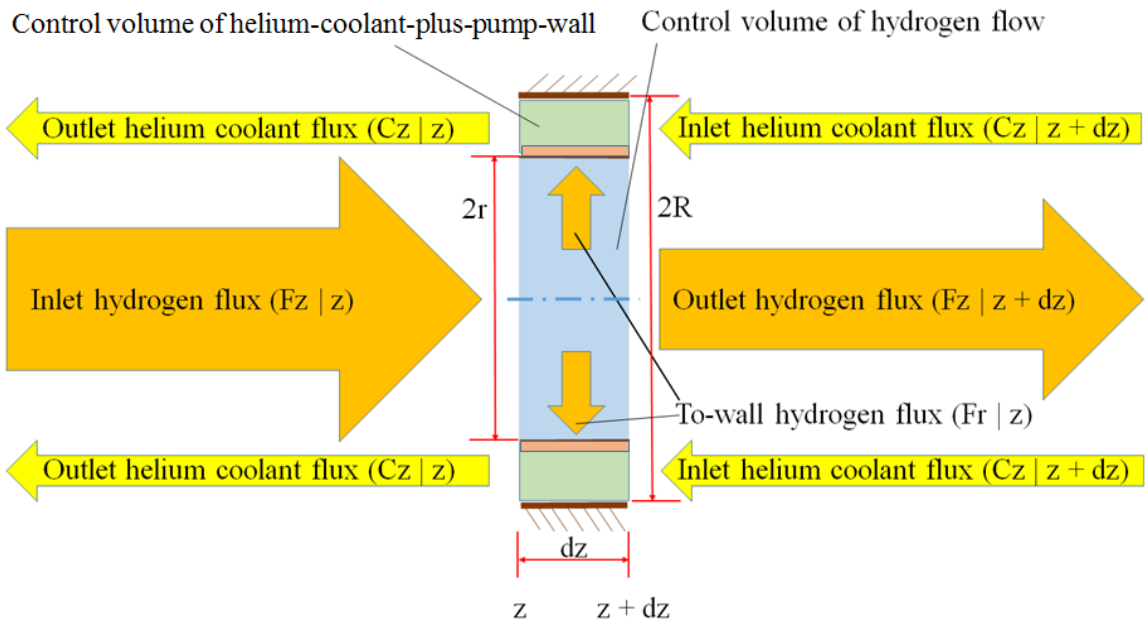

FIGURE 3-5. Control volume of the hydrogen flow at steady state and control volume of the helium-coolant-plus-pump-wall at transient state.

For the control volume of the steady-state hydrogen gas, the general governing equation of the flux in axial (z) direction is the following equation.

$$r\frac{d[F_z]}{dz} + 2F_r = 0. \qquad 25)$$

The general equation is then specified as follows to represent the conservation in species, z-momentum, and energy respectively.

$$r\frac{d\left[M_{z,H_2}\right]}{dz}+2M_{r,H_2}=0. \quad (26)$$

$$r\frac{d\left[\Phi_{zz}\right]}{dz}+2\Phi_{rz}=0. \quad (27)$$

$$r\frac{d\left[E_z\right]}{dz}+2E_r=0. \quad (28)$$

In the conservation equation of the hydrogen species, the mass flux terms are developed as follows to represent the hydrogen mass flux in the axial (z) direction and in radial (r) direction respectively.

$$M_{z,H_2}=\rho_{H_2}u_z \quad (29)$$

$$M_{r,H_2}=h_m(\rho_{H_2}-\rho_{H_2,w}) \quad (30)$$

The mass transfer coefficient h_m is developed in the similar manner as the heat transfer coefficient h_t , and the two transfer coefficients are calculated as follows.

$$h_t = \frac{Nu \cdot k}{2r}, h_m = \frac{Sh \cdot D_{ab}}{2r} \quad 31)$$

In the conservation equation of z-momentum, the z-momentum flux terms are developed as follows to represent the z-momentum transfer in axial (z) direction and in radial (z) direction respectively.

$$\Phi_{zz} = \rho_{H_2} u_z u_z + P \quad 32)$$

$$\Phi_{rz} = \Delta P_{friction} + M_{r,H_2} u_z \quad 33)$$

Where the pressure loss due to friction $\Delta P_{friction}$ is shown as the following equation.

$$\Delta P_{friction} = \rho_{H_2} f \frac{u_z^{\,2}}{2} \frac{dz}{2r} \quad 34)$$

In the conservation equation of energy, the energy flux terms are developed as follows to represent the energy flux in axial (z) direction and in radial (r) direction respectively.

$$E_z = \rho_{H_2} u_z h_{H_2} + \rho_{H_2} u_z (\frac{1}{2} u_z{}^2) \quad 35)$$

$$E_r = M_{r,H_2} (h_{H_2} + \frac{1}{2} u_z{}^2) + h_t (T - T_w) \quad 36)$$

In addition to the conservation equations, the equation of state is needed and assumed as the ideal gas equation of state because of the close-to-unity compressibility factor.

$$P = \rho R_m T \quad 37)$$

For the control volume of the transient-state helium-coolant-plus-pump-wall (abbreviated as helium coolant). The pump wall is considered to be a lumped system, and the axial conduction is neglected. The Biot number is shown as the following equation.

$$Bi = \frac{th_w h_{coolant}}{k_w} \quad 38)$$

The control volume of the helium coolant is connected to the control volume of hydrogen gas by the radial energy flux. The radial energy flux from the hydrogen gas to

the cryogenic pump wall $E_{r,H_2->w}$ is the sum of the energy change of the radial hydrogen flux and the convection heat transfer flux.

$$E_{r,H_2->w} = M_{r,H_2}(\Delta h_{H_2} + \frac{1}{2}u_z{}^2) + h_t(T - T_w) \quad 39)$$

The enthalpy change of hydrogen gas Δh_{H_2} is the sum of enthalpy change from gas phase at the inlet condition to the gas phase in the gas-solid equilibrium condition and the enthalpy change from the gas phase in the gas-solid equilibrium condition to the corresponding solid phase.

$$\Delta h_{H_2} = \Delta h_{H_2,gas->gas_s} + \Delta h_{H_2,gas_s->solid} \quad 40)$$

The energy governing equation of the control volume of helium-coolant-plus-pump-wall is shown as the following equation.

$$E_{r,H_2->w} A_s = Q_{r,w->coolant} + \frac{\Delta U_w}{\Delta t} \quad 41)$$

Where the term $\frac{\Delta U_w}{\Delta t}$ represents the rate of change of the pump-wall internal energy. The Energy transfer rate from the pump wall to the helium coolant ($Q_{r,w->coolant}$) is developed as the following equation.

$$Q_{r,w->coolant} = \Delta H_{coolant} + \frac{\Delta U_{coolant}}{\Delta t} \quad 42)$$

Where the term $\frac{\Delta U_{coolant}}{\Delta t}$ represents the rate of change of the helium-coolant internal energy.

Additionally, $Q_{r,w->coolant}$ can be expressed by the following equation.

$$Q_{r,w->coolant} = \frac{T_w - T_{coolant}}{R_{coolant}} \quad 43)$$

Where the term $R_{coolant}$ represents the thermal resistance between the pump wall and the helium coolant flow.

It takes about 377 seconds for the helium coolant to travel though the pump. The history of the helium coolant thus affects the initial temperature of the helium coolant contained in the pump at the beginning of the time, a feature that is included in the model.

The initial pump-surface temperature is set by a linear interpolation of the experimental data.

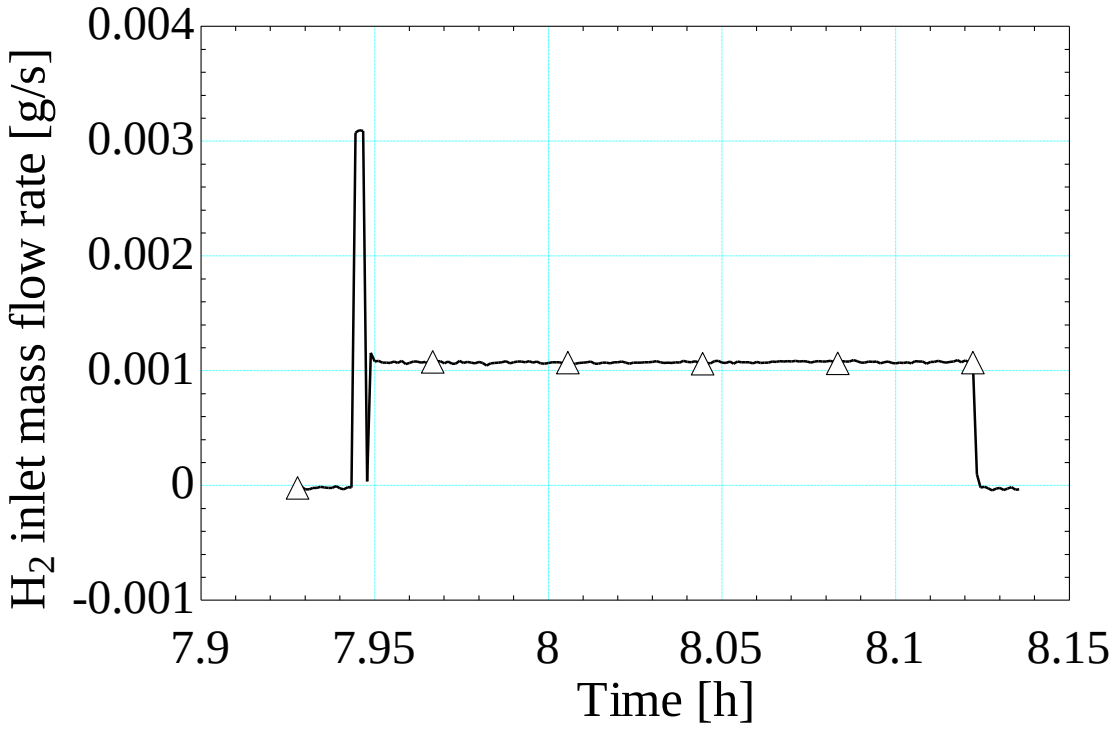

FIGURE 3-6. Hydrogen inlet mass flow rate as a function of time.

FIGURE 3-6 shows the inlet hydrogen mass flow rate being set in the experiment. After the hydrogen mass controller is turned on, the mass flow rate initially rises to about 0.003 g/s for the first 12 seconds, falls to near 0 g/s for the next 6 seconds, and finally remains constant at about 0.0011 g/s.

In order to compare with the experimental data, the initial time of the transient model is set at the 7.95 hour mark as recorded by the experiment.

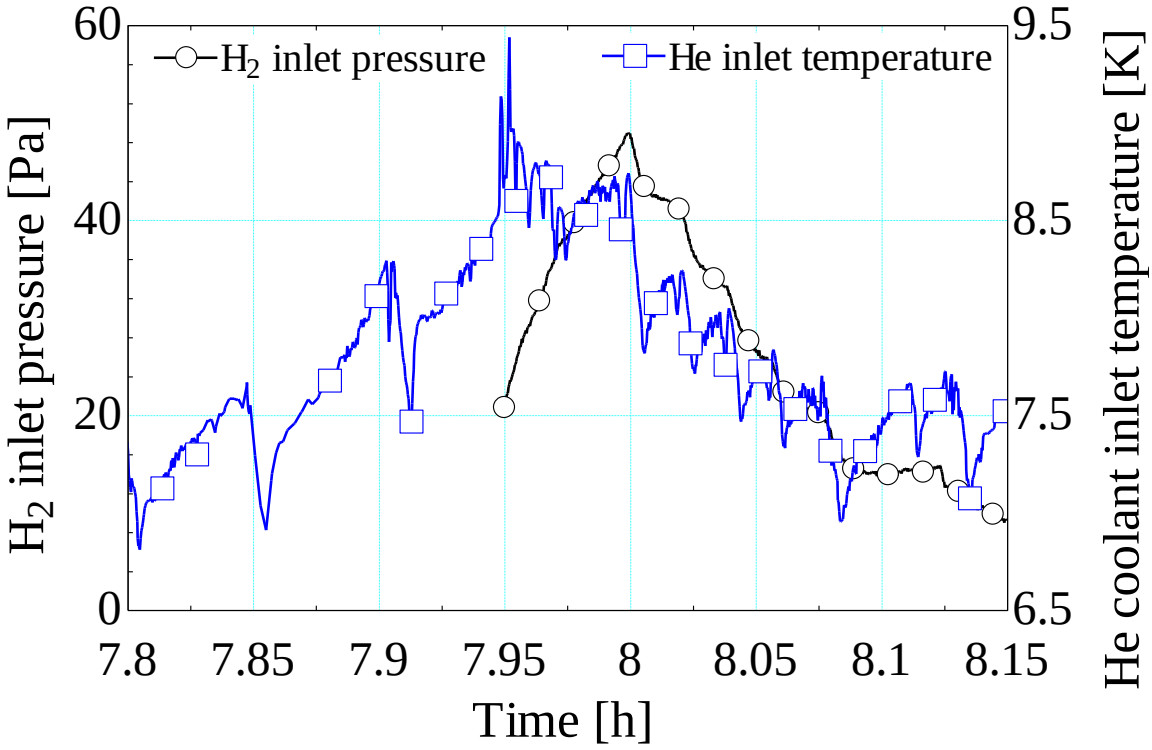

FIGURE 3-7. Inlet hydrogen gas pressure and inlet helium coolant temperature as a function of time (the experimental data set I).

FIGURE 3-7 shows the time dependence of the inlet hydrogen gas pressure and the inlet helium coolant temperature. They are directly plotted from the experimental data set I. The inlet hydrogen pressure follows the trend of the inlet helium coolant temperature in a delayed manner.

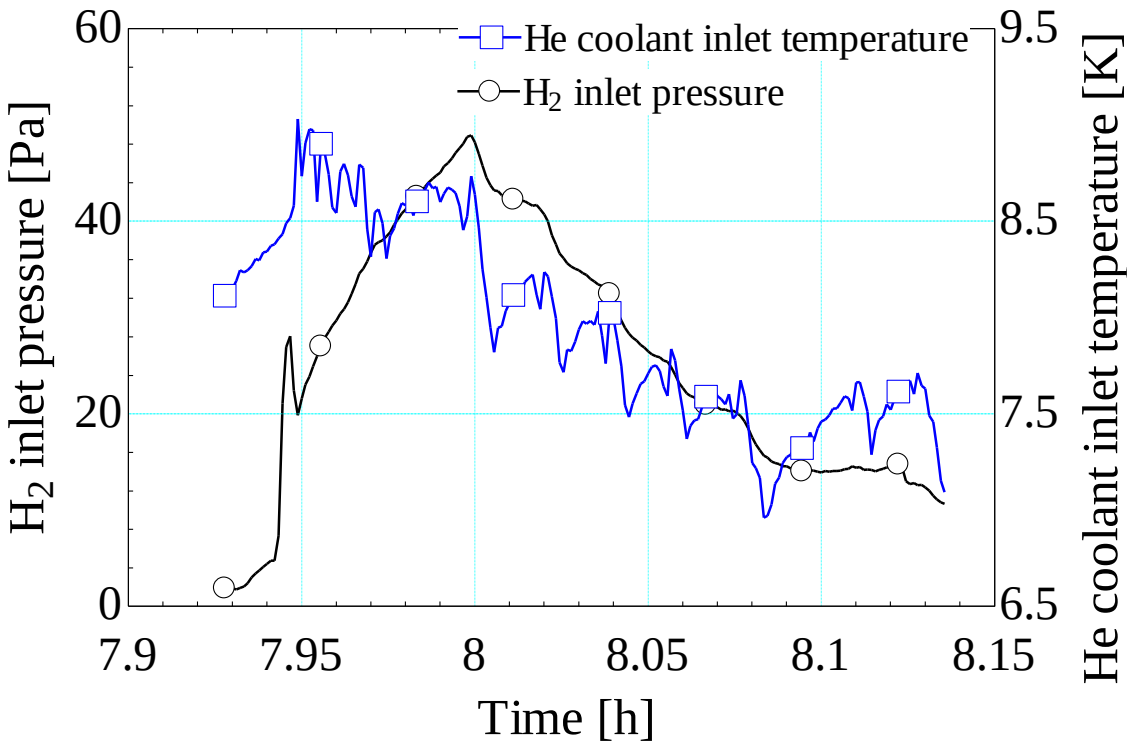

FIGURE 3-8. Inlet hydrogen gas pressure and inlet helium coolant temperature as a function of time (averaged).

FIGURE 3-8 shows the inlet hydrogen gas pressure and inlet helium coolant temperature as a function of time. They are 4-second time-averaged value of the experimental data set I. These two measurements are selected as the input parameters for the transient model. In the experiment, the data are collected every second. However, since the time step in the transient model is about 3.7 seconds, the experimental data is averaged for every 4 seconds. The transient model incorporates a time step size of 4 seconds and uses the 4-second time-averaged experimental data.

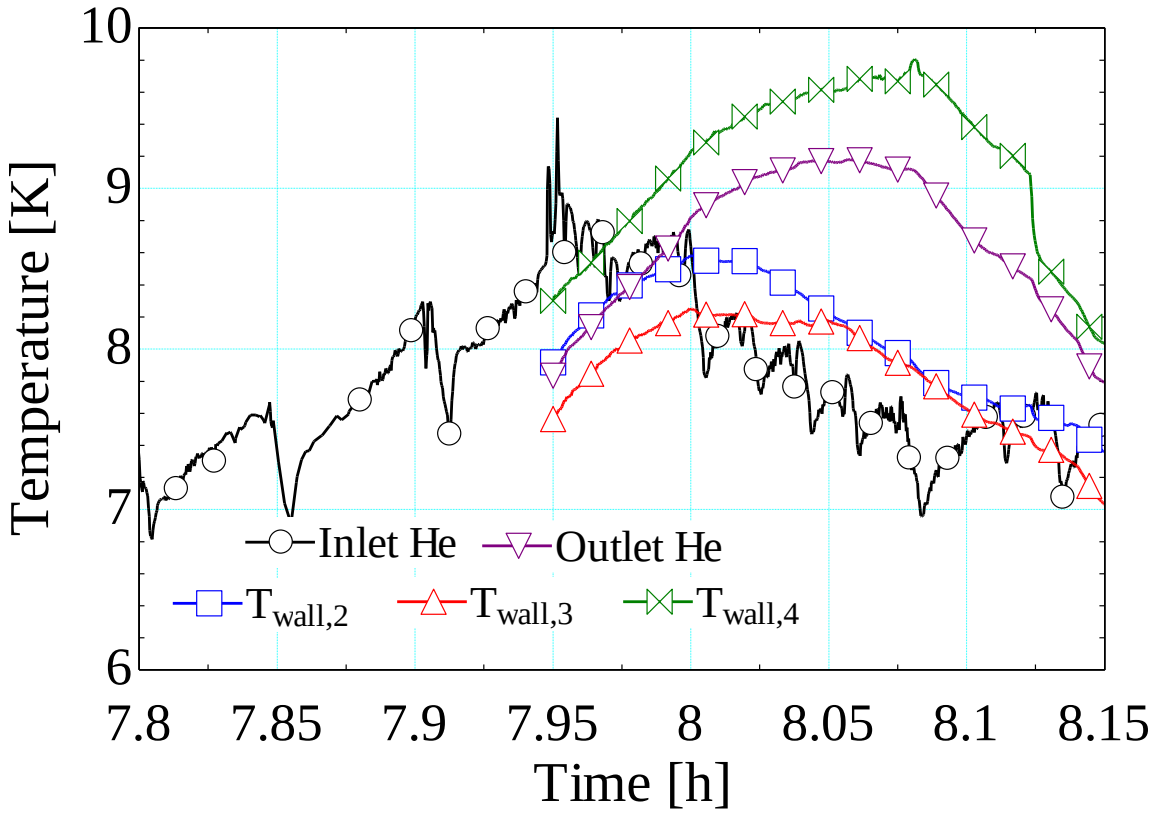

FIGURE 3-9. Inlet and outlet helium coolant temperature and pump wall temperatures as a function of time (experimental data set I).

FIGURE 3-9 shows the temperature measurements as a function of time from the experimental data set I. The inlet helium coolant temperature is taken as an input parameter to the transient model. The other four temperatures will be compared to the modeling results. The wall temperatures response to the inlet helium coolant temperature in a delayed manner.

3.3. The Group-Member numerical technique

The physical analysis generates several governing equations along with the equation of state. However, it is tedious to solve those non-linear coupled equations even

with an assumption of constant thermal and kinetic properties. Furthermore it is not accurate to assume constant thermal and kinetic properties, because properties change with temperature and pressure, and properties at cryogenic temperatures are quite different from those at normal conditions. Additionally, the viscosity and conductivity of the combined hydrogen-helium flow are considered as properties of the gas mixture (Lindsay, 1950) (Wilke, 1950).

3.3.1. Procedure and steps

A novel numerical technique, here named as the Group-Member numerical technique, is proposed to solve such a set of equations with highly-coupled non-linear variables. The Group-Member numerical technique combines an explicit numerical technique with a non-linear equation solving technique, and is basically comprised of three steps as shown in **FIGURE 3-10**. The three steps are Grouping, Numerically Forward Marching, and Solving Non-linear Equations. In the Group-Member numerical technique, the individual unknown variables, which are the ultimate targets to be solved, are referred to as Members, and the combinations of those individual variables, which are the intermediary targets to be solved, are referred to as Groups. In fact, the technique might have been named as Member-Group-Member numerical technique according to its procedure.

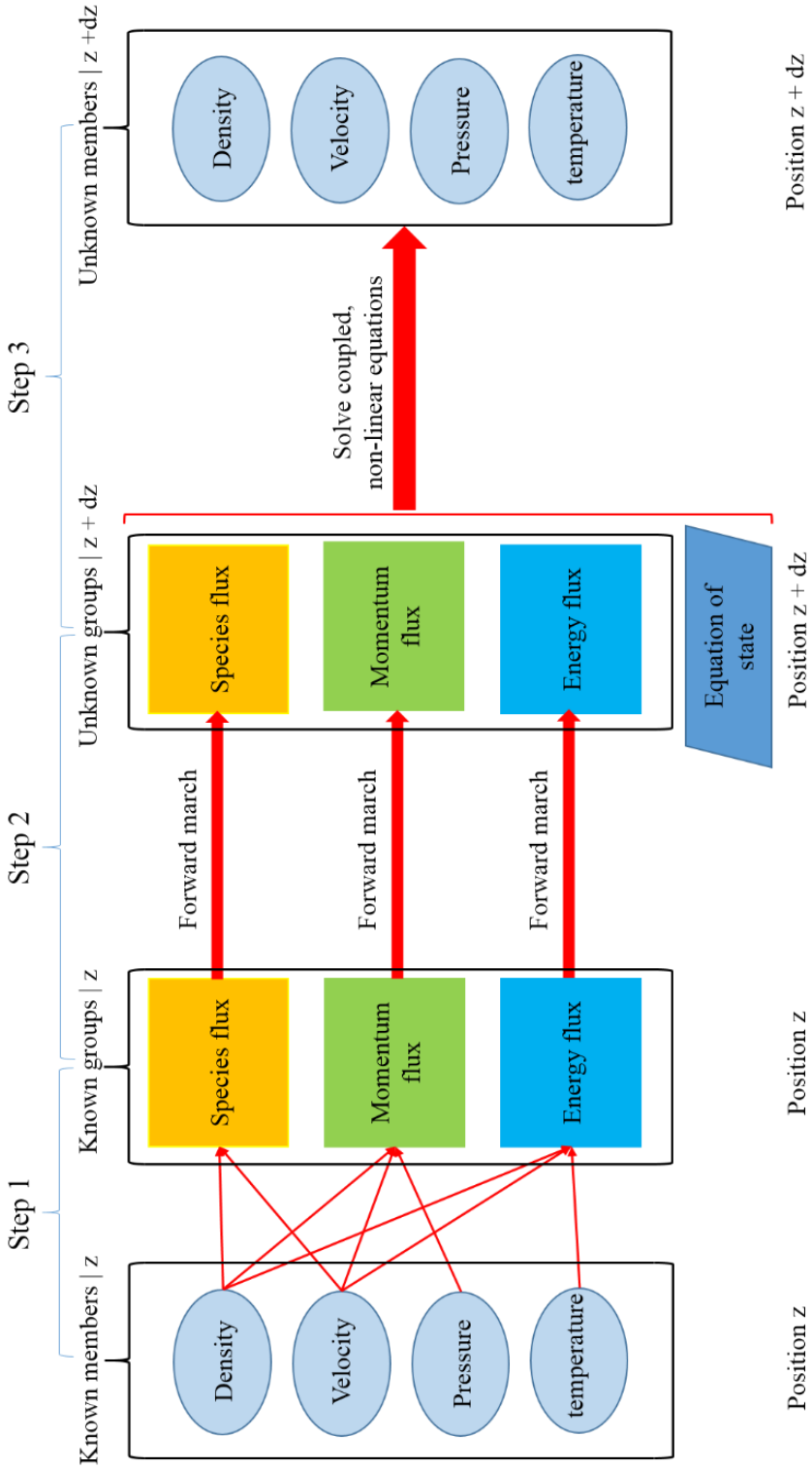

FIGURE 3-10. A flowchart of Group-Member numerical technique for the 1D numerical model.

The first step, Grouping, is to group and transform individual ultimate target variables (Members) into several combinations (Groups) according to the physical meaning and ease of numerically forward marching. In this particular case, the Members are hydrogen density, helium density, axial bulk velocity, bulk temperature, hydrogen pressure, and helium pressure. The Groups are hydrogen mass flux, helium mass flux, axial momentum flux, and energy flux. Since the information of all the individual variables (Members) at the calculation boundary are known, the information of the combinations (Groups) at the calculation boundary are known. In the particular case, the inlet densities, bulk velocity, bulk temperature, and pressures are known, and thus the inlet mass fluxes, momentum flux, and energy flux values are known. There are no assumptions or approximations in step one, and therefore there are also no numerical errors in step one. It is a step of packaging the information and getting ready for Step Two. It should be noticed that the six Members are combined into four Groups, which is equal to the number of the governing equations. In other words, the number of the Groups is not determined by the number of Members but is determined by the number of governing relationships that would be used for numerically marching forward in Step Two. No information is missing as a result of the grouping, because the two equations of state (of hydrogen and helium) are directly adopted in Step Three, and there is no need to numerically march forward using the two equations of state. The result of Step One is that the Groups are formed and serve as new variables that are used in Step Two.

Step Two, numerically marching forward, explicitly solves the new variables (Groups) formed in Step One at a new position under the constraint of the governing equations. The governing equations used in Step Two are the physics governing the process of a problem. And thus the governing equations control the differential change of the variables (Groups). In this particular case, the governing equations are the balance equations of species, momentum, and energy, and they constrain the differential change of mass flux, momentum flux, and energy flux. The explicit numerical method adopted in Step Two determines the order of the Group-Member numerical technique. In this particular case, Euler's method is adopted as the explicit numerical method, and thus the order of the Group-Member numerical technique is first order. If higher order methods are adopted, the order of the Group-Member numerical technique will be increased accordingly. One difference from the common numerical method is that in Step Two, only one numerical step is taken, which means that Groups are only calculated at the position of $z + dz$ based on the values at the position of z, and then Step Two is over. The result of Step Two is that the Groups at the new position of $z + dz$ are now known values. Furthermore, the combinations of the ultimate individual variables (Members) are known values as well.

Step Three, solving the non-linear equations, solves for the ultimate individual variables (Members) at the new position of $z + dz$ based on the value of the Groups at the new position of $z + dz$, which are numerically solved in Step Two. The values of the four Groups generate four equations, which, along with the additional equation of state for hydrogen and helium provide enough equations to solve for the individual Members. As

long as the coupled non-linear equations have physically sound roots, a proper method should be able to find them.

Using the Group-Member numerical technique, the one-dimensional numerical model is solved using the Engineering Equation Solver software, or EES.

3.3.2. Discussions and justifications

The innovation in the Group-Member numerical method is to connect the two separate domains, namely the numerical method and the equation solving technique. The idea of the Group-Member numerical technique is to take advantage of both the numerical technique and the non-linear equation solving technique while at the same time avoiding the cost of both methods. The explicit numerical technique is convenient for marching forward and generating a solution from a known starting point (an information source). However, in the existing situation of non-linear coupled variables it is usually necessary to linearize and uncouple those variables before numerically marching forward. The required effort and skill for the linearization process can be significantly increased with an increase in the complexity of equations. Furthermore, when equation parameters, such as conductivity and viscosity, are functions of unknown variables (temperature, pressure and composition) and cannot be treated as constants, it is even more time-and-effort consuming to solve those set of equations. Further, when the unknown variables appear inside a complicated operation, for example an operation involving the third power of the unknown variable, the linearization step could be impossible. On the other hand, a non-linear equation solving technique is convenient for solving non-linear coupled equations. However, non-linear equation solving techniques can only work on a control volume at

one position where the equations and unknowns are located. There is no information transfer from other positions. The Group-Member numerical technique takes advantage of both techniques.

The goal of the Group-Member numerical technique is to let information travel without tedious effort.

3.4. Results and discussion

The transient model developed to explain experimental data set I includes numerical approximation in both axial position and time step. The specific modeling results discussed in this section are based on the setup of 51 numerical nodes and 155 time steps. The associated node length is 0.02092 m and the time step is 4 seconds.

This section is divided as follows. **SECTION** 3.4.1. Variable profiles as a function of axial position) and **SECTION** 3.4.2. Time dependence of variable discuss the variable profiles as a function of axial position and as a function of time respectively. The results of the transient model are compared with the experimental data in **SECTION** 2.2.1. Experimental data set I**. SECTION** 3.4.3. Hydrogen pressure and adsorption discusses the hydrogen pressure and adsorption.

3.4.1. Variable profiles as a function of axial position

The modeling results that use the data shown in **FIGURE 3-8** as input information are presented as follows. The profile of the hydrogen gas temperature as a function of axial position is shown as **FIGURE 3-11**, **FIGURE 3-12**, and **FIGURE 3-13**. The profile of the pump wall temperature is shown as **FIGURE 3-14** and **FIGURE 3-15**. The profile of the helium coolant temperature is shown as **FIGURE 3-16**. The profile of the hydrogen gas

pressure is shown as **FIGURE 3-17**. The profile of the hydrogen gas bulk density is shown as **FIGURE 3-18**. The profile of the axial hydrogen gas bulk velocity is shown as **FIGURE 3-19**. The profile of the radial hydrogen mass flux is shown as **FIGURE 3-20**. The profile of the radial energy flux is shown as **FIGURE 3-21** and **FIGURE 3-22**. The profile of the radial convection heat flux is shown as **FIGURE 3-23** and **FIGURE 3-24**. The profile of the axial hydrogen gas mass flux is shown as **FIGURE 3-25**.

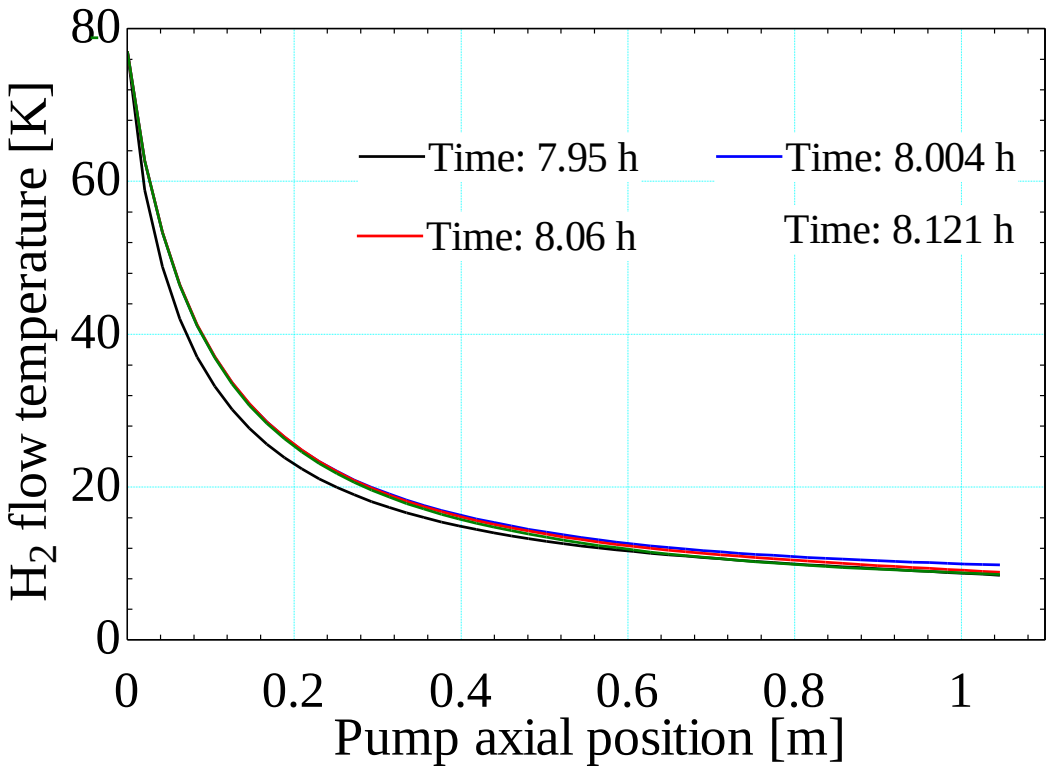

FIGURE 3-11. Hydrogen gas temperature as a function of pump axial position at 4 time steps (I).

FIGURE 3-11 shows the profiles of the hydrogen flow bulk temperature as a function of the axial pump position. The profiles are plotted for 4 time steps that are 7.95 h, 8.004 h, 8.06 h, and 8.121 h.

Since the hydrogen gas is precooled by a nitrogen bath at 77 K in the experiment, the inlet temperature of the hydrogen gas is set at a constant value of 77 K in the transient model.

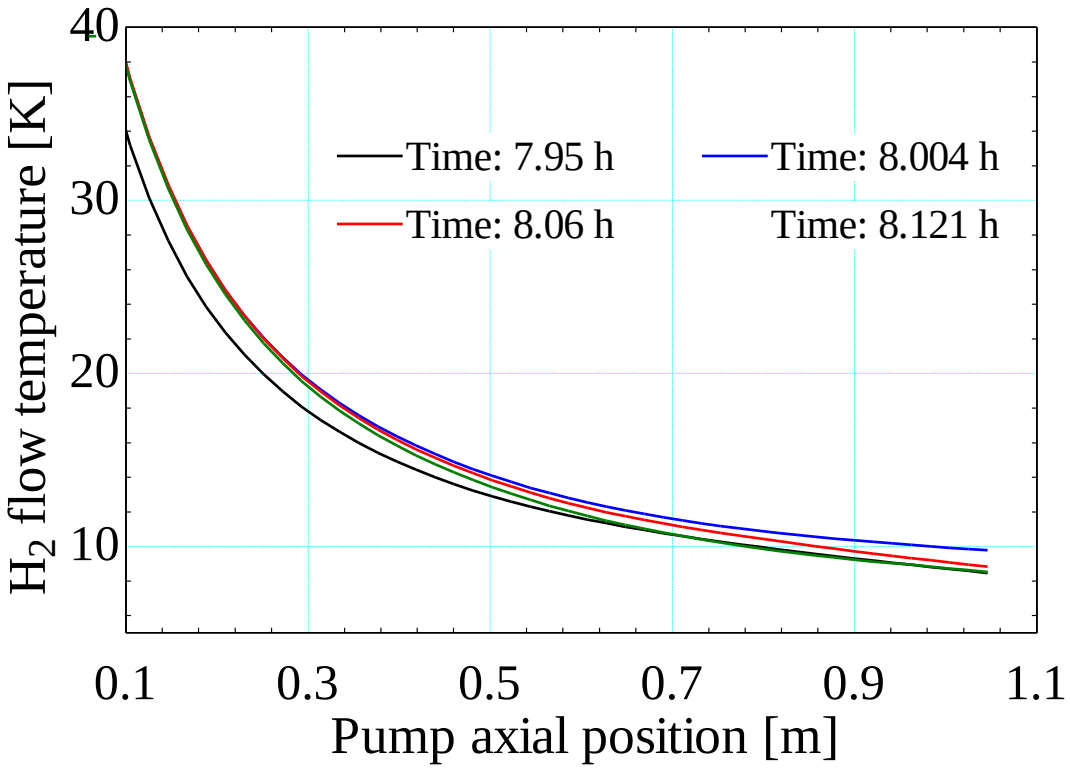

FIGURE 3-12. Hydrogen gas temperature as a function of pump axial position at 4 time steps (II).

Note significantly, the rapid temperature drop of the gas at the entrance of the pump. This feature is due to the large temperature difference and the high heat transfer coefficient in this region. Compared to **FIGURE 3-11**, **FIGURE 3-12** shows that the hydrogen temperature drops to half of its inlet value within the first 0.1 m.

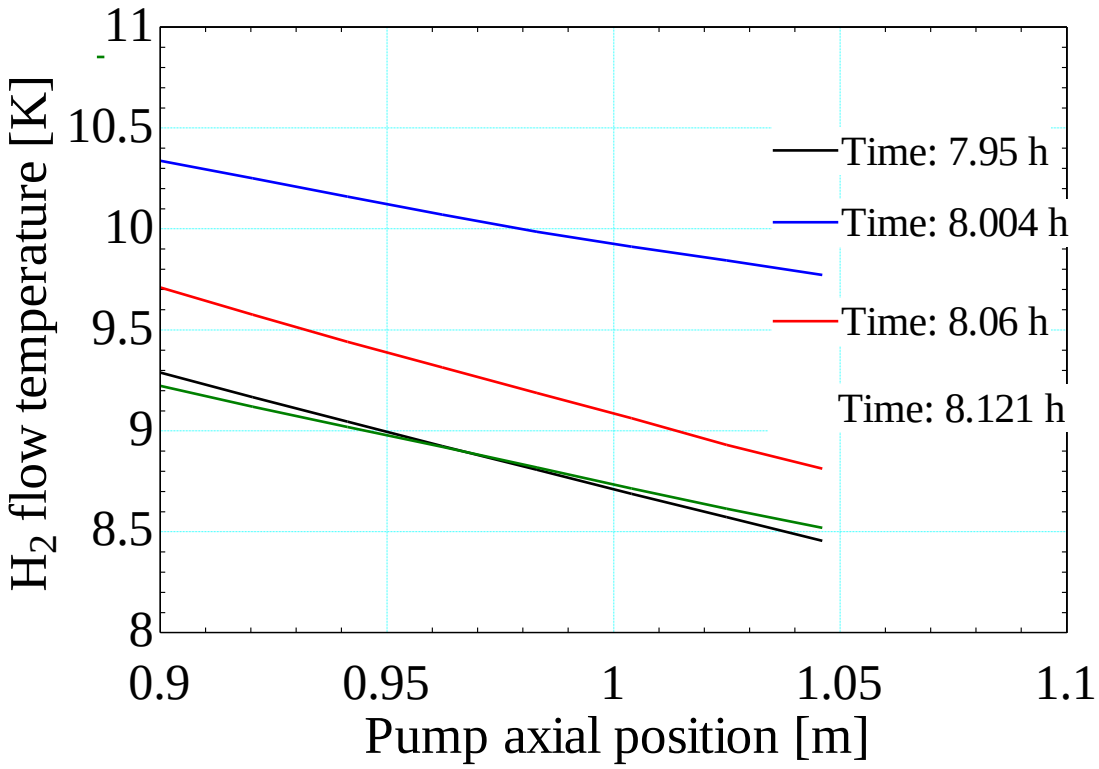

FIGURE 3-13. Hydrogen gas temperature as a function of pump axial position at 4 time steps (III).

At the outlet end of pump, the hydrogen gas temperature is close to and dominantly determined by the inlet helium coolant. The inlet helium coolant temperature is read from the experimental data and it varies with time. The effect of that variation is shown as **FIGURE 3-13**.

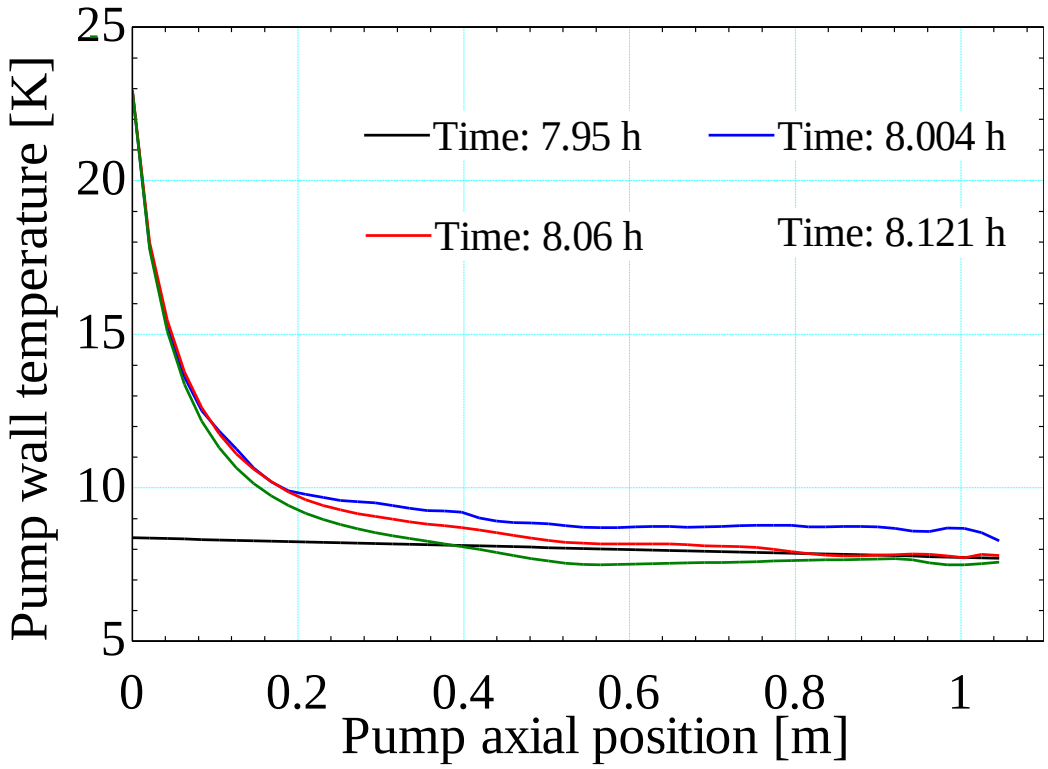

FIGURE 3-14. Pump wall temperature as a function of axial position at 4 time steps (I).

FIGURE 3-14 shows the pump wall temperature as a function of axial pump position. The temperature profiles at 4 time steps are plotted.

In the experiment, the pump is precooled by the helium coolant. The transient model thus sets the initial pump wall temperature (at Time: 7.95 h) accordingly. Once the hydrogen gas is introduced, the pump wall temperature rises immediately at the pump entrance. The pump wall temperature at the hydrogen inlet end (near the axial position of 0 m) is dominantly determined by the inlet hydrogen gas. Since the inlet hydrogen

temperature is maintained as 77 K, the pump wall temperature at the entrance is almost a constant.

A little farther into the pump (beyond the axial position of 0.2 m), the pump wall temperature is dominantly controlled by the helium coolant. It means that the helium coolant has enough cooling power under the current experimental setting.

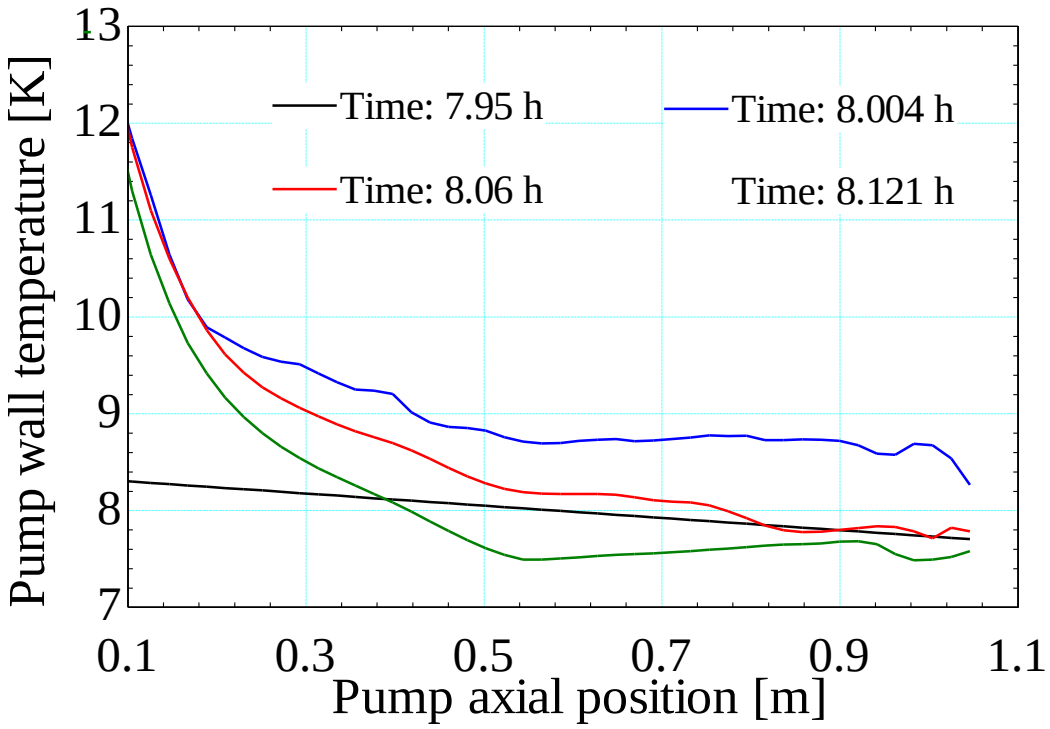

FIGURE 3-15. Pump wall temperature as a function of axial position at 4 time steps (II).

FIGURE 3-15 shows the pump wall temperature beyond the axial position of 0.1 m. The variation in the temperature is clear and it is primarily due to the variation in the inlet helium coolant temperature. The pump (beyond the axial position of 0.2 m) is sufficiently cooled and maintained at low temperatures by the helium coolant. As long as

the inlet helium coolant temperature is low enough, hydrogen molecules will be absorbed at those positions. Since the pump wall temperature is lower at the outlet end, the adsorption of hydrogen molecules occurs at the locations farther into the pump instead of near the entrance. This is a desirable feature because the entrance will not be blocked.

The pump wall temperature rises (from the Time of 7.95 h to the Time of 8.004 h) and then drops (from the Time of 8.004 h to the Time of 8.121 h). At the pump entrance, the rise is because of the introduction of the warm hydrogen gas. At the pump outlet, the rise is due to the increase of the inlet helium coolant temperature (**FIGURE 3-16**). The drop is because of the variation in the inlet helium coolant temperature.

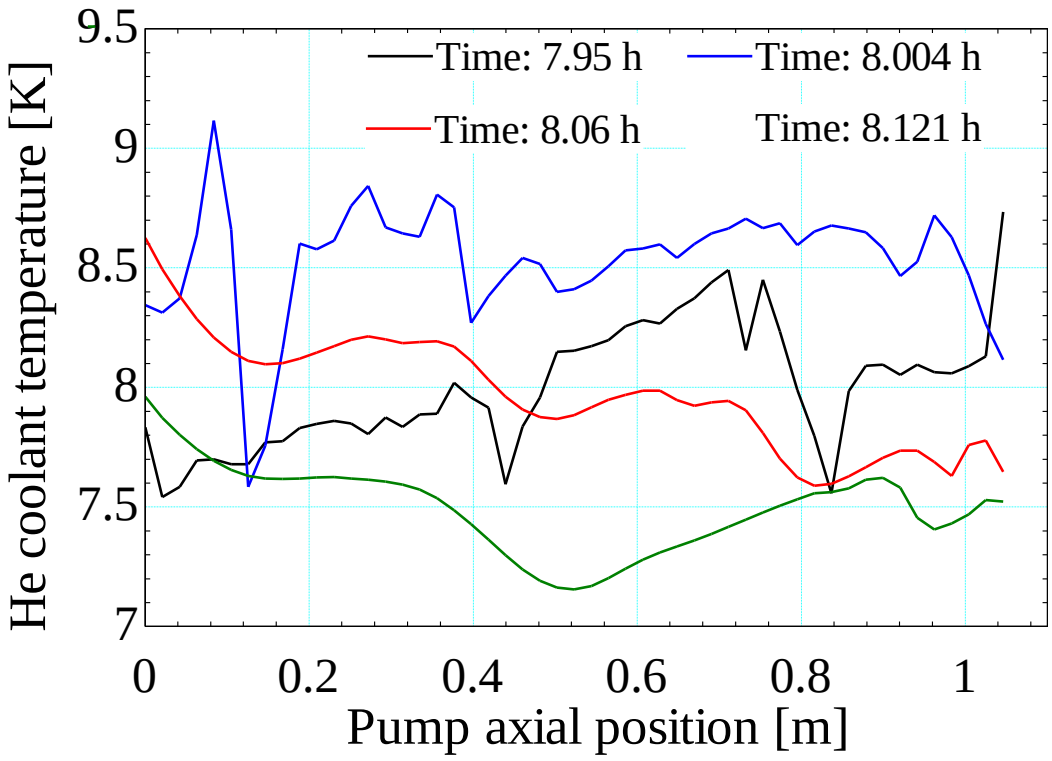

FIGURE 3-16. Helium coolant temperature as a function of axial position for four time steps.

FIGURE 3-16 shows the helium coolant temperature as a function of axial pump position. The initial temperature (at the Time of 7.95 h) of the helium coolant contained in the pump is set by consideration the history of the helium coolant temperature. There is thus a variation in the temperature at the Time of 7.95 h. The variation fades out with time. The inlet helium coolant temperature is read from the experimental data. As mentioned above it is not experimentally controlled as a constant parameter, and this feature significantly affects the helium temperature in the pump.

The helium coolant temperature does not change significantly as it flows through the pump, because its heat capacity is much larger than that of the hydrogen gas and the pump wall.

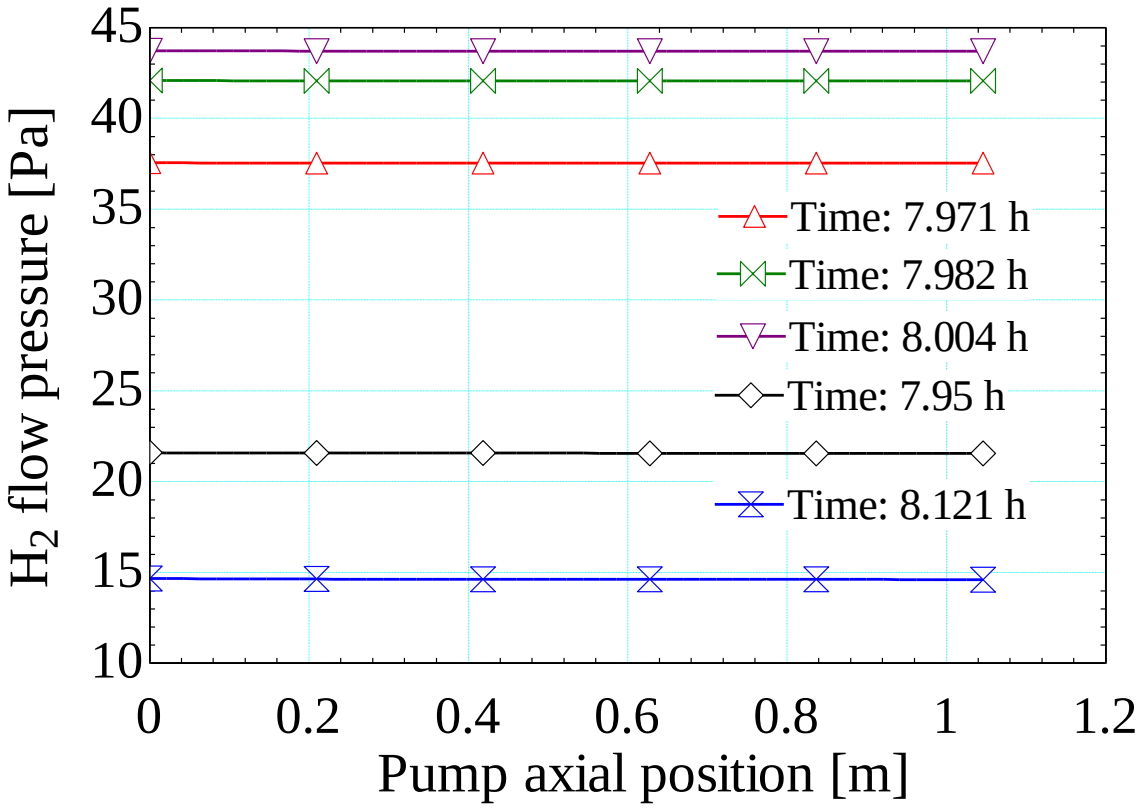

FIGURE 3-17. Hydrogen flow pressure as a function of pump axial position.

FIGURE 3-17 shows the hydrogen gas pressure as a function of axial pump position. The pressure varies with time. However at any given moment, the spatial pressure drop through the pump is negligibly small. The pressure drop in the pump is due to the wall friction that is small for gas flow.

The variation of pressure with time is due to the wall-temperature-dependent sublimation or adsorption of the hydrogen molecules. The sublimation or adsorption process is a boundary condition for the control volume of the hydrogen gas. Any change in the boundary condition immediately affects the hydrogen gas pressure, because that information travels at the speed of sound. The sublimation or adsorption process strongly

depends on the pump wall temperature. A 1-K change in the wall pump temperature can lead to orders of magnitude change in the adsorption rate (indicated by the hydrogen vapor pressure). The change is reflected by the hydrogen pressure.

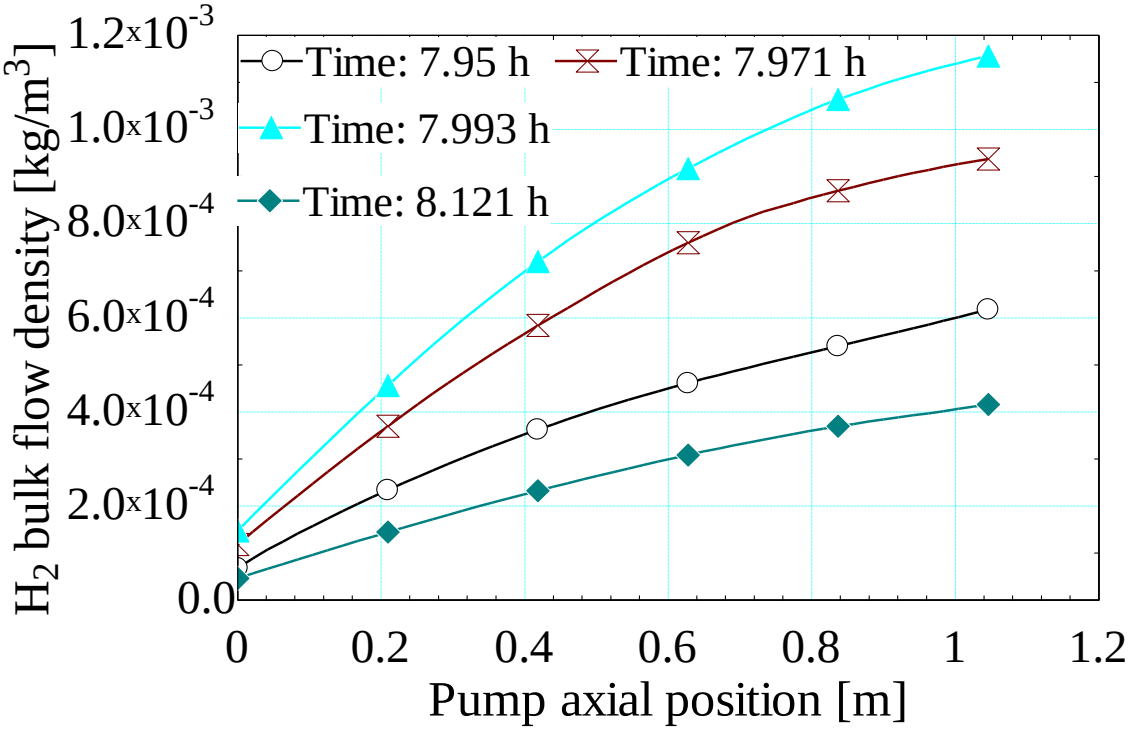

FIGURE 3-18. Hydrogen bulk density as a function of pump axial position.

FIGURE 3-18 shows the profiles of the hydrogen gas density. The density goes up as the hydrogen gas travels into the pump, because the gas is cooled by the pump. The inlet density varies with time is actually the reflection of the time dependence of the inlet hydrogen pressure.

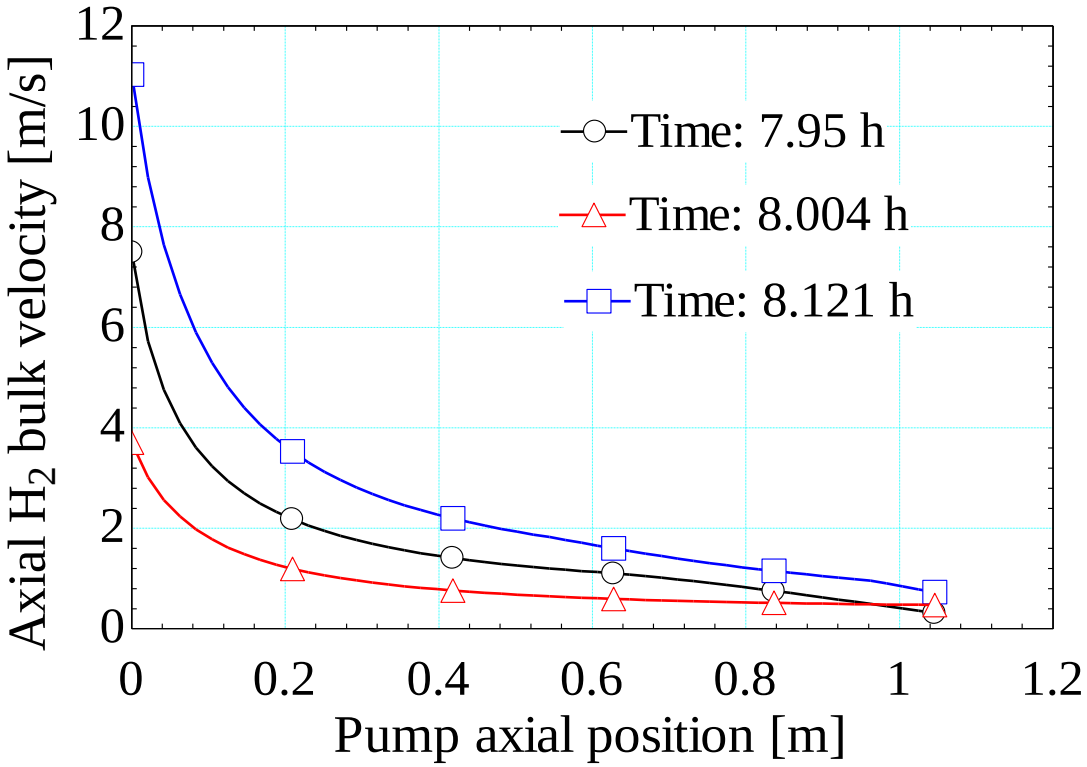

FIGURE 3-19. Axial hydrogen bulk velocity as a function of pump axial position.

FIGURE 3-19 shows the profiles of the axial hydrogen bulk velocity. The axial hydrogen bulk velocity decreases as the gas travels into the pump. That decrease is mainly due to the cooling effect. As the gas is cooled and the pressure remains constant, the density rises. Therefore the velocity has to decrease in order to maintain the same mass flow rate.

The inlet velocity is not a constant as a result of the changing inlet hydrogen pressure. The inlet hydrogen mass flow rate is controlled as a constant by the mass controller. The inlet temperature is maintained as a constant by the nitrogen bath. The inlet pressure changes with time because of changing adsorption power due to the variable inlet helium coolant temperature. And the inlet density thus changes according to the equation

of state. And therefore the inlet velocity has to change accordingly to maintain a constant inlet mass flow rate.

The density increases to the maximum at the pump outlet in **FIGURE 3-18** while the bulk velocity decreases to the minimum at the same location in **FIGURE 3-19**.

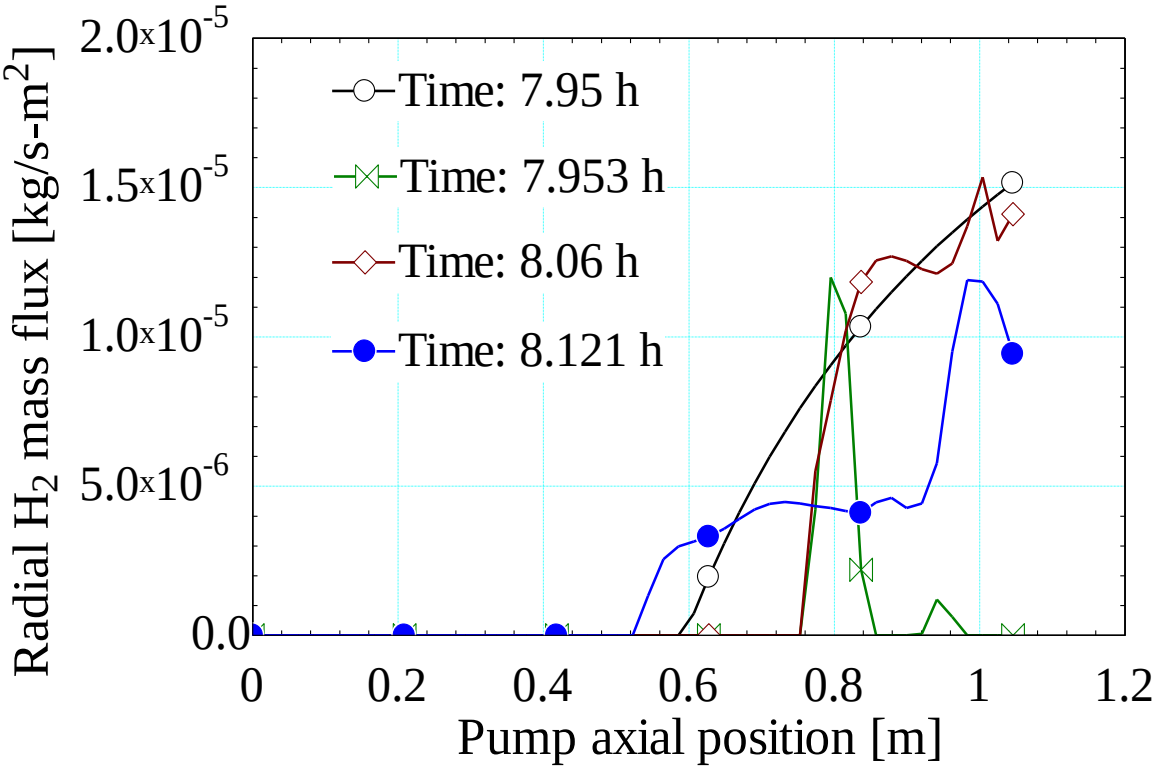

FIGURE 3-20. Radial hydrogen mass flux as a function of pump axial position.

FIGURE 3-20 shows the profiles of the radial hydrogen mass flux. The radial hydrogen flux is the adsorption flux of hydrogen molecules onto the pump wall. The adsorption happens where the pump wall is cold enough. The result agrees with the pump wall temperature in **FIGURE 3-14** and **FIGURE 3-15**.

The mass flux is the maximum at the Time of 7.95 h because the pump wall is precooled and initially at its lowest temperature. As the pump wall temperature increases, the mass flux decreases. **FIGURE 3-20** shows the flux variation with time and location. That variation is again the result of the variation of the pump wall temperature.

The hydrogen molecules are mainly absorbed in the downstream half of the pump, where the pump wall is cooled to low temperatures. There the corresponding hydrogen vapor pressure is so low that the hydrogen molecules are deposited onto the pump wall. The deposition is modeled as the diffusion process driven by the hydrogen density difference.

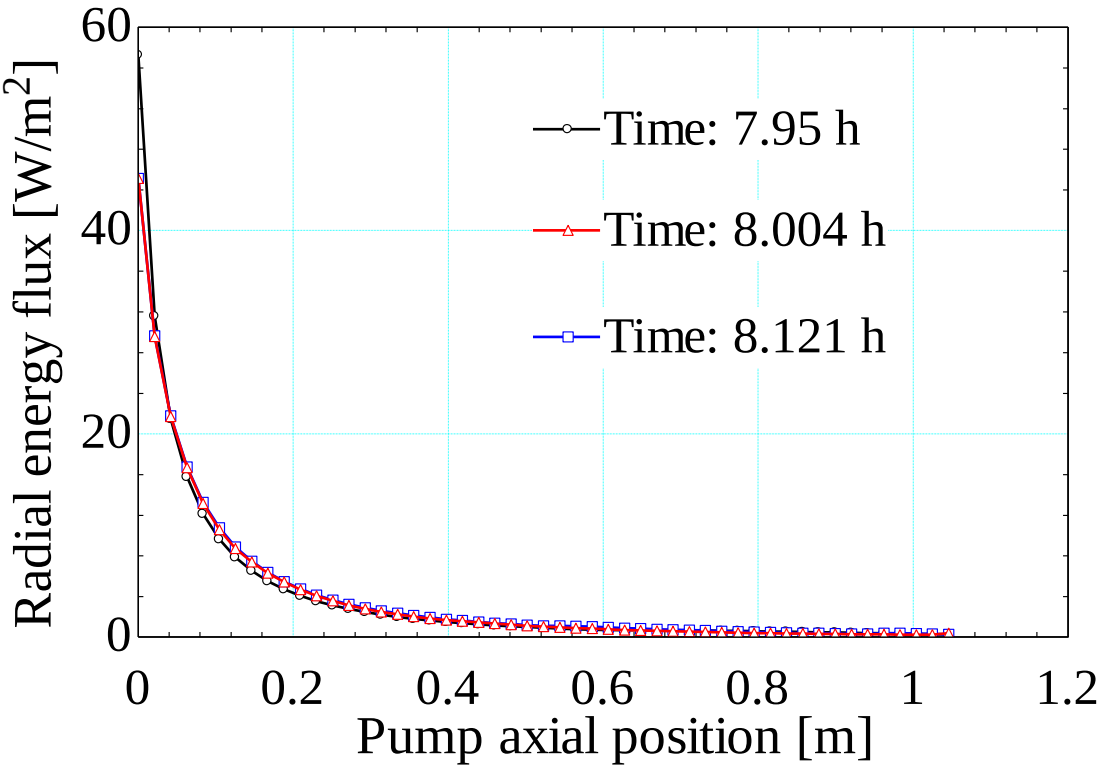

FIGURE 3-21. Radial energy flux as a function of pump axial position (I).

FIGURE 3-21 shows the profiles of the radial energy flux. The radial energy flux is the total energy flux transferred from the hydrogen gas to the pump wall, and is the sum of the convection heat transfer flux and the adsorption energy flux.

Most of the energy transfer occurs within the first 0.2 m because both the heat transfer coefficient and the temperature difference is high at the pump entrance. The profile remains nearly constant with time.

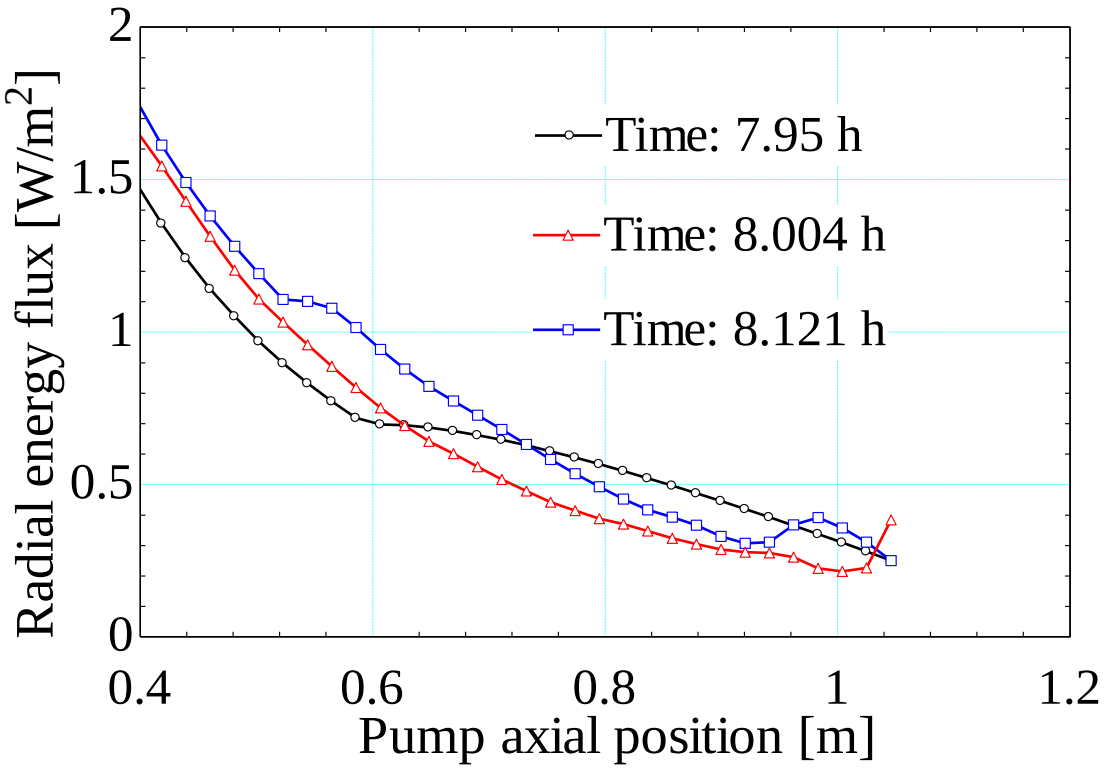

FIGURE 3-22. Radial energy flux as a function of pump axial position (II).

FIGURE 3-22 shows the profiles of the radial energy flux for the second half of the pump. The lumps in the profiles are the result of the adsorption heat of the hydrogen molecules. Note that the convective heat transfer is much larger than the adsorption heat.

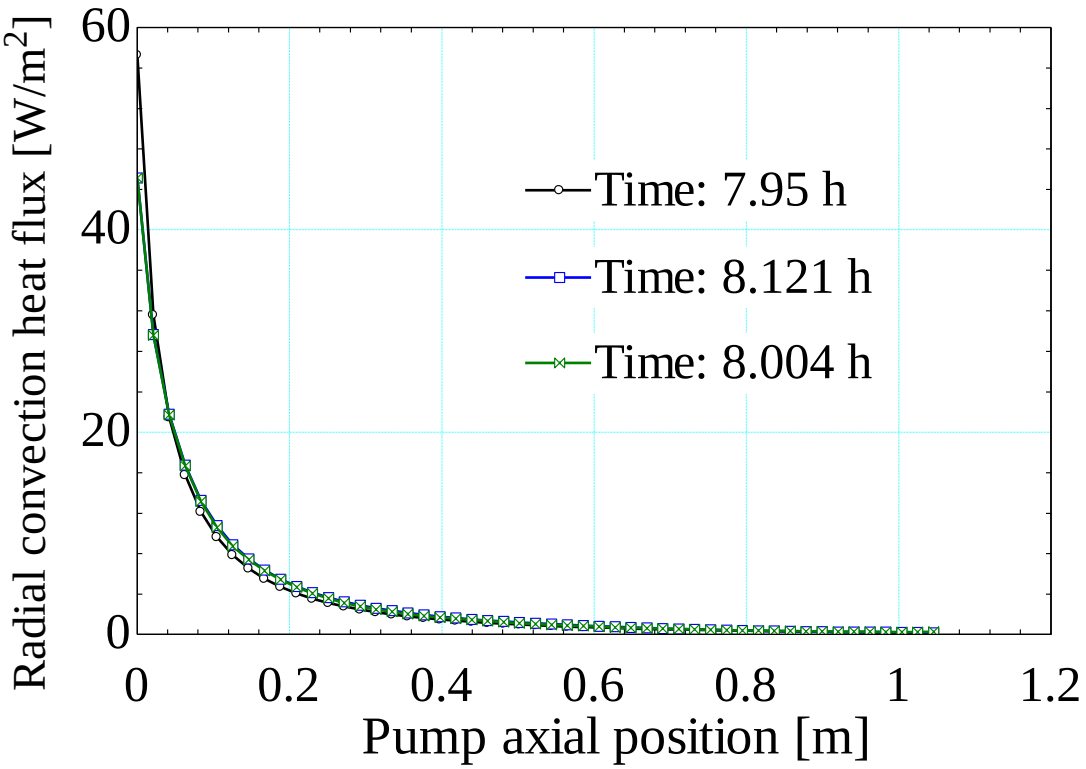

FIGURE 3-23. Radial convection heat flux as a function of pump axial position (I).

FIGURE 3-23 shows the profiles of the radial convective heat flux. They are very similar to the profiles of the total energy flux. Most of the convective heat flux happens at the pump entrance. Within the first 0.2 m, the heat flux nearly drops by a factor of 10.

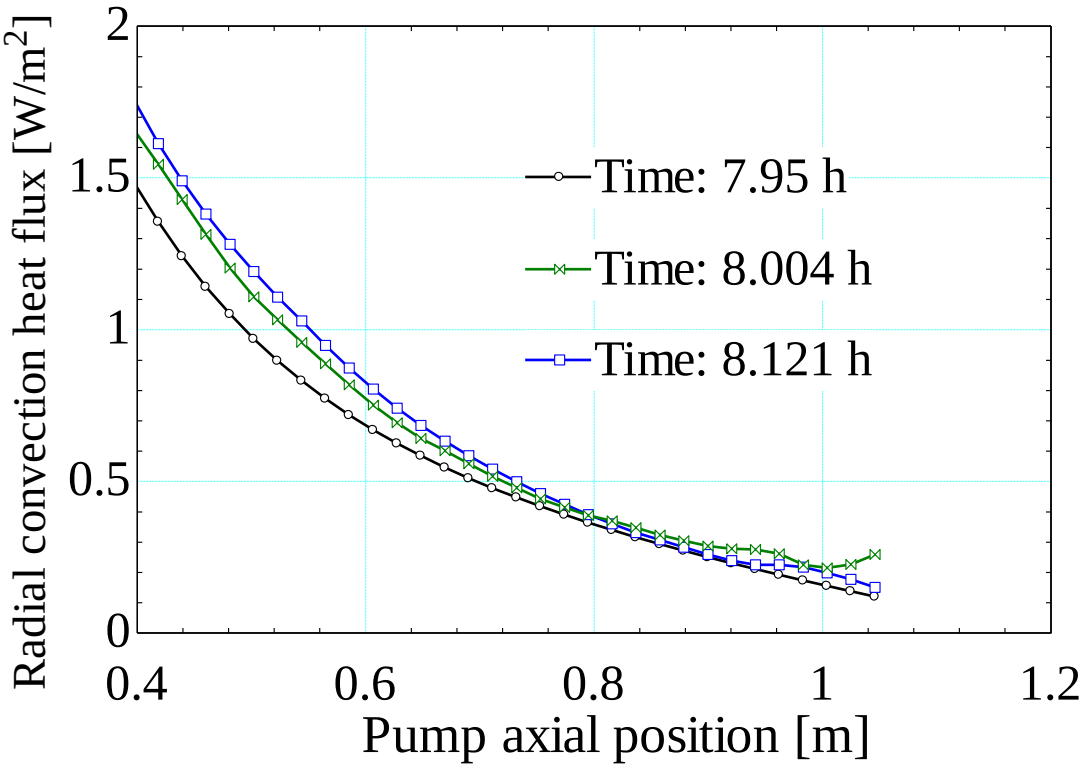

FIGURE 3-24. Radial convection heat flux as a function of pump axial position (II).

FIGURE 3-24 shows the profiles of the convective heat flux for the second half of the pump. Compared to **FIGURE 3-22**, it is clear that the adsorption heat is the reason for the lumps of the profiles in **FIGURE 3-22**. The difference between **FIGURE 3-22** and **FIGURE 3-24** is the adsorption heat flux.

In future iterations of the model, the convection heat transfer coefficient should be reduced since the adsorbed molecules do not transfer the wall information back to the gas, and thus a smaller number of molecules are available to transfer the energy.

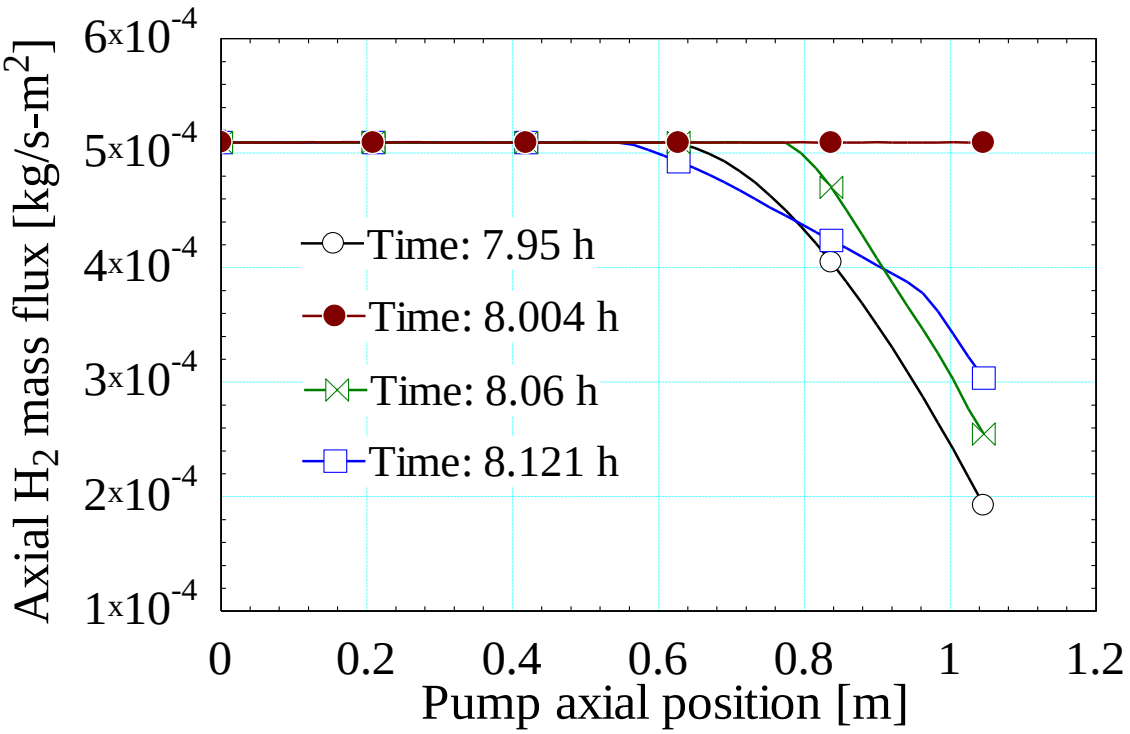

FIGURE 3-25. Axial hydrogen mass flux as a function of pump axial position.

FIGURE 3-25 shows the profiles of the axial hydrogen mass flux. When adsorption occurs, the axial hydrogen mass flux decreases. Initially (at the Time of 7.95 h), the pump wall is at the lowest temperature and the axial hydrogen mass flux decreases the most. As the pump wall temperature increases, the axial mass flux decreases less. At the Time of 8.004 h, the pump wall temperature is so high that the axial hydrogen mass flux essentially remains constant.

3.4.2. Time dependence of variables

In this section some results of the transient model are compared with the experimental data set I, as shown in **FIGURE 3-26**, **FIGURE 3-27**, **FIGURE 3-28**, and

FIGURE 3-29. Some of the modeling results do not have matching experimental data, and they are shown in **FIGURE 3-30** - **FIGURE 3-38**.

In the experiment, four thermometers are mounted on the outer surface of the inner tube. Three of them, $T_{wall,2}$ (at the axial position of 0.7112 m), $T_{wall,3}$ (at the axial position of 0.4064 m), and $T_{wall,4}$ (at the axial position of 0.1016 m) provide measurement data. Additionally, the inlet and outlet helium coolant temperatures are measured.

The results of the transient model for the pump wall temperatures at the axial positions of 0.7112 m, 0.3974 m, and 0.1046 m, and the outlet helium coolant temperature are compared with the experimental measurements taken at approximately the same locations.

Note significantly, the wall temperature measurements in the experiment are only close to the wall temperature. The thermometers are not exactly on the pump wall, and their measurements are affected by the helium coolant flow. In contrast, the modeling results presented below are exactly the pump wall temperatures.

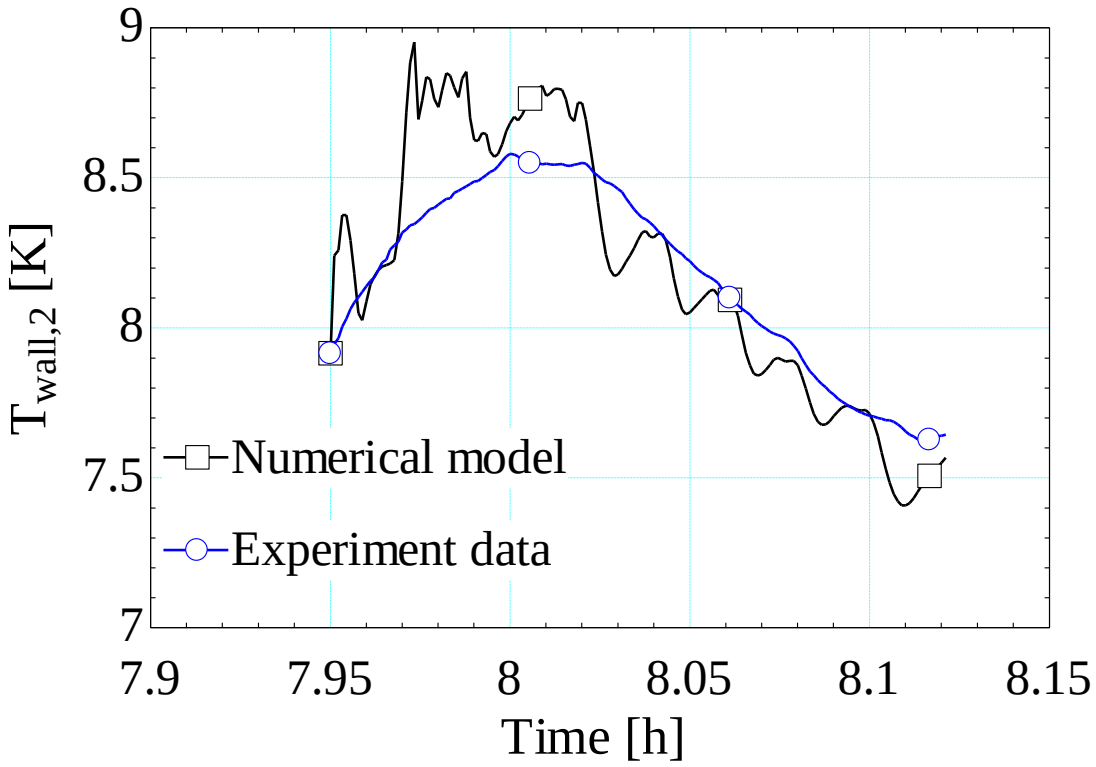

FIGURE 3-26. Modeling result and experiment measurement for $T_{wall,2}$ as a function of time.

FIGURE 3-26 compares the results of the transient model with the experimental data set I for the thermometer $T_{wall,2}$. The modeling results show more variation than the experimental data because of their sensitivity to the inlet helium coolant temperature that varies significantly with time.

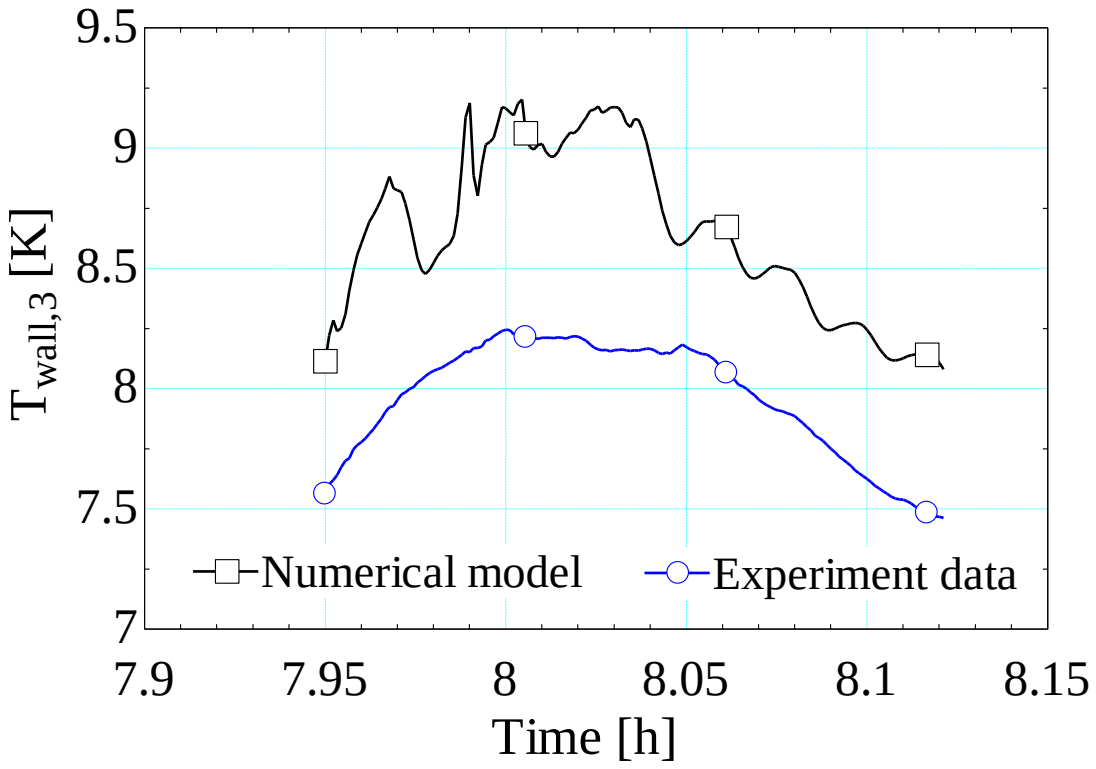

FIGURE 3-27. Modeling result and experiment data for $T_{wall,3}$ as a function of time.

FIGURE 3-27 compares the modeling results with the experimental data for thermometer $T_{wall,3}$. The model results and the experimental data follow the same trend, but display a noticeable temperature difference. **FIGURE 3-9** (The experimental data set I) shows the curious feature that $T_{wall,3}$ is lower than $T_{wall,2}$. $T_{wall,2}$ is closer to the inlet helium coolant end and thus should be lower than $T_{wall,3}$. The temperature difference shown in may therefore be due to a measurement error associated with thermometer $T_{wall,3}$.

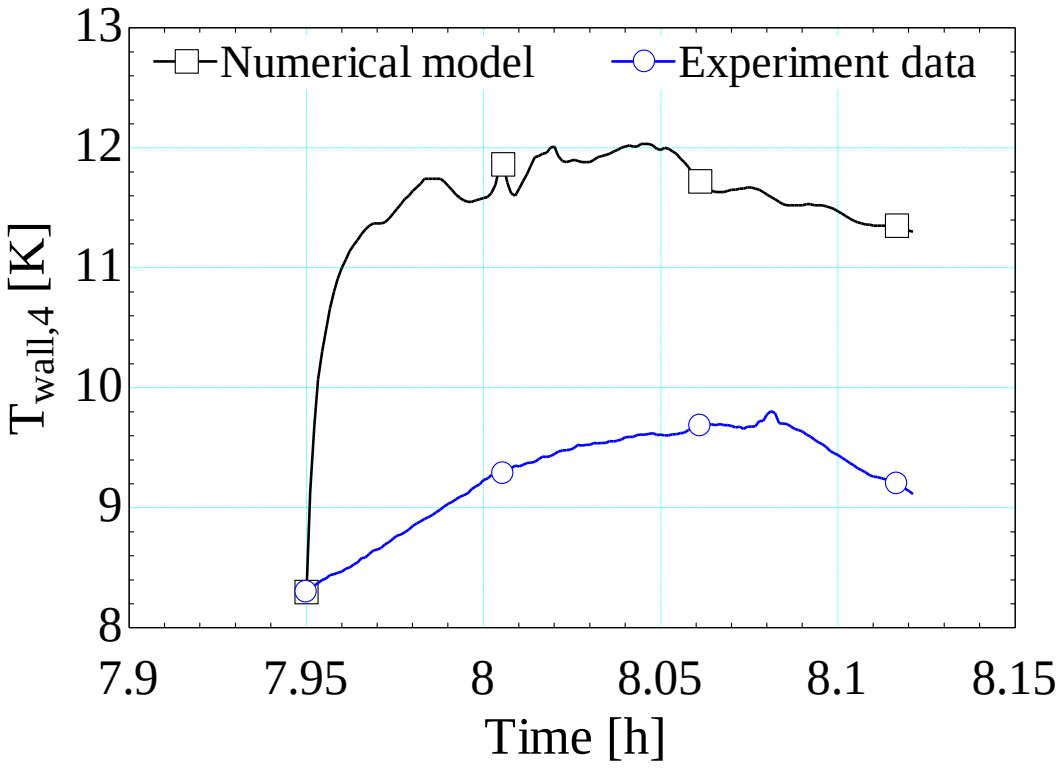

FIGURE 3-28. Modeling result and experiment data for $T_{wall,4}$ as a function of time.

FIGURE 3-8 compares the modeling results with the experimental data at the thermometer of $T_{wall,4}$. There is a temperature difference between the model and the data. Again the thermometers are not exactly on the pump surface, and are affected by the helium coolant. The insulation of thermometers in the experiment may not be perfect.

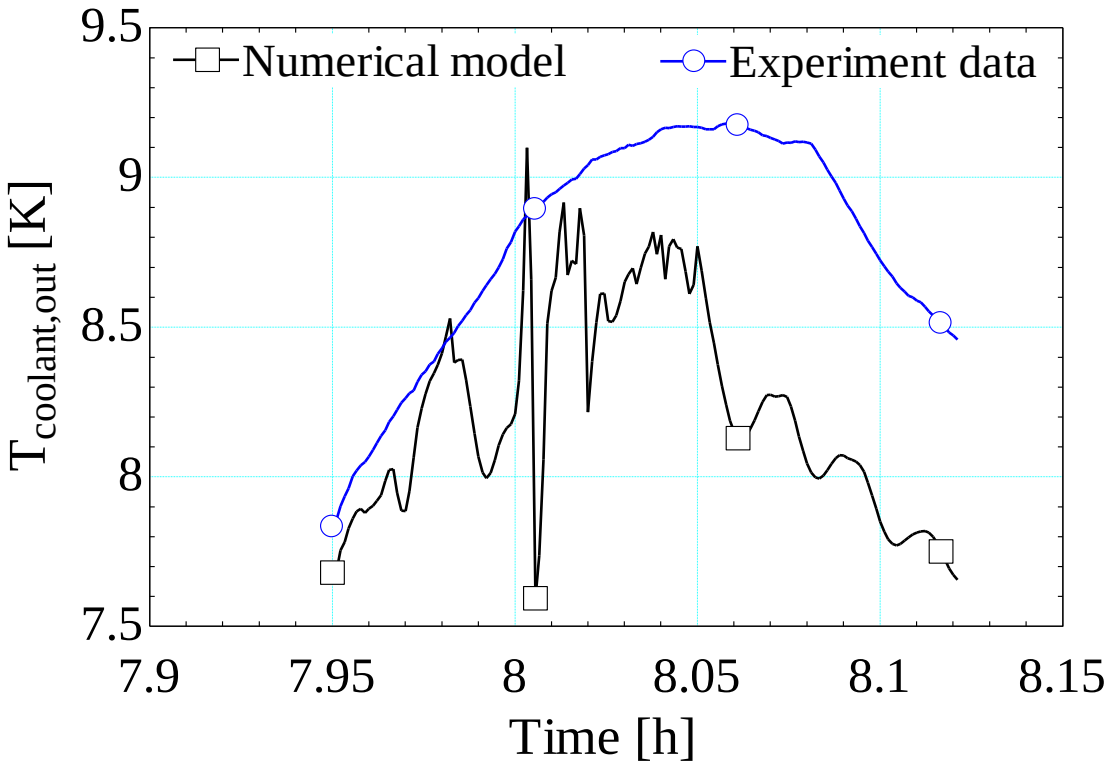

FIGURE 3-29. Modeling result and experiment data for $T_{outlet,He}$ as a function of time.

FIGURE 3-29 compares the modeling results and the experimental data for the outlet helium coolant temperature. The fluctuations in the modeling results are due to the variation in the initial helium coolant temperature.

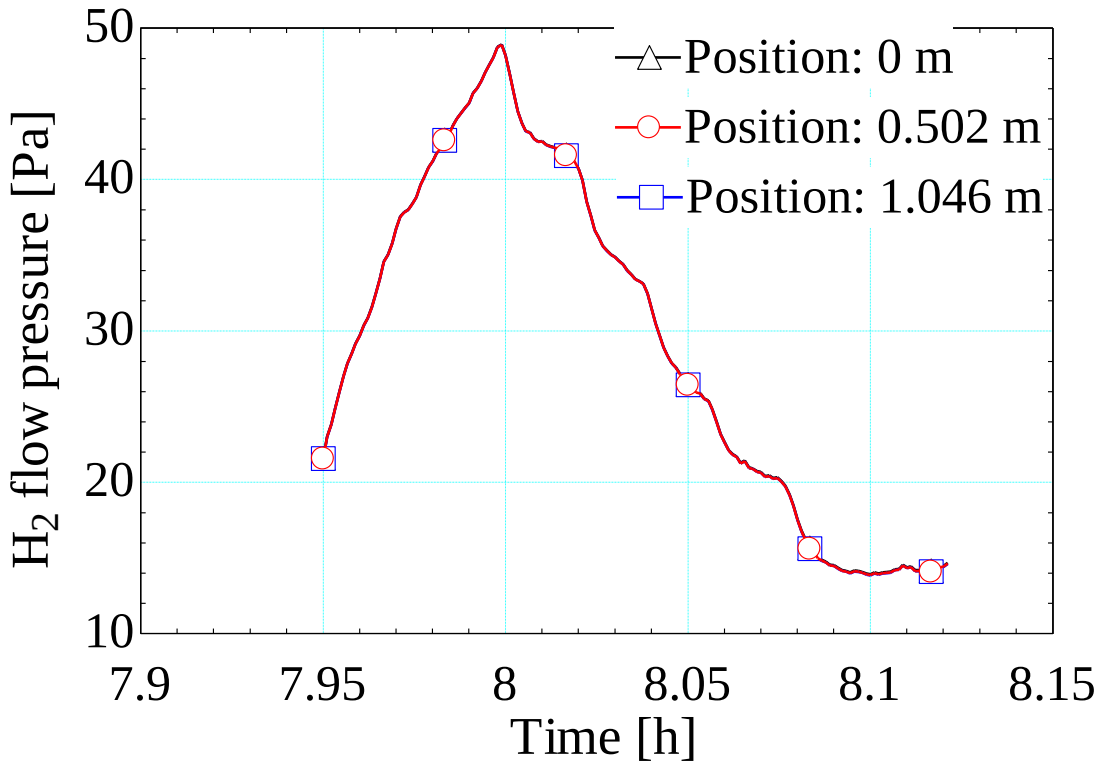

FIGURE 3-30. Hydrogen flow pressure as a function of time.

FIGURE 3-30 shows the time dependence of the hydrogen pressure at three axial positions. The pressure varies with time but it is spatially uniform at any given moment. The hydrogen pressure changes with time because of the changing pumping power. The spatial difference is negligible because of small friction. Note that only the pressure at the position of 0 m is used as the input parameter to the model, and that the other two pressures (at the position of 0.502 m and 1.046 m) are calculated from the model. That implies the negligibly small pressure drop in the pump.

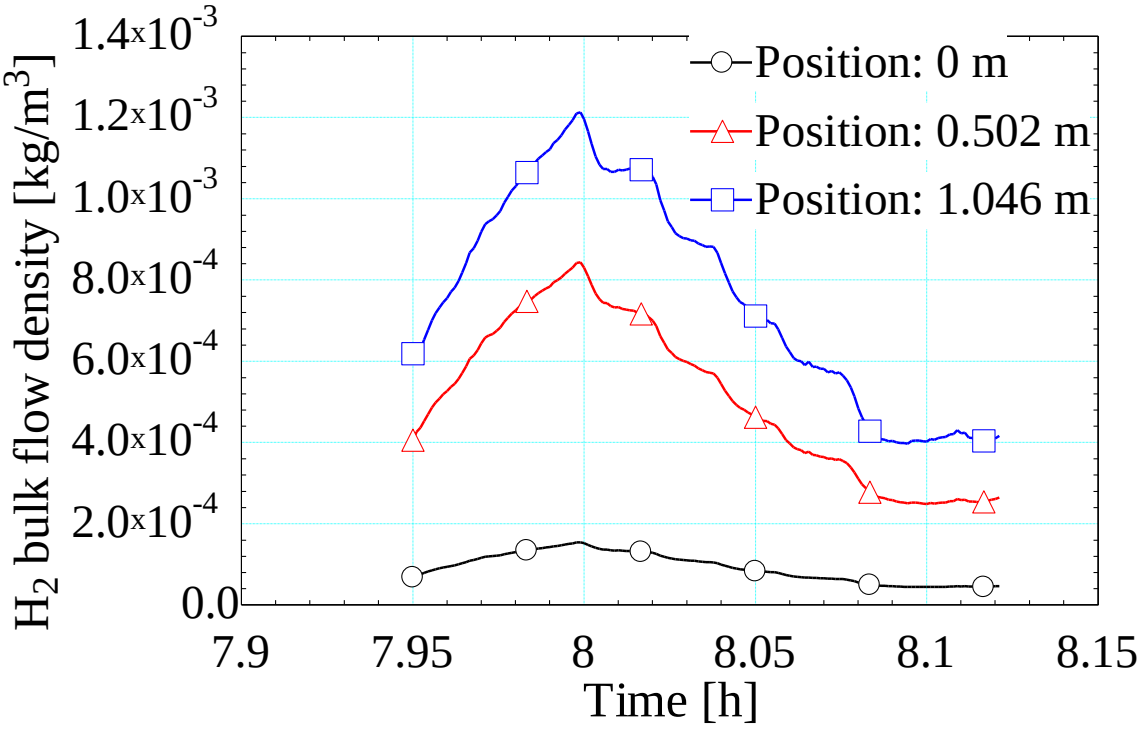

FIGURE 3-31. Hydrogen bulk density as a function of time.

FIGURE 3-31 shows the time dependence of the hydrogen gas density at three axial positions. In time, the density follows the same trend as the hydrogen pressure. Spatially, the density increases as the hydrogen gas travels along the pump and is cooled, reaching its maximum value at the end of the pump.

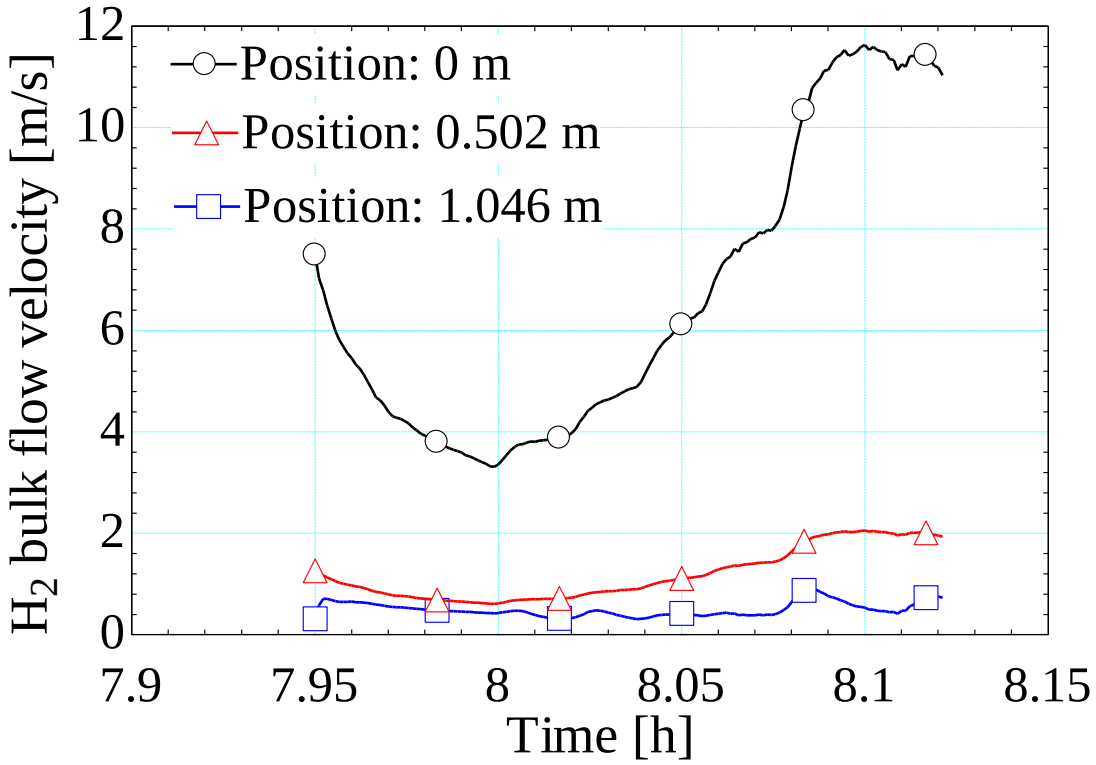

FIGURE 3-32. Hydrogen bulk velocity as a function of time.

FIGURE 3-32 shows the time dependence of the hydrogen bulk velocity at three axial positions. The bulk velocity decreases as the hydrogen gas flows along the pump. The inlet bulk velocity (at the axial position of 0 m) changes with time due to the change in the hydrogen pressure.

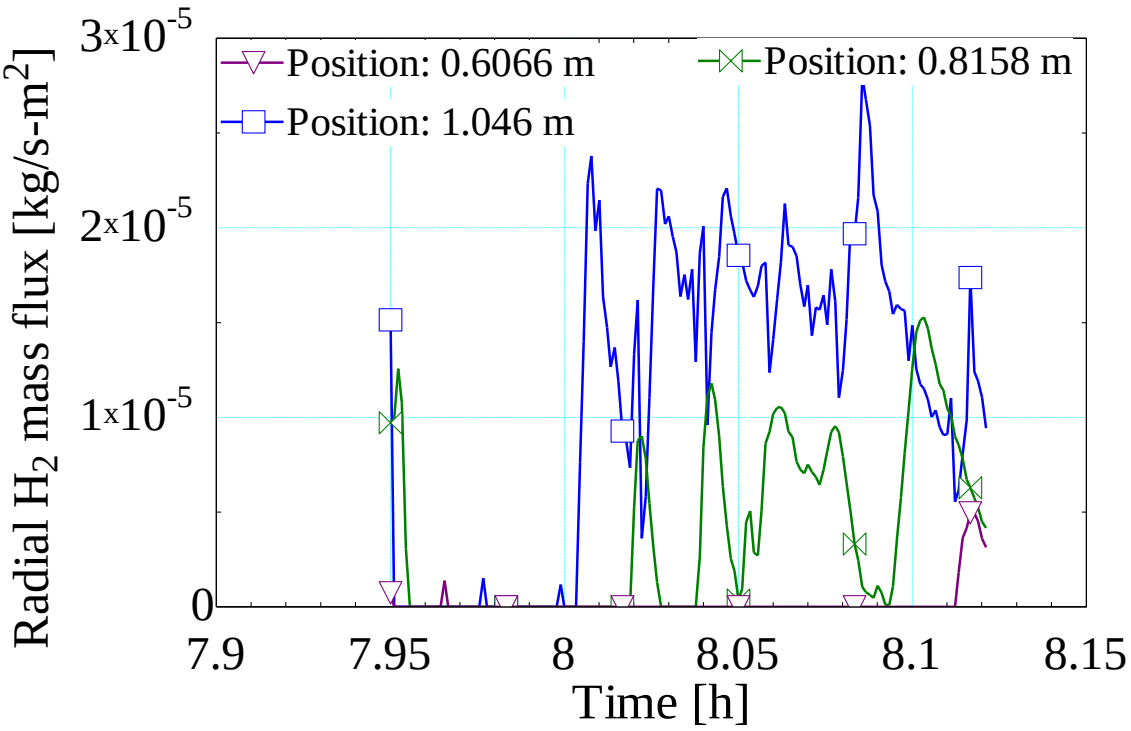

FIGURE 3-33. Radial hydrogen mass flux as a function of time.

FIGURE 3-33 shows the time dependence of the radial hydrogen mass flux at three axial positions. The radial hydrogen flux (adsorption) occurs solely in the downstream half of the pump. The variation with time is due to the associated variation of the pump wall temperature. Note that the absorption rate is largest near the end of the pump (at the axial position of 1.046 m).

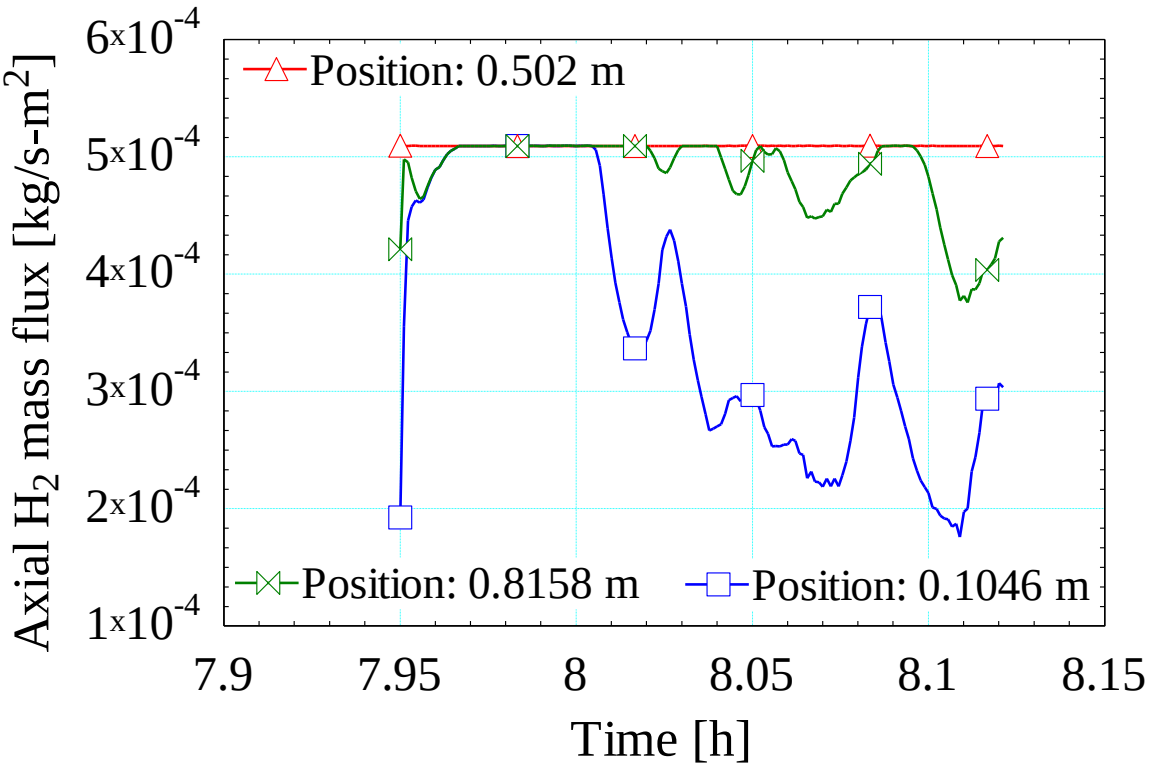

FIGURE 3-34. Axial hydrogen mass flux as a function of time.

FIGURE 3-34 shows the time dependence of the axial hydrogen mass flux at three axial positions. The axial hydrogen mass flux decreases when adsorption occurs. Most of the adsorption occurs in the downstream half of the pump, and it strongly depends on the pump wall temperature.

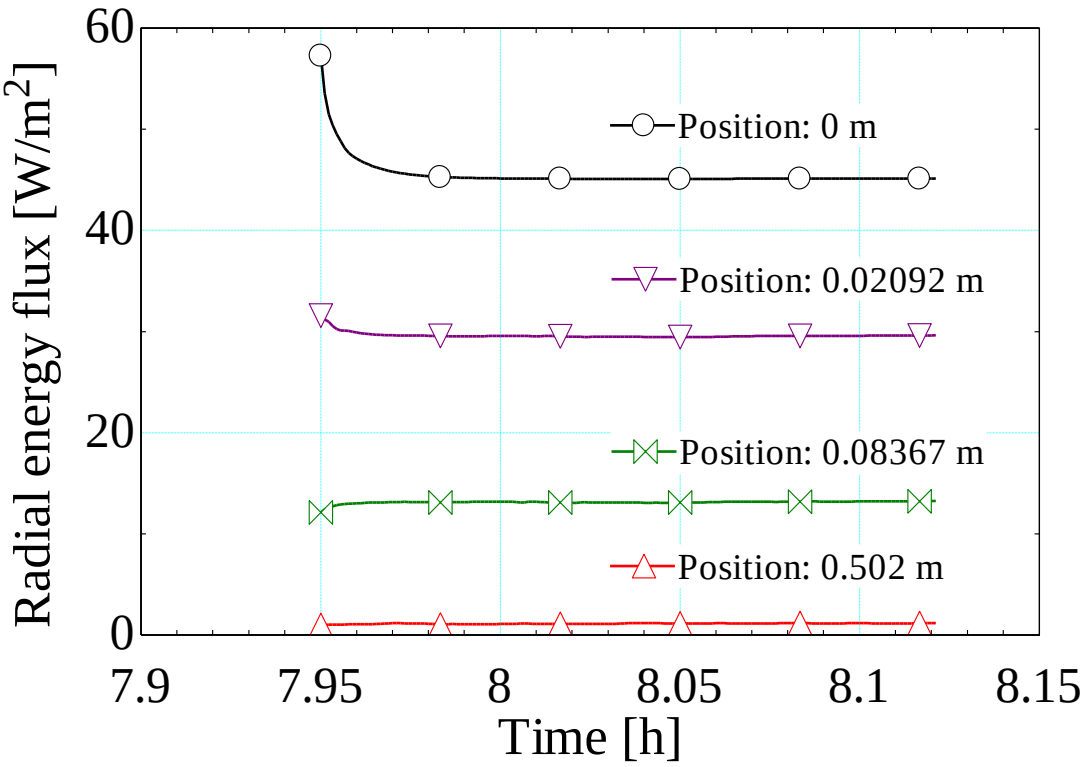

FIGURE 3-35. Radial energy flux as a function of time (I).

FIGURE 3-35 shows the time dependence of the radial energy flux at four axial positions. Most of the radial energy flux occurs within the first 10 cm. At the pump entrance, the energy flux is much higher because of the larger temperature difference and heat transfer coefficient. At the pump entrance, the energy flux decreases with time because the hydrogen gas warms up the pump wall.

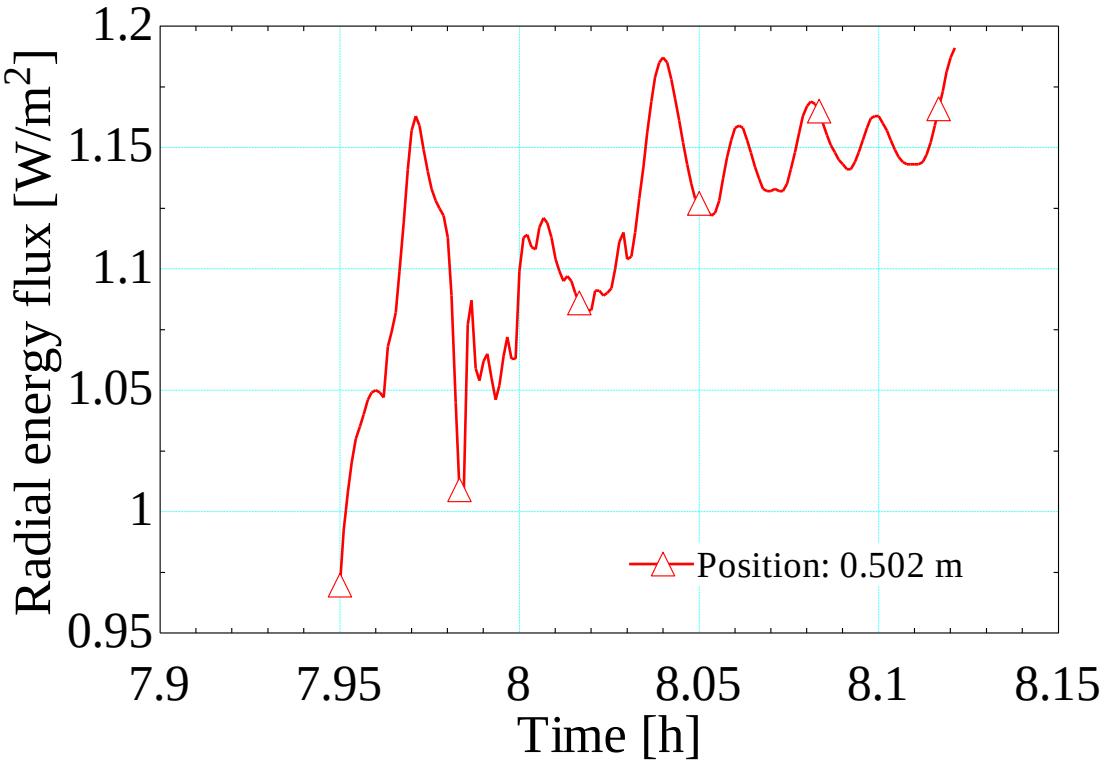

FIGURE 3-36. Radial energy flux as a function of time (II).

FIGURE 3-36 shows the time dependence of the radial energy flux in the middle of the pump. The variation can be seen clearly. And that variation is due to the variation of the pump wall temperature. It means that the model can capture precise variations.

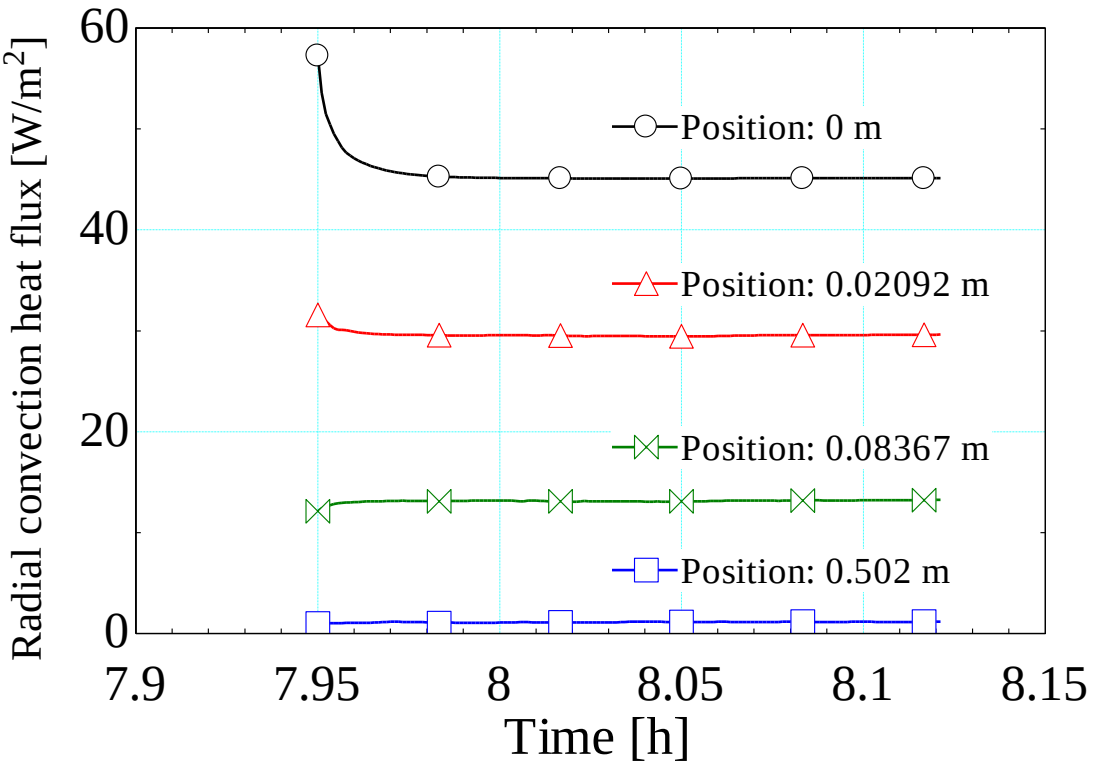

FIGURE 3-37. Radial convection heat flux as a function of time (I).

FIGURE 3-37 shows the time dependence of the radial convection heat flux at four axial positions. They are very similar to the profiles of the total energy flux in **FIGURE 3-35**, because the convection heat flux is much larger than the adsorption heat flux.

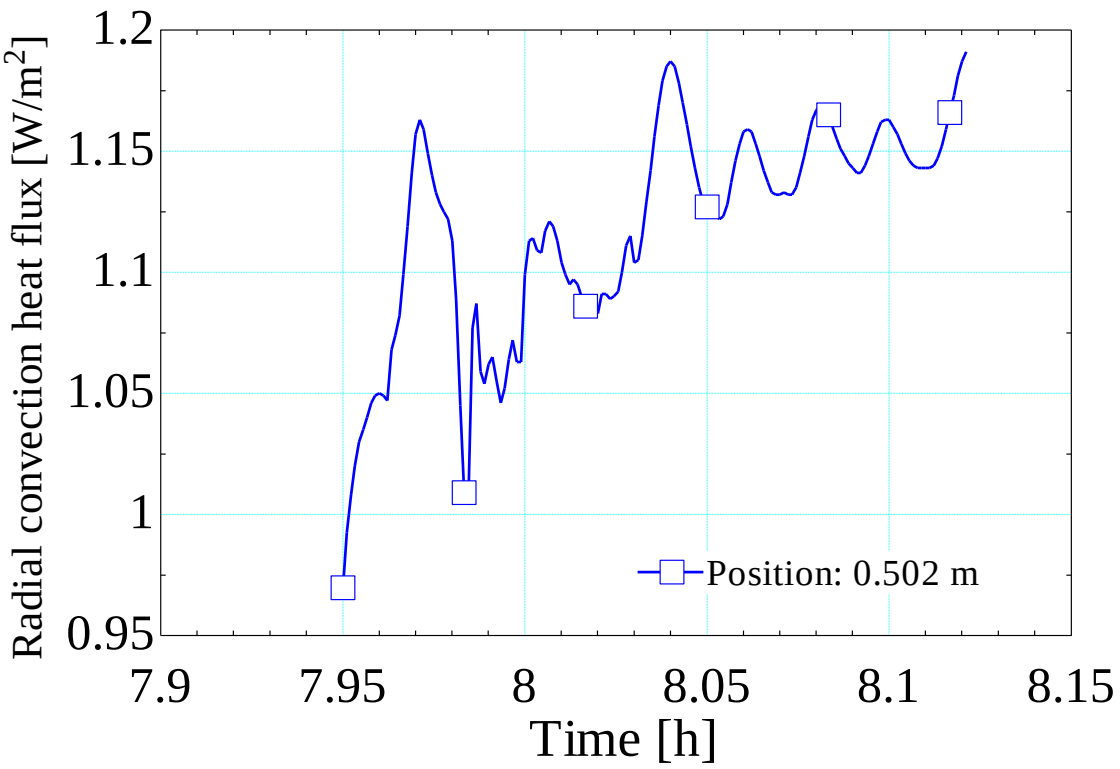

FIGURE 3-38. Radial convection heat flux as a function of time (II).

FIGURE 3-38 shows the profile of the radial convection heat flux in the middle of the pump. The variation can be clearly seen.

3.4.3. Hydrogen pressure and adsorption

The pumping performance is mainly determined by the pump wall temperature. The helium coolant cools the pump wall to cryogenic temperatures, and the cold wall adsorbs hydrogen molecules. As a result, it is appropriately named a cryogenic pump.

As shown in the experimental data, the inlet hydrogen gas pressure is an important indicator for the pumping performance. Without any adsorption or sublimation of the hydrogen molecules, the inlet hydrogen gas pressure remains constant (**FIGURE 2-10**)

while with adsorption or sublimation, the inlet hydrogen gas pressure varies with time (**FIGURE 2-11** and **FIGURE 2-12**).

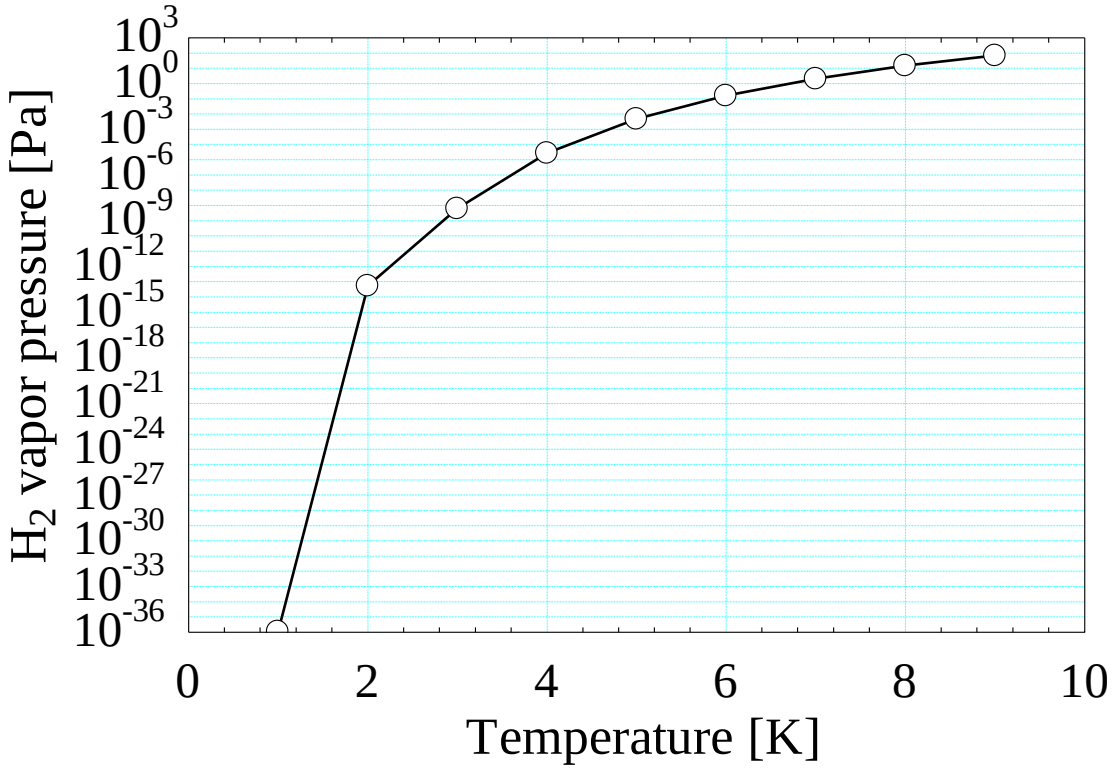

FIGURE 3-39. Hydrogen vapor pressure as a function of temperature [1 K, 9K].

FIGURE 3-39 plots the experimental data of the hydrogen vapor pressure (Ahlers, 1964) (H. M. Roder, 1973) (J. C. Mullins, 1961) (R. D. McCarty, 1981) (Roder, 1977). The vapor pressure of hydrogen decreases dramatically with the decrease of temperature. When the vapor pressure associated with a surface temperature is smaller than the pressure of some adjacent hydrogen gas, the hydrogen molecules in the hydrogen gas are adsorbed onto the pump surface. Without maintaining an equivalent supply of gas molecules, the

adsorption of the hydrogen molecules noticeably reduces the hydrogen gas pressure. An exchange of molecules between the gas and the surface will then occur until an equilibrium pressure is reached. The inlet hydrogen pressure approaches the equilibrium pressure, and the difference drives the deposition.

A comparison between the inlet hydrogen gas pressure and the hydrogen vapor pressure corresponding to the coldest wall temperature is presented in **FIGURE 3-40**. The inlet hydrogen gas pressure (the upstream hydrogen pressure in the experiment) is measured by the pressure gauge that is mounted with a capillary tube located 7 cm from the top of the pump. The hydrogen vapor pressure is the vapor-solid phase equilibrium pressure, based on the minimum pump wall temperature that is obtained from the transient model. The mathematical relationship between the hydrogen vapor pressure and the temperature is interpolated from the reported experimental data (J. C. Mullins, 1961) (Ahlers, 1964) (H. M. Roder, 1973) (Roder, 1977) (R. D. McCarty, 1981).

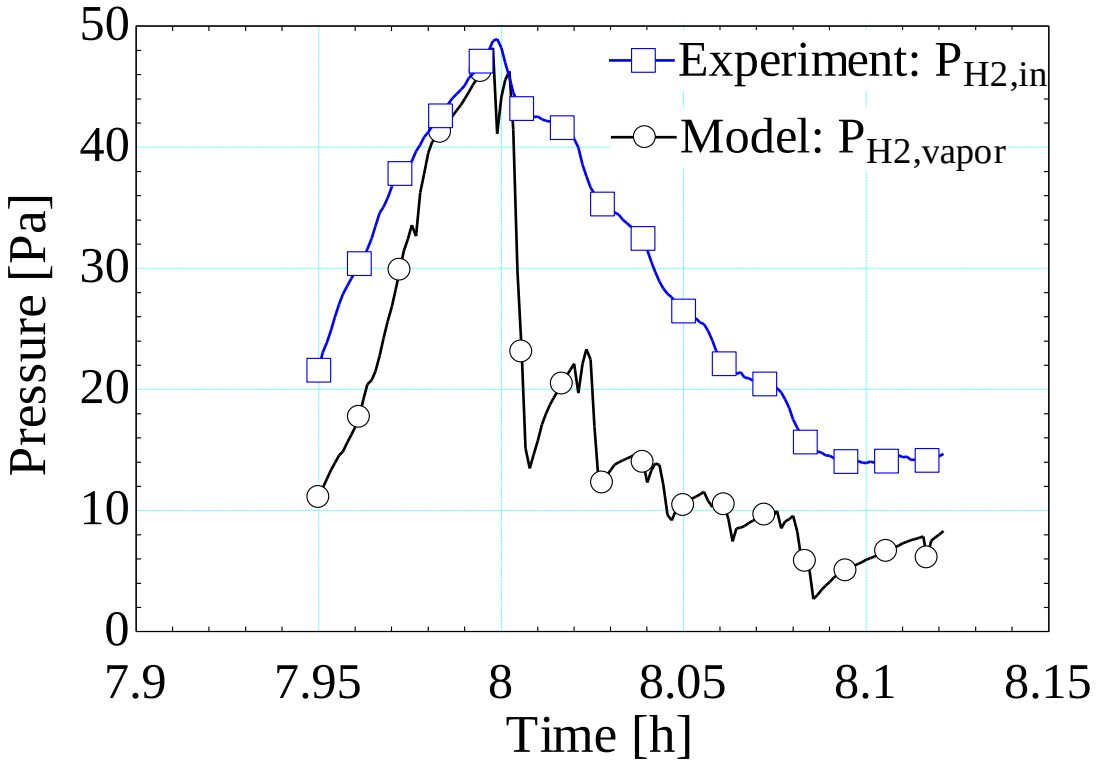

FIGURE 3-40. Inlet hydrogen gas pressure (the experimental data set I) and the hydrogen vapor pressure (calculated by the transient model) as a function of time.

The **FIGURE 3-40** shows that the inlet hydrogen gas pressure does follow the hydrogen vapor pressure.

Chapter 4 Steady-state model

The transient model being discussed in the former section explains the experimental data set I. However, the experimental conditions are not ideal for generating the best cryopumping performance. The steady-state model is thus developed to investigate and design optimum conditions for the ITER cryogenic fore pump. The steady-state model is also a model developed for the viscous flow regime.

The analysis here provides a steady-state model instead of a transient model for the following three reasons. First, the steady-state model provides a simple method to obtain a good estimate. Secondly, the transient process in the experimental data is mainly induced by the variation in the inlet helium coolant temperature that should be controlled at a constant value. From a design point the variation in the variable profiles are not as interesting as the pumping performance. Finally, the experimentally measured inlet hydrogen pressure provides a necessary boundary condition for the transient model, and that information is not generally available.

The steady-state model follows the same analysis for the control volume of the hydrogen gas as that used in the transient model. It further assumes that the control volume of the helium-coolant-plus-the-pump-wall is at steady state, a significant difference from the transient model.

4.1. Analysis and governing equations

Similar to the transient model, the general flux balance on the control volume of the hydrogen gas at steady state is as follows.

$$r\frac{d[F_z]}{dz}+2F_r=0. \quad (44)$$

The general flux equation is then specified as the following three equations to represent the conservation of species, momentum and energy respectively.

Conservation of the hydrogen mass:

$$r\frac{d[M_{z,H_2}]}{dz}+2M_{r,H_2}=0. \quad (45)$$

Conservation of the axial (z) momentum:

$$r\frac{d[\Phi_{zz}]}{dz}+2\Phi_{rz}=0. \quad (46)$$

Conservation of the energy:

$$r\frac{d[E_z]}{dz}+2E_r=0. \quad (47)$$

The mass flux terms in the conservation equation of the hydrogen mass are developed as the following two equations.

The hydrogen mass flux in axial (z) direction:

$$M_{z,H_2} = \rho_{H_2} u_z \tag{48}$$

The hydrogen mass flux in radial (r) direction:

$$M_{r,H_2} = h_m(\rho_{H_2} - \rho_{H_2,w}) \tag{49}$$

Where the mass transfer coefficient h_m is developed in the similar manner as the heat transfer coefficient h_t :

$$h_t = \frac{Nu \cdot k}{2r}, h_m = \frac{Sh \cdot D_{ab}}{2r} \tag{50}$$

The z -momentum flux terms in the conservation equation of the axial (z) momentum are developed as the following two equations.

The axial (z) momentum flux transferred in axial (z) direction:

$$\Phi_{zz} = \rho_{H_2} u_z u_z + P \qquad 51)$$

The axial (z) momentum flux transferred in radial (r) direction:

$$\Phi_{rz} = \Delta P_{friction} + M_{r,H_2} u_z \qquad 52)$$

Where the pressure loss due to friction $\Delta P_{friction}$ is expresses as follow.

$$\Delta P_{friction} = \rho_{H_2} f \frac{u_z^{\,2}}{2} \frac{dz}{2r} \qquad 53)$$

The energy flux terms in the conservation equation of energy are developed as the following two equations.

The energy flux in axial (z) direction:

$$E_z = \rho_{H_2} u_z h_{H_2} + \rho_{H_2} u_z (\frac{1}{2} u_z^{\,2}) \qquad 54)$$

The energy flux in radial (r) direction:

$$E_r = M_{r,H_2}(h_{H_2} + \frac{1}{2}u_z{}^2) + h_t(T - T_w) \quad 55)$$

In addition to the conservation equations, the ideal gas law is used for the equation of state because the compressibility factor is close to unity.

$$P = \rho R_m T \quad 56)$$

The pump wall and the helium coolant in the annular tube are assumed to be at steady state with their temperatures determined by the heat transfer from the hydrogen gas.

4.2. Results and discussion

The results of the steady-state model are discussed in two sections, **SECTION** 4.2.1. Inlet hydrogen pressure and inlet helium coolant temperature and **SECTION** 4.2.2. Best pumping performance. In the first section, the relationship between the inlet hydrogen pressure and the inlet helium coolant temperature is discussed. The second section discusses how to achieve the best pumping performance by decreasing the inlet helium coolant temperature.

The results of 5 cases are presented. Among those, case 1-4 are discussed in the first section and case 5 is discussed in the second section. The 5 cases are summarized in **TABLE 2**.

TABLE 2. Inlet and outlet conditions of helium coolant and hydrogen gas

Case	Helium Coolant Conditions			Hydrogen Gas Conditions				
	$\dot{m}_{He}$	$T_{He,in}$	$T_{He,out}$	$\dot{m}_{H2}$	$P_{H_2,in}$	$T_{H_2,in}$	$T_{H_2,out}$	R
	[g/s]	[K]	[K]	[g/s]	[Pa]	[K]	[K]	[-]
1	0.4921	7.483	7.734	0.001	10	77	7.484	50%
2	0.4921	8.028	8.281	0.001	20	77	8.029	50%
3	0.4921	8.181	8.435	0.001	30	77	8.182	50%
4	0.4921	8.336	8.59	0.001	40	77	8.336	50%
5	0.4921	7.378	7.628	0.001	10	77	7.379	97.7%

As shown in **TABLE 2**, the inlet mass flow rate of the helium coolant $\dot{m}_{He}$, the inlet mass flow rate of the hydrogen gas $\dot{m}_{H2}$, and the inlet hydrogen gas temperature $T_{H_2,in}$ are set as constants. In addition, the inlet helium coolant pressure is always set at 1.4 bar.

For cases 1-4, the adsorption percentage of the hydrogen gas R is set at 50%. Subsequently, the inlet helium coolant temperature $T_{He,in}$ is adjusted in order to achieve that adsorption rate for the various inlet hydrogen gas pressures $P_{H_2,in}$.

For case 5, the inlet hydrogen gas pressure is set at 10 Pa, and the inlet helium coolant temperature is decreased in order to achieve the "best" pumping performance.

4.2.1. Inlet hydrogen pressure and inlet helium coolant temperature

The results of the steady-state model for cases 1-4 are discussed in this section. The inlet helium coolant temperature is adjusted to yield the same adsorption percentage (50%) of the inlet hydrogen molecules. The inlet helium coolant temperature is a critical factor for the cryogenic pump performance, and it is closely related to the inlet hydrogen gas pressure.

The inlet helium coolant determines the pumping performance in that it sets the pump wall temperature. A small variation of that temperature leads to orders of magnitude change in the hydrogen vapor pressure. The vapor pressure in turn is an indicator for the pumping power. The smaller the vapor pressure is, the stronger the pumping power is.

Given the same inlet hydrogen mass flow rate and temperature, the change of the hydrogen gas pressure is an indicator for the adsorption of the hydrogen molecules. As shown in the experimental data, without adsorption the inlet hydrogen pressure stays constant, while with adsorption, the pressure decreases.

The modeling results are presented as follows. Cases 1-4 are represented by different inlet hydrogen pressures, being 10 Pa, 20 Pa, 30 Pa, and 40 Pa respectively.

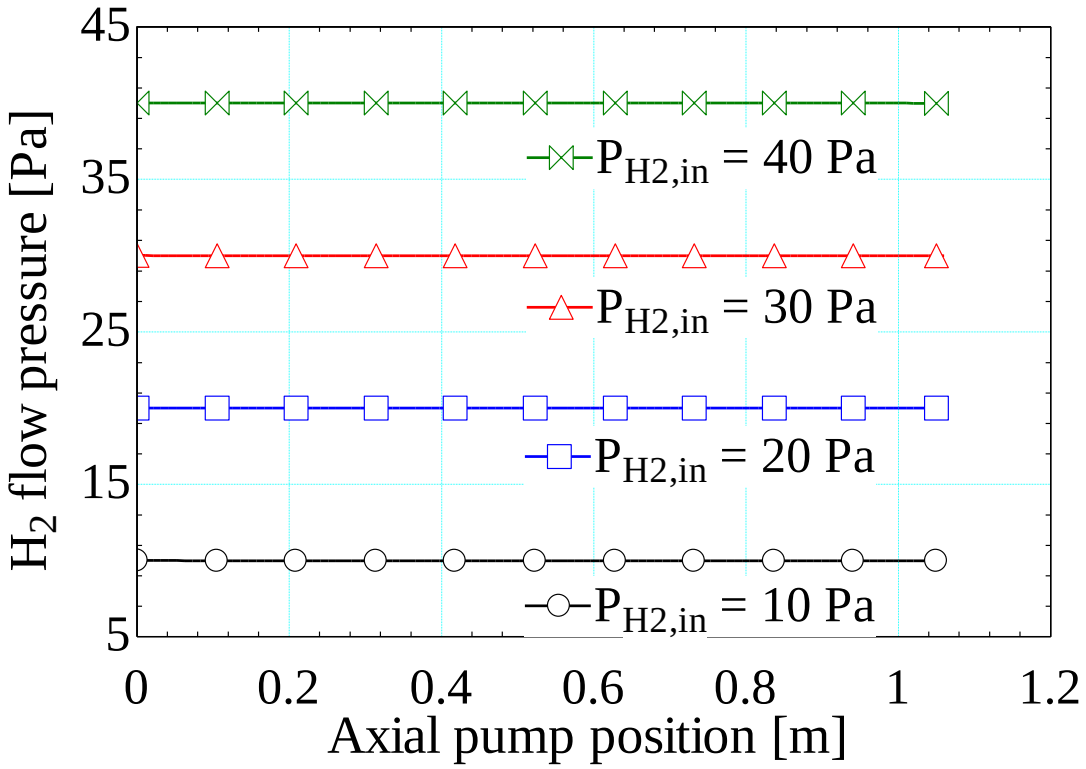

FIGURE 4-1. Hydrogen gas pressure as a function of axial pump position.

FIGURE 4-1 shows the profiles of the hydrogen gas pressure. The pressure drop is negligibly small because of the small friction factor. As a result, the outlet pressure is almost the same as the inlet pressure, in agreement with the experimental data shown in **FIGURE 2-20**.

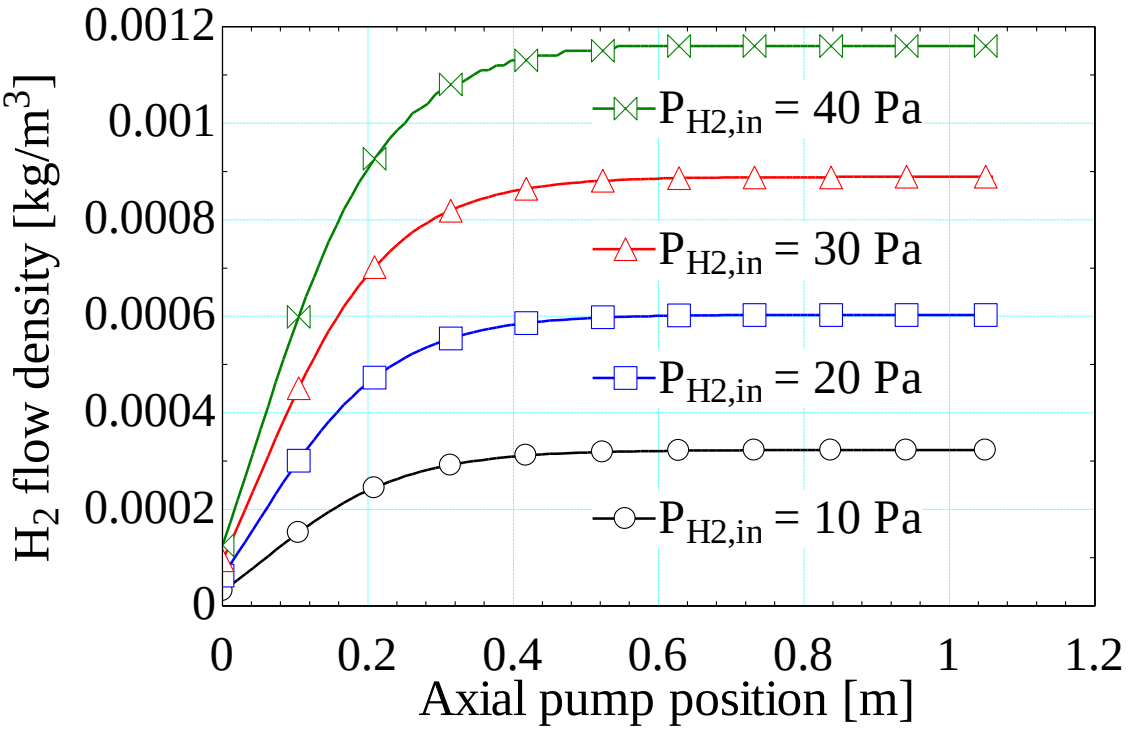

FIGURE 4-2. Hydrogen flow density as a function of axial pump position.

FIGURE 4-2 shows the profiles of the hydrogen gas density. The inlet density varies case by case, according to the ideal gas equation of state, the pressure, and the same inlet temperature. As the hydrogen gas travels along the pump and is cooled, the density increases. The density rise is sharp at first because of the large heat flux, and it then gradually becomes stable. The density for case 4 (pressure being 40 Pa) is about 4 times as large as that for case 1 (pressure being 10 Pa).

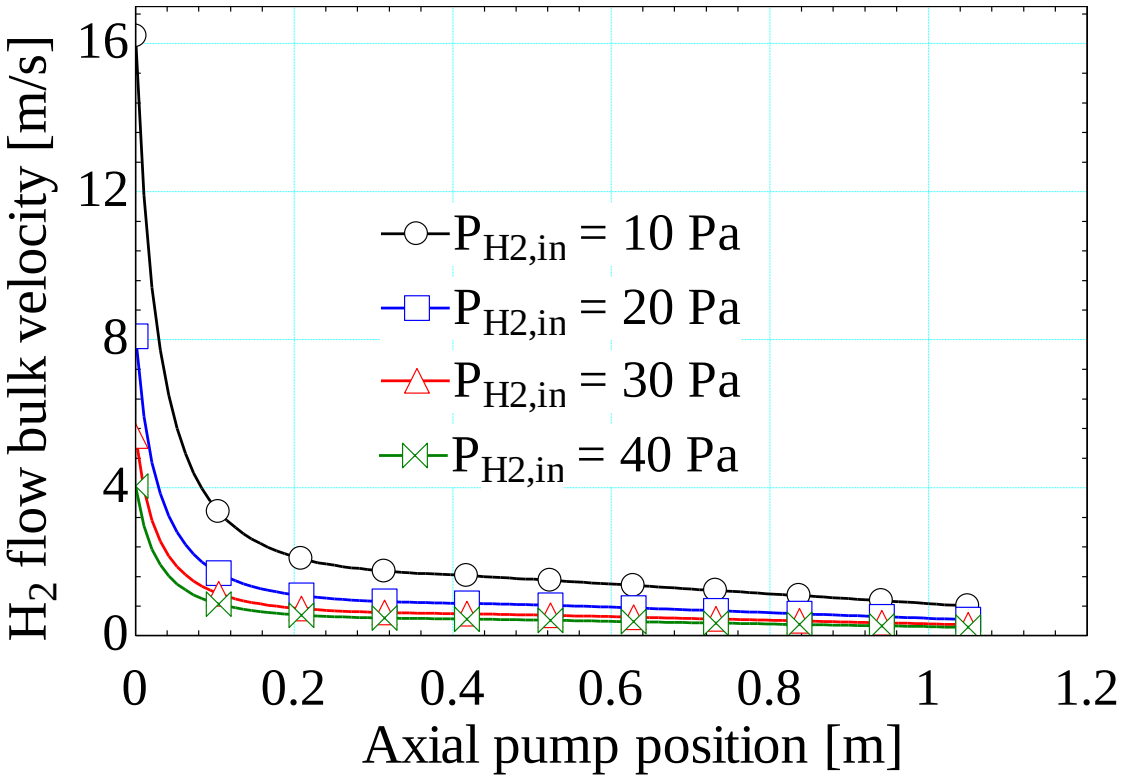

FIGURE 4-3. Hydrogen gas bulk velocity as a function of axial pump position (I).

FIGURE 4-3 shows the profiles of the hydrogen gas bulk velocity. The inlet velocity varies case by case because of the same inlet hydrogen mass flow rate with different densities. The outlet velocities approach 0 m/s.

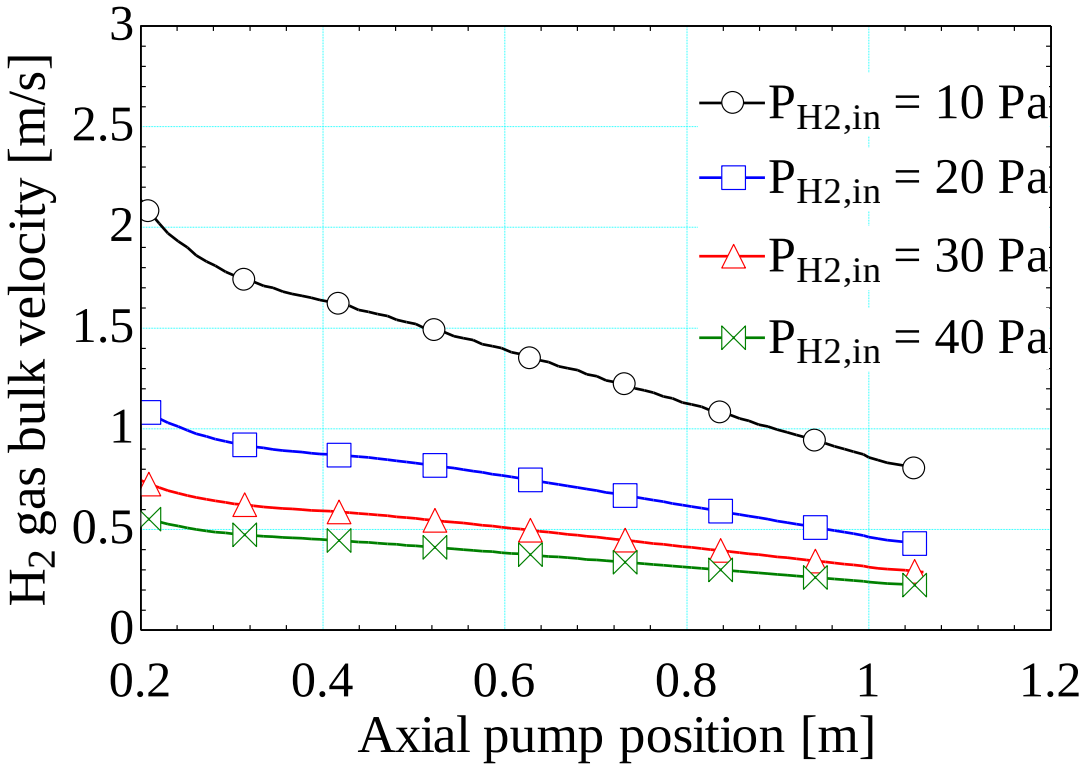

FIGURE 4-4. Hydrogen gas bulk velocity as a function of axial pump position (I).

FIGURE 4-4 shows the profiles of the hydrogen gas velocity beyond the axial position of 0.2 m. The bulk velocity decreases as the hydrogen gas flows along the pump. It is constrained by the conservation of mass, and therefore decreases since the density increases due to the cooling effect. Mathematically, a higher inlet velocity provides a larger margin for the velocity drop.

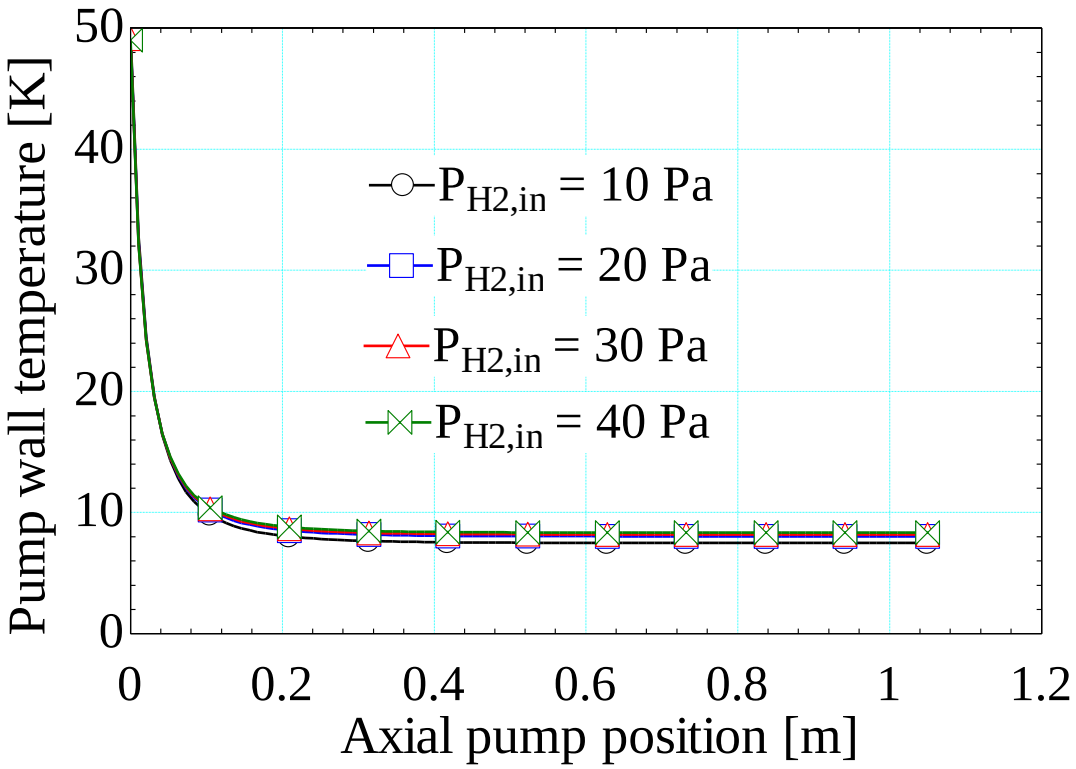

FIGURE 4-5. Pump wall temperature as a function of axial pump position (I).

FIGURE 4-5 shows the profiles of the pump wall temperature, and these seem to be very similar for the 4 cases. The similarity is especially close at the pump entrance because at that location the pump wall temperature is dominantly determined by the inlet hydrogen temperature (77 K) at the entrance. Small variations exist at the end of the pump.

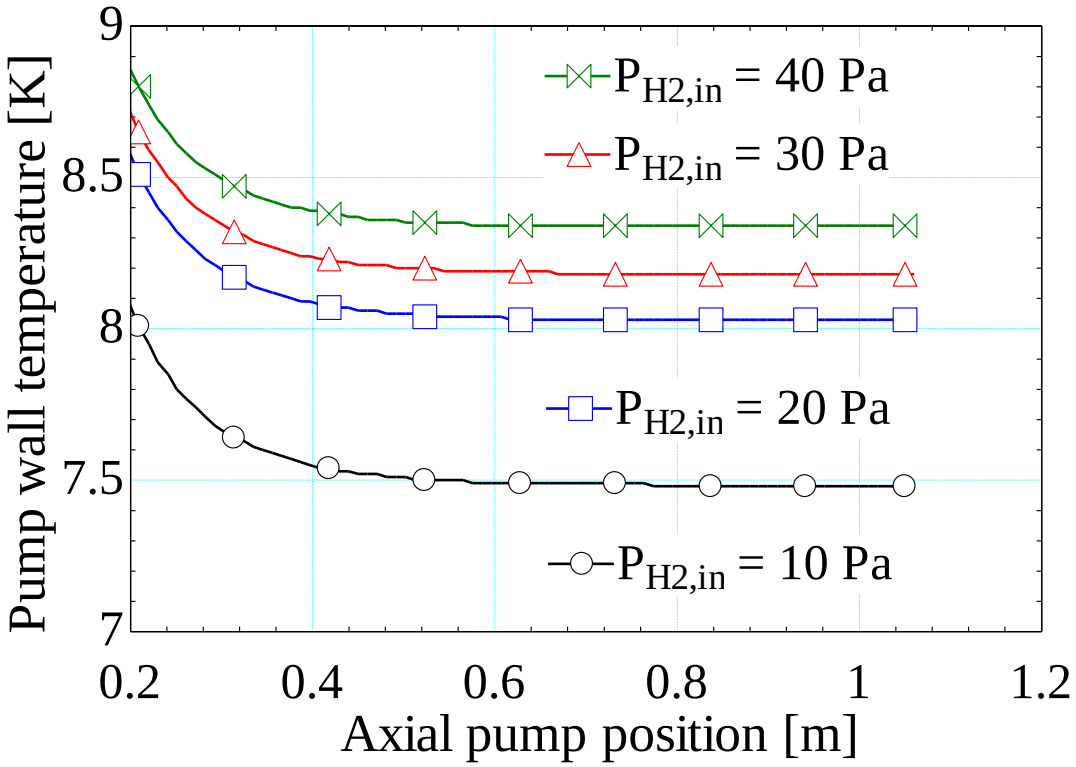

FIGURE 4-6. Pump wall temperature as a function of axial pump position (II).

FIGURE 4-6 shows the profiles of the pump wall temperature beyond the axial position of 0.2 m. The variations for the different cases are noticeable. However, the difference is less than 1 K, because the pump the wall temperature at this end is dominantly determined by the inlet helium coolant temperature that varies only between 7.483 K and 8.336 K.

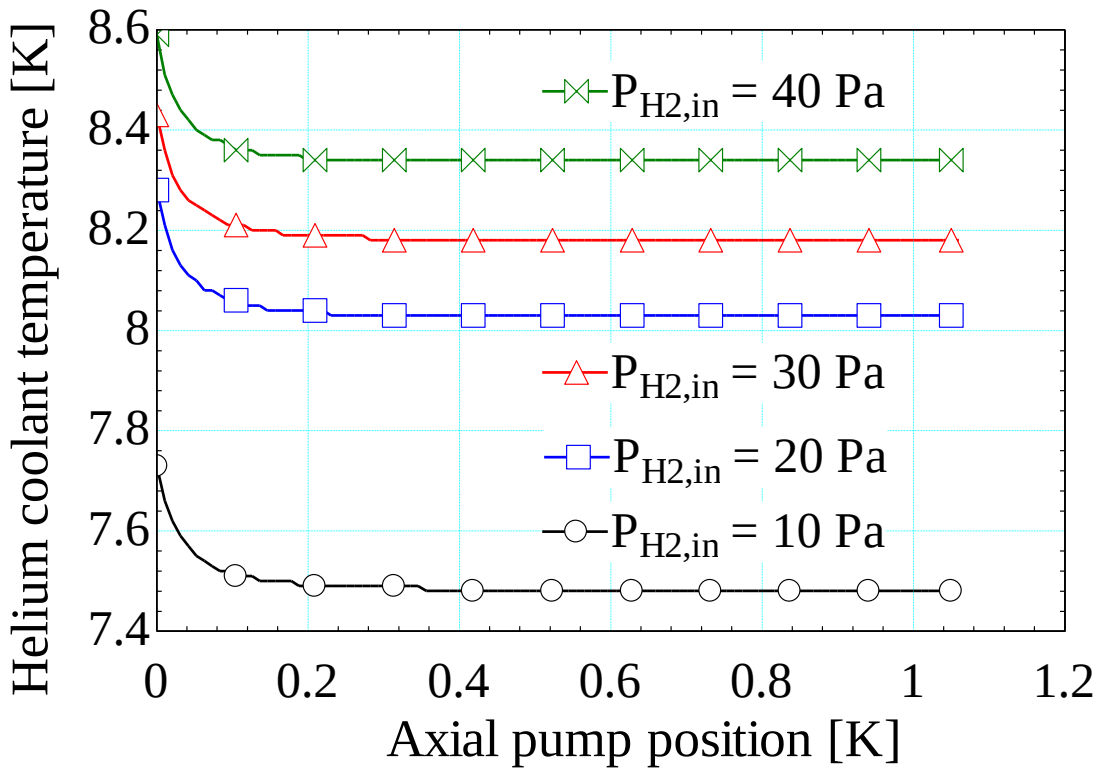

FIGURE 4-7. Helium coolant temperature as a function of axial pump position.

FIGURE 4-7 shows the profiles for the helium coolant temperatures. The outlet helium coolant temperature (at the axial position of 0 m) only rises about 0.3 K compared to the inlet helium coolant temperature (at the axial position of 1.06 m), thereby indicating that the cooling power of the current helium coolant is strong enough.

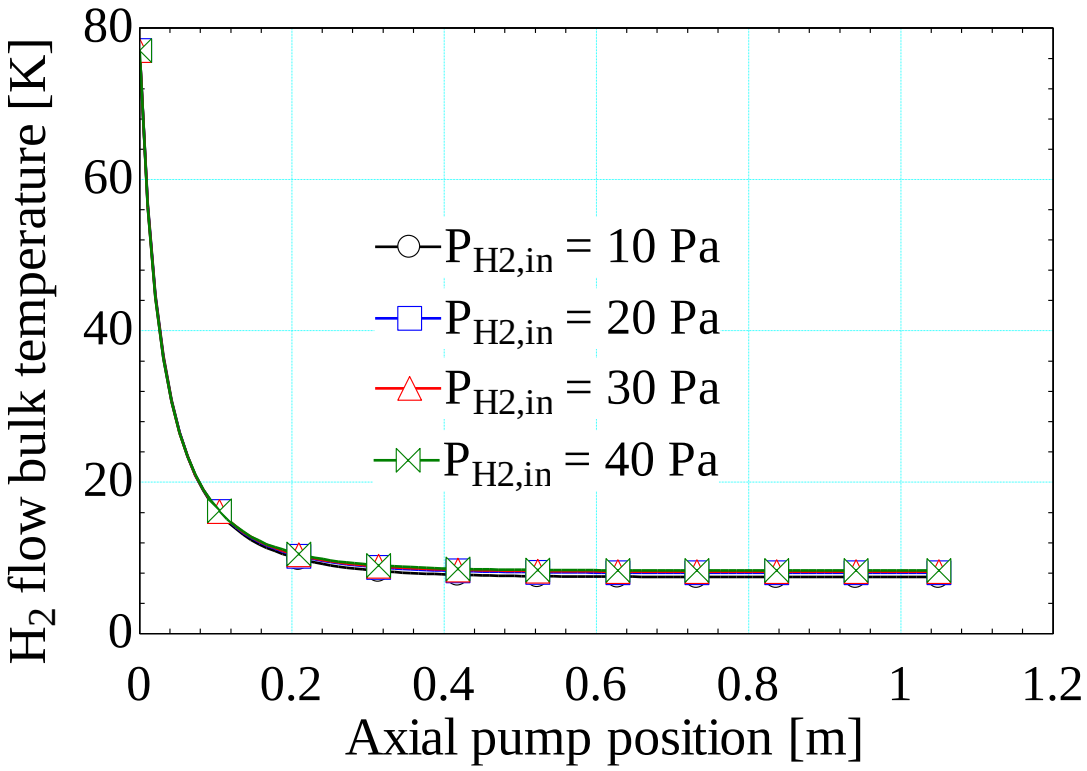

FIGURE 4-8. Hydrogen gas bulk temperature as a function of axial pump position.

FIGURE 4-8 shows the profiles of the hydrogen gas bulk temperatures. The profiles look very similar for the 4 cases. The temperature drops sharply at the pump entrance.

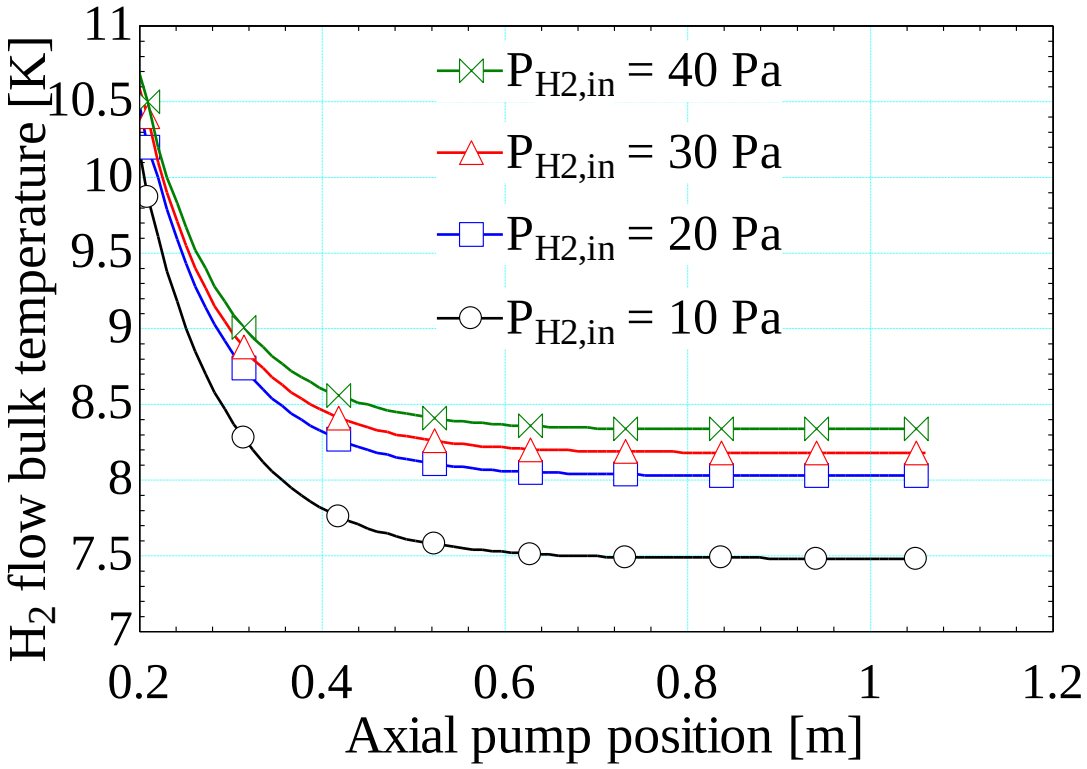

FIGURE 4-9. Hydrogen flow bulk temperature as a function of axial pump position.

FIGURE 4-9 shows the profiles of the hydrogen gas temperature beyond the axial position of 0.2 m.

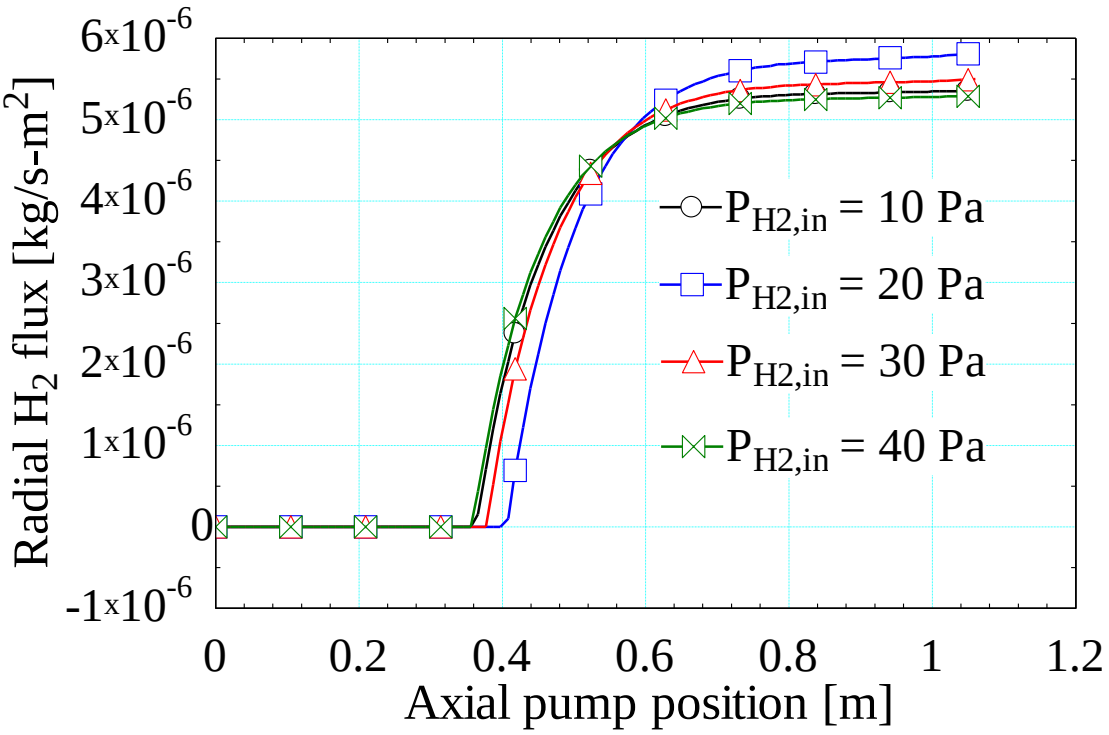

FIGURE 4-10. Radial hydrogen mass flux as a function of axial pump position.

FIGURE 4-10 shows the profiles of the radial hydrogen mass flux. The mass flux is the diffusion-driven mass flux due to the adsorption of hydrogen molecules onto the pump wall. The diffusion occurs where the pump wall temperature is low enough. Since the adsorption percentage is set to be the same (50%) for the 4 cases, the area under the profile curve is the same for all four cases.

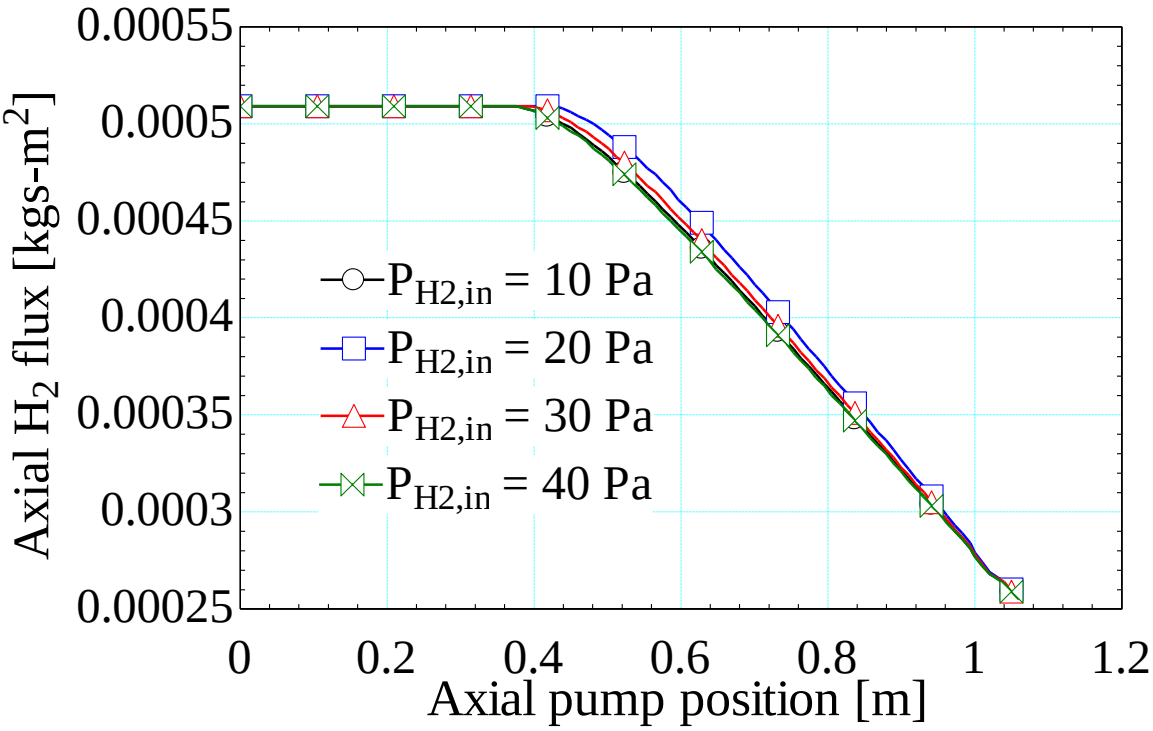

FIGURE 4-11. Axial hydrogen mass flux as a function of axial pump position.

FIGURE 4-11 shows the profiles of the axial hydrogen mass flux. The mass flux decreases because of the adsorption of the hydrogen molecules. Since the adsorption percentages are the same, the outlet hydrogen mass fluxes are the same for the 4 cases.

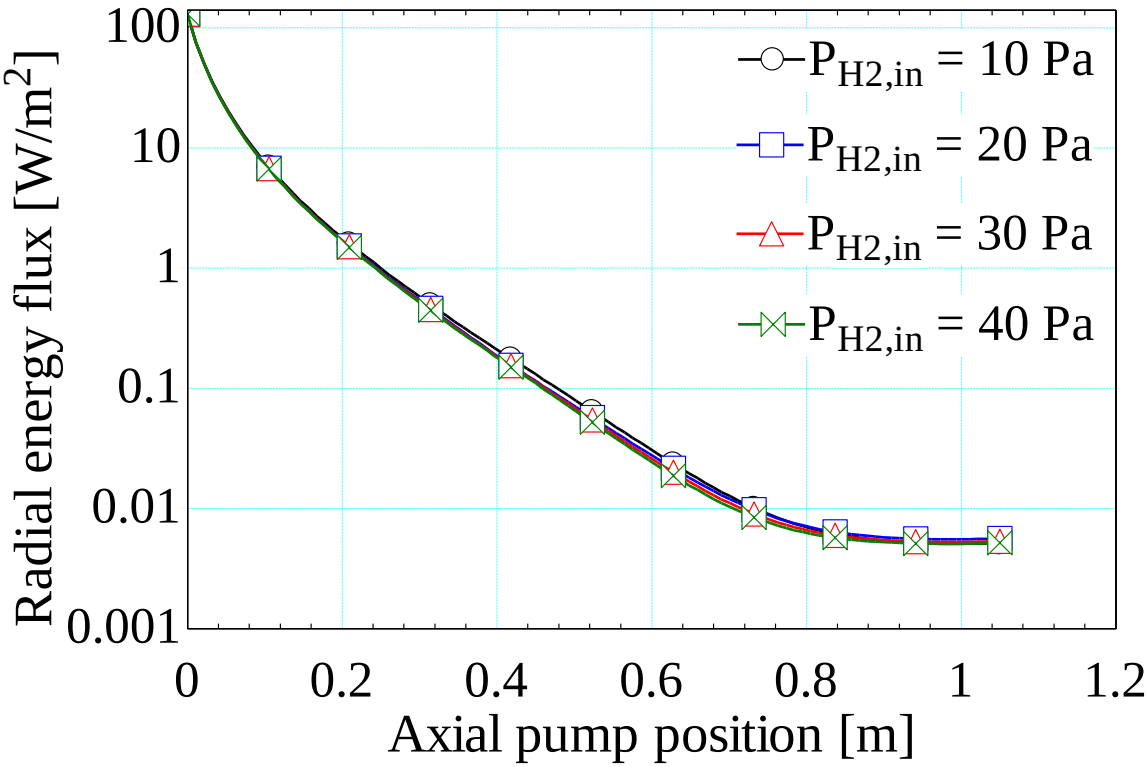

FIGURE 4-12. Radial energy flux as a function of axial pump position (I).

FIGURE 4-12 shows the profiles of the radial energy flux on a log scale. The energy flux is the sum of the convection flux and the adsorption energy flux. The fluxes are almost identical for the four cases because of the very similar temperature settings.

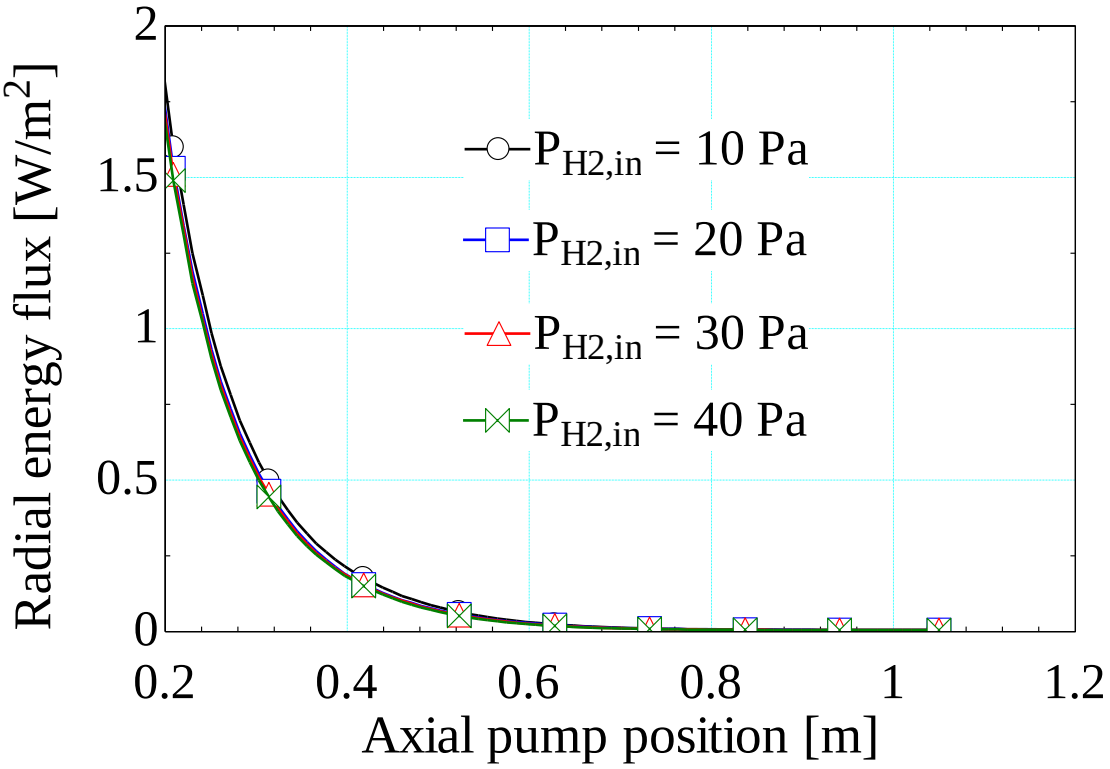

FIGURE 4-13. Radial energy flux as a function of axial pump position (II).

FIGURE 4-13 shows the profiles of the radial energy flux beyond the axial position of 0.2 m. The energy flux becomes much smaller in that region.

4.2.2. Best pumping performance

The modeling result of case 5 in **TABLE 2** is presented in this section. Given the same conditions as those in case 1, the inlet helium temperature is decreased to increase the adsorption percentage of the hydrogen molecules. When the inlet helium temperature researches 7.378 K, the adsorption percentage approaches 97.7%. At such condition, the pump will be blocked by the adsorbed hydrogen molecules in about 16.52 hours. The time period is calculated from the highest radial hydrogen mass flux.

The profiles of the important variables are plotted as follows.

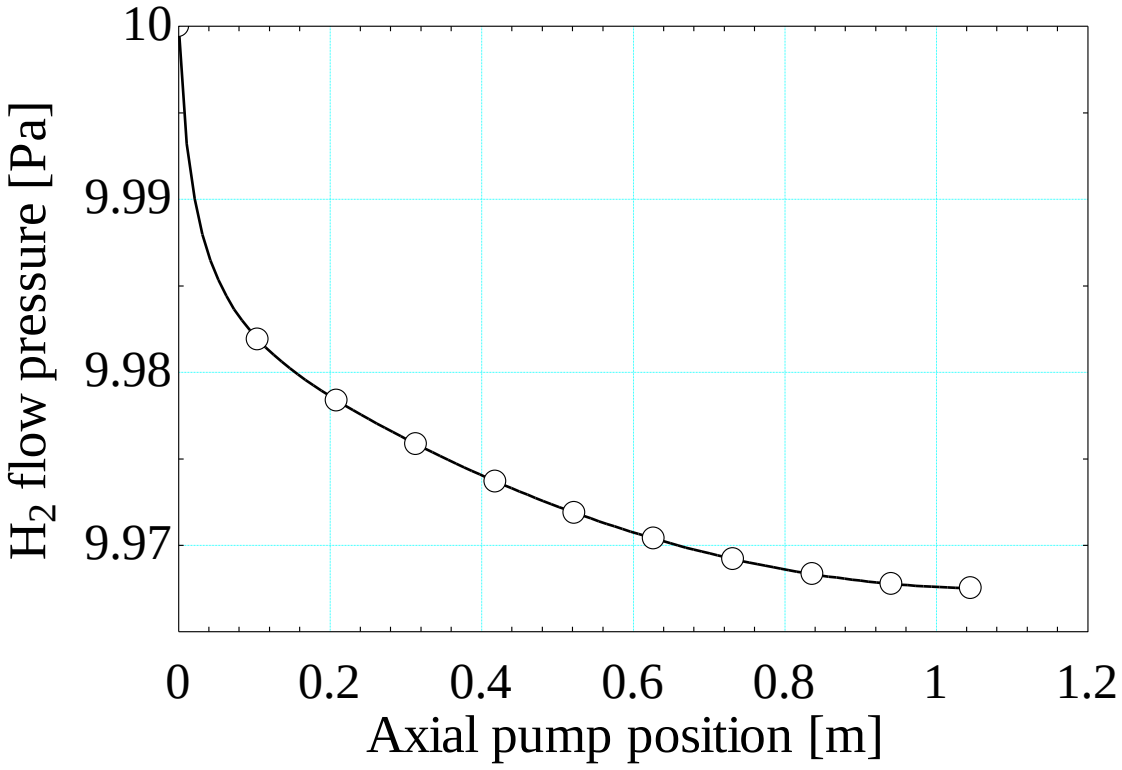

FIGURE 4-14. Hydrogen gas pressure as a function of axial pump position.

FIGURE 4-14 shows the profile of the hydrogen gas pressure. The pressure drop is negligibly small because of the small friction between the pump wall and the hydrogen gas.

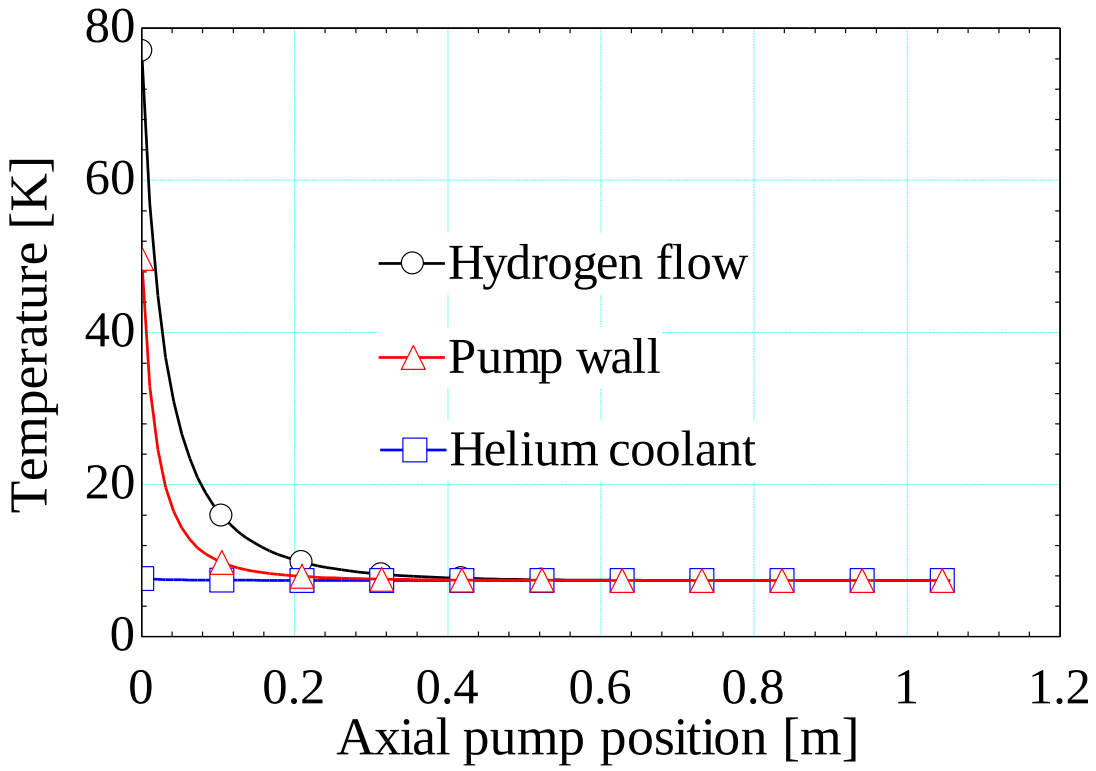

FIGURE 4-15. Temperature profiles of the hydrogen flow, pump wall and helium coolant as a function of axial pump position (I).

FIGURE 4-15 shows the profiles of the hydrogen gas temperature, the pump wall temperature, and the helium coolant temperature. At the pump entrance, the temperature changes dramatically due to the high heat transfer coefficient and large temperature difference. Beyond the axial position of 0.2 m, the temperatures are dominantly determined by the inlet helium coolant temperature.

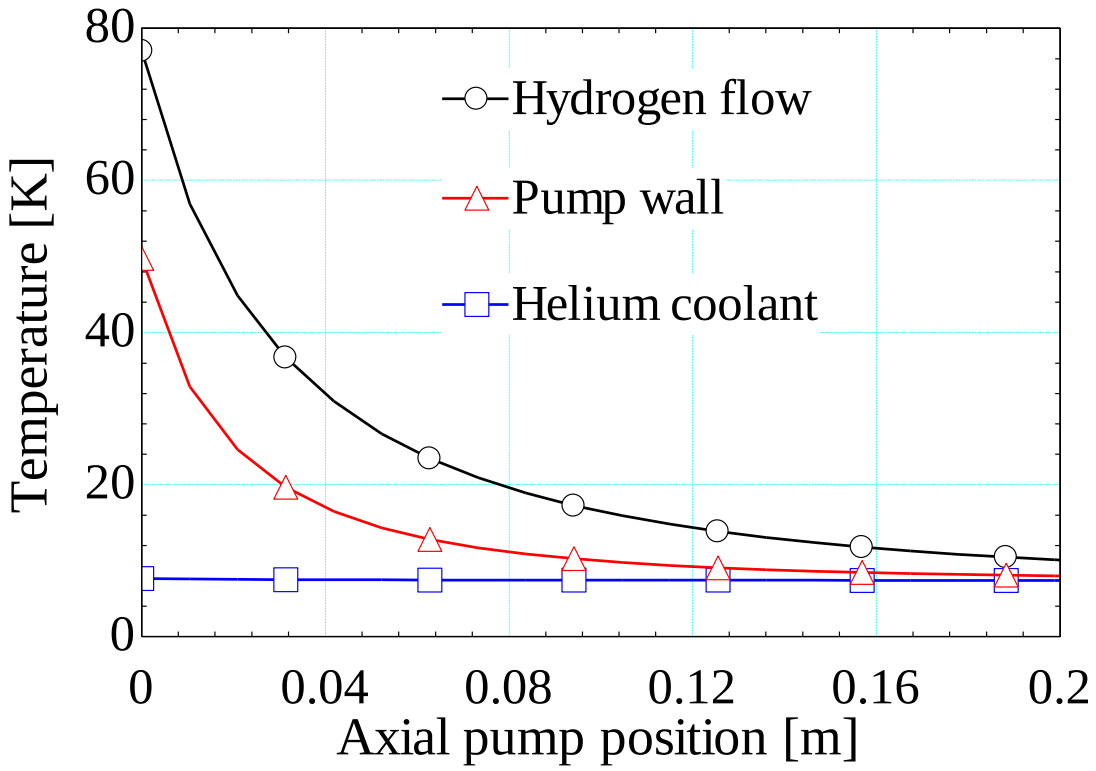

FIGURE 4-16. Temperature profiles of the hydrogen flow, pump wall, and helium coolant as a function of axial pump position (II).

FIGURE 4-16 shows the temperature profiles before the axial position of 0.2 m. The hydrogen gas temperature decreases about 8 times and the pump wall temperature decreases about 5 times. However, the helium coolant temperature changes moderately, again indicating its sufficient cooling power.

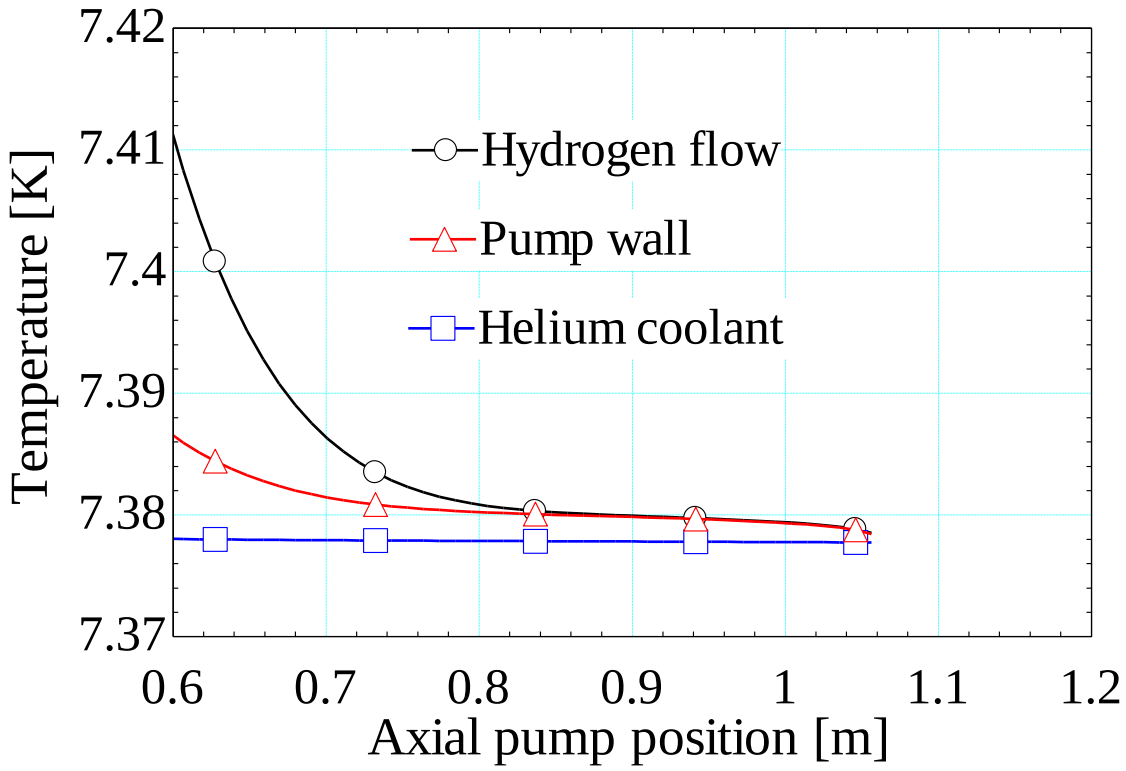

FIGURE 4-17. Temperature profiles of the hydrogen flow, pump wall, and helium coolant as a function of axial pump position (III).

FIGURE 4-17 shows the temperature profiles after the axial position of 0.6 m. The small differences are visible. The larger difference between the pump wall and the helium coolant implies the larger thermal resistance of the helium coolant.

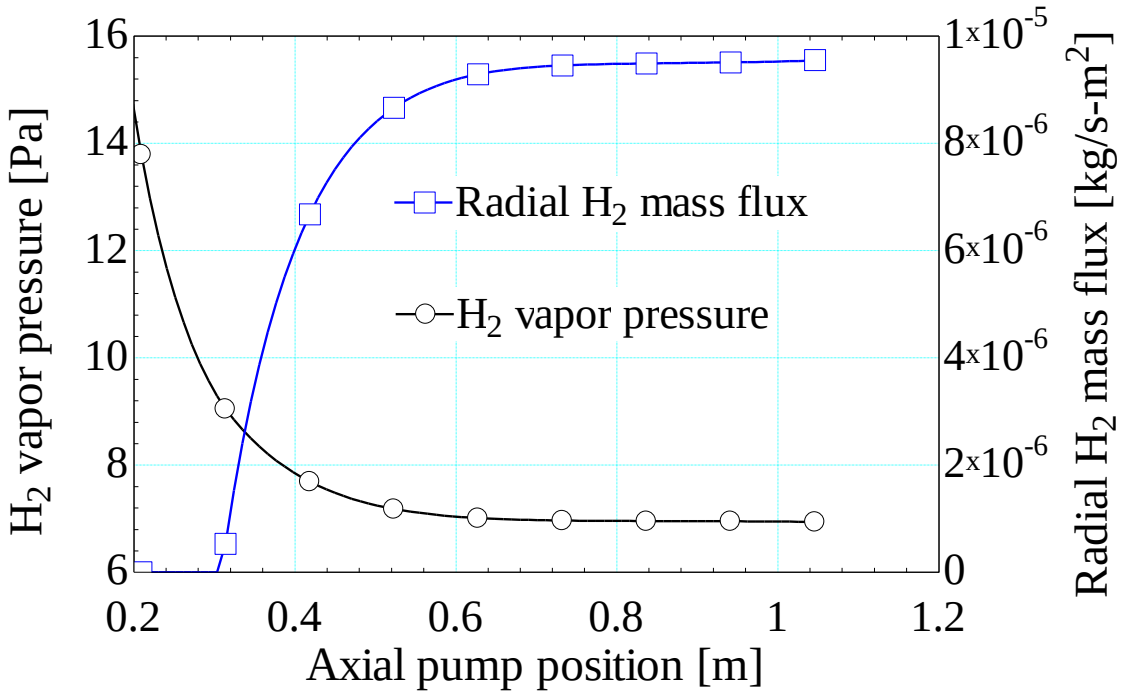

FIGURE 4-18. Hydrogen vapor pressure corresponding to the pump wall temperature and radial hydrogen mass flux as a function of axial pump position.

FIGURE 4-18 shows the profiles of the hydrogen vapor pressure and the radial hydrogen mass flux. The hydrogen vapor pressure is the vapor-solid equilibrium pressure at the local pump wall temperature. As may be observed, it could serve as an indicator for the adsorption rate, that is the cryogenic pumping power. The radial hydrogen mass flux is the adsorption mass flux of the hydrogen molecules onto the pump wall. It is driven by the radial density difference. Notice that the smaller the hydrogen vapor pressure corresponds to a higher adsorption rate.

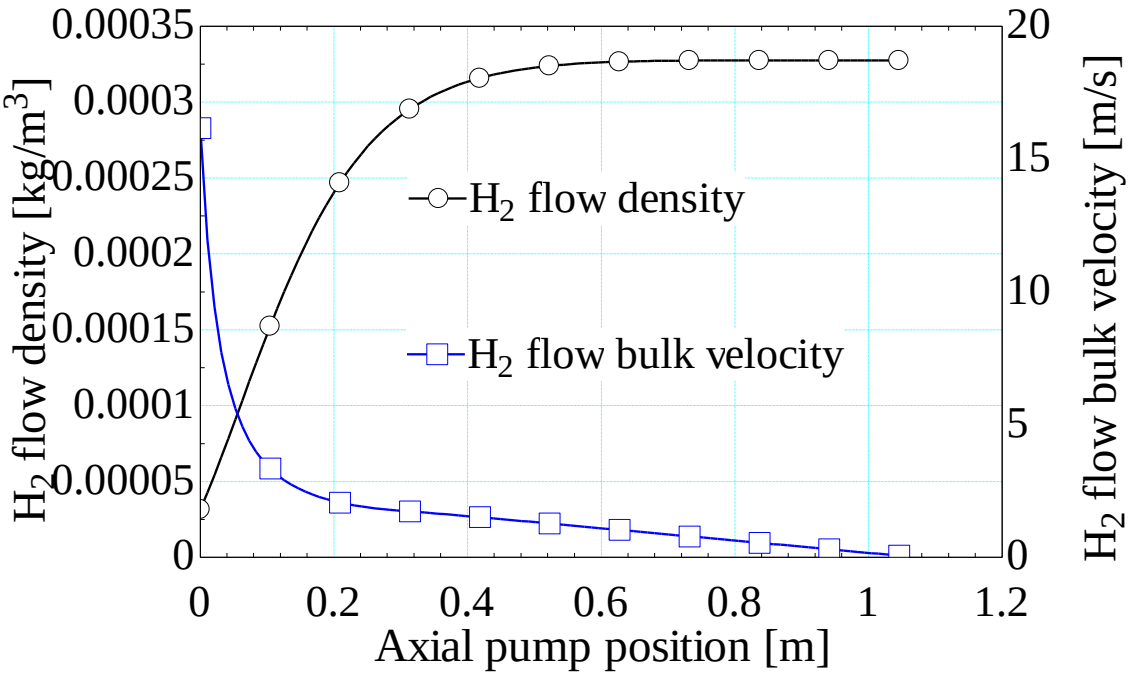

FIGURE 4-19. Hydrogen gas density and bulk velocity as a function of axial pump position.

FIGURE 4-19 shows the profiles of the hydrogen gas density and the bulk velocity. The density increases due to the cooling effect as the hydrogen gas flows through the pump. Constrained by the mass balance, the bulk velocity decreases.

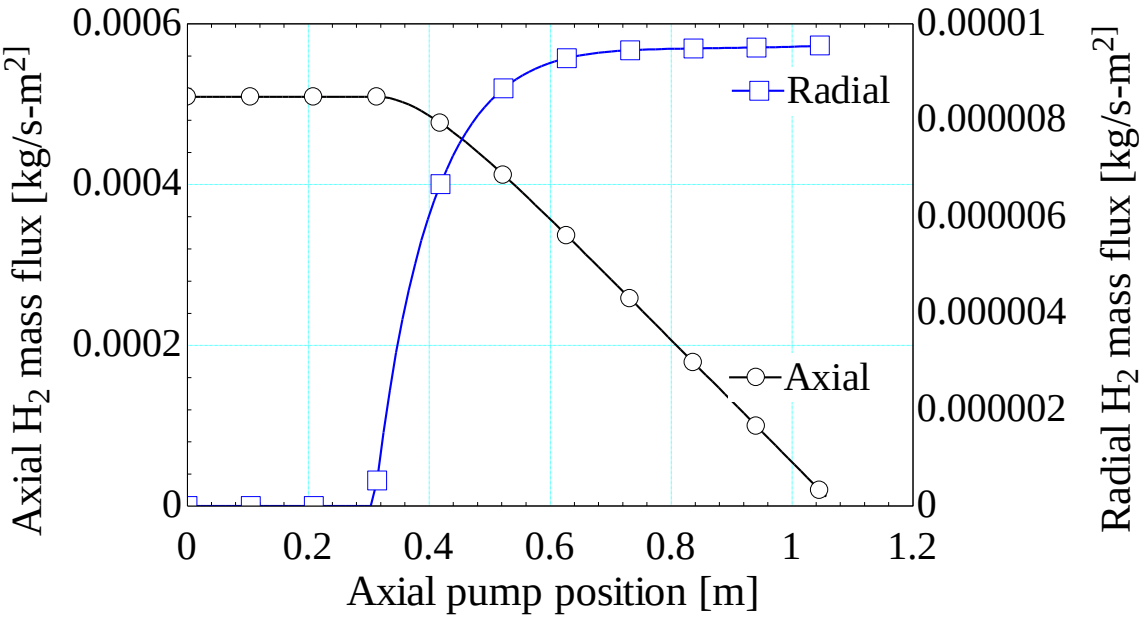

FIGURE 4-20. Axial hydrogen mass flux and radial hydrogen mass flux as a function of axial pump position.

FIGURE 4-20 shows the profiles of the axial hydrogen mass flux and the radial hydrogen mass flux. As the hydrogen molecules are adsorbed on the pump wall (represented by radial hydrogen mass flux), the mass flow rate of the bulk hydrogen gas (represented by axial hydrogen mass flux) decreases.

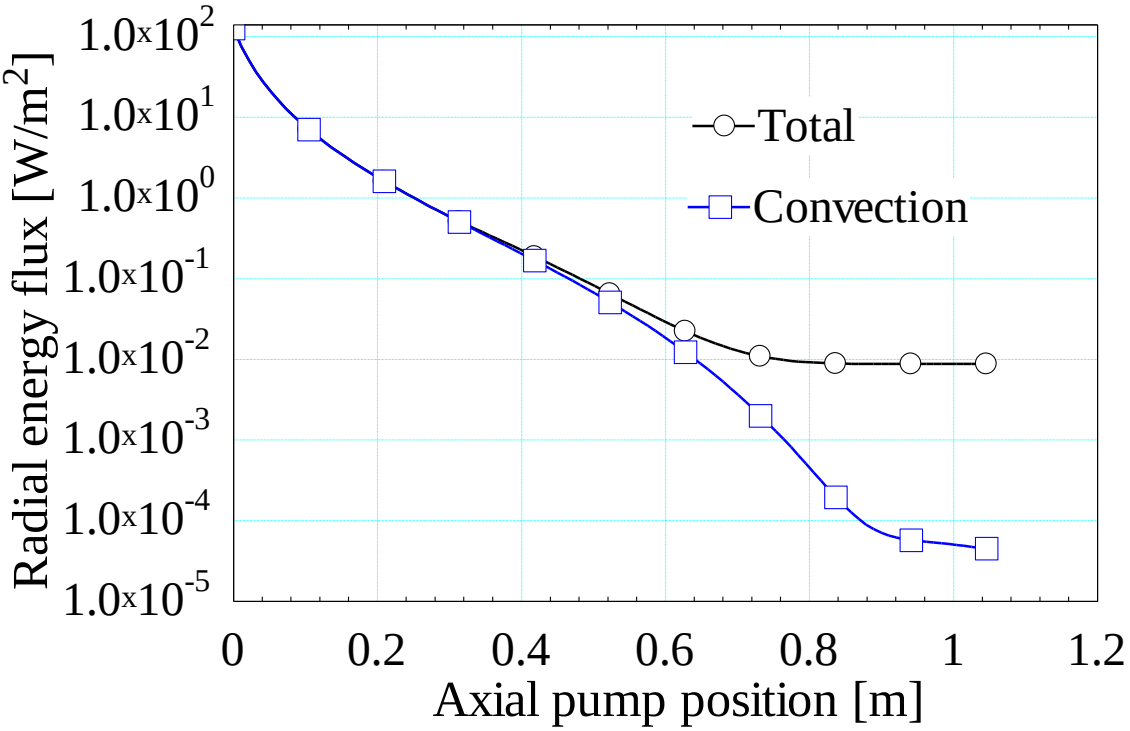

FIGURE 4-21. Total radial energy flux and convection energy flux as a function of axial pump position (I).

FIGURE 4-21 shows the profiles of the total radial energy flux and the convection energy flux. The total energy flux is the sum of the convection energy flux and the adsorption energy flux. On the log-scale figure, one can observe that the adsorption energy flux (the difference between the two profiles) dominates beyond 0.7 m.

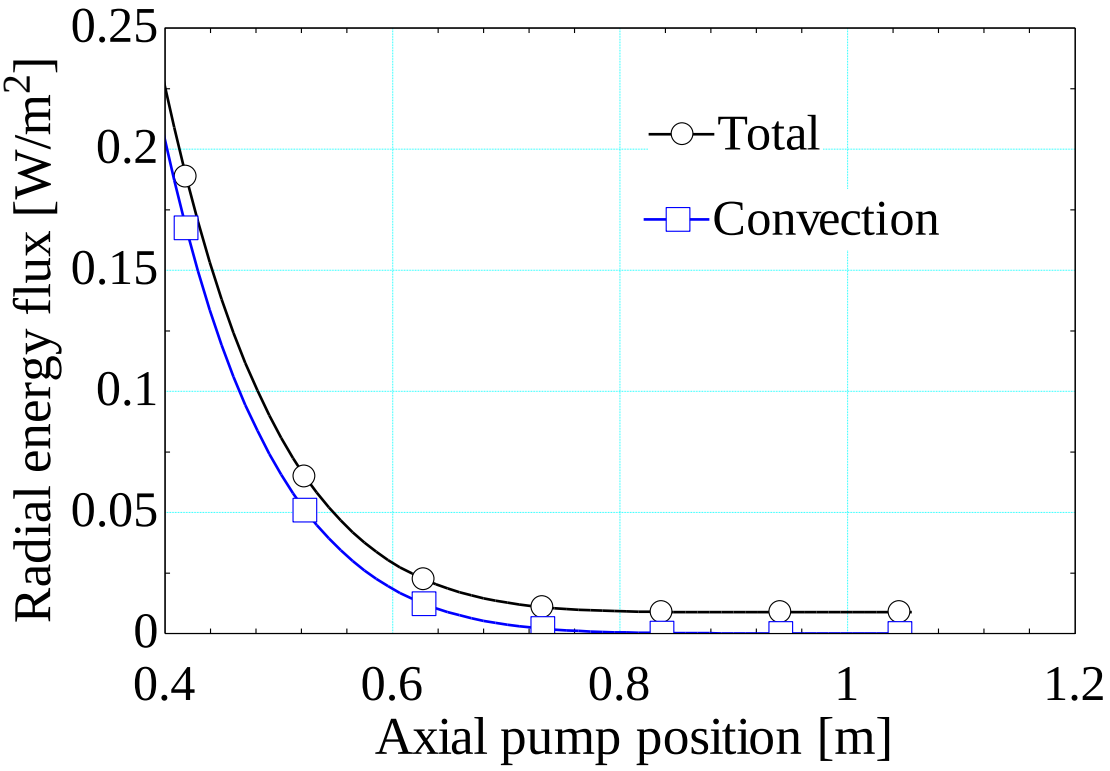

FIGURE 4-22. Total radial energy flux and convection energy flux as a function of axial pump position (II).

FIGURE 4-22 shows the profiles of the total radial energy flux and the convection energy flux after the axial pump position of 0.4 m. The difference is the adsorption energy flux.

Chapter 5 Hemisphere model

The transient model explains the experimental data set I. The steady-state model investigates the "best" performance of the cryogenic pump. However, both of the two models are developed for the pump working in the viscous regime. The hemisphere model being discussed in this section is the model for the pump working in the molecular regime. It also incorporates a transient change of the pump wall temperature.

Whether the pump works in viscous regime or molecular regime depends on the Knudsen number (Kn) of the hydrogen gas. For the cryogenic pump, the Kn number is defined as the radio of the mean free path (λ) of the hydrogen gas to the inner tube diameter (D_{in}) of the pump.

$$Kn = \frac{\lambda}{D_{in}} \tag{57}$$

When the Kn number is smaller than unity, the hydrogen gas is in the viscous regime. When the Kn number is comparable to or greater than unity, the hydrogen gas is in the molecular regime.

The mean free path λ is inversely proportional to the hydrogen gas pressure P . As the pressure P decreases, the mean free path λ approaches the characteristic length

D_{in}. At 80 K, when the pressure P is 0.066 Pa, the mean free path becomes comparable to the characteristic length D_{in}.

$$\lambda = \frac{k_B T}{\sqrt{2}\pi d^2 P} \quad 58)$$

Note significantly, the hydrogen vapor pressure is 0.00476 Pa at 5 K, and is 2.08E-7 mmHg (about 0.00003 Pa) at 4 K. The supercritical helium coolant that will be used for the ITER cryogenic fore pump is at about 4.5 K. And it means that a stream of hydrogen gas alone will be in the molecular regime once the pump wall temperature approaches 5 K. Under that condition, the hemisphere model is relevant.

5.1. Analysis and governing equations

The inlet helium coolant temperature dominantly determines the pump wall temperature. When the cooling power is strong enough, the pump wall temperature can be decreased to about 5 K. At that temperature, the hydrogen vapor pressure is smaller than the critical pressure of 0.066 Pa at which the mean free path λ is comparable to the characteristic length D_{in}. In other words, the hydrogen gas is in the molecular regime.

In the molecular flow regime the inlet hydrogen molecules are very efficiently adsorbed by the pump. The molecules colliding onto the pump wall are adsorbed and never come back to the hydrogen gas again. The adsorbed hydrogen molecules seem to disappear. In other words, the sticking coefficient S is very close to unity.

In such a case, the pump wall to the inlet hydrogen molecules is not a physical boundary any more. Instead, the pump wall is similar to a vacuum space where the hydrogen molecules seem to disappear.

There are two major differences between the hemisphere model and the transient model together with the steady-state model. One difference is the mass adsorption rate and the other is the thermal resistance network. The following discussion addresses the mass adsorption rate of the hydrogen molecules.

The following two figures (**FIGURE 5-1** and **FIGURE 5-2**) illustrate the key idea. **FIGURE 5-1** is the cryogenic pump as seen by the hydrogen gas in the viscous regime, while **FIGURE 5-2** is the apparent cryogenic pump as seen by the hydrogen gas when the pump wall temperature results in the molecular flow regime for the hydrogen molecules. The transient model and the steady-state model are developed based on **FIGURE 5-1**. The hemisphere model is developed based on **FIGURE 5-2**.

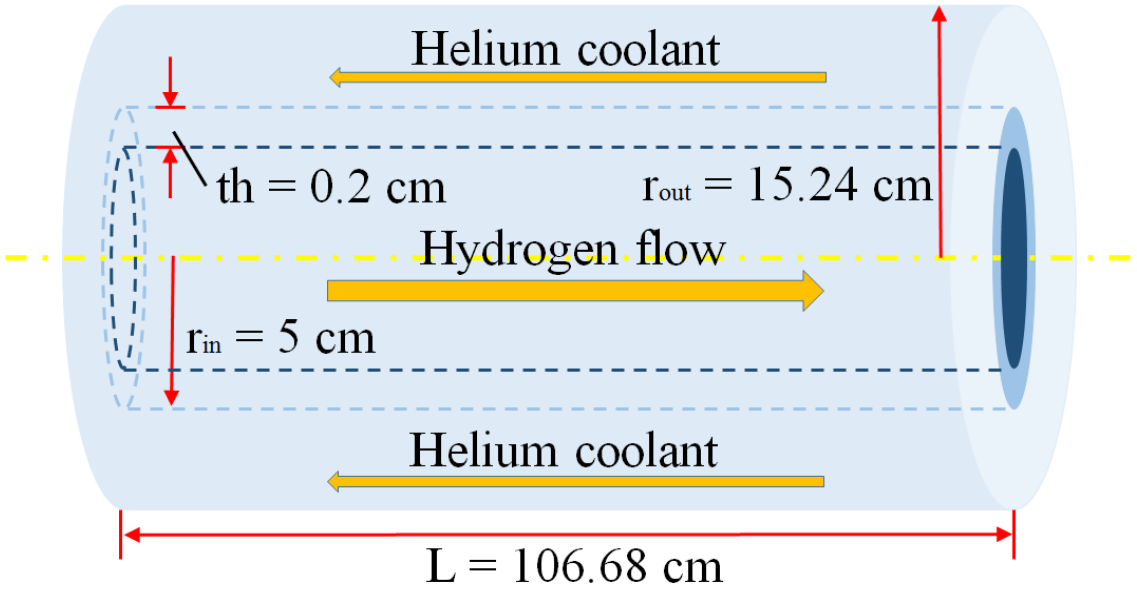

FIGURE 5-1. The cryogenic fore pump working at viscous flow region (not to scale).

FIGURE 5-1 shows the geometry of the cryogenic pump. It is a concentric tube-in-tube arrangement. The hydrogen gas flows in the inner tube while the helium coolant counter flows in the annular tube. The geometry in the figure is not to scale.

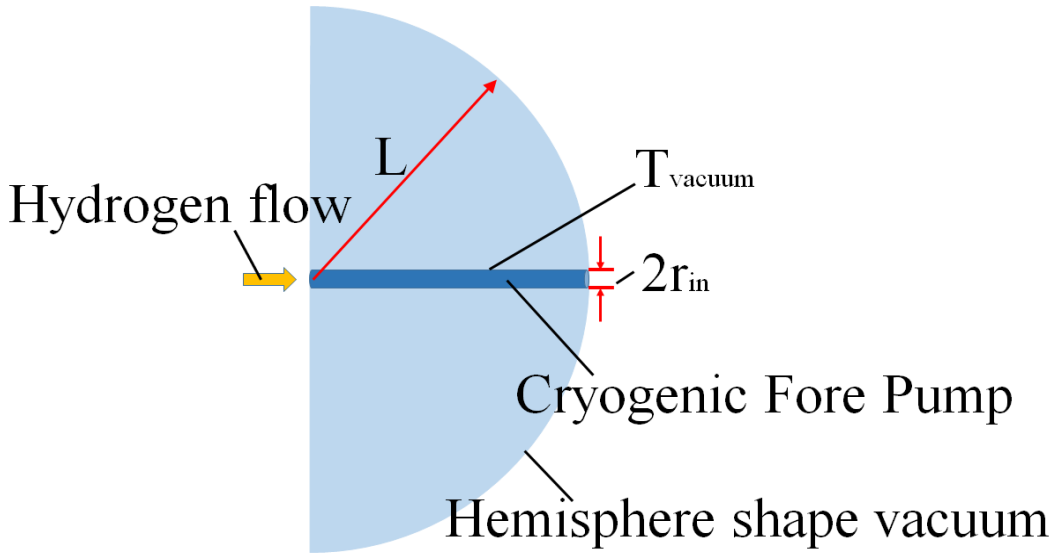

FIGURE 5-2. Hemisphere model for the cryogenic fore pump working at vacuum region.

FIGURE 5-2 shows the apparent cryogenic pump seen by the inlet hydrogen molecules, and illustrates how the idea of the hemisphere model is developed. Note significantly, the cryogenic pump is represented by the thin tube, located along the diameter of the hemisphere. When the pump wall is cold enough to adsorb most of the incoming hydrogen molecules, the pump wall behaves like a vacuum space to the hydrogen molecules. The hydrogen molecules entering the pump don't see the pump. Instead they see a hemisphere-shape vacuum space with the radius of the hemisphere defined by the pump length.

At the pump entrance, the inlet hydrogen molecules can be treated as a point source at the center of the hemisphere. The inlet hydrogen molecules travel in random directions into the hemisphere. The amount of the hydrogen molecules hitting a particular location on

the hemisphere depends on the ratio of that surface area to the total hemisphere area. This ratio can be expressed by the solid angle α in **FIGURE 5-3**.

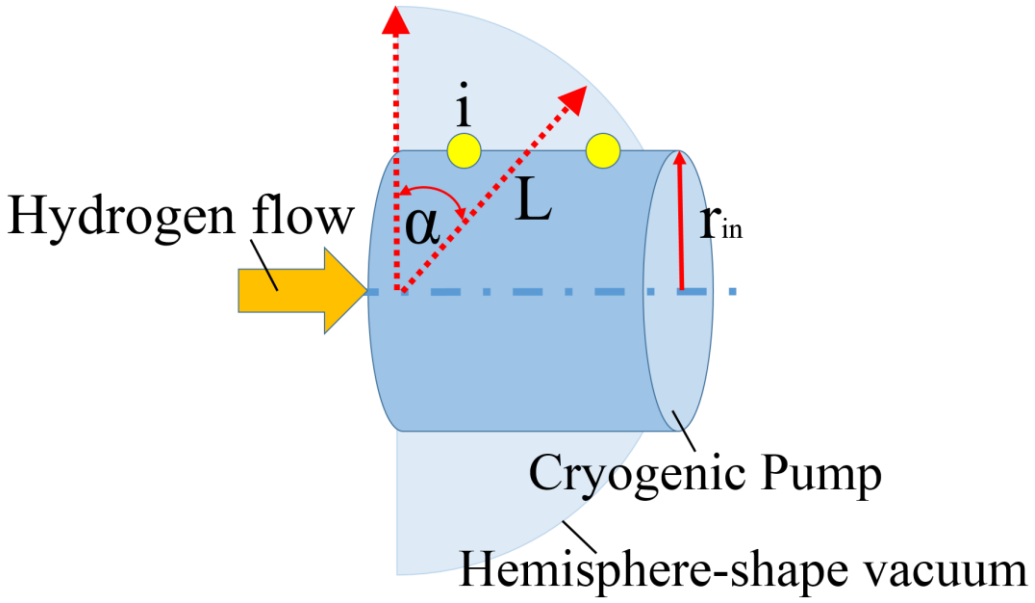

FIGURE 5-3. Hemisphere model and the cryogenic fore pump.

FIGURE 5-3 shows the hemisphere model and the cryogenic pump (not to scale). The numerical nodes on the pump wall define a cylindrical shaped surface. The amount of the hydrogen molecules colliding onto that surface can is a portion of the total inlet hydrogen molecules. And that portion can be calculated based on the angle α. The angle α can be calculated from the ratio of the corresponding surface area on the hemisphere

to the total hemisphere area. The values for the first 5 nodes are 0.4033, 0.3032, 0.2012, 0.1332, and 0.09167 respectively.

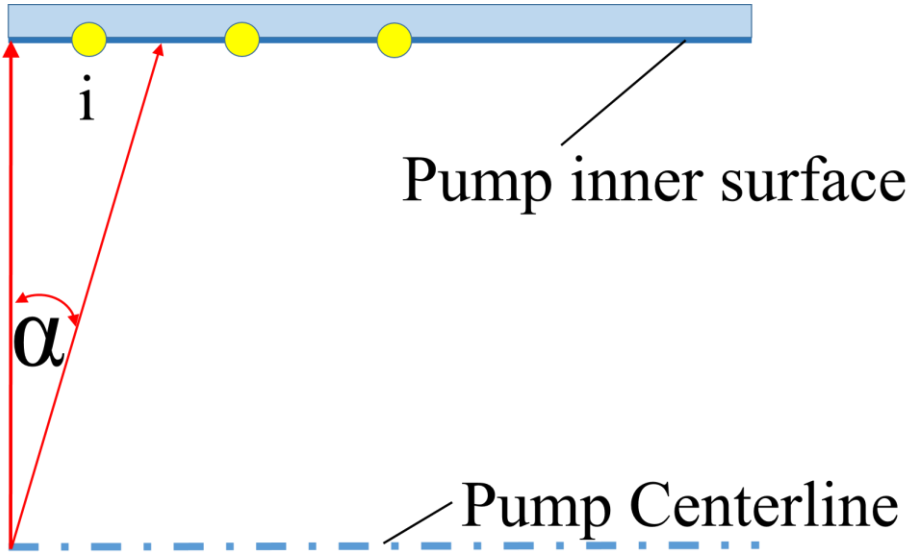

FIGURE 5-4. The angle of point source of the hydrogen molecules.

FIGURE 5-4 shows the angle α and half of the pump (not to scale). Numerical nodes are placed on the pump wall, represented as the yellow dots in **FIGURE 5-4**. The positions of the nodes are the axial pump positions in the numerical models.

Based on the analysis, the mass flow rate of the hydrogen molecules colliding on the node i surface, $m_{w,H_2,i}$, is calculated as follow.

$$m_{w,H_2,i} = m_{H_2} \frac{\alpha}{(\pi/2)} \quad 59)$$

Where m_{H_2} is the total inlet mass rate of the hydrogen molecules into the cryogenic pump.

It is assumed here that the pump wall temperature is low enough that any hydrogen molecules colliding with the pump wall are adsorbed. In other words, $m_{w,H_2,i}$ is the mass rate of the hydrogen molecules that is adsorbed by the node i surface.

Following the discussion of the mass rate of the adsorbed hydrogen molecules, the thermal resistance network is discussed by comparing **FIGURE 5-5** and **FIGURE 5-6**. **FIGURE 5-5** shows the thermal resistance network for the pump in the viscous regime, that forms the basis of the transient model and the steady-state model. **FIGURE 5-6** shows the thermal resistance network for the cryogenic pump in the molecular regime, that forms the basis of the hemisphere model.

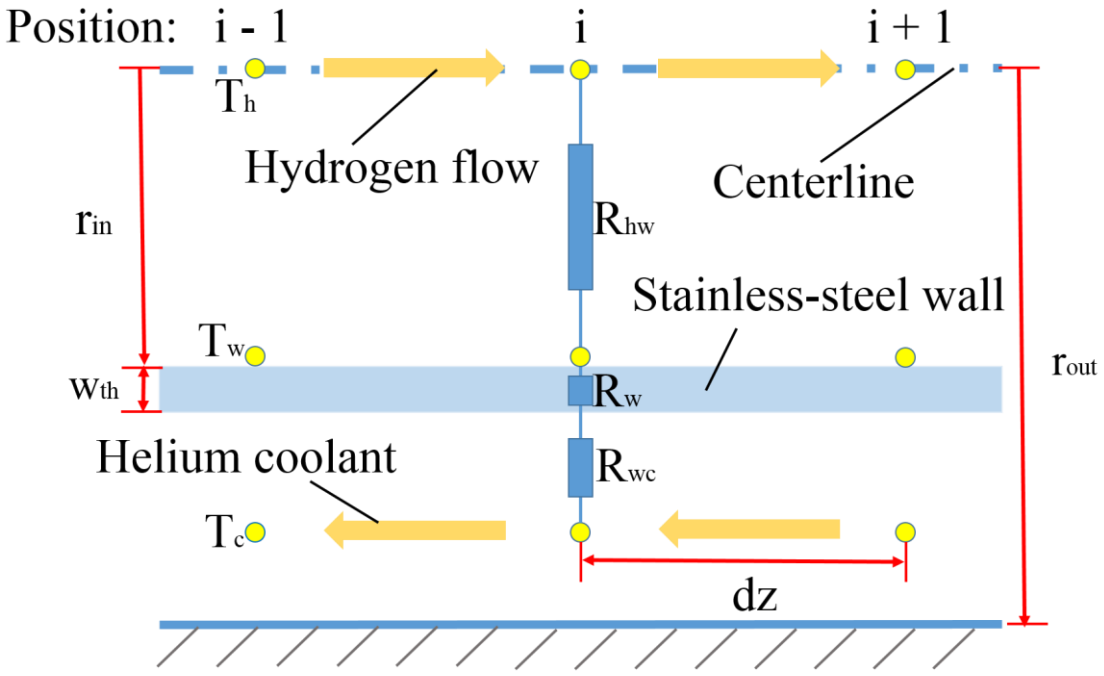

FIGURE 5-5. Thermal resistance network for cryogenic fore pump in viscous flow region.

FIGURE 5-5 shows the thermal resistance network for the cryogenic pump in the viscous regime. The heat transfers from the hydrogen gas to the helium coolant by passing through three thermal resistances, R_{hw}, R_w, and R_{wc}. R_{hw} is the convective resistance from the hydrogen gas to the inner pump wall, R_w is the conductive resistance through the pump wall, and R_{wc} is the convective resistance from the outside of the pump wall to the helium coolant. The total energy transferred to the inner pump wall is the sum of the convective heat from the hydrogen gas and the adsorption energy of the hydrogen molecules.

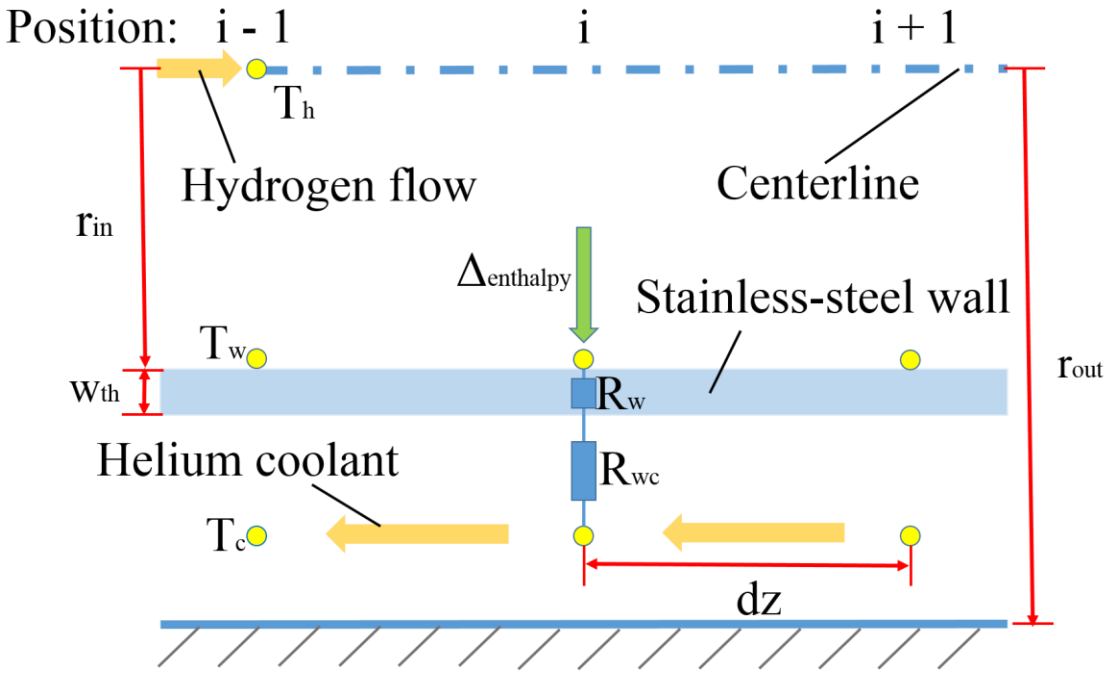

FIGURE 5-6. Thermal resistance for the cryogenic fore pump in the hemisphere model.

FIGURE 5-6 shows the thermal resistance network for the cryogenic pump in the molecular regime. Compared to **FIGURE 5-5**, there is no equivalent thermal resistance R_{hw} in **FIGURE 5-6**. In other words, there is no convective heat transfer from the hydrogen gas to the inner pump wall, because of the lack of the viscous hydrogen gas flow. The hydrogen molecules hitting the pump wall are adsorbed and do not return back to the hydrogen gas. As a result, there is no information traveling from the pump wall to the hydrogen gas. The energy transferred from the hydrogen gas to the pump inner wall is the adsorption energy. The other two the thermal resistances are the same.

Based on the analysis, for the hemisphere model the energy transfer rate to the node i due to the adsorption of the hydrogen molecules, $E_{H_2->w}$, is the product of the mass rate $m_{w,H_2,i}$ and the adsorption energy $\Delta E_{adsorption}$.

$$E_{H_2->w} = m_{w,H_2,i}\Delta E_{adsorption} \quad 60)$$

For the particular cryogenic pump, the adsorption process is the deposition of the hydrogen molecules into the solid phase. And the adsorption energy $\Delta E_{adsorption}$ is expressed as the following equation.

$$\Delta E_{adsorption} = \Delta h_{H_2} + \frac{1}{2}u_z^{\,2} \quad 61)$$

Where Δh_{H_2} and $\frac{1}{2}u_z^{\,2}$ are the enthalpy change of the adsorbed hydrogen molecules and the kinetic energy of the adsorbed hydrogen molecules respectively.

The enthalpy change Δh_{H_2} includes two parts, $\Delta h_{H_2,inet->gas_s}$ and $\Delta h_{H_2,gas_s->solid}$. $\Delta h_{H_2,inet->gas_s}$ is the enthalpy change from the gas phase at the inlet condition to the gas

phase in the gas-solid equilibrium condition. $\Delta h_{H_2,gas_s->solid}$ is the enthalpy change from the gas phase in the gas-solid equilibrium condition to the corresponding solid phase.

$$\Delta h_{H_2} = \Delta h_{H_2,inet->gas_s} + \Delta h_{H_2,gas_s->solid} \quad 62)$$

The conservation equation of energy on the control volume of the pump wall is shown as follows.

$$E_{H_2->w} = Q_{w->c} + \frac{\Delta U_w}{\Delta t} \quad 63)$$

Here $Q_{w->c}$ is energy transfer rate from the pump wall to the helium coolant, and $\frac{\Delta U_w}{\Delta t}$ is the internal energy change rate of the pump wall.

The conservation equation of energy on the control volume of the helium coolant is shown as follows.

$$Q_{w->c} = \Delta H_c + \frac{\Delta U_c}{\Delta t} \quad 64)$$

Here ΔH_c is the rate of enthalpy change for the helium coolant passing through the node, and $\frac{\Delta U_c}{\Delta t}$ is the rate of internal energy change of the resident helium coolant.

The energy transfer rate from the outer pump wall to the helium coolant $Q_{w->c}$ is constrained by the following energy equation.

$$Q_{w->c} = \frac{T_w - T_c}{R_{wc}} \quad 65)$$

Where R_{wc} is the convective thermal resistance from the outer pump wall to the helium coolant.

5.2. Results and discussion

The results of the hemisphere model are presented in this section. Note that axial conduction along the pump wall is neglected. The initial condition and the inlet conditions of the hydrogen gas and the helium coolant are as follows.

The pump wall temperature and the residence helium coolant in the pump are initially set to be at 5 K. The mass flow rate of the inlet hydrogen gas is set at 0.001 g/s with the temperature of 77 K. At 77 K, the enthalpy of hydrogen is 1056 kJ/kg for the pressure range of [1 Pa, 100 Pa] (reference state: 298.15 K, 101.325 kPa: enthalpy = 3932 kJ/kg). As is typical of an ideal gas the pressure dependence of the enthalpy is negligible.

The mass flow rate of the inlet helium coolant is set at 0.53 g/s with the temperature of 5 K and the pressure of 1.4 bar.

At such conditions, most of the hydrogen molecules are adsorbed within the first 0.2 m of the cryogenic pump, and in that region the pump wall temperature rises due to the adsorption energy.

Once the temperature rises to a critical value, (5.8 K for the 5 cm diameter) the assumption of molecular flow is not valid. The critical temperature yields a hydrogen vapor pressure for which the mean free path is comparable to the pump diameter. In this situation the point source of the hydrogen gas can be treated as moving forward into the pump to the region where the pump wall temperature is low and the hemisphere model works again. In other words, the hemisphere model works in the region where the pump wall temperature is lower than the critical temperature. As long as the inlet helium coolant has enough cooling power to maintain some portion of the wall at a temperature below the critical temperature, such a region always exists.

As mentioned above, most of the hydrogen molecules are adsorbed onto the cryogenic pump before the axial position of 0.2 m. The pump wall beyond 0.2 m is not significantly affected by the inlet hydrogen molecules, and the temperature of that part does not rise. As a result, the modeling results of the hemisphere model are only shown for the region before the axial position of 0.2 m as follows.

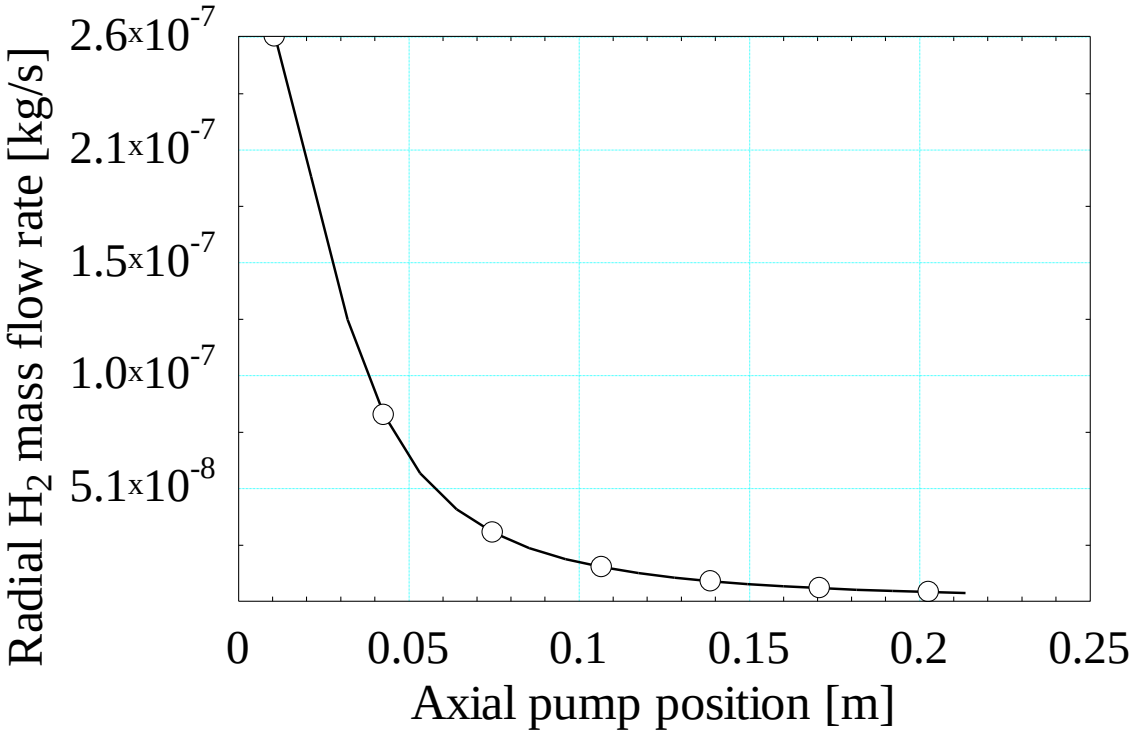

FIGURE 5-7. Radial hydrogen mass flow rate as a function of axial pump position.

FIGURE 5-7 shows the profile of the mass flow rate of the adsorbed hydrogen molecules. Most of the hydrogen molecules are adsorbed on the pump entrance. Before the pump wall temperature rises above the critical temperature, the profile of the mass rate does not change.

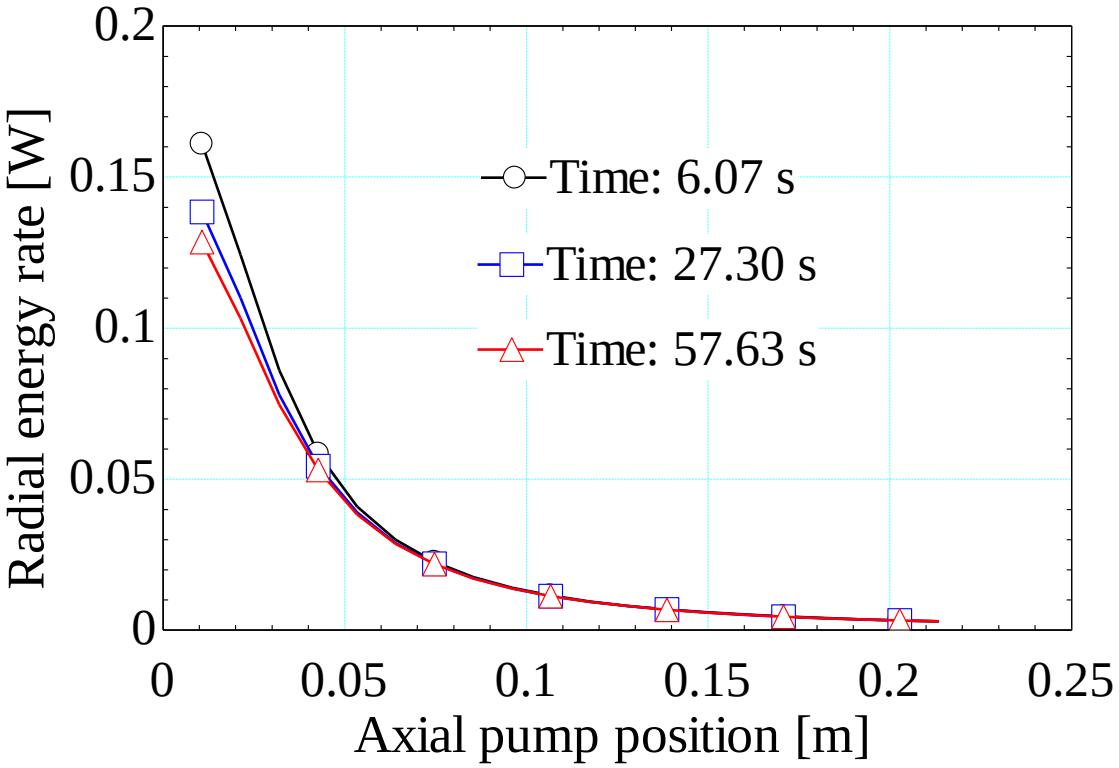

FIGURE 5-8. Radial energy rate transferred to the pump wall as a function of axial pump position.

FIGURE 5-8 shows profiles of the radial energy rate transferred to the pump wall. The energy rate is only due to adsorption of the hydrogen molecules, but includes the change of enthalpy plus the negligible kinetic energy.

The energy rate is high at the pump entrance because of the large amount of adsorbed hydrogen molecules. Due to the adsorption energy, the pump wall temperature rises. As the temperature difference between the hydrogen gas and the pump wall decreases, the radial energy rate also decreases.

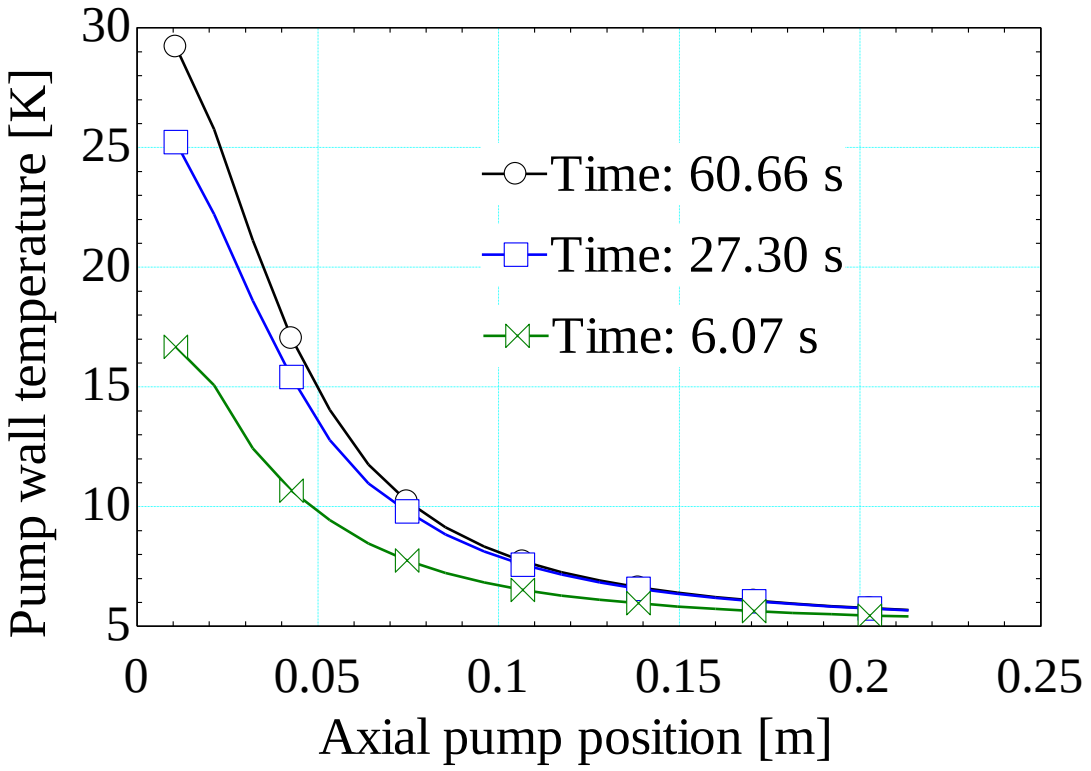

FIGURE 5-9. Pump wall temperature as a function of axial pump position.

FIGURE 5-9 shows the profiles of the pump wall temperature. The pump wall temperature rises significantly from 5 K at the pump entrance due to the large amount of adsorbed hydrogen molecules. After the pump wall temperature exceeds the critical temperature, the point source of the hydrogen gas can be moved forward into the pump.

The significant pump wall temperature rise is also due to the high inlet hydrogen gas temperature. As the gas temperature decreases, the adsorption energy (enthalpy change) also decreases, leading to a smaller temperature rise of the pump wall.

Thus, the cryogenic pump can be divided into two parts. The first part precools the hydrogen gas, and the transient model or the steady-state model can be used in this region.

The second part uses the hemisphere model when the inlet hydrogen gas temperature is low and the mass flow rate is small.

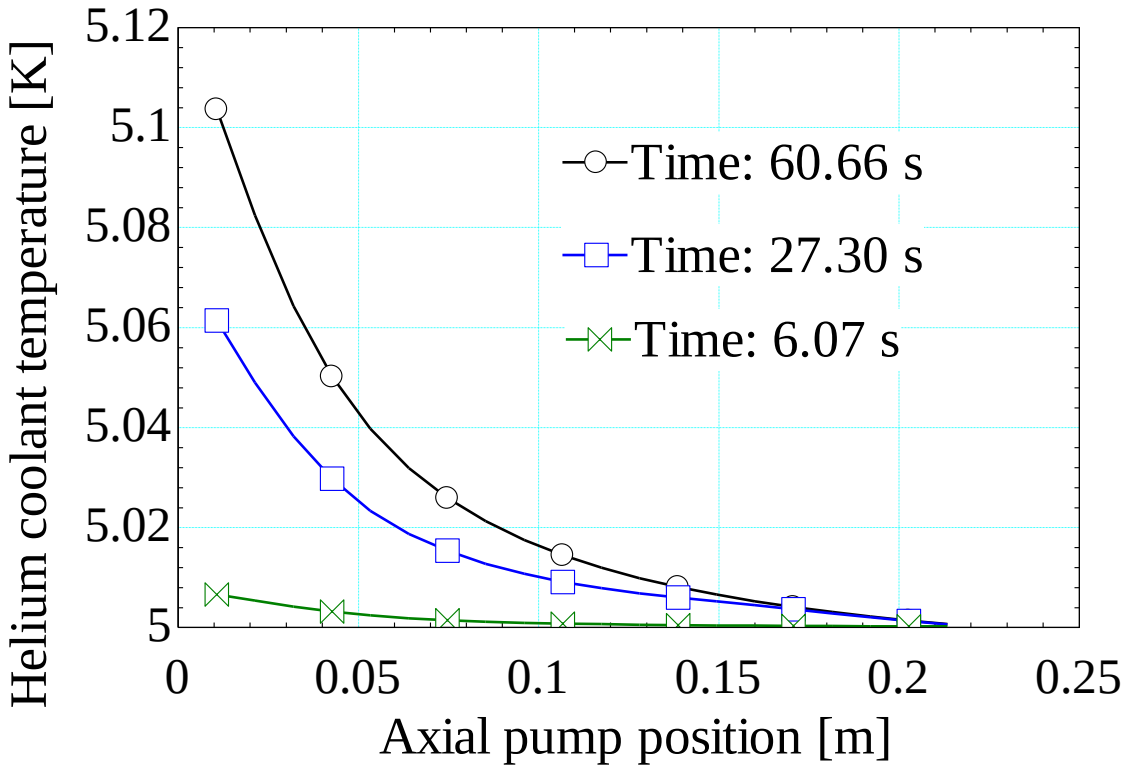

FIGURE 5-10. Helium coolant temperature as a function of axial pump position.

FIGURE 5-10 shows the profiles of the helium coolant temperature. The helium coolant temperature only increases mildly. Even at the pump entrance, the temperature increases only 0.1 K in about 60 seconds. The small temperature rise is due to the relatively large heat capacity of the helium coolant compared to the other components. From this perspective, one may observe that the helium coolant provides a strong cooling power.

Chapter 6 Conclusions

The thesis summarizes the modeling effort carried out at UW-Madison regarding the cryogenic fore pump being designed for use in ITER. The investigation is based on our understanding of the associated theory and physics, and is formulated in terms of numerical models. The numerical models can provide a starting point and reference for future work on similar problems involving viscous cryopumping.

6.1. Modeling of cryogenic fore pump

Three numerical models are developed; the transient model, the steady-state model, and the hemisphere model. The transient model and the steady-state model apply when the cryogenic fore pump operates in the viscous flow regime, and the hemisphere model applies when the pump operates in the molecular flow regime.

By comparing the transient model with the experimental data set I provided by colleagues at ORNL, this thesis has been able to both explain the experimental data, and verify the transient model.

The steady-state model provides a method for designing an optimally performing cryogenic pump. It investigates the two important parameters, namely the inlet hydrogen gas pressure and the inlet helium coolant temperature. It explores the relationship between the two parameters, and clearly shows how the inlet helium coolant temperature determines the cryogenic pumping performance and how the inlet hydrogen pressure reflects that performance.

The hemisphere model is developed for the condition where the pump wall temperature yields a sufficiently low hydrogen vapor pressure so that the molecules

according to molecular flow, rather than viscous flow, dynamics. When the helium coolant provides sufficient cooling power, the pump wall temperature drops below a critical temperature, and the corresponding hydrogen vapor pressure is in the molecular flow regime. In this regime, the mean free path of the hydrogen molecules is comparable to the pump diameter.

The three numerical models capture the overall performance of the cryogenic fore pump and should be adopted according to the specific conditions.

6.2. Future investigations

The possibility of better models always exists.

First, additional property data are needed. For helium, thermodynamic properties are available using the fundamental equation of state given by Reiner Tillner-Roth (Tillner-Roth, 1998), and the temperature of applicability is as low as 2.1768 K. Transport properties of helium are also available. However, for normal hydrogen, thermodynamic properties are provided in the temperature range from 13.957 K and above; gas phase viscosity is available from 18 K and above; and gas phase thermal conductivity is available from 14 K and above. The data for deuterium are even more strictly limited: The range of applicability for equation of state is from 18.71 K to 423 K.

Secondly, in the work carried out for this thesis, access to the raw experimental data provided a turning point in the model development. It is thus of benefit to access and compare more experimental data with the numerical models.

Chapter 7 References

Ahlers, G. (1963). *Some properties of solid hydrogen at small molar volumes.* Berkeley: Lawrence Radiation Laboratory, University of California, Berkeley.

Baylor, L. M., Barbier, C., Combs, S., Duckworth, R., Edgemon, T., Fehling, D. R., . . . Boisson, J. (2011). Cryogenic viscous compressor development and modeling for the ITER vacuum system. *Fusion Engineering (SOFE), 2011 IEEE/NPSS 24th Symposium on*, (pp. 1 - 4). Chicago.

Bentley, P. (1980). The modern cryopump. *Vacuum*, 145–158.

C. Day, D. B. (2005). Performance of ITER-Relevant Cryopump Panels for Tritiated Gases. *7th Tritium Science and Technology Conference* (pp. 29-34). Baden Baden, Germany: Fusion Science and Technology.

C. Day, D. M. (2009). The vacuum systems of ITER. *Vacuum*, 773-778.

M. Dremel, C. D. (2009). Cryopump design development for the ITER Neutral Beam Injector. *Fusion Engineering and Design*, 689-693.

C. Tzemos, M. G. (1986). Design and Performance of a Liquid Helium Cryopump Operating in the Viscous Flow Regime. *Advances in Cryogenic Engineering*, 575-581.

Deen, W. M. (1998). *Analysis of Transport Phenomena (Topics in Chemical Engineering).* New York: Oxford University Press.

Duckworth, R. C., Baylor, L. R., Meitner, S. J., Combs, S. K., Rasmussen, D. A., Hechler, M., . . . Boissin, J.-C. (2012). Development and demonstration of a supercritical helium-cooled cryogenic viscous compressor prototype for the iter vacuum system.

Private communication from Robert C. Duckworth

Edwards, M. F. (1968). Gas dispersion in packed beds. *Chemical Engineering Science*, 109-123.

Ferziger, J. H. (1996). *Computational methods for fluid dynamics.* Springer.

Foster, C. A. (2005). A Continuous Cryogenic Diffusion Pump For Fusion Reactors. *Fusion Engineering 2005, Twenty-First IEEE/NPS Symposium on* (pp. 1-4). Knoxville, TN: IEEE.

Furry, W. H. (1939). On the theory of isotope separation by thermal diffusion. *Physical Review*, 1083.

Govers, T. R. (1980). Molecular beam experiments on the sticking and accommodation of molecular hydrogen on a low-temperature substrate. *The Journal of Chemical Physics*, 5446.

Gregory Nellis, S. K. (2008). *Heat transfer.* Cambridge.

Hands, B. (1976). Introduction to cryopump design. *Vacuum*, 11-16.

Hornbeck, R. W. (1965). An all-numerical method for heat transfer in the inlet of a tube. *ASME*.

J. M. COULSON, J. F. (1990). *Chemical Engineering , Vol. 1*. Pergamon Press.

J. W. Leachman, R. T. (2009). Fundamental equations of state for parahydrogen, normal hydrogen, and orthohydrogen. *Journal of Physical and Chemical Reference Data*, 721.

K. Munakataa, S. B. (2007). Experimental and simulation study on adsorption of hydrogen isotopes on MS5A at 77K. *Fusion Engineering and Design*, 2303-2310.

Kennard, E. H. (1938). *Kinetic theory of gases: with an introduction to statistical mechanics*. New York: McGraw-hill.

Lafferty, J. M. (1998). *Foundations of Vacuum Science and Technology*. John Wiley & Sons, Inc.

Lindsay, A. L. (1950). Thermal conductivity of gas mixtures. *Industrial & Engineering Chemistry*, 1508-1511.

Luo, X. (2011). Experimental results and numerical modeling of a high-performance large-scale cryopump. I. Test particle Monte Carlo simulation. *Journal of Vacuum Science & Technology A: Vacuum, Surfaces, and Films*, 041601 - 041601-7.

M.F. Edwards1, J. R. (1968). Gas dispersion in packed beds. *Chemical Engineering Science*, 109–123.

McCarty, R. D. (1981). *Selected properties of hydrogen (engineering design data)*. Boulder, CO (USA): National Engineering Lab.(NBS).

Mullins, J., Ziegler, W., & Kirk, S. (1961). *Thermodynamic properties of parahydrogen from 1 to 22/sup 0/K*. Atlanta (USA): Georgia Inst. of Tech.

Myers, G. E. (1998). *Analytical Methods in Conduction Heat Transfer*. Amch.

Nastaj, J. F. (2006). Simulation studies of a vacuum and temperature swing adsorption process for the removal of VOC from waste air streams. *International communications in heat and mass transfer*, 80-86.

Nordlander, P. S. (1984). Hydrogen adsorption on metal surfaces. *Surface science*, 59-81.

O'Hanlon, J. F. (2004). *A User's Guide to Vacuum Technology*. Hoboken, NJ, USA: John Wiley & Sons, Inc.

P Dwivedi, V. G. (2004). Comparative study of removal of volatile organic compounds by cryogenic condensation and adsorption by activated carbon fiber. *Separation and Purification Technology*, 23-37.

R. K. Shah, A. L. (1978). *Laminar Flow Forced Convection in Ducts: a Source Book for Compact Heat Exchanger Analytical Data, Supl. 1*. New York: Academic Press.

RB Bird, W. S. (2007). *Transport phenomena*. Wiley. com.

Reid, R., Prausnitz, J., & Poling, B. (1987). *The properties of gases and liquids.* New York, NY: McGraw Hill Book Co.

Roder, H. M. (1977). *The thermodynamic properties of slush hydrogen and oxygen.* Boulder, Co, USA: National Bureau of Standards.

Roder, H. M., Childs, G. E., McCarty, R. D., & Angerhofer, P. E. (1973). *Survey of the properties of the hydrogen isotopes below their critical temperatures.* Boulder, Co, USA: National Bureau of Standards (U.S.).

Ruthven, D. M. (1984). *Principles of adsorption and adsorption processes.* New York: Wiley.

S Varoutis, C. D. (2011). Follow-up vacuum study of the ITER model cryopump by the direct simulation Monte Carlo method. *Verhandlungen der Deutschen Physikalischen Gesellschaft*.

S. Farooq, D. R. (1991). Numerical simulation of a kinetically controlled pressure swing adsorption bulk separation process based on a diffusion model. *Chemical Engineering Science*, 2213–2224.

Sanford Klein, G. N. (2011). *Thermodynamics.* Cambridge.

Schork, J. M. (1988). Parametric analysis of thermal regeneration of adsorption beds. *Industrial & engineering chemistry research*, 457-469.

Stylianos Varoutis, C. D. (2012). Numerical modeling of an ITER type Cryopump. *Fusion Engineering and Design*, 1395-1398.

Tannehill, J. C., Anderson, D. A., & Pletcher, R. H. (1997). *Computational Fluid Mechanics and Heat Transfer.* Pennsylvania, U.S.A.: Bristol.

Tillner-Roth, R. (1998). *Fundamental Equations of State.* Shaker.

Wakao, N. a. (1978). Effect of fluid dispersion coefficients on particle-to-fluid mass transfer coefficients in packed beds: Correlation of Sherwood numbers. *Chemical Engineering Science*, 1375-1384.

Wakao, N. T. (1978). Effect of fluid dispersion coefficients on particle-to-fluid mass transfer coefficients in packed beds: Correlation of Sherwood numbers. *Chemical Engineering Science*, 1375-1384.

Wilke, C. R. (1950). A viscosity equation for gas mixtures. *The Journal of Chemical Physics*, 517.

Yang, R. (1997). *Gas Separation by Adsorption Processes.* UK: Imperial College Press.

D. S. Zhang, F. K. (2014). Modeling results for the ITER cryogenic fore pump. *AIP Conf. Proc.* (p. 618). Anchorage, Alaska, USA: AIP Publishing.

Chapter 8 Appendix

Appendix A. Transient model code

```
$UnitSysytem SI mass kg J m s rad Pa K
$Tabstops 0.2 0.4 0.6 0.8 1 in
"initial condition: initial T_c, T_w  --> heat flux --> next setp T_c, T_w"

"so sensitive to guess value of pressure"


Procedure enthalpy_ad(T,P:h)   "hydrogen enthalpy"
    G1$='Hydrogen'
    M_1=MolarMass(G1$)
    if (T<=14 [K]) then
        h=(521047[J/kmol] + 20616.7[J/kmol-K]*T)/M_1
    else
        h=256598[J/kg] + 10357.4[J/kg-K]*T
        {h=Enthalpy(G1$,T=T,P=P)}
    endif
end

Procedure mix(T,P_1:mu,k,cp)  "mixture thermal and kinetic properties"
    G1$='Hydrogen'
    M_1=MolarMass(G1$)
    if (T>18[K]) then
        mu_1=Viscosity(G1$,T=T,P=P_1)
    else
        mu_1=7.64217E-07[Pa-s] + 3.39265E-08[Pa-s/K]*T
    endif
{   mu_1=Viscosity(G1$,T=T,P=P_1)}
    if (T>14[K]) then
        k_1=Conductivity(G1$,T=T,P=P_1)
    else
        k_1=0.00559606[W/m-K] + 0.000629187[W/m-K^2]*T
    endif
{   k_1=Conductivity(G1$,T=14[K],P=P_1)}
    mu=mu_1"viscosity"
    k=k_1 "conductivity"
    if (T<10[K]) then
        cp_1=(35.065[J/kmol-K] - 73.0795[J/kmol-K^2]*T + 27.5904[J/kmol-
K^3]*T^2)/M_1
```

```
    else
        if (T>=10[K]) and (T<13.957[K]) then
            cp_1=(4469.83[J/kmol-K] - 1147.04[J/kmol-K^2]*T + 89.2029[J/kmol-
K^3]*T^2)/M_1
        else
            cp_1=SpecHeat(G1$,T=T,P=P_1)
        endif
    endif
    cp=cp_1   "specific heat"
end


Procedure Wall(P_1,T:P)     "wall boundary conditions"
G1$='Hydrogen'
    if (T>10[K]) then
        P=P_1
    else
        if (T<=10[K]) and (T>9[K]) then
            P=min(P_1,-1587.87[Pa] + 184.345[Pa/K]*T)
        else
            if (T<=9[K]) and (T>8[K]) then
                P=min(P_1,-435.724[Pa] + 56.3287[Pa/K]*T)
            else
                if (T<=8[K]) and (T>7[K]) then
                    P=-87.6888[Pa] + 12.8243[Pa/K]*T
                else
                    if (T<=7[K]) and (T>6[K]) then
                        P=-11.3689[Pa] + 1.92144[Pa/K]*T
                    else
                        P=max(0.0001[Pa],-0.770044[Pa] + 0.154961[Pa/K]*T)
                        {if (T<=6[K]) and (T>=4.5[K]) then
                            P=max(0.0001[Pa],-0.770044[Pa] + 0.154961[Pa/K]*T)
                        else
                            P=4[Pa]                    "attention, T should be greater than 4.5 K"
                        endif}
                    endif
                endif
            endif
        endif
    endif
end
```

```
Procedure
cooling(h,mf_s,cvh_s,T_w,P_1_w:{Delta_H_vs,Delta_H_vv,DH_s_p,DH_s_c,}Ef_w_p{
,Ef_w_c})     "wall boundary conditions"
    G1$='Hydrogen'
    M_1=MolarMass(G1$)
    CA=100000[J/kmol]/M_1
    if (T_w<=14 [K]) then
        h_1_w=(521047[J/kmol] + 20616.7[J/kmol-K]*T_w)/M_1
    else
        h_1_w=256598[J/kg] + 10357.4[J/kg-K]*T_w
{       h_1_w=Enthalpy(G1$,T=T_w,P=P_1_w)}
    endif
    Delta_H_vs=769.897[J/kg] + 19.6193[J/kg-K]*T_w
    Delta_H_vv=h-h_1_w    "enthalpy change from vapor to vapor, lack of data"
    DH_s_p=mf_s*(Delta_H_vv+Delta_H_vs)
    DH_s_c=mf_s*(Delta_H_vv+CA)
    Ef_w_p=DH_s_p+cvh_s
    Ef_w_c=DH_s_c+cvh_s
end

Procedure ms(h_m, rho_1, rho_1_w, P_1_w,P_1_b:mf_s)   "mass flux to the wall"
    S=1
    if (P_1_w>=P_1_b) then
        mf_s=0[kg/s-m^2]
    else
        mf_s=max(0[kg/s-m^2],S*h_m*(rho_1-rho_1_w))
    endif
end

Procedure sphelium(A,m_dot,T,P:rho,u,cp,h, mu, k, Pr)      "properties of super critical
helium"
    G2$='Helium'
    rho=Density(G2$,T=T,P=P)
    u=m_dot/rho/A
    cp=Cp(G2$,T=T,P=P)
    h=Enthalpy(G2$,T=T,P=P)
    mu=Viscosity(G2$,T=T,P=P)
    k=Conductivity(G2$,T=T,P=P)
    Pr=Prandtl(G2$,T=T,P=P)
    {Re=4*m_dot_c/(pi*mu*D_c)}
end

"----------------------------------------------------------------------------------------------------
----setting"
```

```
"H2 flow and He coolant"
G1$='Hydrogen'
G2$='Helium'
MW_1=MolarMass(G1$)
R_1=R#/MW_1

"cryogenic fore pump, double-pipe"
L=42[in]*convert(in,m)            "pump length"
D=0.05[m]    "inner diameter"
r=D/2
Ltw4=4[in]*convert(in,m)   "thermometer 4, pump wall"
Ltw3=(4+12)[in]*convert(in,m)
Ltw2=(4+12+12)[in]*convert(in,m)
Ltw1=(4+12+12+12)[in]*convert(in,m)     "no experiment data for this location"
Ltco=4[in]*convert(in,m)    "thermometer, coolant outlet"
Ltci=42[in]*convert(in,m)

"supercritical helium pipe"
D_c=0.1524{0.06}{0.1524}[m]      "outer diameter"
r_c=D_c/2
A_a=pi*(r_c^2-r^2)  "annular cross-sectional area"
D_h=r_c-r     "hydraulic diameter"
r|star=r/r_c
th=0.002[m]  "pump wall thickness"
{A_c=pi*((D_c)^2-(D+th)^2)/4"similar to A_a"}

"grid"
N=51{102}        "number of nodes."
dy=L/N
A_s=pi*D*dy     "node surface area"
dy_bar=(2/r)*dy
duplicate i=1,N
   y[i]=dy*(i-1)
   xoverD[i]=(y[i]+dy/2)/D  "hydrogen flow"
    xoverD_h[i]=(L-(y[i]+dy/2))/D_h    "coolant flow"
end

"inlet H2 flow condition"
T_H2_in=77{80}[K]     "constant inlet temperature"
m_dot_H2_in=0.001[g/s]*convert(g/s,kg/s)     "mass flow rate is controled"

{u[1,1]=6.228{8.6}{16.3}{3.35}{3.697}{9.242}{13.69}{11.2}{3.361}{3.361}[m/s]}
```

```
"inlet helium coolant condition"
T_c_in=8[K] "estimated coolant inlet temperature"
P_c=1.4[bar]*convert(bar,Pa)
m_dot_c={0.0002}0.4186[g/s]*convert(g/s,kg/s)

"time step"
cv_c=Cv(G2$,T=T_c_in, P=P_c)
rho_c=Density(G2$, T=T_c_in, P=P_c)
m_dot_c=rho_c*A_a*u_c
dy=u_c*t_ct  "t_ct is time_coolant travel"
{t_step=t_ct/2     "time step"}
t_step=4[s]    "determined by time experiment data"
M=26{6}{floor(720/t_step)}     "number of time steps" "720 s is the total time period "
M_plus=28


"-------------------------------------------------------------------------------------------------------
---------------------------- -read from lookup table" "modification needed"
"M=26"
duplicate k=1,N
    T_w[k,M-1]=Lookup('9',k,'T_w[i,25]') "for H2"
    T_c[k,M-1]=Lookup('9',k,'T_c[i,25]')   "for H2"
    Ef_w_p[k,M-1]=Lookup('9',k,'Ef_w_p[i,25]')
    T_w[k,M]=Lookup('9',k,'T_w[i,26]')    "for H2"
    T_c[k,M]=Lookup('9',k,'T_c[i,26]') "for H2"
    u_s[k,M]=Lookup('9',k,'u_s[i,26]')
    u_c[k,M]=Lookup('9',k,'u_c[i,26]')
end
"-------------------------------------------------------------------------------------------------------
---------------------------- -read from lookup table""modification needed"


"pump wall property"
T_w=8[K]     "estimated pump temperature for property"
rho_s=Density(Stainless_AISI304, T=T_w)
m_s=rho_s*dy*pi*((D+th)^2-D^2)/4

"-------------------------------------------------------------------------------------------------------
----setting"


"-----------------------------------------------------------------------------------------control
parameters"
```

```
"-------------------------------------------------------------------------------------------------------------
---------------------------- -read from lookup table"

"inlet helium coolant"
duplicate k=M,M_plus
    T_c_in[k]=Lookup('BC new',k+20,'T_c_in')    "read from line 26 excel copy 3-1"
end
{   T_c_in[1]=8.6[K]      "coolant inlet temperature"
    T_c_in[2]=8.901[K]  "coolant inlet temperature"
    T_c_in[3]=8.855[K]  "coolant inlet temperature"
    T_c_in[4]=8.742[K]  "coolant inlet temperature"
    T_c_in[5]=8.57[K]    "coolant inlet temperature"
    T_c_in[6]=8.542[K]  "coolant inlet temperature"
    T_c_in[7]=8.758[K]}
"-------------------------------------------------------------------------------------------------------------
---------------------------- -read from lookup table"

duplicate j=M,M_plus
{   T_c_in[j]=8.5[K]"coolant inlet temperature"}
    h_c_in[j]=Enthalpy(G2$,T=T_c_in[j],P=P_c)  "coolant inlet enthalpy, flowing into
node N"
end


"-----------------------------------------------------------------------------------------control
parameters"


"-------------------------------------------------------------------------------------------------------------
-----------?"
{duplicate j=2,M
P=P[1,1]
        P[1,j]=P
end}
"-------------------------------------------------------------------------------------------------------------
---------------------------- -read from lookup table"
duplicate k=M,M_plus
    P[1,k]=Lookup('BC new',k+20,'P_H2_in')  "read from line 26 excel copy 3-1"
end
{
P[1,1]=25.97046667{20.8129}{81}{13.5}{50}[Pa]
P[1,2]=27.0284[Pa]
P[1,3]=27.85233333[Pa]
P[1,4]=28.50343333[Pa]
```

```
P[1,5]=29.14936667[Pa]
P[1,6]=29.67833333[Pa]
P[1,7]=30.38026667[Pa]
}
"-------------------------------------------------------------------------------------------------------------
------------------------------ -read from lookup table"


duplicate j=M,M_plus    "warning"
    P_1_b[j]=P[1,j]
end
"-------------------------------------------------------------------------------------------------------------
-----------?"

"-------------------------------------------------------------------------------------------------------------
---- adjust "
ad=1{5}
ad_d=1
sb=5
"-------------------------------------------------------------------------------------------------------------
---- adjust "

"-----------------------------------------------------------------------------------------------initial
condition"
{{
"read from experiment"
Tw4=7.8[K]  "thermometer 4, pump wall"
Tw3=7.2[K]
Tw2=7.6[K]
Tco=7.5[K]   "thermometer, coolant outlet"
Tci=8[K]
}}


{{
"initial pump wall temperature" "the temperature profile curve is needed for the pump
wall"
T_w[1,1]=53{8.5}{30}{40}{50}[K]    "guess value" "from pure hydrogen final cec paper
case 3"
T_w[2,1]=30{8.5}{30}{40}{50}[K]    "guess value"
T_w[3,1]=20{8.5}{30}{40}{50}[K]    "guess value"
T_w[4,1]=15{8.5}{30}{40}{50}[K]    "guess value"
T_w[5,1]=12{8.5}{30}{40}{50}[K]    "guess value"
T_w[6,1]=10{8.5}{30}{40}{50}[K]    "guess value"
```

```
duplicate i=7,N
    T_w[i,1]=8.5[K]  "guess value"
end

T_c_ini=8.4[K]
"initial coolant temperature----------------------------------------------------?"
T_c[1,1]=T_c_ini+0.9[K]
T_c[2,1]=T_c_ini+0.3[K]
T_c[3,1]=T_c_ini+0.12[K]
T_c[4,1]=T_c_ini+0.08[K]
T_c[5,1]=T_c_ini+0.06[K]
T_c[6,1]=T_c_ini+0.03[K]
duplicate i=7,N
    T_c[i,1]=T_c_ini
end


m_dot_H2_in=rho[1,1]*u[1,1]*pi*r^2
}}
{{
(7.915[K]-8.3[K])/(Ltw2-Ltw4)=xie
duplicate i=1,N
    T_w[i,1]=xie*(y[i]-Ltw4)+8.3[K]    "guess value based on BC new line 21"
end

L=u_c*time_zhihou
time_zhihou+Table=18850+82
T_c[1,1]=Lookup('BC new',1+20,'T_c_out')

duplicate i=2,N-1
    T_c[i,1]=Lookup('Initial T_c',i,'T_c_in_p')+0.7[K]*(50-i)/50     "guess value based on
BC new line 21"
end

T_c[N,1]=Lookup('BC new',1+20,'T_c_in')
}}

duplicate j=M,M_plus    "constant H2 flow rate"
    m_dot_H2_in=rho[1,j]*u[1,j]*pi*r^2
end

"----------------------------------------------------initial condition: march to node 2 from node
1"
```

```
{{
"wall boundary"
Call Wall(P_1_b[1],T_w[1,1]:P_1_w[1,1])
rho_1_w[1,1]=P_1_w[1,1]/(R_1*T_w[1,1])

rho[1,1]=P[1,1]/(R_1*T_H2_in)
Call enthalpy_ad(T_H2_in,P[1,1]:h[1,1])
Call mix(T_H2_in,P[1,1]:mu[1,1],k[1,1],cp[1,1])
nu[1,1]=mu[1,1]/rho[1,1]

Re[1,1]=u[1,1]*D/nu[1,1]    "Reynolds number"
D_ab[1,1]=ad_d*D_12_gas(G1$,G1$,T_H2_in,P[1,1])       "diffusion coefficient"
Sc[1,1]=nu[1,1]/D_ab[1,1]  "Schmidt number"
call PipeFlow_N_local(Re[1,1],Sc[1,1],xoverD[1],0: Sh_T_x[1,1],Sh_H_x[1],f[1])
     "warning: xoverD should be >0.1"
Sh_T_x[1,1]=h_m[1,1]*D/D_ab[1,1]    "Sherwood number" "choose the worst case"
call ms(h_m[1,1], rho[1,1], rho_1_w[1,1], P_1_w[1,1],P_1_b[1]:mf_s[1,1])          "radial
mass flux"

Pr[1,1]=cp[1,1]*mu[1,1]/k[1,1]
call PipeFlow_N_local(Re[1,1],Pr[1,1],xoverD[1],0:
Nusselt_T_x[1,1],Nusselt_H_x[1],f_x[1,1])
Nusselt_T_x[1,1]=h_t[1,1]*D/k[1,1]     "choose the lower limit"
cvh[1,1]=h_t[1,1]*(T_H2_in-T_w[1,1])     "convection heat flux"
dP_f_c[1,1]=rho[1,1]*f_x[1,1]*(u[1,1]^2/2)*(dy/D)

Call
cooling(h[1,1],mf_s[1,1],cvh[1,1],T_w[1,1],P_1_w[1,1]:{Delta_H_vs[1],Delta_H_vv[1],
DH_s_p[1],DH_s_c[1],}Ef_w_p[1,1]{,Ef_w_c[1]}) "total energy flux"

"balance equations"
u[2,1]*rho[2,1]=u[1,1]*rho[1,1]-dy_bar*mf_s[1,1]   "hydrogen mass balance"
u[2,1]^2*rho[2,1]+P[2,1]=u[1,1]^2*rho[1,1]+P[1,1]{-dP_f[1]}-dP_f_c[1,1]-
dy_bar*mf_s[1,1]*u[1,1]     "momentum balance"
u[2,1]*rho[2,1]*(h[2,1]+0.5*u[2,1]^2)=u[1,1]*rho[1,1]*(h[1,1]+0.5*u[1,1]^2)-
dy_bar*(mf_s[1,1]*(h[1,1]+0.5*u[1,1]^2)+cvh[1,1])          "energy balance"

rho[2,1]=P[2,1]/(R_1*T[2,1])
Call enthalpy_ad(T[2,1],P[2,1]:h[2,1])
Call mix(T[2,1],P[2,1]:mu[2,1],k[2,1],cp[2,1])

}}
```

```
"-------------------------------------------------------------------------------------------------------------
------------------------------move forward with time"
duplicate j=M,M_plus
    "wall boundary"
    Call Wall(P_1_b[j],T_w[1,j]:P_1_w[1,j])
    rho_1_w[1,j]=P_1_w[1,j]/(R_1*T_w[1,j])

    rho[1,j]=P[1,j]/(R_1*T_H2_in)
    Call enthalpy_ad(T_H2_in,P[1,j]:h[1,j])
    Call mix(T_H2_in,P[1,j]:mu[1,j],k[1,j],cp[1,j])
    nu[1,j]=mu[1,j]/rho[1,j]

    Re[1,j]=u[1,j]*D/nu[1,j] "Reynolds number"
    D_ab[1,j]=ad_d*D_12_gas(G1$,G1$,T_H2_in,P[1,j])    "diffusion coefficient"
    Sc[1,j]=nu[1,j]/D_ab[1,j]      "Schmidt number"
    call PipeFlow_N_local(Re[1,j],Sc[1,j],xoverD[1],0: Sh_T_x[1,j],Sh_H_x[1,j],f[1,j])
    "warning: xoverD should be >0.1"
    Sh_T_x[1,j]=h_m[1,j]*D/D_ab[1,j] "Sherwood number" "choose the worst case"
    call ms(h_m[1,j], rho[1,j], rho_1_w[1,j], P_1_w[1,j],P_1_b[j]:mf_s[1,j])          "radial
mass flux"

    Pr[1,j]=cp[1,j]*mu[1,j]/k[1,j]
    call PipeFlow_N_local(Re[1,j],Pr[1,j],xoverD[1],0:
Nusselt_T_x[1,j],Nusselt_H_x[1,j],f_x[1,j])
    Nusselt_T_x[1,j]=sb*h_t[1,j]*D/k[1,j]  "choose the lower limit"
    cvh[1,j]=h_t[1,j]*(T_H2_in-T_w[1,j])
    dP_f_c[1,j]=rho[1,j]*f_x[1,j]*(u[1,j]^2/2)*(dy/D)

    Call
cooling(h[1,j],mf_s[1,j],cvh[1,j],T_w[1,j],P_1_w[1,j]:{Delta_H_vs[1],Delta_H_vv[1],D
H_s_p[1],DH_s_c[1],}Ef_w_p[1,j]{,Ef_w_c[1]}) "total energy flux"

    {u[1+1,j]=u[1,j]  "To let the shasha know"}

    "energy equation"
    u[2,j]*rho[2,j]=u[1,j]*rho[1,j]-dy_bar*mf_s[1,j]  "hydrogen mass balance"
    u[2,j]^2*rho[2,j]+P[2,j]=u[1,j]^2*rho[1,j]+P[1,j]{-dP_f[1]}-dP_f_c[1,j]-
dy_bar*mf_s[1,j]*u[1,j] "momentum balance"
    u[2,j]*rho[2,j]*(h[2,j]+0.5*u[2,j]^2)=u[1,j]*rho[1,j]*(h[1,j]+0.5*u[1,j]^2)-
dy_bar*(mf_s[1,j]*(h[1,j]+0.5*u[1,j]^2)+cvh[1,j])   "energy balance"

    {rho[2,j]=P[2,j]/(R_1*T[2,j])}   "hard for shasha"
```

```
    0=P[1+1,j]-rho[1+1,j]*R_1*T[1+1,j]

    Call enthalpy_ad(T[2,j],P[2,j]:h[2,j])

    Call mix(T[2,j],P[2,j]:mu[2,j],k[2,j],cp[2,j])

end

{{

duplicate i=2,N"N"
    nu[i,1]=mu[i,1]/rho[i,1]
    Re[i,1]=u[i,1]*D/nu[i,1] "Reynolds number"
    D_ab[i,1]=ad_d*D_12_gas(G1$,G1$,T[i,1],P[i,1])        "diffusion coefficient"
    Sc[i,1]=nu[i,1]/D_ab[i,1]      "Schmidt number"
    call PipeFlow_N_local(Re[i,1],Sc[i,1],xoverD[i],0: Sh_T_x[i,1],Sh_H_x[i],f[i])
    "warning: xoverD should be >0.1"
    Sh_T_x[i,1]=h_m[i,1]*D/D_ab[i,1] "Sherwood number" "choose the worst case"

    Call Wall(P_1_b[1],T_w[i,1]:P_1_w[i,1])
    rho_1_w[i,1]=P_1_w[i,1]/(R_1*T_w[i,1])
    call ms(h_m[i,1], rho[i,1], rho_1_w[i,1], P_1_w[i,1],P_1_b[1]:mf_s[i,1])         "radial
mass flux"

    Pr[i,1]=cp[i,1]*mu[i,1]/k[i,1]
    call PipeFlow_N_local(Re[i,1],Pr[i,1],xoverD[i],0:
Nusselt_T_x[i,1],Nusselt_H_x[i],f_x[i,1])
    Nusselt_T_x[i,1]=h_t[i,1]*D/k[i,1]  "choose the lower limit"
    cvh[i,1]=h_t[i,1]*(T[i,1]-T_w[i,1])  "convection heat"
    dP_f_c[i,1]=rho[i,1]*f_x[i,1]*(u[i,1]^2/2)*(dy/D)
    Call
cooling(h[i,1],mf_s[i,1],cvh[i,1],T_w[i,1],P_1_w[i,1]:{Delta_H_vs[i],Delta_H_vv[i],DH
_s_p[i],DH_s_c[i],}Ef_w_p[i,1]{,Ef_w_c[i]}) "total energy flux"

    "balance equation"
    0=(u[i+1,1]*rho[i+1,1])-(u[i,1]*rho[i,1]-dy_bar*mf_s[i,1])        "hydrogen mass
balance"
    0=(u[i+1,1]^2*rho[i+1,1]+P[i+1,1])-(u[i,1]^2*rho[i,1]+P[i,1]{-dP_f[i]}-dP_f_c[i,1]-
dy_bar*mf_s[i,1]*u[i,1])     "momentum balance"
    0=(u[i+1,1]*rho[i+1,1]*(h[i+1,1]+0.5*u[i+1,1]^2))-
(u[i,1]*rho[i,1]*(h[i,1]+0.5*u[i,1]^2)-dy_bar*(mf_s[i,1]*(h[i,1]+0.5*u[i,1]^2)+cvh[i,1]))
    "energy balance"
```

```
    0=(rho[i+1,1])-(P[i+1,1]/(R_1*T[i+1,1]))
    Call enthalpy_ad(T[i+1,1],P[i+1,1]:h[i+1,1])
    Call mix(T[i+1,1],P[i+1,1]:mu[i+1,1],k[i+1,1],cp[i+1,1])
end
}}

duplicate j=M,M_plus
    duplicate i=2,N"N"
""""""""""""""""""""""""""""""""""""""""""""""""""""""""""""""""""""""""""""""""""""""""""""""""""
        nu[i,j]=mu[i,j]/rho[i,j]
        Re[i,j]=u[i,j]*D/nu[i,j]    "Reynolds number"
        D_ab[i,j]=ad_d*D_12_gas(G1$,G1$,T[i,j],P[i,j])      "diffusion coefficient"
        Sc[i,j]=nu[i,j]/D_ab[i,j]   "Schmidt number"
        call PipeFlow_N_local(Re[i,j],Sc[i,j],xoverD[i],0: Sh_T_x[i,j],Sh_H_x[i,j],f[i,j])
    "warning: xoverD should be >0.1"
        Sh_T_x[i,j]=h_m[i,j]*D/D_ab[i,j]    "Sherwood number" "choose the worst case"

        Call Wall(P_1_b[j],T_w[i,j]:P_1_w[i,j])
        rho_1_w[i,j]=P_1_w[i,j]/(R_1*T_w[i,j])
        call ms(h_m[i,j], rho[i,j], rho_1_w[i,j], P_1_w[i,j],P_1_b[j]:mf_s[i,j])

        Pr[i,j]=cp[i,j]*mu[i,j]/k[i,j]
        call PipeFlow_N_local(Re[i,j],Pr[i,j],xoverD[i],0:
Nusselt_T_x[i,j],Nusselt_H_x[i,j],f_x[i,j])
        Nusselt_T_x[i,j]=sb*h_t[i,j]*D/k[i,j]     "choose the lower limit"
        cvh[i,j]=h_t[i,j]*(T[i,j]-T_w[i,j])
        dP_f_c[i,j]=rho[i,j]*f_x[i,j]*(u[i,j]^2/2)*(dy/D)
        Call
cooling(h[i,j],mf_s[i,j],cvh[i,j],T_w[i,j],P_1_w[i,j]:{Delta_H_vs[i],Delta_H_vv[i],DH_s_
p[i],DH_s_c[i],}Ef_w_p[i,j]{,Ef_w_c[i]})

{
        u[i+1,j]=u[i,j] "To let the shasha know"
}
        "balance equations"
        0=(u[i+1,j]*rho[i+1,j])-(u[i,j]*rho[i,j]-dy_bar*mf_s[i,j])       "hydrogen mass
balance"
        0=(u[i+1,j]^2*rho[i+1,j]+P[i+1,j])-(u[i,j]^2*rho[i,j]+P[i,j]{-dP_f[i]}-dP_f_c[i,j]-
dy_bar*mf_s[i,j]*u[i,j])  "momentum balance"
        0=(u[i+1,j]*rho[i+1,j]*(h[i+1,j]+0.5*u[i+1,j]^2))-
(u[i,j]*rho[i,j]*(h[i,j]+0.5*u[i,j]^2)-dy_bar*(mf_s[i,j]*(h[i,j]+0.5*u[i,j]^2)+cvh[i,j]))
    "energy balance"
```

```
        0=P[i+1,j]-rho[i+1,j]*R_1*T[i+1,j]
        {0=(rho[i+1,j])-(P[i+1,j]/(R_1*T[i+1,j]))}  "hard for shasha"

        Call enthalpy_ad(T[i+1,j],P[i+1,j]:h[i+1,j])

        Call mix(T[i+1,j],P[i+1,j]:mu[i+1,j],k[i+1,j],cp[i+1,j])

    end
end



{{

duplicate j=M,M_plus
    duplicate i=5,5{N}"N"
""""""""""""""""""""""""""""""""""""""""""""""""""""""""""""""""""""""""""""""""""""
        nu[i,j]=mu[i,j]/rho[i,j]
        Re[i,j]=u[i,j]*D/nu[i,j]    "Reynolds number"
        D_ab[i,j]=ad_d*D_12_gas(G1$,G1$,T[i,j],P[i,j])      "diffusion coefficient"
        Sc[i,j]=nu[i,j]/D_ab[i,j]   "Schmidt number"
        call PipeFlow_N_local(Re[i,j],Sc[i,j],xoverD[i],0: Sh_T_x[i,j],Sh_H_x[i,j],f[i,j])
    "warning: xoverD should be >0.1"
        Sh_T_x[i,j]=h_m[i,j]*D/D_ab[i,j]    "Sherwood number" "choose the worst case"

        Call Wall(P_1_b[j],T_w[i,j]:P_1_w[i,j])
        rho_1_w[i,j]=P_1_w[i,j]/(R_1*T_w[i,j])
        call ms(h_m[i,j], rho[i,j], rho_1_w[i,j], P_1_w[i,j],P_1_b[j]:mf_s[i,j])

        Pr[i,j]=cp[i,j]*mu[i,j]/k[i,j]
        call PipeFlow_N_local(Re[i,j],Pr[i,j],xoverD[i],0:
Nusselt_T_x[i,j],Nusselt_H_x[i,j],f_x[i,j])
        Nusselt_T_x[i,j]=h_t[i,j]*D/k[i,j]     "choose the lower limit"
        cvh[i,j]=h_t[i,j]*(T[i,j]-T_w[i,j])
        dP_f_c[i,j]=rho[i,j]*f_x[i,j]*(u[i,j]^2/2)*(dy/D)
        Call
cooling(h[i,j],mf_s[i,j],cvh[i,j],T_w[i,j],P_1_w[i,j]:{Delta_H_vs[i],Delta_H_vv[i],DH_s_
p[i],DH_s_c[i],}Ef_w_p[i,j]{,Ef_w_c[i]})

{
        u[i+1,j]=u[i,j]-0.3[m/s]    "To let the shasha know"
}
        "balance equations"
```

```
        0=(u[i+1,j]*rho[i+1,j])-(u[i,j]*rho[i,j]-dy_bar*mf_s[i,j])       "hydrogen mass
balance"
        0=(u[i+1,j]^2*rho[i+1,j]+P[i+1,j])-(u[i,j]^2*rho[i,j]+P[i,j]{-dP_f[i]}-dP_f_c[i,j]-
dy_bar*mf_s[i,j]*u[i,j])  "momentum balance"
        0=(u[i+1,j]*rho[i+1,j]*(h[i+1,j]+0.5*u[i+1,j]^2))-
(u[i,j]*rho[i,j]*(h[i,j]+0.5*u[i,j]^2)-dy_bar*(mf_s[i,j]*(h[i,j]+0.5*u[i,j]^2)+cvh[i,j]))
    "energy balance"

        {0=(rho[i+1,j])-(P[i+1,j]/(R_1*T[i+1,j]))}  "hard for shasha"
        0=P[i+1,j]-rho[i+1,j]*R_1*T[i+1,j]
        Call enthalpy_ad(T[i+1,j],P[i+1,j]:h[i+1,j])
        Call mix(T[i+1,j],P[i+1,j]:mu[i+1,j],k[i+1,j],cp[i+1,j])

    end
end
}}

"-----------------------------------------------------------------------------------------------------------
---------"
{T_c_in_c=T_c[N]
error=Abs(T_c_in-T_c[N])  "error=2.956 [K] for 102 N"}
"-----------------------------------------------------------------------------------------------------------
mass flux"


{duplicate i=1,N
    mf[i,1]=rho[i,1]*u[i,1]
end
N_mf=(mf[1,1]-mf[N,1])/mf[1,1]}


"-----------------------------------------------------------connection between two control
volumes"


{{
duplicate i=1,N
    Ef_w_p[i,1]*A_s=q_sc[i,1]+DELTAU_dot_s[i,1]
end

}}
```

```
duplicate j=M,M_plus
    duplicate i=1,{4}N
        Ef_w_p[i,j]*A_s=q_sc[i,j]+DELTAU_dot_s[i,j]        "should be Ef_w_p[i,j]*A_s"
    end
end



"-----------------------------------------------------------connection between two control volumes"

{{
"-------------------------------------------------------------------------------for time step 1, one more equation than the rest time step"
"coolant helium node N-----------------------------------------------move forward with time"
q_sc[N,1]=DELTA_E_dot[N,1]+DELTAU_dot[N,1]          "energy balance"
Call sphelium(A_a,m_dot_c,T_c[N,1],P_c: rho_c[N,1],vel_c[N,1],cp_c[N,1],h_c[N,1], mu_c[N,1], k_c[N,1], Pr_c[N,1])
m_c[N,1]=rho_c[N,1]*dy*A_a "control volume mass"
u_c[N,1]=IntEnergy(G2$,T=T_c[N,1],P=P_c)
DELTA_E_dot[N,1]=m_dot_c*(h_c[N,1]-h_c_in[1])          "enthalpy difference"
DELTAU_dot[N,1]=m_c[N,1]*(u_c[N,2]-u_c[N,1])/t_step "internal energy change"
u_c[N,2]=IntEnergy(G2$,T=T_c[N,2],P=P_c)

"coolant helium node 1, N-1-------------------------------------------move forward with time"
duplicate i=1,N-1
    q_sc[N-i,1]=DELTA_E_dot[N-i,1]+DELTAU_dot[N-i,1]
    DELTA_E_dot[N-i,1]=m_dot_c*(h_c[N-i,1]-h_c[N+1-i,1])
    DELTAU_dot[N-i,1]=m_c[N-i,1]*(u_c[N-i,2]-u_c[N-i,1])/t_step
    Call sphelium(A_a,m_dot_c,T_c[N-i,1],P_c: rho_c[N-i,1],vel_c[N-i,1],cp_c[N-i,1],h_c[N-i,1], mu_c[N-i,1], k_c[N-i,1], Pr_c[N-i,1])
    m_c[N-i,1]=rho_c[N-i,1]*dy*A_a
    u_c[N-i,2]=IntEnergy(G2$,T=T_c[N-i,2],P=P_c)
    u_c[N-i,1]=IntEnergy(G2$,T=T_c[N-i,1],P=P_c)
end
"-------------------------------------------------------------------------------for time step 1, one more equation than the rest time step"

}}

duplicate j=M,M_plus
```

```
    Call sphelium(A_a,m_dot_c,T_c[N,j],P_c: rho_c[N,j],vel_c[N,j],cp_c[N,j],h_c[N,j],
mu_c[N,j], k_c[N,j], Pr_c[N,j])
    m_c[N,j]=rho_c[N,j]*dy*A_a
    q_sc[N,j]=DELTA_E_dot[N,j]+DELTAU_dot[N,j]

    DELTA_E_dot[N,j]=m_dot_c*(h_c[N,j]-h_c_in[j])
    DELTAU_dot[N,j]=m_c[N,j]*(u_c[N,j+1]-u_c[N,j])/t_step
    u_c[N,j+1]=IntEnergy(G2$,T=T_c[N,j+1],P=P_c)


    duplicate i=1,N-1
        Call sphelium(A_a,m_dot_c,T_c[N-i,j],P_c: rho_c[N-i,j],vel_c[N-i,j],cp_c[N-
i,j],h_c[N-i,j], mu_c[N-i,j], k_c[N-i,j], Pr_c[N-i,j])
        m_c[N-i,j]=rho_c[N-i,j]*dy*A_a
        q_sc[N-i,j]=DELTA_E_dot[N-i,j]+DELTAU_dot[N-i,j]

        DELTA_E_dot[N-i,j]=m_dot_c*(h_c[N-i,j]-h_c[N+1-i,j])
        DELTAU_dot[N-i,j]=m_c[N-i,j]*(u_c[N-i,j+1]-u_c[N-i,j])/t_step
        u_c[N-i,j+1]=IntEnergy(G2$,T=T_c[N-i,j+1],P=P_c)

    end


end



duplicate j=M,M_plus
    duplicate i=1,N
        Re_c[i,j]=m_dot_c*D_h/(A_a*mu_c[i,j])
        call AnnularFlow_N_local(Re_c[i,j], Pr_c[i,j], xoverD_h[i], r|star, 0:
Nusselt_c_T_x[i,j],Nusselt_c_H_x[i,j], f_c_x[i,j])
        Nusselt_c_T_x[i,j]=hh_c[i,j]*D_h/k_c[i,j]  "choose the lower limit"
        R_c[i,j]=1/(hh_c[i,j]*pi*D*dy)
    end
end


{{
"----------------------------------------------------------------------------------------for time step
1, one more equation than the rest time step"
duplicate j=1,1
    duplicate i=1,N
        Re_c[i,j]=m_dot_c*D_h/(A_a*mu_c[i,j])
```

```
        call AnnularFlow_N_local(Re_c[i,j], Pr_c[i,j], xoverD_h[i], r|star, 0:
Nusselt_c_T_x[i,j],Nusselt_c_H_x[i,j], f_c_x[i,j])
        Nusselt_c_T_x[i,j]=hh_c[i,j]*D_h/k_c[i,j]  "choose the lower limit"
        R_c[i,j]=1/(hh_c[i,j]*pi*D*dy)
    end
end
"the pump wall lumped"

duplicate i=1,N
    q_sc[i,1]=(T_w[i,1]-T_c[i,1])/R_c[i,1]
    u_s[i,1]=IntEnergy(Stainless_AISI304, T=T_w[i,1])
    DELTAU_dot_s[i,1]=m_s*(u_s[i,1+1]-u_s[i,1])/t_step
    u_s[i,1+1]=IntEnergy(Stainless_AISI304, T=T_w[i,1+1])
end
"----------------------------------------------------------------------------------------for time step
1, one more equation than the rest time step"

}}

duplicate j=M,M_plus
    duplicate i=1,N
        q_sc[i,j]=(T_w[i,j]-T_c[i,j])/R_c[i,j]
        DELTAU_dot_s[i,j]=m_s*(u_s[i,j+1]-u_s[i,j])/t_step

        u_s[i,j+1]=IntEnergy(Stainless_AISI304, T=T_w[i,j+1])

    end
end

time_total=t_step*M



{T_critical=6[K]
duplicate time_steps=1,M
    pointer[time_steps]=pointer(time_steps, T_w[1,time_steps], T_critical)
end}
```

Appendix B. Steady-state model code

```
$UnitSysytem SI mass kg J m s rad Pa K
$Tabstops 0.2 0.4 0.6 0.8 1 in

"so sensitive to guess value of pressure"


Procedure enthalpy_ad(T,P:h)   "hydrogen enthalpy"
    G1$='Hydrogen'
    M_1=MolarMass(G1$)
    if (T<=14 [K]) then
        h=(521047[J/kmol] + 20616.7[J/kmol-K]*T)/M_1
    else
        h=256598[J/kg] + 10357.4[J/kg-K]*T
        {h=Enthalpy(G1$,T=T,P=P)}
    endif
end

Procedure mix(T,P_1:mu,k,cp)  "mixture thermal and kinetic properties"
    G1$='Hydrogen'
    M_1=MolarMass(G1$)
    if (T>18[K]) then
        mu_1=Viscosity(G1$,T=T,P=P_1)
    else
        mu_1=7.64217E-07[Pa-s] + 3.39265E-08[Pa-s/K]*T
    endif
{   mu_1=Viscosity(G1$,T=T,P=P_1)}
    if (T>14[K]) then
        k_1=Conductivity(G1$,T=T,P=P_1)
    else
        k_1=0.00559606[W/m-K] + 0.000629187[W/m-K^2]*T
    endif
{   k_1=Conductivity(G1$,T=14[K],P=P_1)}
    mu=mu_1"viscosity"
    k=k_1 "conductivity"
    if (T<10[K]) then
        cp_1=(35.065[J/kmol-K] - 73.0795[J/kmol-K^2]*T + 27.5904[J/kmol-
K^3]*T^2)/M_1
    else
        if (T>=10[K]) and (T<13.957[K]) then
            cp_1=(4469.83[J/kmol-K] - 1147.04[J/kmol-K^2]*T + 89.2029[J/kmol-
K^3]*T^2)/M_1
        else
```

```
            cp_1=SpecHeat(G1$,T=T,P=P_1)
        endif
    endif
    cp=cp_1   "specific heat"
end

{Procedure Wall(L,y,P_1_b:T_w,P_1_w)  "wall boundary conditions"
    if (y<L/3) then
        T_w=(10-90*(y-L/3)/L)*1[K]
        P_1_w=P_1_b
    else
        T_w=(5-15*(y-L)/(2*L))*1[K]
        P_1_w=min(P_1_b,-2235.54[Pa] + 1783.52[Pa/K]*T_w - 569.28[Pa/K^2]*T_w^2
+ 91.0669[Pa/K^3]*T_w^3 - 7.31871[Pa/K^4]*T_w^4 + 0.237041[Pa/K^5]*T_w^5)
    endif
end}

{Procedure Wall(P_1_b,T_w:P_1_w)   "wall boundary conditions"
    if (T_w>10[K]) then
        P_1_w=P_1_b
    else
        P_1_w=min(P_1_b,-2235.54[Pa] + 1783.52[Pa/K]*T_w - 569.28[Pa/K^2]*T_w^2
+ 91.0669[Pa/K^3]*T_w^3 - 7.31871[Pa/K^4]*T_w^4 + 0.237041[Pa/K^5]*T_w^5)
    endif
end}


Procedure Wall(P_1,T:P)     "wall boundary conditions"
G1$='Hydrogen'
    if (T>10[K]) then
        P=P_1
    else
        if (T<=10[K]) and (T>9[K]) then
            P=min(P_1,-1587.87[Pa] + 184.345[Pa/K]*T)
        else
            if (T<=9[K]) and (T>8[K]) then
                P=min(P_1,-435.724[Pa] + 56.3287[Pa/K]*T)
            else
                if (T<=8[K]) and (T>7[K]) then
                    P=-87.6888[Pa] + 12.8243[Pa/K]*T
                else
                    if (T<=7[K]) and (T>6[K]) then
                        P=-11.3689[Pa] + 1.92144[Pa/K]*T
                    else
```

```
                    P=max(0.0001[Pa],-0.770044[Pa] + 0.154961[Pa/K]*T)
                    {if (T<=6[K]) and (T>=4.5[K]) then
                        P=max(0.0001[Pa],-0.770044[Pa] + 0.154961[Pa/K]*T)
                    else
                        P=4[Pa]                "attention, T should be greater than 4.5 K"
                    endif}
                endif
            endif
        endif
    endif
end

Procedure
cooling(h,mf_s,t_s,T_w,P_1_w:Delta_H_vs,Delta_H_vv,DH_s_p,DH_s_c,Ef_w_p,Ef_w
_c)"wall boundary conditions"
    G1$='Hydrogen'
    M_1=MolarMass(G1$)
    CA=100000[J/kmol]/M_1
    if (T_w<=14 [K]) then
        h_1_w=(521047[J/kmol] + 20616.7[J/kmol-K]*T_w)/M_1
    else
        h_1_w=256598[J/kg] + 10357.4[J/kg-K]*T_w
{       h_1_w=Enthalpy(G1$,T=T_w,P=P_1_w)}
    endif
    Delta_H_vs=769.897[J/kg] + 19.6193[J/kg-K]*T_w
    Delta_H_vv=h-h_1_w    "enthalpy change from vapor to vapor, lack of data"
    DH_s_p=mf_s*(Delta_H_vv+Delta_H_vs)
    DH_s_c=mf_s*(Delta_H_vv+CA)
    Ef_w_p=DH_s_p+t_s
    Ef_w_c=DH_s_c+t_s
end

Procedure ms(h_m, rho_1, rho_1_w, P_1_w,P_1_b:mf_s)   "mass flux to the wall"
    S=1
    if (P_1_w>=P_1_b) then
        mf_s=0[kg/s-m^2]
    else
        mf_s=max(0[kg/s-m^2],S*h_m*(rho_1-rho_1_w))
    endif
end

Procedure sphelium(A,m_dot,T,P:rho,u,cp,h, mu, k, Pr)      "properties of super critical
helium"
```

```
    G2$='Helium'
    rho=Density(G2$,T=T,P=P)
    u=m_dot/rho/A
    cp=Cp(G2$,T=T,P=P)
    h=Enthalpy(G2$,T=T,P=P)
    mu=Viscosity(G2$,T=T,P=P)
    k=Conductivity(G2$,T=T,P=P)
    Pr=Prandtl(G2$,T=T,P=P)
    {Re=4*m_dot_c/(pi*mu*D_c)}
end

"-----------------------------------------------------------------------------------------------"
adjust "
ad=1
ad_d=1
N_mf=0.5
G1$='Hydrogen'

"cryogenic fore pump"
L=42[in]*convert(in,m)          "pump length"
D=0.05[m]
r=D/2

"supercritical helium pipe"
D_c=0.1524{0.06}{0.1524}[m]
r_c=D_c/2
A_a=pi*(r_c^2-r^2)
D_h=r_c-r
r|star=r/r_c

"inlet gas mixture condition"
{m_dot_H2_in=0.0011[g/s]*convert(g/s,kg/s)}
m_dot_H2_in=rho[1]*u[1]*pi*r^2
{m_dot_H2_in=0.008[g/s]*convert(g/s,kg/s)}

u[1]=8.087{4.043}{3.697}{9.242}{13.69}{11.2}{3.361}{3.361}[m/s]

{u[1]=14.5[m/s]}
P[1]=20{13.5}{50}[Pa]
x_1[1]=1
P_1[1]=P[1]*x_1[1]
T[1]=77{80}[K]

MW_1=MolarMass(G1$)
```

```
R_1=R#/MW_1

"inlet supercritical helium condition"
T_c_in=7[K]
P_c_in=1.4[bar]*convert(bar,Pa)
P_c_out=1.4[bar]*convert(bar,Pa)
m_dot_c={0.0002}0.4921[g/s]*convert(g/s,kg/s)

"grid"
N=102          "number of nodes."
dy=L/N
A_s=pi*D*dy
dy_bar=(2/r)*dy
duplicate i=1,N
   y[i]=dy*(i-1)
   xoverD[i]=(y[i]+dy/2)/D
    xoverD_h[i]=(L-(y[i]+dy/2))/D_h
end

P_1_b=P_1[1]
{duplicate i=1,N
    Call Wall(L,y[i],P_1_b:T_w[i] ,P_1_w[i])
    rho_1_w[i]=P_1_w[i]/(R_1*T_w[i])
end}

"----------------------------------------------------------------------------------------------march to
node 2 from node 1"
{T_w[1]=50[K]  "guess value"}
Call Wall(P_1_b,T_w[1]:P_1_w[1])
{h_1_w[1]=Enthalpy(G1$,T=T_w[1],P=P_1_w[1])}
rho_1_w[1]=P_1_w[1]/(R_1*T_w[1])

rho_1[1]=P_1[1]/(R_1*T[1])
rho[1]=rho_1[1]

Call enthalpy_ad(T[1],P_1[1]:h_1[1])
{h_1[1]=Enthalpy(G1$,T=T[1],P=P_1[1])}

h[1]=h_1[1]  "h[2] another equation"
Call mix(T[1],P_1[1]:mu[1],k[1],cp[1])
nu[1]=mu[1]/rho[1]

Re[1]=u[1]*D/nu[1] "Reynolds number"
D_ab[1]=ad_d*D_12_gas(G1$,G1$,T[1],P[1])     "diffusion coefficient"
```

```
Sc[1]=nu[1]/D_ab[1]     "Schmidt number"
call PipeFlow_N_local(Re[1],Sc[1],xoverD[1],0: Sh_T_x[1],Sh_H_x[1],f[1])
    "warning: xoverD should be >0.1"
Sh_T_x[1]=h_m[1]*D/D_ab[1] "Sherwood number" "choose the worst case"
call ms(h_m[1], rho_1[1], rho_1_w[1], P_1_w[1],P_1_b:mf_s[1])

Pr[1]=cp[1]*mu[1]/k[1]
call PipeFlow_N_local(Re[1],Pr[1],xoverD[1],0: Nusselt_T_x[1],Nusselt_H_x[1],f_x[1])
Nusselt_T_x[1]=h_t[1]*D/k[1]  "choose the lower limit"
t_s[1]=h_t[1]*(T[1]-T_w[1])
dP_f_c[1]=rho[1]*f_x[1]*(u[1]^2/2)*(dy/D)

Call
cooling(h_1[1],mf_s[1],t_s[1],T_w[1],P_1_w[1]:Delta_H_vs[1],Delta_H_vv[1],DH_s_p[
1],DH_s_c[1],Ef_w_p[1],Ef_w_c[1])

{{T_c_out={9.4}{8.7}8.3{8.295}{8.351}{9.195}{5.23}[K]          "guess value"}}
T_c[1]=T_c_out
P_c[1]=P_c_out
Call sphelium(A_a,m_dot_c,T_c[1],P_c[1]:rho_c[1],u_c[1],cp_c[1],h_c[1], mu_c[1],
k_c[1], Pr_c[1])
cp_c=cp_c[1]
mu_c=mu_c[1]
Pr_c= Pr_c[1]
k_c=k_c[1]
Re_c[1]=m_dot_c*D_h/(A_a*mu_c[1])

call AnnularFlow_N_local(Re_c[1], Pr_c[1], xoverD_h[1], r|star, 0:
Nusselt_c_T_x[1],Nusselt_c_H_x[1], f_c_x[1])
Nusselt_c_T_x[1]=hh_c[1]*D_h/k_c[1]     "choose the lower limit"
q_c[1]=hh_c[1]*(T_w[1]-T_c[1])
ad*Ef_w_p[1]=q_c[1]
dP_c_f[1]=rho_c[1]*f_c_x[1]*(u_c[1]^2/2)*(dy/D_h)

{u[2]=u[1]}
{dP_f[1]=2*R_1*T[1]*mf_s[1]/r}
dP_f[1]=P[1]*(2*dy*mf_s[1]/(u[1]*rho[1]*r))
u[2]*rho_1[2]=u[1]*rho_1[1]-dy_bar*mf_s[1]      "hydrogen mass balance"

u[2]^2*rho[2]+P[2]=u[1]^2*rho[1]+P[1]{-dP_f[1]}-dP_f_c[1]-dy_bar*mf_s[1]*u[1]
    "momentum balance"

u[2]*rho[2]*(h[2]+0.5*u[2]^2)=u[1]*rho[1]*(h[1]+0.5*u[1]^2)-
dy_bar*(mf_s[1]*(h[1]+0.5*u[1]^2)+t_s[1])    "energy balance"
```

```
rho_1[2]=P_1[2]/(R_1*T[2])

rho[2]=rho_1[2]
P[2]=P_1[2]

"the last equation"
{P[2]=100[Pa]    "guess for another equation"}
Call enthalpy_ad(T[2],P_1[2]:h_1[2])
{h_1[2]=Enthalpy(G1$,T=T[2],P=P_1[2])}
h[2]=h_1[2]  "h[2] another equation"

Call mix(T[2],P_1[2]:mu[2],k[2],cp[2])


duplicate i=2,N"N"
    nu[i]=mu[i]/rho[i]
    Re[i]=u[i]*D/nu[i]    "Reynolds number"
    D_ab[i]=ad_d*D_12_gas(G1$,G1$,T[i],P[i])   "diffusion coefficient"
    Sc[i]=nu[i]/D_ab[i]   "Schmidt number"
    call PipeFlow_N_local(Re[i],Sc[i],xoverD[i],0: Sh_T_x[i],Sh_H_x[i],f[i])
    "warning: xoverD should be >0.1"
    Sh_T_x[i]=h_m[i]*D/D_ab[i]    "Sherwood number" "choose the worst case"
{   T_w[i]=18[K]     "guess value"}
    Call Wall(P_1_b,T_w[i]:P_1_w[i])
{   h_1_w[i]=Enthalpy(G1$,T=T_w[i],P=P_1_w[i])}
    rho_1_w[i]=P_1_w[i]/(R_1*T_w[i])
    call ms(h_m[i], rho_1[i], rho_1_w[i], P_1_w[i],P_1_b:mf_s[i])

    Pr[i]=cp[i]*mu[i]/k[i]
    call PipeFlow_N_local(Re[i],Pr[i],xoverD[i],0: Nusselt_T_x[i],Nusselt_H_x[i],f_x[i])
    Nusselt_T_x[i]=h_t[i]*D/k[i]     "choose the lower limit"
    t_s[i]=h_t[i]*(T[i]-T_w[i])
    dP_f_c[i]=rho[i]*f_x[i]*(u[i]^2/2)*(dy/D)
    Call
cooling(h_1[i],mf_s[i],t_s[i],T_w[i],P_1_w[i]:Delta_H_vs[i],Delta_H_vv[i],DH_s_p[i],D
H_s_c[i],Ef_w_p[i],Ef_w_c[i])
    P_c[i]=P_c[i-1]
    T_c[i]=T_c[i-1]-q_c[i-1]*A_s/(m_dot_c*cp_c[i-1])       "super critical helium
temperature"
    Call sphelium(A_a,m_dot_c,T_c[i],P_c[i]:rho_c[i],u_c[i],cp_c[i],h_c[i], mu_c[i],
k_c[i], Pr_c[i])
    Re_c[i]=m_dot_c*D_h/(A_a*mu_c[i])
```

```
    call AnnularFlow_N_local(Re_c[i], Pr_c[i], xoverD_h[i], r|star, 0:
Nusselt_c_T_x[i],Nusselt_c_H_x[i], f_c_x[i])
    dP_c_f[i]=rho_c[i]*f_c_x[i]*(u_c[i]^2/2)*(dy/D_h)
    Nusselt_c_T_x[i]=hh_c[i]*D_h/k_c[i]  "choose the lower limit"
    q_c[i]=hh_c[i]*(T_w[i]-T_c[i])
    ad*Ef_w_p[i]=q_c[i]

{   u[i+1]*rho_1[i+1]=u[i]*rho_1[i]-dy_bar*mf_s[i]          "hydrogen mass balance"
    u[i+1]^2*rho[i+1]+P[i+1]=u[i]^2*rho[i]+P[i]-dP_f[i]-dy_bar*mf_s[i]*u[i]
    "momentum balance"
    u[i+1]*rho[i+1]*(h[i+1]+0.5*u[i+1]^2)=u[i]*rho[i]*(h[i]+0.5*u[i]^2)-
dy_bar*(mf_s[i]*(h[i]+0.5*u[i]^2)+t_s[i]) "energy balance"
    rho_1[i+1]=P_1[i+1]/(R_1*T[i+1])}

{   u[i+1]=u[i]}
{   dP_f[i]=2*R_1*T[i]*mf_s[i]/r}
    dP_f[i]=P[i]*(2*dy*mf_s[i]/(u[i]*rho[i]*r))
    0=(u[i+1]*rho_1[i+1])-(u[i]*rho_1[i]-dy_bar*mf_s[i])   "hydrogen mass balance"
    0=(u[i+1]^2*rho[i+1]+P[i+1])-(u[i]^2*rho[i]+P[i]{-dP_f[i]}-dP_f_c[i]-
dy_bar*mf_s[i]*u[i])     "momentum balance"
    0=(u[i+1]*rho[i+1]*(h[i+1]+0.5*u[i+1]^2))-(u[i]*rho[i]*(h[i]+0.5*u[i]^2)-
dy_bar*(mf_s[i]*(h[i]+0.5*u[i]^2)+t_s[i]))     "energy balance"
    0=(rho_1[i+1])-(P_1[i+1]/(R_1*T[i+1]))

    {rho[i+1]=rho_1[i+1]
    P[i+1]=P_1[i+1]}
    0=rho[i+1]-rho_1[i+1]
    0=P[i+1]-P_1[i+1]
    "the last equation"
    {P_1[i+1]=99[Pa]}   "guess for another equation"
    {u[i+1]=14.5[m/s]}

    Call enthalpy_ad(T[i+1],P_1[i+1]:h_1[i+1])
{   h_1[i+1]=Enthalpy(G1$,T=T[i+1],P=P_1[i+1])}
    h[i+1]=h_1[i+1]  "h[2] another equation"

    Call mix(T[i+1],P_1[i+1]:mu[i+1],k[i+1],cp[i+1])
end

{duplicate i=N-2,N
    nu[i]=mu[i]/rho[i]
    Re[i]=u[i]*D/nu[i]    "Reynolds number"
    D_ab[i]=ad_d*D_12_gas(G1$,G1$,T[i],P[i])   "diffusion coefficient"
    Sc[i]=nu[i]/D_ab[i]   "Schmidt number"
```

```
    call PipeFlow_N_local(Re[i],Sc[i],xoverD[i],0: Sh_T_x[i],Sh_H_x[i],f[i])
    "warning: xoverD should be >0.1"
    Sh_T_x[i]=h_m[i]*D/D_ab[i]   "Sherwood number" "choose the worst case"
{   T_w[i]=18[K]     "guess value"}
    Call Wall(P_1_b,T_w[i]:P_1_w[i])
    rho_1_w[i]=P_1_w[i]/(R_1*T_w[i])
    call ms(h_m[i], rho_1[i], rho_1_w[i], P_1_w[i],P_1_b:mf_s[i])

    Pr[i]=cp[i]*mu[i]/k[i]
    call PipeFlow_N_local(Re[i],Pr[i],xoverD[i],0: Nusselt_T_x[i],Nusselt_H_x[i],f_x[i])
    Nusselt_T_x[i]=h_t[i]*D/k[i]    "choose the lower limit"
    t_s[i]=h_t[i]*(T[i]-T_w[i])
    dP_f[i]=rho[i]*f_x[i]*(u[i]^2/2)*(dy/D)
    Call
cooling(h_1[i],mf_s[i],t_s[i],T_w[i],P_1_w[i]:Delta_H_vs[i],Delta_H_vv[i],DH_s_p[i],D
H_s_c[i],Ef_w_p[i],Ef_w_c[i])
    P_c[i]=P_c[i-1]
    T_c[i]=T_c[i-1]-q_c[i-1]*A_s/(m_dot_c*cp_c[i-1])       "super critical helium
temperature"
    Call sphelium(A_a,m_dot_c,T_c[i],P_c[i]:rho_c[i],u_c[i],cp_c[i],h_c[i], mu_c[i],
k_c[i], Pr_c[i])
    Re_c[i]=m_dot_c*D_h/(A_a*mu_c[i])
    call AnnularFlow_N_local(Re_c[i], Pr_c[i], xoverD_h[i], r|star, 0:
Nusselt_c_T_x[i],Nusselt_c_H_x[i], f_c_x[i])
    dP_c_f[i]=rho_c[i]*f_c_x[i]*(u_c[i]^2/2)*(dy/D_h)
    Nusselt_c_T_x[i]=hh_c[i]*D_h/k_c[i]  "choose the lower limit"
    q_c[i]=hh_c[i]*(T_w[i]-T_c[i])
    ad*Ef_w_p[i]=q_c[i]

{   u[i+1]*rho_1[i+1]=u[i]*rho_1[i]-dy_bar*mf_s[i]          "hydrogen mass balance"
    u[i+1]^2*rho[i+1]+P[i+1]=u[i]^2*rho[i]+P[i]-dP_f[i]-dy_bar*mf_s[i]*u[i]
    "momentum balance"
    u[i+1]*rho[i+1]*(h[i+1]+0.5*u[i+1]^2)=u[i]*rho[i]*(h[i]+0.5*u[i]^2)-
dy_bar*(mf_s[i]*(h[i]+0.5*u[i]^2)+t_s[i]) "energy balance"
    rho_1[i+1]=P_1[i+1]/(R_1*T[i+1])}
    0=(u[i+1]*rho_1[i+1])-(u[i]*rho_1[i]-dy_bar*mf_s[i])   "hydrogen mass balance"
    0=(u[i+1]^2*rho[i+1]+P[i+1])-(u[i]^2*rho[i]+P[i]-dP_f[i]-dy_bar*mf_s[i]*u[i])
    "momentum balance"
    0=(u[i+1]*rho[i+1]*(h[i+1]+0.5*u[i+1]^2))-(u[i]*rho[i]*(h[i]+0.5*u[i]^2)-
dy_bar*(mf_s[i]*(h[i]+0.5*u[i]^2)+t_s[i]))     "energy balance"
    0=(rho_1[i+1])-(P_1[i+1]/(R_1*T[i+1]))

    {rho[i+1]=rho_1[i+1]
    P[i+1]=P_1[i+1]}
```

```
    0=rho[i+1]-rho_1[i+1]
    0=P[i+1]-P_1[i+1]
    "the last equation"
    {P_1[i+1]=99[Pa]}    "guess for another equation"
    {u[i+1]=14.5[m/s]}

    Call enthalpy_ad(T[i+1],P_1[i+1]:h_1[i+1])
{   h_1[i+1]=Enthalpy(G1$,T=T[i+1],P=P_1[i+1])}
    h[i+1]=h_1[i+1]  "h[2] another equation"

    Call mix(T[i+1],P_1[i+1]:mu[i+1],k[i+1],cp[i+1])
end}
{T_c[N]=T_c_in+error}

"-------------------------------------------------------------------------------------------------------
---------"
T_c_in_c=T_c[N]
error=Abs(T_c_in-T_c_in_c)    "error=2.956 [K] for 102 N"
"-------------------------------------------------------------------------------------------------------
mass flux"
duplicate i=1,N
    mf[i]=rho[i]*u[i]
end
N_mf=(mf[1]-mf[N])/mf[1]
```

Appendix C. Hemisphere model code

```
$Unitsystem SI m s kg PA N J Rad K
$Tabstops 0.2 0.4 0.6 0.8 1 in

Function pointer(time_steps, T_s_1, T_critical)
    If (T_s_1>T_critical) Then q=time_steps Else q=-1
    pointer=q
end

Procedure enthalpy_ad(T,P:h)   "hydrogen enthalpy"
    G1$='Hydrogen'
    M_1=MolarMass(G1$)
    if (T<=14 [K]) then
        h=(521047[J/kmol] + 20616.7[J/kmol-K]*T)/M_1
    else
        h=256598[J/kg] + 10357.4[J/kg-K]*T
        {h=Enthalpy(G1$,T=T,P=P)}
    endif
end

Procedure Wall(P_1,T:P)    "wall boundary conditions"
G1$='Hydrogen'
    if (T>10[K]) then
        P=P_1
    else
        if (T<=10[K]) and (T>9[K]) then
            P=min(P_1,-1587.87[Pa] + 184.345[Pa/K]*T)
        else
            if (T<=9[K]) and (T>8[K]) then
                P=min(P_1,-435.724[Pa] + 56.3287[Pa/K]*T)
            else
                if (T<=8[K]) and (T>7[K]) then
                    P=-87.6888[Pa] + 12.8243[Pa/K]*T
                else
                    if (T<=7[K]) and (T>6[K]) then
                        P=-11.3689[Pa] + 1.92144[Pa/K]*T
                    else
                        P=max(0.0001[Pa],-0.770044[Pa] + 0.154961[Pa/K]*T)
                        {if (T<=6[K]) and (T>=4.5[K]) then
                            P=max(0.0001[Pa],-0.770044[Pa] + 0.154961[Pa/K]*T)
                        else
                            P=4[Pa]                    "attention, T should be greater than 4.5 K"
                        endif}
```

```
                endif
            endif
        endif
    endif
endif
end

Procedure cooling(h,mf_s,T_w:DH_s_p)   "wall boundary conditions"
    G1$='Hydrogen'
    M_1=MolarMass(G1$)
    CA=100000[J/kmol]/M_1
    if (T_w<=14 [K]) then
        h_1_w=(521047[J/kmol] + 20616.7[J/kmol-K]*T_w)/M_1
    else
        h_1_w=256598[J/kg] + 10357.4[J/kg-K]*T_w
{       h_1_w=Enthalpy(G1$,T=T_w,P=P_1_w)}
    endif
    Delta_H_vs=769.897[J/kg] + 19.6193[J/kg-K]*T_w
    Delta_H_vv=h-h_1_w    "enthalpy change from vapor to vapor, lack of data"
    DH_s_p=mf_s*(Delta_H_vv+Delta_H_vs)
    {DH_s_c=mf_s*(Delta_H_vv+CA)}
end

Procedure mix(T,P_1:mu,k,cp)  "mixture thermal and kinetic properties"
    G1$='Hydrogen'
    M_1=MolarMass(G1$)
    if (T>18[K]) then
        mu_1=Viscosity(G1$,T=T,P=P_1)
    else
        mu_1=7.64217E-07[Pa-s] + 3.39265E-08[Pa-s/K]*T
    endif
{   mu_1=Viscosity(G1$,T=T,P=P_1)}
    if (T>14[K]) then
        k_1=Conductivity(G1$,T=T,P=P_1)
    else
        k_1=0.00559606[W/m-K] + 0.000629187[W/m-K^2]*T
    endif
{   k_1=Conductivity(G1$,T=14[K],P=P_1)}
    mu=mu_1"viscosity"
    k=k_1 "conductivity"
    if (T<10[K]) then
        cp_1=(35.065[J/kmol-K] - 73.0795[J/kmol-K^2]*T + 27.5904[J/kmol-
K^3]*T^2)/M_1
    else
```

```
        if (T>=10[K]) and (T<13.957[K]) then
            cp_1=(4469.83[J/kmol-K] - 1147.04[J/kmol-K^2]*T + 89.2029[J/kmol-
K^3]*T^2)/M_1
        else
            cp_1=SpecHeat(G1$,T=T,P=P_1)
        endif
    endif
    cp=cp_1   "specific heat"
end

Procedure sphelium(A,m_dot,T,P:rho,vel,cp,h, mu, k, Pr)    "properties of super critical
helium"
    G2$='Helium'
    rho=Density(G2$,T=T,P=P)
    vel=m_dot/rho/A
    cp=Cp(G2$,T=T,P=P)
    h=Enthalpy(G2$,T=T,P=P)
    mu=Viscosity(G2$,T=T,P=P)
    k=Conductivity(G2$,T=T,P=P)
    Pr=Prandtl(G2$,T=T,P=P)
    {Re=4*m_dot_c/(pi*mu*D_c)}
end
M=20
T_c_i=6[K]
T_s_i=6[K]
T_s=6[K]

m_dot_c=0.53[g/s]*convert(g/s,kg/s)

    G1$='Hydrogen'
L=42[in]*convert(in,m)          "pump length"

D=0.05[m]
r=D/2
th=0.002[m]
N=100
dy=L/N
D_o=0.1524[m]
r_o=D_o/2
D_h=r_o-r
r|star=r/r_o
```

```
duplicate i=1,N
    y[i]=i*dy
   xoverD[i]=(y[i]+dy/2)/D

    xoverD_h[i]=(L-(y[i]+dy/2))/D_h
end

theta[1]=arctan(y[1]/r)
duplicate i=2,N
    theta[i]=arctan(y[i]/r)
end

alpha[1]=theta[1]
duplicate i=2,N
    alpha[i]=theta[i]-theta[i-1]
end

check_alpha=sum(alpha[1..N])+arctan(r/L)-pi/2

duplicate i=1,N
    pc[i]=alpha[i]/(pi/2)
end

m_dot_H2_in=0.001[g/s]*convert(g/s,kg/s)

duplicate i=1,N
    m_dot_H2[i]=pc[i]*m_dot_H2_in
end

P_1=50[Pa]
T_w=5[K]
Call Wall(P_1,T_w:P)

P_in=50[Pa]
T_in=77[K]
h_in=Enthalpy(G1$,T=T_in,P=P_in)


duplicate j=1,M
    duplicate i=1,20
        Call cooling(h_in,m_dot_H2[i],T_s[i,j]: DH_s_p[i,j])
    end
end
{{
```

```
duplicate i=1,20
    Call cooling(h_in,m_dot_H2[i],T_w: DH_s_p[i])
end
}}
Call cooling(h_in,m_dot_H2_in,T_w: DH_s_p_total)


m_dot_c=rho_c*A_c*u_c
dy=u_c*t_ct  "t_ct is time_coolant travel"


k_s=Conductivity(Stainless_AISI304, T=T_s)


cv_s=Cv(Stainless_AISI304, T=T_s)

rho_s=Density(Stainless_AISI304, T=T_s)

Ac_s=pi*((D+th)^2-D^2)/4

m_s=rho_s*dy*pi*((D+th)^2-D^2)/4
alpha_s=k_s/(rho_s*cv_s)
th=2*sqrt(alpha_s*time_s)
{duplicate i=1, N
    cv_s*m_s*1[K]=DH_s_p[i]*time_s[i]
end}

{D_c=0.06[m]}

{T_c=5[K]}
P_c=1.4[bar]*convert(bar,Pa)
cp_c=Cp(Helium,T=T_c_i, P=P_c)
cv_c=Cv(Helium,T=T_c_i, P=P_c)
rho_c=Density(Helium, T=T_c_i, P=P_c)
alpha_c=k_c/(rho_c*cv_c)
A_c=pi*((D_o)^2-(D+th)^2)/4
(D_o-(D+th))/2=2*sqrt(alpha_c*time_c)

Bi=0.5792
Bi=th*hh_c/k_s

k_c=Conductivity(Helium, T=T_c_i, P=P_c)

{DH_s_p[1]/(pi*D*dy)=k_s*DT/th}
```

```
{T_s_i=5[K]
duplicate i=1,N
    T_s[i]=T_s_i
end}



duplicate i=1,20
    T_c[i,1]=T_c_i
end


{T_c[21,1]=T_c_i}
{T_c_o[20]=T_c_i}

duplicate j=1,M
    h_c[21,j]=Enthalpy(Helium,T=T_c_i,P=P_c)  "from node 21 to node 20"
end
t_step=t_ct/2

"energy balance on 20"

{DH_s_p[20]=DELTA_E_dot[20,1]+DELTAU_dot[20,1]}
q_sc[20,1]=DELTA_E_dot[20,1]+DELTAU_dot[20,1]

DELTA_E_dot[20,1]=m_dot_c*(h_c[20,1]-h_c[21,1])
DELTAU_dot[20,1]=m_c[20,1]*(u_c[20,2]-u_c[20,1])/t_step
Call sphelium(A_a,m_dot_c,T_c[20,1],P_c:
rho_c[20,1],vel_c[20,1],cp_c[20,1],h_c[20,1], mu_c[20,1], k_c[20,1], Pr_c[20,1])
{h_c[20,1]=Enthalpy(Helium,T=T_c[20,1],P=P_c)
rho_c[20,1]=Density(Helium, T=T_c[20,1], P=P_c)}
m_c[20,1]=rho_c[20,1]*dy*A_c
u_c[20,2]=IntEnergy(Helium,T=T_c[20,2],P=P_c)
u_c[20,1]=IntEnergy(Helium,T=T_c[20,1],P=P_c)

duplicate i=1,19
{   DH_s_p[20-i]=DELTA_E_dot[20-i,1]+DELTAU_dot[20-i,1]}
    q_sc[20-i,1]=DELTA_E_dot[20-i,1]+DELTAU_dot[20-i,1]
    DELTA_E_dot[20-i,1]=m_dot_c*(h_c[20-i,1]-h_c[20+1-i,1])
    DELTAU_dot[20-i,1]=m_c[20-i,1]*(u_c[20-i,2]-u_c[20-i,1])/t_step
    Call sphelium(A_a,m_dot_c,T_c[20-i,1],P_c: rho_c[20-i,1],vel_c[20-i,1],cp_c[20-
i,1],h_c[20-i,1], mu_c[20-i,1], k_c[20-i,1], Pr_c[20-i,1])
{   h_c[20-i,1]=Enthalpy(Helium,T=T_c[20-i,1],P=P_c)
```

```
    rho_c[20-i,1]=Density(Helium, T=T_c[20-i,1], P=P_c)}
    m_c[20-i,1]=rho_c[20-i,1]*dy*A_c
    u_c[20-i,2]=IntEnergy(Helium,T=T_c[20-i,2],P=P_c)
    u_c[20-i,1]=IntEnergy(Helium,T=T_c[20-i,1],P=P_c)
end

duplicate j=2,M
    Call sphelium(A_a,m_dot_c,T_c[20,j],P_c:
rho_c[20,j],vel_c[20,j],cp_c[20,j],h_c[20,j], mu_c[20,j], k_c[20,j], Pr_c[20,j])
{   h_c[20,j]=Enthalpy(Helium,T=T_c[20,j],P=P_c)
    rho_c[20,j]=Density(Helium, T=T_c[20,j], P=P_c)}
    m_c[20,j]=rho_c[20,j]*dy*A_c
    {u_c[20,j]=IntEnergy(Helium,T=T_c[20,j],P=P_c)}
{   DH_s_p[20]=DELTA_E_dot[20,j]+DELTAU_dot[20,j]}
    q_sc[20,j]=DELTA_E_dot[20,j]+DELTAU_dot[20,j]
    DELTA_E_dot[20,j]=m_dot_c*(h_c[20,j]-h_c[21,j])
    DELTAU_dot[20,j]=m_c[20,j]*(u_c[20,j+1]-u_c[20,j])/t_step
    u_c[20,j+1]=IntEnergy(Helium,T=T_c[20,j+1],P=P_c)

duplicate i=1,19
    Call sphelium(A_a,m_dot_c,T_c[20-i,j],P_c: rho_c[20-i,j],vel_c[20-i,j],cp_c[20-
i,j],h_c[20-i,j], mu_c[20-i,j], k_c[20-i,j], Pr_c[20-i,j])
{   h_c[20-i,j]=Enthalpy(Helium,T=T_c[20-i,j],P=P_c)
    rho_c[20-i,j]=Density(Helium, T=T_c[20-i,j], P=P_c)}
    m_c[20-i,j]=rho_c[20-i,j]*dy*A_c
{   DH_s_p[20-i]=DELTA_E_dot[20-i,j]+DELTAU_dot[20-i,j]}
    q_sc[20-i,j]=DELTA_E_dot[20-i,j]+DELTAU_dot[20-i,j]
    DELTA_E_dot[20-i,j]=m_dot_c*(h_c[20-i,j]-h_c[20+1-i,j])
    DELTAU_dot[20-i,j]=m_c[20-i,j]*(u_c[20-i,j+1]-u_c[20-i,j])/t_step
    u_c[20-i,j+1]=IntEnergy(Helium,T=T_c[20-i,j+1],P=P_c)
{   u_c[20-i,j]=IntEnergy(Helium,T=T_c[20-i,j],P=P_c)}
end



end
A_a=pi*(r_o^2-r^2)
{duplicate j=1,M
duplicate i=1,20
    {T_s[i,1]=5[K]}
    k_s[i,j]=Conductivity(Stainless_AISI304, T=T_s[i,j])
    rho_s[i,j]=Density(Stainless_AISI304, T=T_s[i,j])
    c_s[i,j]=Cv(Stainless_AISI304, T=T_s[i,j])
    alpha_s[i,j]=k_s[i,j]/(rho_s[i,j]*c_s[i,j])
```

```
    th=2*sqrt(alpha_s[i,j]*time_diff[i,j])
    R_s[i,j]=ln(r_o/r)/(2*pi*dy*k_s[i,j])


    Re_c[i,j]=m_dot_c*D_h/(A_a*mu_c[i,j])
    call AnnularFlow_N_local(Re_c[i,j], Pr_c[i,j], xoverD_h[i], r|star, 0:
Nusselt_c_T_x[i,j],Nusselt_c_H_x[i,j], f_c_x[i,j])
    Nusselt_c_T_x[i,j]=hh_c[i,j]*D_h/k_c[i,j]  "choose the lower limit"
    R_c[i,j]=1/(hh_c[i,j]*pi*D*dy)




    T_s[i,j]-T_c[i,j]=DH_s_p[i]*(R_s[i,j]+R_c[i,j])
end
end}

duplicate j=1,M
    duplicate i=1,20
        Re_c[i,j]=m_dot_c*D_h/(A_a*mu_c[i,j])
        call AnnularFlow_N_local(Re_c[i,j], Pr_c[i,j], xoverD_h[i], r|star, 0:
Nusselt_c_T_x[i,j],Nusselt_c_H_x[i,j], f_c_x[i,j])
        Nusselt_c_T_x[i,j]=hh_c[i,j]*D_h/k_c[i,j]  "choose the lower limit"
        R_c[i,j]=1/(hh_c[i,j]*pi*D*dy)
    end
end

P_1[1]=P_in
T[1]=T_in
MW_1=MolarMass(G1$)
R_1=R#/MW_1
P_in=rho_1_in*R_1*T_in
Call mix(T_in,P_in:mu_in,k_in,cp_in)
m_dot_H2_in=rho_1_in*u_in*pi*r^2
dy=u_in*t_ht
t_H2_l*u_in=L

alpha_H2=k_in/(rho_1_in*cp_in)
r=2*sqrt(alpha_H2*time_H2)

nu_in=mu_in/rho_1_in
Re_in=u_in*D/nu_in
Pr_in=cp_in*mu_in/k_in
call PipeFlow_N_local(Re_in,Pr_in,dy/(2*D),0: Nusselt_T_x_in,Nusselt_H_x_in,f_x_in)
```

```
Nusselt_T_x_in=hh_in*D/k_in
A_s=pi*D*dy
q_in=hh_in*(T_in-5[K])*A_s
q_in*time=cv_s*m_s*(5.1[K]-5[K])
q_in=m_dot_H2_in*(h_in-h_min_H2)
Call enthalpy_ad(T_min_H2,P_in:h_min_H2)
Bi_hs=th*hh_in/k_s
R_s_in=ln(r_o/r)/(2*pi*dy*k_s)
R_in_h=1/(hh_in*A_s)


"the pump wall lumped"

"node 1"
{q_hs[1,1]=0.03[W]
T_s[1,1]=5[K]
q_sc[1,1]=(T_s[1,1]-T_c[1,1])/R_c[1,1]
u_s[1,1]=IntEnergy(Stainless_AISI304, T=T_s[1,1])
q_hs[1,1]=q_sc[1,1]+DELTAU_dot_s[1,1]
DELTAU_dot_s[1,1]=m_s*(u_s[1,1+1]-u_s[1,1])/t_step
u_s[1,1+1]=IntEnergy(Stainless_AISI304, T=T_s[1,1+1])}

duplicate i=1,20
    T_s[i,1]=T_s_i
    q_hs[i,1]=DH_s_p[i,1]
end

duplicate i=1,20
    duplicate j=2,M
        q_hs[i,j]=DH_s_p[i,j]
    end
end

duplicate i=1,20

    q_sc[i,1]=(T_s[i,1]-T_c[i,1])/R_c[i,1]
    u_s[i,1]=IntEnergy(Stainless_AISI304, T=T_s[i,1])
    q_hs[i,1]=q_sc[i,1]+DELTAU_dot_s[i,1]
    DELTAU_dot_s[i,1]=m_s*(u_s[i,1+1]-u_s[i,1])/t_step
    u_s[i,1+1]=IntEnergy(Stainless_AISI304, T=T_s[i,1+1])
end

duplicate j=2,M
    duplicate i=1,20
```

```
        q_sc[i,j]=(T_s[i,j]-T_c[i,j])/R_c[i,j]
        q_hs[i,j]=q_sc[i,j]+DELTAU_dot_s[i,j]
        DELTAU_dot_s[i,j]=m_s*(u_s[i,j+1]-u_s[i,j])/t_step
        u_s[i,j+1]=IntEnergy(Stainless_AISI304, T=T_s[i,j+1])
    end
end

time_total=t_step*M

T_critical=6[K]
duplicate time_steps=1,M
    pointer[time_steps]=pointer(time_steps, T_s[1,time_steps], T_critical)
end

{DELTAU_dot[20-i,j]=m_c[20-i,j]*(u_c[20-i,j+1]-u_c[20-i,j])/t_step
u=IntEnergy(Stainless_AISI304, T=T)}
{Re[1]=u[1]*D/nu[1]     "Reynolds number"
Pr[1]=cp[1]*mu[1]/k[1]
call PipeFlow_N_local(Re[1],Pr[1],xoverD[1],0:
Nusselt_T_x[1],Nusselt_H_x[1],f_x[1])}

{T_s_bar=10[K]
T_s_bar-5[K]=DH_s_p_bar*(R_s[1,1]+R_c[1,1])

Call cooling(h_bar,m_dot_H2[1],T_s_bar:DH_s_p_bar)
h_bar=Enthalpy(G1$,T=T_bar,P=P_in)}

{duplicate i=1,20
    {T_s[i,1]=5[K]}
    k_s[i,j]=Conductivity(Stainless_AISI304, T=T_s[i,j])
    R_s[i,j]=ln(r_o/r)/(2*pi*dy*k_s[i,j])
end

A_a=pi*(r_o^2-r^2)
duplicate i=1,20
    Re_c[i,1]=m_dot_c*D_h/(A_a*mu_c[i,1])
    call AnnularFlow_N_local(Re_c[i,1], Pr_c[i,1], xoverD_h[i], r|star, 0:
Nusselt_c_T_x[i,1],Nusselt_c_H_x[i,1], f_c_x[i,1])
    Nusselt_c_T_x[i,1]=hh_c[i,1]*D_h/k_c[i,1]     "choose the lower limit"
    R_c[i,1]=1/(hh_c[i,1]*pi*D*dy)
end

duplicate i=1,20
    T_s[i,1]-T_c[i,1]=DH_s_p[i]*(R_s[i,1]+R_c[i,1])
```

```
end}
{
DH_s_p[20]=DELTA_E_dot[20]+DELTAU_dot[20]
DELTA_E_dot[20]=m_dot_c*(h_c[20]-h_c[21])
DELTAU_dot[20]=m_c[20]*(u_c_n[20]-u_c_o[20])/t_step
h_c[20]=Enthalpy(Helium,T=T_c_o[20],P=P_c)
rho_c[20]=Density(Helium, T=T_c_o[20], P=P_c)
m_c[20]=rho_c[20]*dy*A_c
u_c_n[20]=IntEnergy(Helium,T=T_c_n[20],P=P_c)
u_c_o[20]=IntEnergy(Helium,T=T_c_o[20],P=P_c)

duplicate i=1,19
    DH_s_p[20-i]=DELTA_E_dot[20-i]+DELTAU_dot[20-i]
    DELTA_E_dot[20-i]=m_dot_c*(h_c[20-i]-h_c[20+1-i])
    DELTAU_dot[20-i]=m_c[20-i]*(u_c_n[20-i]-u_c_o[20-i])/t_step
    h_c[20-i]=Enthalpy(Helium,T=T_c_o[20-i],P=P_c)
    rho_c[20-i]=Density(Helium, T=T_c_o[20-i], P=P_c)
    m_c[20-i]=rho_c[20-i]*dy*A_c
    u_c_n[20-i]=IntEnergy(Helium,T=T_c_n[20-i],P=P_c)
    u_c_o[20-i]=IntEnergy(Helium,T=T_c_o[20-i],P=P_c)
end}
```